

University of Nottingham
UK | CHINA | MALAYSIA

# SRPK1 inhibition and other treatments for Acute Myeloid Leukaemia

University of Nottingham

School of Life Sciences

Viola Erdelyi

Thesis submitted for the degree of Doctor of Philosophy

University of Nottingham

2023

*"I climbed into the machine and signalled to Peter and Ian to push the button for a single pulse. There was an audible crack but I felt nothing. I then signalled to start the scan. The magnet was enclosed in aluminium sheeting forming an RF screen. Due to lack of time there was no light inside. I was therefore clamped in the magnet vertically and in pitch darkness for 50 minutes until the procedure was completed."*

*-Sir Peter Mansfield-*

# ACKNOWLEDGEMENTS

This is the hardest thing I have ever done in my life. It nearly broke me. To whom reading this, please know, I gave it my all.

I would like to dedicate this thesis to my family; my mum, my grandma, my sisters and to all the strong women who carved the way before me.

And to my beloved grandpa, András, who was never told which type of leukaemia he was dying from. I am still heartbroken that you left us when I needed you the most.

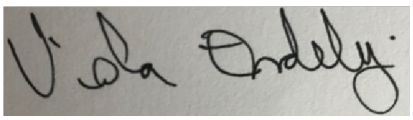
I am forever grateful to Prof David Bates for believing in me and to Dr Kiren Yacub-Usman for all the 'You've got this, Babe's'.

Fabio, my love, I wouldn't be writing this without your support and watching over me. You and our son make the world go around.

I would also like to thank my friends and colleagues who helped me all along the way, Yang-Fan, Simon, Robbie, Pardeep, Joe, Rawan, Razan, Amer, Rachel, Monika & Nikki. The people from BSU, Dr Róbert Márkus from SLIM and the hardworking, dedicated technicians from SOLS. I am truly indebted to all my friends and colleagues from TVBL, especially Jason, James, Jyoti, Ayse, Yizhuo. I am also deeply grateful for my GP and therapist who put me back together.

# AUTHOR'S DECLARATION

I, Viola Erdelyi, confirm that the work presented in this thesis was carried out in accordance with the requirements of the University's Regulations and Code of Practice for Research Degree Programs and that it has not been submitted for any other academic award. I confirm that the work and views demonstrated in this thesis are my own. Where information has been derived from other sources, I confirm this has been indicated in the thesis. All figures were created with BioRender Premium Licence, unless stated otherwise. Figures and data analysis were created in GraphPad Prism 9.5.0.



# ABSTRACT

Acute Myeloid Leukaemia (AML) is a heterogeneous disease of haematopoietic stem cells. It is characterised by poor prognosis and many sub-types carry genetic alterations that make it harder to treat. The current treatment of AML takes heavy tolls on patients, especially on children, causing life changing consequences. AML usually appears in a *de novo* form, although there are multiple cases of therapy-related AML reported due to the use of temozolomide, that is used for the treatment of Glioblastoma Multiforme (GBM).

Previous studies showed that SRPK1 (serine/arginine rich splicing factor protein kinase 1) inhibition reduces AML burden in *in vivo* models of MLL-translocated cells, by prohibiting cell proliferation and causing cell cycle arrest. SRPK1 is known for its role in phosphorylating the serine/arginine rich proteins, especially SRSF1 (serine/arginine rich splicing factor 1), which then plays a role in alternative mRNA splicing. Six AML cell lines were tested, three of the AML cell lines carry an MLL translocation (MLL-TL with AF9, AF10 fusion genes) whilst the other three do not, and therefore classed as wild-type (MLL-WT). It has been reported that cells which carry a translocation are more sensitive to SRPK1 inhibitor treatment than cells without this genetic mutation. This thesis aims to demonstrate the efficacy of a known SRPK1 inhibitor, SPHINX-31, and other unpublished inhibitors for the treatment of AML and solid tumours.

As an off-target effect, SRPK1 has also been shown to alter survival and BRD4 (Bromodomain-containing protein 4) splicing in AML cells. It was shown that

SPHINX-31 can change the BRD4 isoform in AML from the short (BRD4s), oncogenic, to the long (BRD4l), tumour-suppressive form and thus significantly halt cancer progression. To rule out confounding factors, other genes were also tested that are commonly overexpressed in cancer such as MYC, HOXA9, BCL-2 which all showed a decrease in expression in response to increasing levels of inhibitor treatment. To test the clinical relevance of these inhibitors primary AML cells were also treated with SPHINX-31 and Griffin 51 in colony forming units. The data showed promising results that were previously seen with AML cell lines, e.g. the BRD4s isoform is reduced, and all downstream targets are significantly decreased.

Cdc-like kinase 1 (CLK1) is known for its synergistic effect in combination with SRPK1 and their similar role in phosphorylating SR proteins, therefore the previous studies were repeated with a highly selective CLK1 inhibitor which also resulted in reduced cell viability and a significant decrease in all downstream targets. CLK1 inhibition caused a similar effect in BRD4 splice change, where increasing levels of a CLK1 inhibitor caused an upregulation in the tumour-suppressor BRD4l isoform and a down regulation in BRD4s isoform.

BRD4 has been found to be overexpressed not only in AML but in solid tumour cancers such as GBM. And often AML occurs as a side effect to therapy applied to treat GBM. As both AML and GBM have poor survival rates, there is a great unmet clinical need to find potential drug targets for both. To that end, SPHINX-31 and Griffin 51 were used to treat GBM cells and test their response to treatment. A 3D model of the Blood-Brain barrier was also created to mimic the natural environment of GBM.

# TABLE OF CONTENTS

*ACKNOWLEDGEMENTS* *III*

*AUTHOR'S DECLARATION* *IV*

*ABSTRACT* *V*

*ABBREVIATIONS* *XXII*

*1. Chapter Introduction* *1*

**1.1. Haematopoiesis** **1**

**1.2. Leukaemia** **2**

**1.3. Leukaemia classification** **3**

**1.4. Acute Myeloid Leukaemia** **9**

**1.5. Risk factors and pathogenesis** **11**

**1.6. Therapy and management** **12**

**1.7. Chromosomal abnormalities in AML** **14**

**1.8. The FAB system and clinical diagnosis** **14**

**1.9. Constitutive and alternative splicing** **18**

**1.10. Pre-mRNA splicing** **20**

**1.11. Regulatory elements and splice factors of constitutive and alternative splicing** **23**

**1.12. Aberrant splicing in cancer** **24**

**1.13. Aberrant alternative splicing in cancer** **25**

**1.14. Aberrant alternative splicing in leukaemia** **26**

**1.15. Serine/arginine-rich (SR) proteins** **27**

**1.16. Serine/arginine protein kinase 1 (SRPK1) 30**

**1.17. Regulation of SRPK1 activity 31**

**1.18. The role of SRPK1 in cancer 32**

**1.19. SRPK1 expression in leukaemia and its therapy targets 33**

**1.20. CDC-like kinase 1 (CLK1) 34**

**1.21. SRPK1 selective inhibitors 35**

**1.21.1. Second generation SRPK1 inhibitors (ET1126, ET1132, ET3002) 37**

**1.22. CLK1 selective inhibitors 38**

**1.23. Alternative splicing of BRD4 41**

**1.24. BRD4 as a therapeutic target in AML 43**

**1.25. SRPK1 inhibition in solid tumours 44**

***2. Chapter 46***

***Aims and objectives 46***

***3. Chapter 49***

***Materials and methods 49***

**3.1. Acute Myeloid Leukaemia (AML) cell lines and clinical samples 50**

3.1.1. OCI-AML2 50

3.1.2. THP-1 51

3.1.3. MOLM-13 51

3.1.4. OCI-AML3 51

3.1.5. HL60 52

3.1.6. TF1a 52

**3.2. Non-AML cell lines: 53**

3.2.1. HEK 293FT 53

3.2.2. U87 53

**3.3. Growth conditions 54**

3.4. Extraction of cortical astrocytes 54

3.5. Primary brain pericytes and endothelial culture 56

**3.5.1. Serum free media composites for primary cells 57**

**3.6. Detachment and passaging of adherent cells 58**

**3.7. Maintaining suspension cell lines 59**

**3.8. Culture vessels 59**

**3.9. Cell counting 59**

**3.10. Cell viability assays 60**

**3.11. Colony forming units (CFU) 60**

**3.12. Molecular Biology Methods 63**

**3.12.2. RNA isolation from clinical samples 64**

**3.12.3. Quantification of nucleic acid and assessment of purity 64**

**3.12.4. cDNA synthesis 64**

**3.12.5. Primer design 65**

**3.12.6. Polymerase Chain Reaction (PCR) 65**

**3.12.7. Semi-Quantitative PCR 66**

**3.13. Digital Droplet PCR 68**

**3.14. Agarose gel electrophoresis 69**

**3.15. NanoBRET target engagement intracellular kinase assay 70**

***4. Chapter 73***

*SRPK1 inhibition in AML* *73*

**4.1. Aims and objectives** **74**

**4.2. Introduction** **74**

**4.3. Downstream targets after SPHINX-31 treatment in AML cell lines** **75**

**4.4. Cell viability assay** **81**

**4.5. Discussion** **84**

4.5.1. Downstream target levels after SPHINX-31 treatment 85

4.5.2. Cell viability levels in response to treatment 85

***5. Chapter*** ***87***

***BRD4 Splice change in response to SPHINX-31 treatment*** ***87***

**5.1. Aims and objectives** **88**

**5.2. Introduction** **88**

**5.3. Results** **89**

**5.4. Discussion and conclusion** **96**

5.4.1. BRD4 splice change in AML cell lines 96

5.4.2. Concluding remarks 97

***6. Chapter*** ***98***

**Second generation inhibitor treatment in AML** **98**

**6.1. Aims and objectives** **99**

**6.2. Introduction** **99**

**6.3. Intracellular kinase target engagement assay** **100**

6.3.1. SRPKBNP tracer optimisation 101

6.3.2. SRPK1 assays 103

6.4. Downstream target levels in response to ET1126 inhibitor treatment 107

**6.5. Downstream target levels in response to ET1132 inhibitor treatment 113**

6.6. Downstream target levels in response to ET3002 treatment 120

**6.7. Discussion 129**

6.7.1. Intracellular target engagement assay 130

**6.7.2. Downstream targets after ET1126 inhibitor treatment 130**

**6.7.3. Downstream target levels after ET1132 treatment 131**

**6.7.4. Downstream target levels after ET3002 inhibitor treatment 133**

***7. Chapter 135***

7.1. Aims and objectives 136

7.2. Introduction 136

7.3. Griffin 51 treatment on AML cell lines 137

7.4. CLK1 intracellular TE assays 137

7.4.1. Cell viability assays after Griffin 51 treatment 141

**7.5. Downstream targets after Griffin 51 treatment in AML cell lines 143**

7.6. IC50 values of different AML cells after SPHINX-31 and Griffin 51 treatment 150

**7.7. BRD4 splice change after Griffin 51 treatment in AML cell lines 152**

**7.8. $IC_{50}$ data for BRD4 splice change in AML cells 159**

**7.9. Discussion and conclusion 161**

**7.9.1. Intracellular target engagement assay 162**

**7.9.2. Cell viability assays 163**

**7.9.3. BRD4 splice change in response to Griffin 51 treatment 163**

**7.9.4. Downstream target levels after inhibitor treatments 164**

**7.10. Concluding remarks 166**

***8. Chapter 167***

***The effect of SRPK1 and CLK1 inhibition in primary AML cells 167***

***8.1. Inhibitor treatment on AML primary samples 168***

**8.2. SRPK1 inhibition in AML primary cells 168**

**8.3. CLK1 inhibition in primary AML cells 173**

**8.4. BRD4 isoform change in AML clinical samples 176**

8.4.1. Colony forming units 182

8.4.2. CFU assay images- MLL-WT 184

8.4.3. CFU images- MLL-TL 186

**8.5. Discussion and Conclusion 187**

**8.5.1. SRPK1 and CLK1 inhibition in primary AML cells 187**

8.5.2. BRD4 splice change in AML clinical samples 187

**8.6. Colony forming units (CFU) 189**

***9. Chapter 190***

**9.1. Aims and Objectives 191**

**9.2. Introduction 191**

**9.3. Downstream targets after SPHINX-31 and Griffin 51 treatment in U87 cells 193**

**9.4. The role of the BBB in Glioblastoma therapy 195**

**9.5. Serum free cell media 197**

9.6. Cytokine treatment on primary astrocytes 198

9.7. Spheroid cultures 204

**9.8. Discussion and conclusions 210**

***10. Chapter 211***

***Conclusion and future work 211***

***Conclusion 212***

**10.1. SRPK1 inhibition in AML 213**

10.2. BRD4 splice change in AML 214

10.3. New generation SRPK1 inhibitors 214

**10.4. CLK1 inhibition in AML 215**

10.5. SRPK1 and CLK1 inhibition in astrocyte derived cancer models 216

10.6. Future Work 216

***11. REFERENCES 218***

***12. APPENDIX I. 234***

**12.1. RT-PCR results of BRD4 splice change in response to inhibitor treatment 234**

12.2. Full size gel images with BRD4 splice change 240

12.3. Primer sequences for PCR 248

**12.4. Protocols 249**

**12.4.1. QIAamp RNA Blood Mini Kit 249**

**12.4.2. CLK1-NanoLuc fusion vector sequence 250**

# LIST OF TABLES

Table 1.1 AML Classification .....9

Table 1.2 The French-American-British system of defining AML subtypes...16

Table 1.3 Prognosis based on genetic abnormalities in AML .....17

Table 3.1 Genetic data of AML samples with translocation and MLL-fused oncogenes. .....62

Table 3.2 PCR reagents per reaction .....67

Table 3.3 Detailed description of the thermocycling steps for PCR .....68

# LIST OF FIGURES

Figure 1.1. Schematic representation of haematopoiesis .....1

Figure 1.2. AML prevalence and mortality rate according to Cancer Research UK's data, arranged in age groups.....10

Figure 1.3. Constitutive and alternative splicing .....19

Figure 1.4. Spliceosome assembly.....21

Figure 1.5. SR protein family and their synonyms.....28

Figure 1.6. The chemical structure of SRPIN 340 .....36

Figure 1.7. Chemical structure of SPHINX-31.....37

Figure 1.8. Chemical structures of new generation inhibitors.....38

Figure 1.9. Chemical structures of different CLK1 inhibitors .....40

Figure 1.10. Chemical structure of Griffin 51.....41

Figure 4.1. Downstream target levels in THP-1 cells after SPHINX-31 treatment .....76

Figure 4.2. Downstream target levels in OCI-AML2 cells after SPHINX-31 treatment .....77

Figure 4.3. Downstream target levels in MOLM-13 cells after SPHINX-31 treatment .....78

Figure 4.4. Downstream target levels in OCI-AML3 cells after SPHINX-31 treatment .....79

Figure 4.5. Downstream target levels in HL60 cells after SPHINX-31 treatment .....80

Figure 4.6. Downstream target levels in TF1a cells after SPHINX-31 treatment .....81

Figure 4.7. Cell viability levels in AML cell lines after SPHINX -31 treatment .....83

Figure 5.1. BRD4 splice change in MOLM-13 cells after SPHINX31 treatment .....90

Figure 5.2. BRD4 splice change in THP-1 cells after SPHINX31 treatment..91

Figure 5.3. BRD4 splice change in OCI-AML2 cells after SPHINX31 treatment .....92

Figure 5.4. BRD4 splice change in TF1a cells after SPHINX31 treatment ...93

Figure 5.5. BRD4 splice change in HL60 cells after SPHINX31 treatment ...94

Figure 5.6. BRD4 splice change in OCI-AML3 cells after SPHINX31 treatment .....95

Figure 5.7. IC50 values for SPHINX31 in MLL-WT and MLL-translocated cell lines for BRD4 splicing. .....96

Figure 6.1. Ilustration of the NanoBRET TE cell assay. .....102

Figure 6.2 Optimisation data for the newly developed SRPKBNP tracer for SRPK1.....103

Figure 6.3. SRPK1 inhibition after Sphinx-31 treatment measured via the NanoBRET Target Engagement assay. .....104

Figure 6.4. SRPK1 inhibition after ET1126 and ET1132 treatment measured via the NanoBRET Target Engagement assay. .....104

Figure 6.5. SRPK1 inhibition after ET1126 treatment measured via the NanoBRET Target Engagement assay. .....105

Figure 6.6. SRPK1 inhibition after ET1132 treatment measured via the NanoBRET Target Engagement assay .....106

Figure 6.7. Downstream target levels in THP-1 cells after ET1126 treatment. .....108

Figure 6.8. Downstream target levels in MOLM-13 cells after ET1126 treatment. .....109

Figure 6.9. Downstream target levels in OCI-AML2 cells after ET1126 treatment. .....110

Figure 6.10. Downstream target levels in OCI-AML3 cells after ET1126 treatment. .....111

Figure 6.11. Downstream target levels in TF1a cells after ET1126 treatment. .....112

Figure 6.12. Downstream target levels in HL60 cells after ET1126 treatment. .....113

Figure 6.13. Downstream target levels in THP-1 cells after ET1132 treatment. .....114

Figure 6.14. Downstream target levels in MOLM-13 cells after ET1132 treatment. .....115

Figure 6.15. Downstream target levels in OCI-AML2 cells after ET1132 treatment. .....116

Figure 6.16 Downstream target levels in OCI-AML3 cells after ET1132 treatment. .....117

Figure 6.17. Downstream target levels in TF1a cells after ET1132 treatment. .....118

Figure 6.18. Downstream target levels in HL60 cells after ET1132 treatment. .....119

Figure 6.19. Downstream target levels in THP-1 cells after ET3002 treatment. .....121

Figure 6.20. Downstream target levels in MOLM-13 cells after ET3002 treatment. .....122

Figure 6.21. Downstream target levels in OCI-AML2 cells after ET3002 treatment. .....123

Figure 6.22. Downstream target levels in OCI-AML3 cells after ET3002 treatment. .....124

Figure 6.23. Downstream target levels in TF1a cells after ET3002 treatment. .....125

Figure 6.24. Downstream target levels in HL60 cells after ET3002 treatment. .....126

Figure 6.25. $EC_{50}$ data of ET1126, ET1132 and ET3002 compared to SPHINX-31on MYC expression levels .....127

Figure 6.26. $EC_{50}$ data of ET1126, ET1132 and ET3002 compared to SPHINX-31on HOXA9 expression levels ..... 128

Figure 6.27. $EC_{50}$ data of ET1126, ET1132 and ET3002 compared to SPHINX-31on BCL-2 expression levels ..... 129

Figure 7.1. CLK1 inhibition after Griffin 51 treatment measured via the NanoBRET Target Engagement assay ..... 138

Figure 7.2. CLK1 inhibition after ET1055 treatment measured via the NanoBRET Target Engagement assay ..... 139

Figure 7.3. CLK1 inhibition after Thiii27 treatment measured via the NanoBRET Target Engagement assay ..... 139

Figure 7.4. CLK1 inhibition after ET1008 treatment measured via the NanoBRET Target Engagement assay ..... 140

Figure 7.5. AML Cell viability levels after Griffin 51 treatment ..... 142

Figure 7.6. Downstream target levels in THP-1 cells after Griffin 51 treatment. ..... 144

Figure 7.7. Downstream target levels in OCI-AML2 cells after Griffin 51 treatment. ..... 145

Figure 7.8. Downstream target levels in MOLM-13 cells after Griffin 51 treatment ..... 146

Figure 7.9. Downstream target levels in OCI-AML3 cells after Griffin 51 treatment ..... 147

Figure 7.10. Downstream target levels in HL60 cells after Griffin 51 treatment ..... 148

Figure 7.11. Downstream target levels in TF1a cells after Griffin 51 treatment .....149

Figure 7.12. Comparison of IC50 values of MYC levels in AML cells .....150

Figure 7.13. Comparison of IC50 values of HOXA9 levels in AML cells .....151

Figure 7.14. Comparison of IC50 values of BCL2 levels in AML cells .....151

Figure 7.15. BRD4 splice change in MOLM-13 cells after Griffin 51 treatment .....153

Figure 7.16. BRD4 splice change in OCI-AML2 cells after Griffin 51 treatment .....154

Figure 7.17. BRD4 splice change in THP-1 cells after Griffin 51 treatment 155

Figure 7.18. BRD4 splice change in TF1a cells after Griffin 51 treatment ..156

Figure 7.19. BRD4 splice change in HL60 cells after Griffin 51 treatment ..157

Figure 7.20. BRD4 splice change in OCI-AML3 cells after Griffin 51 treatment .....158

Figure 7.21. IC50 data for BRD4 splice change in AML cells .....160

Figure 9.1. Cell viability of U87 cells after Griffin 51 and SPHINX-31 treatment .....192

Figure 9.2. BCL2, HOXA9 and MYC levels in U87 cells. .....194

Figure 9.3. The neurovascular unit and the Blood Brain Barrier .....196

Figure 9.4. Primary glia cells in serum free media .....198

Figure 9.5. Astrocytes after 6 hours in the no treatment group. .....199

Figure 9.6 Primary cortical astrocytes after 6 hours of 50ng/mL IL-1b treatment .....199

Figure 9.7 Primary cortical astrocytes after 6 hours of 25ng/mL IL-1b treatment .....200

Figure 9.8 Primary cortical astrocytes after 6 hours of 25ng/mL IL-1b and 20ng/mL TNF-α treatment.....201

Figure 9.9 Primary cortical astrocytes after 6 hours 20ng/mL TNF-α treatment .....202

Figure 9.10 Primary cortical astrocytes after 6 hours 100ng/mL TNF-α treatment .....202

Figure 9.11. Primary astrocytes in a 3D spheroid culture.....204

Figure 9.12. Primary astrocytes in a 3D spheroid culture.....205

Figure 9.13. Primary brain endothelial cells (BECS) in a 3D spheroid model.....206

Figure 9.14. Primary pericytes in a 3D spheroid model.....207

Figure 9.15. Co-culture of primary astrocytes, endothelial cells and pericytes. .....208

Figure 9.16 Co-culture of primary astrocytes, brain endothelial cells and pericytes in a 3D spheroid. .....209

# ABBREVIATIONS

aCMML – Atypical chronic myelomonocytic leukaemia

ACP – Anaplastic lymphoma

AD – Accessory domain

ALL – Acute lymphoblastic leukaemia

ALP – Anaplastic lymphoma proteins

AMD – Acute macular degeneration

AML – Acute myeloid leukaemia

AMMoL – Acute myelomonocytic leukemia

ANOVA – Analysis of variance

APL – Acute Promyelocytic Leukemia

asTF – Alternatively spliced tissue factor

ATRA – All-trans retinoic acid

BBB – Blood brain barrier

BECs – Brain endothelial cells

bFGF – Basic fibroblast growth factor

BPS – Branch point sequence

BRCA1 – Breast cancer gene 1

BRD4 – Bromodomain-containing protein 4

BRET – Bioluminescence resonance energy transfer

BSA – Bovine serum albumin

CBF – Core binding factor

cDNA – Complementary DNA (deoxyribonuclease nucleic acid)

CEBPA – CCAAT enhancer-binding protein alpha.

CESC – cervical squamous cell carcinoma

CFU – Colony forming unit

CLK1 – Cyclin- dependent like kinase 1

CLL – Chronic lymphocytic leukaemia

CML – Chronic lymphocytic leukaemia

CMML – Chronic myelomonocytic leukaemia

CMML – Chronic myelomonocytic leukaemia

CNL – Chronic neutrophilic leukaemia

CNS – Central Nervous System

CT – Cycle Threshold

DAPI – 4′,6-diamidino-2-phenylindole

ddPCR – Digital droplet PCR

DMEM – Dulbecco’s modified eagle medium

DMSO – Dimethyl sulphoxide

DNA – Deoxyribonucleic acid

DNMT3A – DNA methyltransferase 3 alpha

dNTP – Deoxyribonucleotide triphosphate

EDTA – Ethylenediaminetetraacetic acid

ET – Essential thrombocythemia

ETV6 – ETS Variant Transcription Factor 6

EVI1 – ecotropic viral integration site 1

FAB – French-American-British (system)

FBS – Foetal Bovine Serum

FGF – Fibroblast Growth Factor

FGFR1 – Fibroblast growth factor receptor 1

FLT3 – FMS like tyrosine kinase 3

flTF – full length tissue factor

GBM – Glioblastoma

GEO – Gene Expression Omnibus

GFAP – glial fibrillary acidic protein

GRB7 – growth factor receptor bound protein 7

HBSS – Hank's balanced salt solution

HEPES – 4-(2-hydroxyethyl)-1-piperazineethanesulfonic acid

hnRNP – Heterogeneous nuclear ribonucleoproteins

HPRT-1 – hypoxanthine phosphoribosyltransferase 1

IAMp21 – Intrachromosomal amplification of chromosome 21

ICC – Immunocytochemistry

IDH1 – isocitrate dehydrogenase 1

IF – Intermediate filament

IL1$\alpha$ – Interleukin-1 alpha

JAK – Janus kinase

JMML – Juvenile myelomonocytic leukaemia

KO – Knock out

MAPK – mitogen-activated protein kinase

MAPK – Mitogen-activated protein kinases

MCL – Mantle cell lymphoma

MDS/MPN – Myelodysplastic/myeloproliferative neoplasms

MLLT3-KMTZA – mixed-lineage leukemia, translocated to, 3 lysine methyltransferase 2A

MPAL – Mixed phenotype acute leukaemia

MPN – myeloproliferative neoplasms

mRNA – messenger RNA

mRNA – Messenger RNA

NFkB – Nuclear Factor Kappa B

NK – Natural killer (cells)

NO – Nitric oxide

NOS – Nitric oxide synthase

NPM1 – Nucleophosmin 1

PBS – Phosphate buffered saline

PCM1-JAK2 – Pericentriolar material 1 Janus Kinase 2

PCR – Polymerase Chain Reaction

PCV – Polycythaemia rubra vera

PDFG-$\beta$ – Platelet-derived growth factor

PDGFR-$\alpha$ – platelet-derived growth factor receptor alpha

PDX – Patient derived xenograft

PMF – Primary myelofibrosis

PML-RARA – promyelocytic leukemia/retinoic acid receptor alpha

PTEN –Phosphatase and tensin homolog

PV – Polycythaemia vera

qPCR – Quantitative Polymerase Chain Reaction

RNA – Ribonucleic acid

ROS – Reactive oxygen species

RRM – RNA Recognition motif

RRM – RNA recognition motif

RS – Arginine serine

RT – Reverse Transcription

RT – room temperature

RUNX-1 – Runt-related transcription factor 1

siRNA – small interfering RNA

SMCs – Smooth muscle cells

snRNA – Small nuclear RNA

snRNP – small nuclear ribonucleoproteins

SRPK1 – Serine arginine protein kinase 1

SRSF1 – Serine arginine rich splicing factor 1

TAM – Transient abnormal myelopoiesis

TAM – Transient Abnormal Myelopoiesis

TIMP-1 – TIMP Metallopeptidase Inhibitor 1

TNF-a – Tumour Necrosis Factor alpha

TP53 – Tumour protein P53

VEGF – Vascular Endothelial Growth Factor

WHO – World Health Organization

# 1. Chapter Introduction

## 1.1. Haematopoiesis

Haematopiesis is the life-long formation of blood cells. The two main cell types in blood are erythrocytes (red blood cells) and leukocytes (white blood cells) along with small fragments and platelets. Haemocytoblasts or blood stem cells become progenitor cells and later on differentiate to megakaryocytic, erythroid, monocytic, granulocytic, eosinophilic or lymphoid lineages. Haemocytoblasts are created and stored in the bone marrow which than they leave once differentiated. See Fig. 1.1 below.

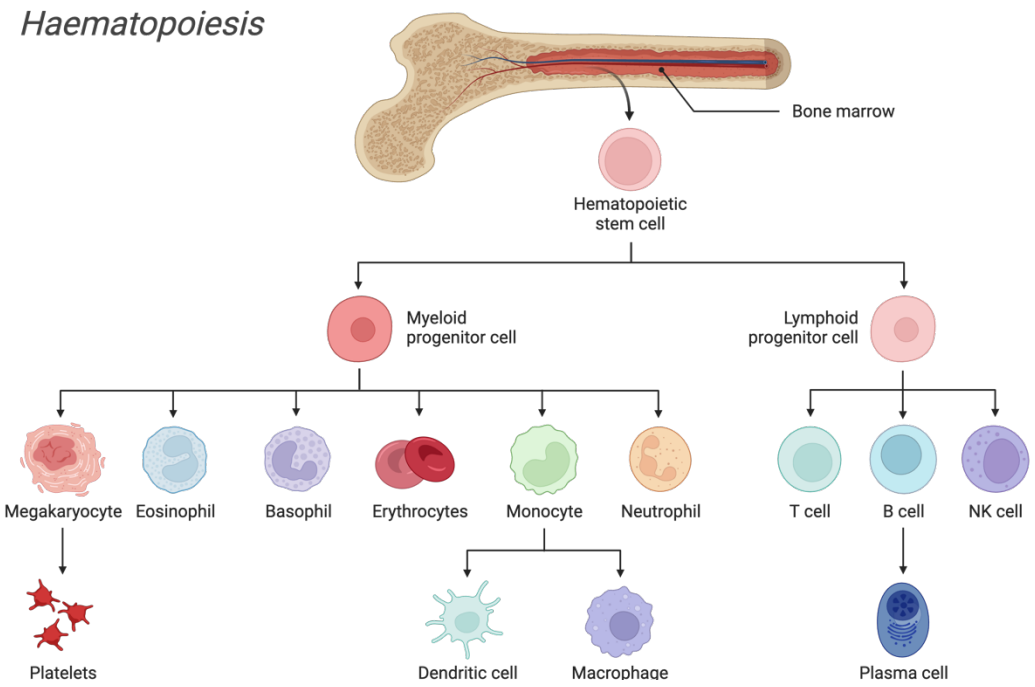



***Figure 1.1. Schematic representation of haematopoiesis***

***The figure shows the maturation process of haematopoietic stem cells to myeloid progenitor or lymphoid progenitor cells. These cells then mature further into the different types of blood cells that are circulating in the blood stream. Image created by BioRender Premium, based on (Lai and Kondo, 2008).***

Haematopoiesis is mediated by cytokines, transcription factors and interleukins. When haematopoietic stem cells undergo their maturation process, they develop into myeloid-lineage cells or lymphoid lineage cells. From then on, they continue their development into their final cell type. Genetic errors in this tightly controlled process are rare, but can result in mutation or deletion which can give rise to cancerous cells (Lee and Hong, 2020). Cancers, such as acute myeloid leukaemia (AML), can be caused by mutations or translocations in the genome. Germ line mutations of RUNX1(runt-related transcription factor 1) gene can result in AML, and other malignant haematology diseases due to haploinsufficiency (Owen *et al.*, 2008).

## 1.2. Leukaemia

Leukaemia stems from the multiplication of haematopoietic stem cells with abnormal clones that become immune to regulatory, differentiation or apoptotic signals (Hanahan and Weinberg, 2000). These cells also multiply to the detriment of healthy haematopoietic stem cells and infiltrate different organs, especially lymph nodes. The most common clinical symptoms are related to bone marrow failure. Patients with suspected leukaemia present at clinic with abnormal bleeding, spontaneous bruising, recurrent infections or severe anaemia (Grigoropoulos *et al.*, 2013). Leukaemia usually has a poor prognosis, and despite recent advancement in the field, many patients will relapse with fatal consequences. According to Public Health England, over

250,000 people were diagnosed with cancer every year, between 2010-2015, from which 130,000 died as a result of the disease. The NHS costs for cancer services were around £5 billion per year, the total cost, including the loss of productivity is estimated to be £18.3 billion (Policy Paper, Public Health England).

## 1.3. Leukaemia classification

The classification of leukaemia is provided by the stage of leukocyte differentiation and cell type. Leukemic cells can come from T-cell or B-cell pre-cursor cells. Depending on the status of the disease leukaemia also divided into acute and chronic subtypes. Acute myeloid leukaemia is characterised by proliferating immature white blood cells in the blast phase, whereas chronic leukaemia is described by the proliferation of mature white blood cells (Grigoropoulos *et al.*, 2013).

The latest revision from the WHO (World Health Organization) on the classification of acute leukaemia and myeloid neoplasms was published in 2016 (Arber *et al.*, 2016). New categories were created, and existing ones modified based on prognostic data, new knowledge on genetic mutations, immunophenotyping and morphology observations. However, the main categories remain the same, acute vs. chronic leukaemia. Within the acute category, they recognise acute lymphoblastic leukaemia (ALL), and acute myeloid leukaemia (AML). Within the chronic category, there is chronic lymphocytic leukaemia (CLL) and chronic myeloid leukaemia (CML). For

further details, see Table 1.1 below. More than half of AML patients (50-60%) will have a non-random chromosomal translocation, which will carry a prognostic factor. Translocation between the chromosomes 8 and 21, translocation or inversion of the chromosome 16, translocation between chromosomes 15 and 17 are generally considered to be favourable abnormalities. Whereas deletion of part of chromosome 5 or 7, translocation or inversion of chromosome 3, translocation between chromosome 6 and 9, translocation between chromosome 9 and 22, etc. are all unfavourable abnormalities. Certain gene mutations also confer poor prognosis. For instance, FLT3 (Fms-like tyrosine kinase 3) mutations occur in approximately 30% of AML patients (the percentage increases with age) and predicts a poor outcome. DNMT3A mutations usually appear in combination with FLT3, NPM1 or IDH1 mutations and are associated with significantly shorter survival (Kumar, 2011).

**Myeloproliferative neoplasms (MPN)**

- Chronic myeloid leukaemia (CML), BCR-ABL11
- Chronic neutrophilic leukaemia (CNL)
- Polycythemia vera (PV)
- Primary myelofibrosis (PMF) PMF, prefibrotic/early stage PMF, overt fibrotic stage Essential thrombocythemia (ET)
- Chronic eosinophilic leukaemia, not otherwise specified
- MPN, unclassifiable
- Mastocytosis

**Myeloid/lymphoid neoplasms with eosinophilia and rearrangement of PDGFRA, PDGFRB, or FGFR1, or with PCM1-JAK2**

- Myeloid/lymphoid neoplasms with PDGFRA rearrangement
- Myeloid/lymphoid neoplasms with PDGFRB rearrangement
- Myeloid/lymphoid neoplasms with FGFR1 rearrangement
- Provisional entity: Myeloid/lymphoid neoplasms with PCM1-JAK2

**Myelodysplastic/myeloproliferative neoplasms (MDS/MPN)**

- Chronic myelomonocytic leukaemia (CMML)
- Atypical chronic myeloid leukaemia (aCML), BCR-ABL12
- Juvenile myelomonocytic leukaemia (JMML)
- MDS/MPN with ring sideroblasts and thrombocytosis (MDS/MPN-RS-T) MDS/MPN, unclassifiable

**Myelodysplastic syndromes (MDS)**

- MDS with single lineage dysplasia
- MDS with ring sideroblasts (MDS-RS)
    - MDS-RS and single lineage dysplasia
    - MDS-RS and multilineage dysplasia
- MDS with multilineage dysplasia
- MDS with excess blasts MDS with isolated del(5q)
- MDS, unclassifiable
- Provisional entity: Refractory cytopenia of childhood
- Myeloid neoplasms with germ line predisposition

**Acute myeloid leukemia (AML) and related neoplasms**

- AML with recurrent genetic abnormalities
    - AML with t(8;21)(q22;q22.1);RUNX1-RUNX1T1
    - AML with inv(16)(p13.1q22) or t(16;16)(p13.1;q22);CBFB-MYH11
    - APL with PML-RARA
    - AML with t(9;11)(p21.3;q23.3);MLLT3-KMT2A
    - AML with t(6;9)(p23;q34.1);DEK-NUP214
    - AML with inv(3)(q21.3q26.2) or t(3;3)(q21.3;q26.2); GATA2, MECOM
    - AML (megakaryoblastic) with t(1;22)(p13.3;q13.3);RBM15-MKL1
    - Provisional entity: AML with BCR-ABL1
    - AML with mutated NPM1
    - AML with biallelic mutations of CEBPA

- Provisional entity: AML with mutated RUNX1

- AML with myelodysplasia-related changes
- Therapy-related myeloid neoplasms
- AML, NOS
  - AML with minimal differentiation
  - AML without maturation
  - AML with maturation
  - Acute myelomonocytic leukemia
  - Acute monoblastic/monocytic leukemia
  - Pure erythroid leukemia
  - Acute megakaryoblastic leukemia
  - Acute basophilic leukaemia Acute panmyelosis with myelofibrosis
- Myeloid sarcoma
- Myeloid proliferations related to Down syndrome
  - Transient abnormal myelopoiesis (TAM)
  - Myeloid leukemia associated with Down syndrome

**Blastic plasmacytoid dendritic cell neoplasm**

**Acute leukaemias of ambiguous lineage**

- Acute undifferentiated leukaemia
- Mixed phenotype acute leukaemia (MPAL) with t(9;22)(q34.1;q11.2); BCR-ABL1 MPAL with t(v;11q23.3); KMT2A rearranged
- MPAL, B/myeloid, NOS

- MPAL, T/myeloid, NOS

**B-lymphoblastic leukaemia/lymphoma**

- B-lymphoblastic leukaemia/lymphoma, NOS
- B-lymphoblastic leukaemia/lymphoma with recurrent genetic abnormalities
- B-lymphoblastic leukaemia/lymphoma with t(9;22)(q34.1;q11.2);BCR-ABL1
- B-lymphoblastic leukaemia/lymphoma with t(v;11q23.3);KMT2A rearranged
- B-lymphoblastic leukaemia/lymphoma with t(12;21)(p13.2;q22.1); ETV6-RUNX1 B-lymphoblastic leukaemia/lymphoma with hyperdiploidy
- B-lymphoblastic leukaemia/lymphoma with hypodiploidy
- B-lymphoblastic leukaemia/lymphoma with t(5;14)(q31.1;q32.3) IL3-IGH
- B-lymphoblastic leukaemia/lymphoma with t(1;19)(q23;p13.3);TCF3-PBX1
- Provisional entity: B-lymphoblastic leukaemia/lymphoma, BCR-ABL1–like
- Provisional entity: B-lymphoblastic leukaemia/lymphoma with iAMP21

**T-lymphoblastic leukaemia/lymphoma**

- Provisional entity: Early T-cell precursor lymphoblastic leukaemia

| |
|---|
| • Provisional entity: Natural killer (NK) cell lymphoblastic leukaemia/lymphoma |

***Table 1.1. AML Classification***

***A list of different type of leukaemias based on the cell of origin and genetic mutations. The list is not comprehensive as the variety of different genetic mutations make it impossible to have a consistently accurate list. Table adapted from Arber et al. 2016.***

## 1.4. Acute Myeloid Leukaemia

Acute myeloid leukaemia (AML) is a heterogeneous disease of immature blood cells. It is characterised by uncontrolled growth and clonal expansion of blast cells which then causes haematopoietic insufficiency and, in most cases, leucocytosis. Genetic mutations in AML can be a prognostic tool for severity and relapse. Van Delft *et al.* found that in ALL with the ETV6-RUNX-1 (TEL-AML1) fusion there is an overall good prognosis, but relapses (type 1-3) almost always occur, often many years later (median range 6.1 years, relapse rate 66.67%) (van Delft *et al.*, 2011). Mutations are found in neonatal blood samples, meaning that they occur prenatally but does not necessary mean that a disease will develop later on (Iwakiri *et al.*, 2002).

According to Cancer Research UK's data, there are around 3,100 new cases of acute myeloid leukaemia in the UK every year. It accounts for less than 1% of all cancer diagnoses (2016-2018) and in 2018 AML accounted for 2% of all deaths caused by cancer. It is most prevalent in people aged from 85 to 89 (National Cancer Registration and Analysis Service, 2021).

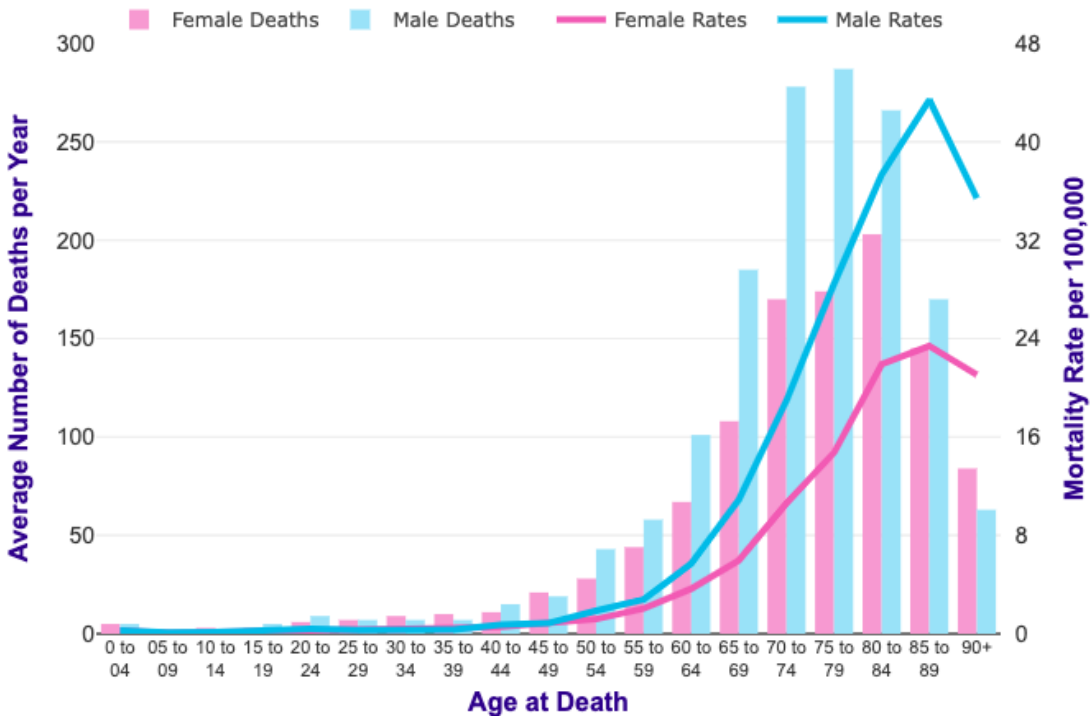



***Figure 1.2. AML prevalence and mortality rate according to Cancer Research UK's data, arranged in age groups.***

***Average number of deaths per year from AML, adjusted to age groups and mortality rate in females (pink) and males (blue) in the UK based on data collected between 2016-2018. Age groups are separated in different columns. Credit: Cancer Research UK.***

## 1.5. Risk factors and pathogenesis

As with many other cancers, the origin of all types of leukaemia is poorly understood. According to CRUK's data, age is a deciding factor, meaning that from the age of 50 it presents in increasing numbers, but the most prevalent age group is 85-89. Lifestyle factors such as smoking, and obesity also increases the chance of developing AML, as well as exposure to benzene (which has since been banned). In their study, (Lan *et al.*, 2004) showed that even low exposure to benzene causes severe effects on progenitor cells and significantly lower white blood cell and platelet counts. Patients who had chemotherapy or were diagnosed with Hodgkin lymphoma or breast cancer previously and were treated with drugs such as chlorambucil, melphalan or cyclophosphamide also have a slightly higher chance of developing AML. Natelson and Pyatt (2010) found that temozolomide, that is used for the treatment of malignant gliomas can develop therapy induced myelodysplasia which may potentially lead to AML (Natelson and Pyatt, 2010). Genetic pre-disposition such as Fanconi anaemia or children with Down's syndrome have a higher chance of developing AML. The presence of blood disorders can also have an adverse effect; myelodysplastic syndrome and myeloproliferative disorders such as Polycythaemia rubra vera (PCV) carry a higher chance of AML comorbidity. Autoimmune diseases such as rheumatoid arthritis, autoimmune haemolytic anaemia and ulcerative colitis also carry a higher risk of developing AML (Laribi *et al.*, 2021).

## 1.6. Therapy and management

In the UK, the NHS currently offers chemotherapy in the induction phase of the treatment, usually Cytarabine (Ara C) and or radiotherapy (National Institute for Health and Care Excellence [NICE], 2022). However, bone marrow or stem cell transplant might also be an option if there is a match for the patient (NICE, 2022 TA787).

The overall survival window of AML is usually approximately 13 months post diagnosis. Apart from Cytarabine other drugs that are also prescribed, such as tipifarnib (farnesyltransferase inhibitor), gemtuzumab, ozogamicin have shown improvements but not increased life expectancy. Patients with high-risk myelodysplastic syndrome showed good response to clofarabine, which is a purine nucleoside antimetabolite agent (Estey *et al.*, 2018).

In their meta-analysis (Medeiros *et al.*, 2015) found that in the USA more than half of newly diagnosed AML patients are over 65 years old, meaning that their treatment is complicated as comorbidities are often present. Among these patients who are enrolled either in Medicare part A or B only 40% received chemotherapy within 3 months of diagnosis. They are more likely to be young, male and without comorbidities. In the older age group, 60% of patients remained untreated, although chemotherapy with suitable drug treatment proved to be a significant factor in overall survival rate. In their study, Konopleva *et al.* (2021) found that combining an FDA approved drug, venetoclax with FLT3 inhibitors, MCL-1 inhibitors or TP53 activators is more effective than just the venetoclax on its own (Konopleva, 2021). Second

generation proteasome inhibitors such bortezomib and carfilzomib for the treatment of multiple myeloma and mantle cell lymphoma were also considered for combination treatment. In light of these findings, many pre-clinical studies started looking at these combined treatment regimens, which showed that proteasome inhibition disrupts proliferative cell signalling pathways and induces autophagy (Csizmar *et al.*, 2016). O'Connor *et al.* (2005) combined bortezomib to determine the anti-tumour activity of the novel proteasome inhibitors in patients with indolent and mantle-cell lymphoma (MCL). Patients in this phase II clinical trial were treated at a dose of 1.5 $mg/m^2$ twice weekly for 2 weeks (days 1, 4, 8, and 11) followed by a 1-week rest period. With a 58% response rate, this study showed a significant activity of bortezomib in patients with indolent non-Hodgkin's lymphoma, especially patients with follicular lymphoma, marginal zone lymphoma, and MCL. They have noted some side effect to bortezomib, such as toxicity, even after a 2-week tolerance period (O'Connor *et al.*, 2005). In recent years (2017-2019) the FDA has approved 8 new drugs for the treatment of AML. It is based on the most common genetic lesions in AML such as the mutant FMS-like tyrosine kinase 3 (FLT3) and isocitrate dehydrogenase 1 and 2 (IDH1 and IDH2), which improved response to therapy. Venetoclax, combined with either decitabine or cytarabine achieved a 54% remission in elderly population in a phase II trial (Wei *et al.*, 2019). Other typical genetic mutations are the t(8;21) and inv(16)/t(16;16), which lead to the balanced translocations *RUNX1–RUNXT1* and *CBFB–MYH11* or inv(16)/t(16;16), t(8;21), t(15;17), inv(3)/t(3:3), t(6;9), and *KMT2A* translocations are the indicators for either an *NPM1* mutation, biallelic *CEBPA* mutations, or recurrent gene fusions (Short

*et al.*, 2020). Daunorubicin is another FDA approved and widely used clinical drug for the treatment of AML, it causes cell arrest and can reverse AML cell development in the bone marrow (Murphy and Yee, 2017).

## 1.7. Chromosomal abnormalities in AML

Interestingly, in some cases of AML, no chromosomal aberration can be detected. In recent studies more and more attention has been paid to genetic mutations within AML with the idea that specific mutations can be treated better with target specific treatment. Core-binding factor (CBF) AML with t(8;21) (q22;q22) and AML with inv(16)(p13q22) or t(8;21)(p13;q22) which then develops RUNX1-RUNX1T1 and CBFB-MYH11 fusion genes significantly affects the clinical management of these patients. This is critically important as 25% of paediatric AML and 15% of de novo adult cases of AML carry these mutations. In 2016 the WHO revised the categories for AML to include genetic and morphology information, immunophenotype and clinical presentation.

## 1.8. The FAB system and clinical diagnosis

AML was initially divided into categories based on the French-American-British (FAB) system that used morphology as a baseline (Kuykendall *et al.*, 2018). The FAB system recognises seven different subtypes of AML (Rose *et*

*al.*, 2017) See Table 1.2 below. The diagnosis of AML is based on examinations of peripheral blood and bone marrow samples. Diagnosis can be established if myeloblasts constitutes more then 30% of the bone marrow or circulating white blood cells, neoplastic promyelocytes, monoblasts and promocytes and megakaryoblasts are also counted in. To differentiate between Acute Myeloid Leukaemia and Acute Lymphoblastic Leukaemia, monoclonal antibodies are used against CD11b, CD13, CD14 and CD33 to determine myeloid differentiation (Barnard *et al.*, 1996).

| *Subtype* | *Description* |
|---|---|
| **M0** | Minimally differentiated acute myeloid leukaemia (AML) |
| **M1** | AML without maturation |
| **M2** | AML with maturation |
| **M4** | Acute myelomonocytic leukaemia (AMMoL) |
| **M4Eo** | AMMoL with eosinophils |
| **M5a** | Acute monoblastic leukaemia |
| **M5b** | Acute monocytic leukaemia |
| **M6** | Acute erythroleukaemia |
| **M7** | Acute megakaryoblastic leukaemia |
| | Acute leukaemia of ambiguous lineage |

***Table 1.2. The French-American-British system of defining AML subtypes***

***The most recent version of the FAB system, one of the most used classification guide of different AML types, published in (Rose et al., 2017).***

In 2017 following the WHO update, the European Leukaemic Network also published an updated classification system with prognostic factors which recognises three categories based on genetic abnormalities and predicted outcomes (Dohner *et al.*, 2017).

| Prognosis | Genetic abnormalities |
|---|---|
| Favourable | • t(8;21)(q22;q22.1);RUNX1-RUNX1T1<br>• Inv(16)(p13.1q22) or t(16;16)(p13.1;q22); CBFB-MYH11<br>• Mutated NMP1 without FLT3-ITD or with FLT3-ITDlow (allelic ratio<0.5);<br>• Biallelic mutated CEBPA |
| Intermediate | • Mutated NPM1 and FLT3-ITDhigh (allelic ratio ≥0.5)<br>• Wild-type NPM1 without FLT3-ITD or with FLT3-ITDlow (without<br>• adverse-risk genetic lesions) t(9;11)(p21.3;q23.3); MLLT3-KMT2A<br>• Cytogenetic abnormalities not classified as favourable or adverse |
| Adverse | • t(6;9)(p23;q34.1); DEK-NUP214 t(v;11q23.3);<br>• KMT2A rearranged t(9;22)(q34.1;q11.2);<br>• BCR-ABL1 inv(3)(q21.3q26.2) or t(3;3)(q21.3;q26.2); GATA2, MECOM<br>• (EVI1) -5 or del(5q); -7; -17/abn(17p)<br>• Complex karyotype (three or more unrelated chromosome abnormalities),<br>• Monosomal karyotype (defined by the presence of 1 single monosomy)<br>• Wild-type NPM1 and FLT3-ITDhigh<br>• Mutated RUNX1<br>• Mutated ASXL1<br>• Mutated TP53 |

***Table 1.3. Prognosis based on genetic abnormalities in AML***

***The European Leukaemic Network's (ELN) classification system of AML. In terms of prognosis and severity AML is categorised in three different groups: favourable, intermediate and adverse. This table sums up the likely prognosis for all AML with different types of genetic abnormalities. Credit: ELN, 2017.***

## 1.9. Constitutive and alternative splicing

The maturation of RNA is achieved by a co-transcriptional modification process of RNA splicing. In constitutive splicing, as it is shown in Fig 1.9 introns are cut out and exons joined together (Ding and Elowitz, 2019). Alternative splicing is a selective process where introns are removed or retained in the co-transcriptional pre-mRNA processing that can result in many mRNAs from a single gene, and therefore can produce several proteins (Zhou *et al.*, 2017a). Close coupling in constitutive splicing with transcription is a signal processing filter that regulates the volume of mRNA. Constitutive splicing might provide other functions such as intron enhanced transcriptional efficacy, increased intronic miRNA retention and other constitutively spliced introns, which in turn can promote evolutionary selection of new phenotypes (Rearick *et al.*, 2011). In their study, Fox-Walsh *et al.* (2015) found that the size of introns can decide if an exon is constitutively or alternatively spliced. When the intron size is between 200 and 250 nucleotides, the splice site is not recognised, which results in the exclusion of exon splice site recognition. The choice of splice site can also be influenced by exons that are flanked by long introns that can result in exon skipping. Splice site recognition is therefore more precise in small introns and exons (Fox-Walsh *et al.*, 2005).

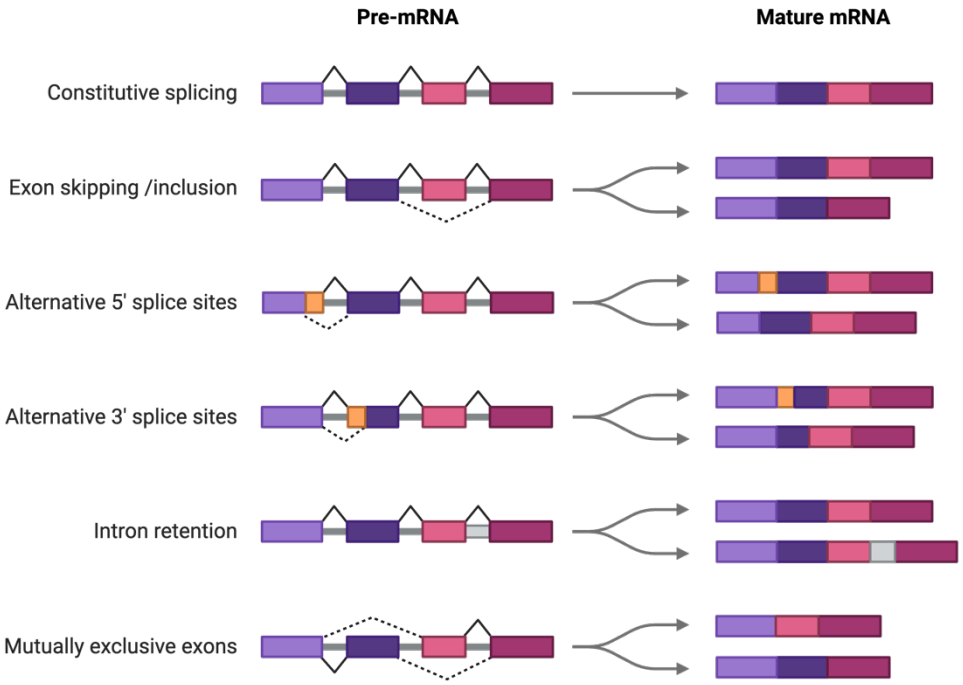



***Figure 1.3. Constitutive and alternative splicing***

***Constitutive and alternative splicing. The exons (rectangles) are connected by introns (black lines), splice site (broken lines). Alternative splicing can be described as exons skipping, intron retention, an alternative 3' or 5' site is used. See also: (Diaba-Nuhoho, 2023)***

Roughly 90-95% of human genes are alternatively spliced (Tazi *et al.*, 2009), which also indicates that alternative splicing plays an important role in most functions. In diseases such as cancer, neurological and vascular disease alternative splicing has been shown to be prevalent (Tazi *et al.*, 2009). Proteomic data shows that due to alternative splicing and alternative splice sites, new protein coding regions were identified. Whilst alternative splicing can modify the structure of proteins, it also affects their stability, binding mechanisms, and activity (Bush *et al.*, 2017).

## 1.10. Pre-mRNA splicing

During pre-mRNA splicing the intron sequence is identified and excised from the pre-mRNA with the ligation of joining exons. The spliceosome assembles the splice sites and binds them. The spliceosome is a large ribonucleoprotein complex which is made up by five small nuclear ribonucleoproteins (snRNPs). Each snRNP is made by from a single uridine-rich small nuclear RNA- snRNA U1, U2, U3, U4, U5, U6 and many other proteins, such as SR proteins, U1 specific proteins etc. (Makarov *et al.*, 2002).

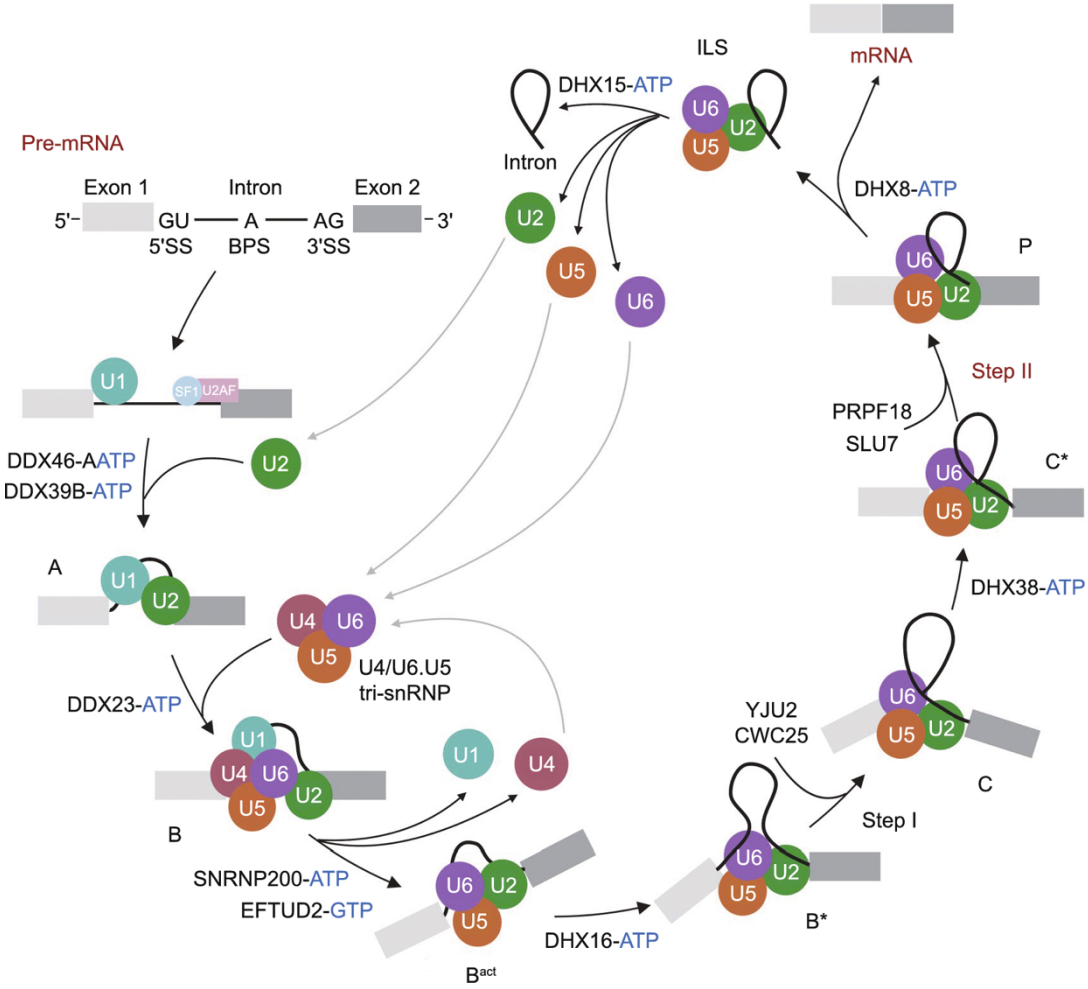



***Figure 1.4. Spliceosome assembly***

***Graphical illustration of spliceosome assembly from pre-mRNA to mRNA with the different small nuclear ribonucleoproteins based on the publication of (Shao et al., 2014)***

The spliceosome assembly starts with the U1 snRNP recognising the 5' splice site and is recruited with SR proteins by RNA polymerase, so that the coupling of splicing is correctly transcribed and deposited at the 5' splice site. Genome stability is achieved by co-transcriptional deposition of SR proteins (ASF/SF2), which then prevents the formation of R loops. R loops are essentially RNA-DNA hybrids that form during replication and are a threat to genome stability (Li and Manley, 2005). The U2 snRNP recognises the functional 3' splice site by base pairing with the branch point sequence (BPS) and the pairing of U2 and the BPS requires help from the auxiliary splice factors such as U2AF. U2AF, a heterodimer, consists of two subunits, U2AF65 and U2AF35. The two subunits bind downstream of the BPS and AG dinucleotide at the 3' end of the intron, which ensures the stability of the branch point. SR proteins are known to interact with U1 and U2AF snRNPs as this spliceosome assembly is the first splice specific complex. The tri-snRNPs U4/U6/U5 forms the A complex, including the U1 and U2 snRNPs and pre-mRNA forming the pre-catalytic B complexes. Afterwards U5 snRNP interact with the 5' and 3' splice site, which destabilises and dissociate the U1 and U4 snRNP association and activating the B complex. The U5 snRNP binds to the 5' splice site and U6 associates with U2 snRNPs in the U2/U5/U6 complex. By activating the B complex and looping the spliced intron, the C complex is formed and when the intron is spliced out, the mature mRNA is completed. Then, having no further use, the U2/U5/U6 complex disassociates and gets recycled (Shao *et al.*, 2014). Before spliceosome assembly, an important step is the recruitment of the pre-assembled tri-snRNP U4/U6/U5 to form Complex A which interacts with the 5' and 3' splice site to form the

pre-catalytic Complex B. Pre-catalytic Complex B is responsible for the release of U1 and U4 and to hydrolyse ATP and GTP by catalysing Brr2 and SNu114 proteins (Hacker *et al.*, 2008). Splicing involves two esterification processes; the first which results in the formation of a lariat structure, the second the 3'OH group of the 5' exon interacts with the 3' splice site, leading to the ligation of the 5' and 3' exon, which, at the end, releases the intron (Makarov *et al.*, 2002).

## 1.11. Regulatory elements and splice factors of constitutive and alternative splicing

The assembly of the spliceosome complex is a multiplex and dynamic process, which is tightly controlled, as splicing errors can be as small as a mistake in adding or removing a single nucleotide. This can affect the open reading frame and a different splice site. snRNAs target specific phosphate bonds, specifically to avoid any errors. The spliceosome must be able to recognise the correct splice site and act accordingly. Exonic and intronic splicing silencers are regulatory elements that help this process (Sun and Chasin, 2000). As splicing either promotes or inhibits exon inclusion, it has to be precise and regulate this process by recruiting trans-acting splice factors, which activate or supress splice site recognition and spliceosome assembly (Chasin, 2007). Serine/arginine (SR) proteins such as SRSF1 (serine and arginine rich splicing factor 1) and SRSF2 (serine and arginine rich splicing factor 2) are known to help assemble spliceosomes which bind to the recognition motif domains. SRSF1 is a known splicing factor that is

phosphorylated by SRPK1 (Serine-arginine protein kinase 1) in the N-terminal region of the RS domain. On the other hand, heterogenous nuclear RNA proteins (hnRNPs) are found to be splice repressors. HnRNPs are known to be able to block the interaction between U1 and U2 snRNPs which causes exon skipping. hnRPN A1 can either misplace the U1 snRNP or bind to a site of exon forming, thus creating a loop. Silencers therefore appear to play a bigger role in alternative splicing than promoters (Fairbrother *et al.*, 2002). SR-proteins with serine/arginine (SR)-rich domain are known to play an important role in splicing by helping in the assembly of spliceosome. SRPK1 (serine rich protein kinase 1) and CLK1 (Cdc-like kinase 1) are known to hyperphosphorylate SR proteins (Bourgeois *et al.*, 2004).

## 1.12. Aberrant splicing in cancer

Alternative splicing is a tightly controlled process, therefore errors in the true and pseudo splice sites are rare, which is necessary for a disease such as cancer to develop. If the alternative pseudo splice site occurs, the untranslated 3' and 5' regions of mRNA alter the stability and translation efficiency of the molecule. Aberrant splicing can also produce a premature stop codon, which makes the mRNA transcript inactive, alters protein function and encodes proteins with undesirable functions (Venables, 2004). Alternative splicing is thought to cause loss of cell cycle control, migration and proliferation of cancer cells, aberrant angiogenesis, cell apoptosis and tumour growth (Sveen *et al.*, 2016). Recently many studies have found that the

presence of alternatively spliced genes can be used for diagnostic and treatment purposes. Small molecule inhibitors, such as SPHINX-31, which is a SRPK1 selective inhibitor can alter the $VEGF_{165}$ isoform from pro-angiogenic to anti-angiogenic, which inhibits the angiogenesis needed for tumour formation but also to prevent macular degeneration in animal models of choroidal neovascularisation the process underlying angiogenesis in AMD patients (Batson *et al.*, 2017). In other cancers, such as glioblastoma (GBM) a recent study identified 14 GBM genes that are thought to be aberrantly spliced to promote tumourigenesis (Cheung *et al.*, 2008). In breast cancer, TP53, BRCA1 and PTEN have been found to be aberrantly spliced. In ovarian cancer, GRB7 and in colon cancer TIMP-1 have been found to have aberrantly spliced isoform (El Marabti and Younis, 2018).

## 1.13. Aberrant alternative splicing in cancer

The splicing machinery can be hijacked in processes such as cancer. As true and pseudo splice sites are easy to mistake, the splicing machinery can be manipulated into choosing an alternative pseudo-splice site instead of the true splice site. This can also affect the mRNA stability and translation efficiency. Aberrant splicing compared to normal splicing has many effects on tumuorigenesis, including proliferation, apoptosis, metabolism and angiogenesis (Venables, 2004). Recently, many studies showed that alternatively spliced genes can be used as diagnostic and therapeutic tools. For instance, U7 snRNA that is normally used to process histone pre-mRNA

can target and block a specific mRNA sequence to deliver a viral based antisense. In beta thalassemia, by modifying the cryptic splice site of β-globin with U1 or U7 snRNA, canonical splicing can be restored by around 50%, compared with healthy adults (Bergsma *et al.*, 2018).

## 1.14. Aberrant alternative splicing in leukaemia

In leukaemia, it has been reported that aberrant splicing increases the number of leukaemic cells. Bozic et al. (2018) showed that DNMT3A (DNA-methytransferase 3A) and transcripts DNMT3A2, DNMT3A4 are key players in haematopoietic cell differentiation and cell proliferation. They found that in the M4 and M5 subgroup (based on the FAB system) of AML DNMT3A2 expression level is lower in high risk patients (Bozic *et al.*, 2018).

A key regulator in the proliferation and differentiation of several haematopoietic stem cells is the *c-Myc* gene. It has been found to have alternative spliced isoforms, which are highly expressed in leukaemia. C-Myc has also been found to be a correlating factor in poor survival groups diagnosed with leukaemia, high expression levels resulted in poorer prognosis (Zhou *et al.*, 2011).

## 1.15. Serine/arginine-rich (SR) proteins

SR proteins, illustrated with Figure 1.15. are a highly conserved family of splicing factors and regulators which consist of the arginine/serine (RS) domain. They are an essential class of splicing regulators and have a characteristically organised structure that contains one or two N-terminal RNA-recognition motifs (RRM), and a C-terminal rich in arginine and serine (RS) dipeptides repeats (Krainer *et al.*, 1990). The SR protein family was identified by using the mAb104 monoclonal antibody which recognises specific phosphoepitopes on SR repeat sequences (Roth *et al.*, 1991)

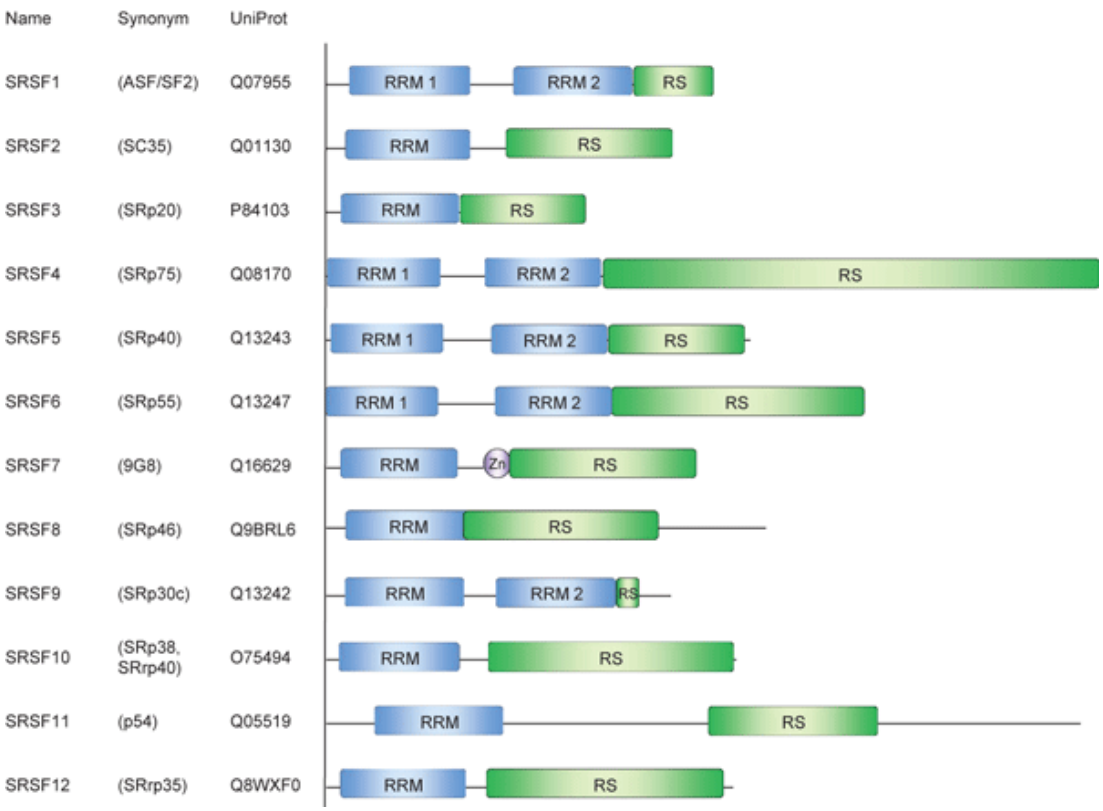



***Figure 1.5. SR protein family and their synonyms***

***The figure presents SR proteins and their synonyms which are often used in literature. It depicts the RRM and RS domains. SR proteins are known to be able to interact simultaneously with RNA and other protein components such as RS domain via an RNA recognition motif (RRM). Image adapted from (Twyffels et al., 2011).***

The classical definition of the SR protein family includes serine/arginine (SRSF) 1-12. Although not identical, as some have RRM1 a RRM2, others only the fused RRM construct, and the zinc knuckle is only to be found in SRSF7 (Twyffels *et al.*, 2011)

SR proteins are located in the nucleoplasm of mammalian cells and often described as ‘speckles’. More precisely, they are found in the interchromatin region where they can be mobilised for active transport. As mentioned before, SR proteins can determine and regulate splice site selection during constitutive and alternative splicing, a function that is performed by the RRM and RS domains, that mediates protein:protein interaction (Cazalla *et al.*, 2002). In other studies, they SR proteins were found to bind non-coding RNA

and exhibit positional RNA binding during regulated alternative splicing events. This indicates that the SR protein level also affects the choice of alternative promoter and polyadenylation sites. It was also noted that SR proteins can act as activators to exonic splicing enhancers in pre-mRNA and recruit proteins to the splicing machinery through the RS-domain:protein interaction. SR proteins affect splice site selection, which affects non-specific binding during early spliceosome assembly, this suggests that phosphorylation and dephosphorylation of RS domain is affected which in turn regulates the role of SR proteins in the splicing cycle. (Bradley *et al.*, 2015).

*In vivo* studies demonstrate that SR proteins are crucial for embryogenesis and general cell viability. It has been shown that the germline deletion of SRSF1, SRSF2, and SRSF3 results in cell or embryonic death in mice (Jumaa *et al.*, 1999, Wang *et al.*, 1996, Xu and Fu, 2005), whereas the deletion of SRSF10 causes a severe cardiac defect and myocardial thinning (Feng *et al.*, 2009). This led to the conclusion that SR proteins are key in early development and gene transcription. For the purposes of this study, we will focus on the enzymes that phosphorylate these SR proteins, SRPK (serine-arginine protein kinases) and CLK (CDC-like) kinase families, which are structurally distinct and differentially expressed in leukaemia and other diseases (Colwill *et al.*, 1996).

## 1.16. Serine/arginine protein kinase 1 (SRPK1)

Serine/arginine-rich protein-specific kinase-1 (SRPK1) is part of the protein family of kinases that phosphorylates the RS-domain of serine/arginine repeat proteins. It was described by Gui et al. (1994) when they observed a new kinase, which was responsible for the redistribution of SR proteins from the nuclear speckle to the nucleoplasm (Gui *et al.*, 1994). The human *srpk1* gene is located on the chromosome 6p21.2-p21.3 and along with *srpk2* (serine/arginine-rich protein-specific kinase-2)(Ghosh and Adams, 2011) is known to be highly preserved (Wang *et al.*, 1999). Like many protein kinases, SRPK1 is characterised by two conserved kinase domains separated by an accessory domain (spacer sequence). The accessory domain is known to regulate SRPK1 shuttling between the cytoplasm and nucleus as the deletion of the accessory domain results in exclusive nuclear localisation (Gout *et al.*, 2012). This finding suggests a role for SRPK1 in spliceosome assembly and in the trafficking of splice factors and subsequent phosphorylation of SR proteins during constitutive and alternative splicing. In terms of structure, the N-terminus and C-terminus are not thought to be conserved and deletion does not activate kinase activity (Ma *et al.*, 2008). Another study found that the N-terminus stabilizes the docking groove of the kinase domain, which helps with high-affinity binding and phosphorylating SR proteins (Ghosh and Adams, 2011), and vice-versa, deleting the N-terminus reduces SR protein recognition and binding efficiency (Hagopian *et al.*, 2008).

As SRPK1 has a short activation loop that does not have a reversible phosphorylation site, it has a stable active site for substrates. It also doesn't require any post-translational modification or any other subunits. This is because the presence of the short activation loop makes it available to extract hydroxyl hydrogen from serine (critical for phosphorylation), which in turn allows for a constitutively active formation of SRPK1 (Plocinik *et al.*, 2011). In a healthy state SRPK1 and SRPK2 are predominantly expressed in testis (Giannakouros *et al.*, 2011). SRPK1 is known to be overexpressed in prostate cancer, breast cancer, lung cancer and in gliomas (Bullock and Oltean, 2017). Other members of the SRPK family have been shown to be expressed in other places, such as the nervous system (SRPK2), muscle cells (SRPK3). This suggests that these different proteins localise at different places and have different roles (Hatcher *et al.*, 2018). SRPK1 mainly localizes in the cytoplasm, with a low presence in the nucleus, while SRPK2 mainly present in the nucleus (Sigala *et al.*, 2021).

## 1.17. Regulation of SRPK1 activity

The accessory domain (AD) of SRPK1 provides a binding surface for chaperone complexes for assembly - the deletion of the binding surface results in SRPK1 being sequestered in the nucleus (Wang *et al.*, 1998). X-ray diffraction studies showed that the AD is a large, cca. 200 amino acid containing unit, it does not have a stable structure, and most of the AD is likely to be an intrinsically disordered region of SRPK1. It could still provide an albeit

unstructured, but large surface for chaperones to bind to unfolded proteins (Plocinik *et al.*, 2011). The chaperone complex assembly is initiated by the binding of Hsp40/Hsp70 to SRPK1 followed by the binding of Hsp90 and Aha1. The creation of SRPK1/chaperone/co-chaperone complex ensures the correct folding of SRPK1 into its active form and prevents proteasome degradation. Previous studies showed that Hsp40 targets a region outside of the accessory domain, and Hsp90 targets the accessory domain. They also showed that the inhibition of Hsp90 chaperone ATPase resulted in the dissociation of the chaperone complex and in the failure SRPK1 nuclear localisation (Zhong *et al.*, 2009).

## 1.18. The role of SRPK1 in cancer

It has been observed in many cases that SRPK1 is upregulated in many forms of cancer, such as prostate, colon, breast cancer, gliomas and AML (Duggan *et al.*, 2022). Nonetheless, the role of SRPK1 in cancer is not entirely clear. Thus far research showed that SRPK1 upregulation promotes tumorigenesis, tumour progression and metastatic dissemination in solid cancers as well as chemotherapy-resistance (Mavrou *et al.*, 2015). In comparison, tumours with a germline mutation showed progressive and metastatic dissemination following the downregulation of SRPK1 (Wang *et al.*, 2014). Wang et al. (2020) showed that high levels of SRPK1 resulted in a poor prognosis, aggressive tumourigenesis, metastases formation in cervical squamous cell carcinoma (CESC) but it also showed potential to be a target for therapy

(Wang *et al.*, 2020). SRPK1 inhibition has also been shown to induce a great effect on angiogenesis and tumour growth both *in vivo* and *in vitro* (Gammons *et al.*, 2014).

## 1.19. SRPK1 expression in leukaemia and its therapy targets

Leukaemias known to be a heterogeneous disease with genomic instability and dysregulated signalling pathways. The complexity of the protein network involved, and kinases involved make it harder to identify druggable targets. As SRPK1 is known to have a role in pre-mRNA splicing, angiogenesis and cell proliferation it could become a potential target (Zhou *et al.*, 2013). In their study, Sanidas et al. (2010) demonstrated that SRPK1 is highly expressed in erythroid and lymphoid cells, which contributes to the cancer proliferation (Sanidas *et al.*, 2010). SRPK1 inhibition in AML has also shown to modify splicing of certain key regulatory genes such as *brd4* (Tzelepis *et al.*, 2018).

There has been increasing interest in targeting SRPK1 as a therapeutic agent, as it has been observed that heightened levels of SRPK1 present in many tumour environments, such as in pancreatic, colon, breast and viral induced T-cell leukaemias (Nikas *et al.*, 2019). Since then, a number of studies have targeted SRPK1 inhibition, specifically to see if this has an effect on cell proliferation, invasion, migration or even, sensitivity to commonly used chemotherapeutics. Wu et al. (2013) found a significant reduction in cell viability in U87, Caco-2 and HL60 cells, after SRPK1 inhibition (Wu *et al.*,

2013). These findings are especially important in the cases of notoriously hard to treat cancers such as leukaemias. There is yet to be a selective SRPK1 inhibitor to be tested in clinical trials and potentially taken to the clinic. This thesis aims to show the potential of a selective SRPK1 inhibitor, called SPHINX-31 and other unpublished inhibitors for the treatment of AML.

## 1.20. CDC-like kinase 1 (CLK1)

CDC-like kinases (CLKs) are an evolutionary conserved group of kinases with dual specificity. They are able to phosphorylate SR proteins (SRSF1-12), which also regulates the spliceosome assembly and consequently pre-mRNA splicing. The CLK family consists of CLK1, CLK2, CLK3, CLK4. All isoforms of CLK can be found in most tissues such as, leukocytes, muscles, brain, liver, lung, kidney, thyroid etc. but the expression levels are very variable (Martin Moyano *et al.*, 2020). CLK1 regulates the alternative splicing of its own gene *clk1* via exon 4 skipping and intron 4 retention. The *clk1* gene consists of 13 exons and the full-length protein consists of 484 amino acids, the first 130 regulates the SR protein interaction while the other 354 is the catalytic domain (Uzor *et al.*, 2018). CLK1 is known to recruit hypophosphorylated SRSF1 from nuclear speckles and form a complex known as CLK1-SRPK1-SRSF1. With SRPK1, CLK1 can work in a complex via the interaction between CLK1 N-terminus and SRPK1 kinase domain and also facilitates the release of hyperphosphorylated SRSF1. In the nucleus, increased levels of CLK1 results in the redistribution of SR proteins and dissolution of the SR speckles (Martin Moyano *et al.*, 2020).

## 1.21. SRPK1 selective inhibitors

As SRPK1 has been found to be highly expressed in numerous cancers such as lung, breast, prostate, colorectal, stomach, liver, pancreatic cancers, gliomas, and leukaemia etc. great efforts have been made to produce an effective inhibitor that can provide treatment. The majority of these cancers are very hard to treat, and patients diagnosed with one of these cancers usually have very poor prognostics. SRPKs were also identified to have a role in infection mechanisms of various viruses, such as HIV, Epstein-Barr virus, hepatitis, dengue. This discovery led Gammons et al. (2014) to screen the efficacy of a newly identified pan-SRPK inhibtior N-(2-(piperidin-1-yl)-5-(trifluoromethyl) phenyl) isonicotinamide, known as SRPIN340. This compound proved to have a significant effect on cellular assays as well as in *in vivo* models. SRPIN340 has proven to be an effective SRPK1 selective inhibitor in melanoma, which significantly reduced cell viability in cell-based assays and *in vivo.* This study also found that SRPIN340 can moderate splicing and switch from pro-angiogenic VEGF-$A_{165}$a to anti-angiogenic VEGF-$A_{165}$b isoforms (Gammons *et al.*, 2014). This proved that a selective SRPK1 inhibitor could become an effective treatment option on its own or to be used in combination with a synergistic compound (Nikas *et al.*, 2019). Another SPRK1 inhibitor, known as SRPKIN-1 is a SRPK1/2 inhibitor which has the same effect on VEGF-$A_{165}$ as SRPIN340.

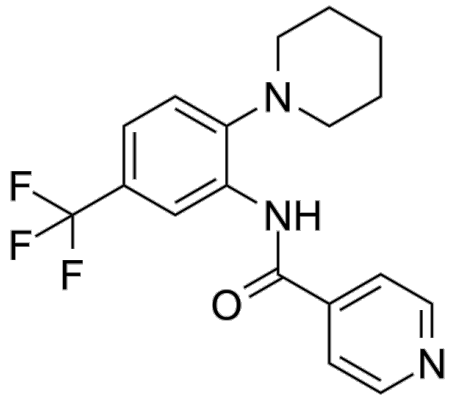



***Figure 1.6. The chemical structure of SRPIN 340***

*(source: MedChemExpress)*

SRPIN340 has an $IC_{50}$ value of 200nM (vs.10μM of SRPKIN-1) and is the first irreversible SRPK inhibitor that forms a covalent bond with a tyrosine phenol group in the ATP-binding pocket and attenuates SR protein phosphorylation at submicromoclar level (Hatcher *et al.*, 2018).

Alectinib (Roche, UK), another SRPK1 inhibitor has made it to the clinical trial stage where anaplastic lymphoma patients (ALP) were treated either with just Alectinib (300mg/day) or in synergy with Crizotinib (approved drug in Japan) that has proven to prolong the life of ALP patients by 10.9 months (Zhou *et al.*, 2019a). Since then, Alectinib has been used for the treatment of non-small-lung cancer under the name of Alecensa (Ramachandran *et al.*, 2018).

SPHINX-31 is a highly selective potent SRPK1 inhibitor, it has been first published by Batson et al. (2017) (Batson *et al.*, 2017). SPHINX-31 is based on a SPHINX scaffold, which is a trifluoromethyl-phenyl-furanyl-carboxamide-piperazine base to which furan and piperazine were added to improve potency, stability, and lower toxicity (Gammons *et al.*, 2014). It has relatively short clearance *in vitro*; $C_{max}$ of 1.2μM at 30 min and a half-life of 12 minutes

in human hepatocytes. Despite the rapid clearance, if continuously administered this compound can inhibit the phosphorylation of SRSF1 after 24 hrs (Tzelepis *et al.*, 2018).

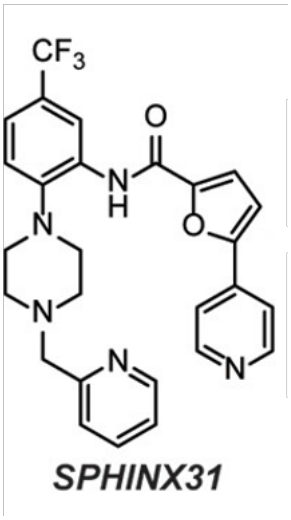



***Figure 1.7. Chemical structure of SPHINX-31***

**Chemical structure of SPHINX-31 as published in Batson et al. (2017) study. Figure copied here with author's and collaborators' permission.**

### 1.21.1. Second generation SRPK1 inhibitors (ET1126, ET1132, ET3002)

ET1126, ET1132 and ET3002 are all unpublished compounds that have been shown good inhibitory effect in previous enzyme studies (© Prof Jonathan Morris, University of New South Wales). ET1126 and ET1132 are Griffin-type inhibitors whereas, ET3002 is part of the ET3000 series of new inhibitors and has an Indole scaffold.

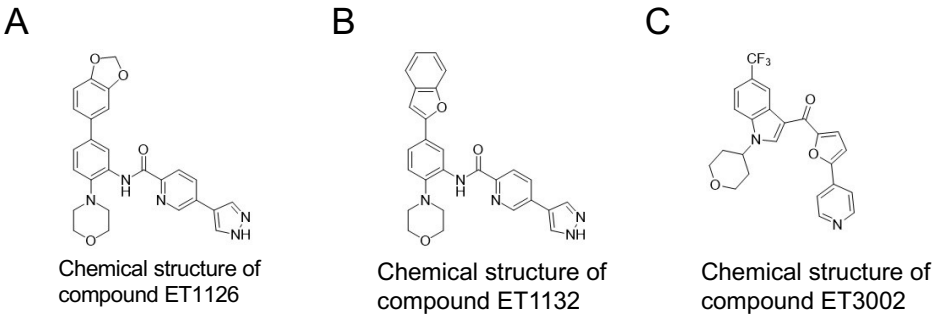



***Figure 1.8. Chemical structures of new generation inhibitors***

**Chemical structure of inhibitors ET1126, ET1132, ET3002. Proprietary information- Emenda Therapeutics Ltd., Gloucester, UK). The images of chemical structures copied here with permission.**

## 1.22. CLK1 selective inhibitors

In primary leukaemic cells, such as acute lymphoblastic leukaemia, CLK1 has been found to be 2.3-fold higher in expression levels than in the control, patient group (Qazi and Uckun, 2010). CLK1 has also been known to be highly expressed in other cancer and particularly in gliomas, which also correlates clinical outcomes and treatment resistance (Zhang *et al.*, 2017).

In recent years, many small molecule CLK inhibitors have been reported but these usually are unselective and also inhibit the structurally similar DYRK and HIPKS families. It has been a challenge so far to find potent but highly selective CLK inhibitors. Most inhibitors usually affect off-targets and PIM and/or CK1 kinases (Martin Moyano *et al.*, 2020).

TG003 is a well-known CLK1 inhibitor, although with many off-target effects. It has been proven to be active in cell-based assays and *in vivo* (Muraki *et al.*, 2004). T-025 is as a pan CLK inhibitor. It has a good selectivity profile that

was based on a screening against 468 kinases, it showed good results in cell based and *in vivo* experiments and it was the first compound to demonstrate anti-tumour activity in mice (Iwai *et al.*, 2018). KH-CB19 another compound showed promise to be a selective CLK1 and DYRK1A inhibitor, against 106 kinases but since it has a molecule that contains a potentially labile ester functionality, it wasn't recommended for *in vivo* work (Fedorov *et al.*, 2011). Other candidates published recently: ML106, ML167, CX-4945,KH-CB19, Leucettine 41, ML315, Thiophene 48, 3A5, cpd-2, SRI 29329, T3,Compound 25, TG693, Indazole 1, KuWal151, CC-671, SGC-CLK-1, SM8502, MU1210, AB1 (Martin Moyano *et al.*, 2020).

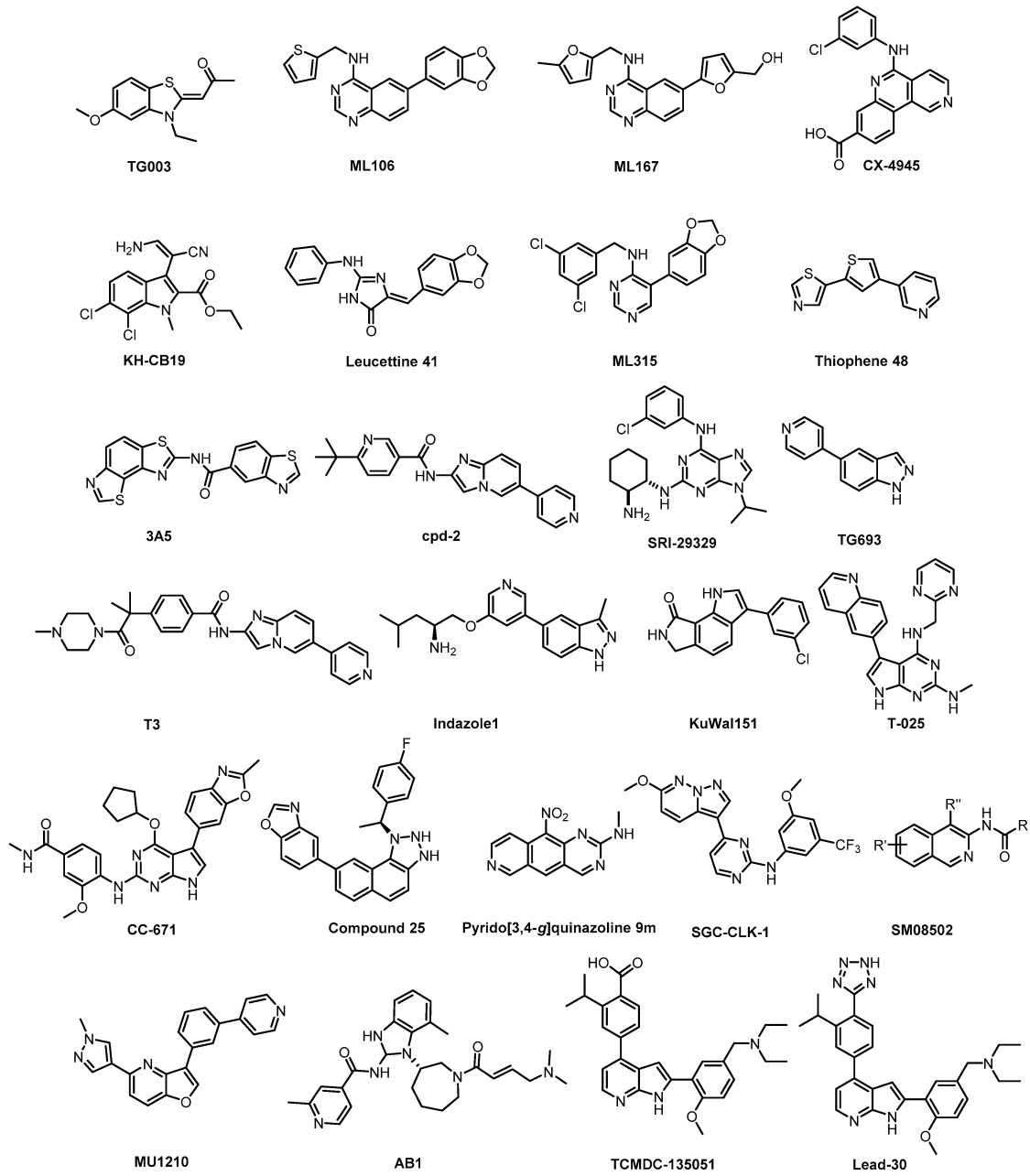



***Figure 1.9. Chemical structures of different CLK1 inhibitors***

***TG003, ML 106, ML167, CX-4945, KH-CB19, Leucettine 41, ML315, Thiophene 48, 3A5, cpd-2, SRI-29329, TG693, T3, Indazole1, KuWal151, T-025, CC-671, Compound 25, Pyridol[3,4]glyqulnazoline 9m, SGC-CLK-1, SM08502,MU1210, A81, TCMDC-135051, Load-30. Adapted from Martin Moyano (2020) article.***

Griffin 51 is a highly selective CLK1 inhibitor which has never been published before. In a pilot study, based on enzyme reactions only, Griffin 51 showed promising results to be a highly selective, potent CLK1 inhibitor that could be a promising drug candidate for the treatment of AML, GBM and other cancers

where high levels of CLK1 expression is present (Proprietary information of Emenda Therapeutics Ltd., Gloucester, UK)

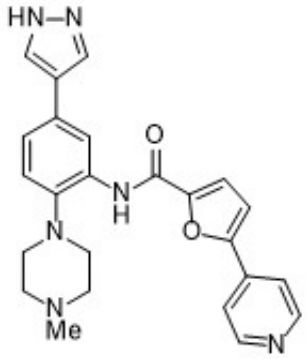



***Figure 1.10. Chemical structure of Griffin 51***

***© Copyright. Intellectual property of Prof Jonathan C Morris (University of New South Wales) and Emenda Therapeutics Ltd., Gloucester, UK.***

## 1.23. Alternative splicing of BRD4

Alternative splicing has been found to have a profound effect on tumorigenesis, as alternative isoforms of the same protein can trigger tumour growth. The splicing alterations (resulting in different isoforms) often linked to cancer driver mutations are making cells vulnerable to drug interaction. These can also have a synergistic effect with classic chemotherapy and radiation, contributing to a better prognosis (Martin Moyano *et al.*, 2020). *BRD4* (Bromodomain-containing protein 4) is an epigenetic and transcriptional regulator for embryogenesis and cancer development. This gene is the member of the BET family, which also includes *BRD2*, *BRD3* (Bromodomain containing protein 2 & 3) and *BRDT* (Bromodomain testis-specific protein). BRD4 also promotes inflammatory responses in numerous cells (Zhou *et al.*, 2019b). Uppal et al. (2019) showed that BRD4 is alternatively spliced in T cell

acute lymphoblastic leukaemia and that BRD4 expression was affected by exon skipping (Uppal *et al.*, 2019). In AML cells, (Tzelepis *et al.*, 2018), showed that SPHINX-31, a selective SRPK1 inhibitor (described below) is effective in changing BRD4 expression in AML cell lines from the short (pro-tumorigenic) to the long (anti-tumorigenic form). BRD4 has been identified to be overexpressed in various cancer types.

In glioblastoma, BRD4 expression is significantly higher than in the surrounding brain tissue. Clinical studies showed that BRD4 inhibitors can successfully penetrate the Blood-Brain barrier but have no effect on healthy brain tissue. As glioblastoma still remains one of the most drug resistant diseases, it is paramount that every effort is made to identify new treatment targets. Even with surgical resection and drug regimen, the median survival time is 13 months (Stupp *et al.*, 2009). The current drug regimen includes radiotherapy with DNA alkylating agent temozolomide, but it does not seem to have a long-term positive effect. Therefore, many small molecule inhibitors were proposed and tested for the treatment of glioblastoma. Small molecule inhibitors displace BET protein complexes from chromatin by binding to BET bromodomains as competitors to acetyl-lysine. One of the most successful was I-BET151, a BET protein inhibitor that effects BRD2, BRD3 and BRDT expression through the NF-κB signalling pathway (Lai *et al.*, 2021). Other pan-bromodomain inhibitors are triazoloazepine (JQ1) or isoxazole derivates such as the I-BET151. With JQ1 they showed $IC_{50}$ values of 77nM, while the I-BET151 was $IC_{50}$ 794nM. Both inhibitors are currently tested in clinical trials but are not approved for clinical use yet (Yang *et al.*, 2021). Given the rate of drug candidates that enter clinical trials but eventually fail to make it to the

clinic there is a constant need to test further compounds that has a potential to offer a much-needed treatment option with the least amount of side effects.

## 1.24. BRD4 as a therapeutic target in AML

Chromatin deregulation is often found in AML patients that contributes to the development and progression of the disease. Next generation sequencing found aberrant DNA methylation, altered chromatin states and mutations in chromatin modifiers (Huang and Figueroa, 2021). KMT2A, also known as histone H3 lysine, 4 methyltransferase protein is altered in most AML cases, genes such as *DNMT3A*, *TET2 (*which is involved in DNA methylation and demethylation) are all mutated in AML as well as transcription factors that leads to altered chromatin structure. BRD4 contains two tandem bromodomain modules that connects BRD4 to chromatin and engages in acetyl lysine recognition. BRD4 is also considered to be a transcriptional coactivator, as it can bind directly to transcription factors. It was thought that BRD4 performs a more general role in genomic regulatory processes, it was found that small molecule inhibitors bind the bromodomains with the acetyl lysine which releases BRD4 from cellular chromatin (Roe and Vakoc, 2016). Zuber et al. (2011) showed that if BRD4 is knocked down via shRNA in a mouse model of AML initiated by the MLL-AF9 oncogene, there is a significant growth arrest, terminal differentiation and apoptosis. They also showed that the BRD4 inhibitor, JQ1 slowed down disease progression in *in vivo* studies as well as caused a pronounced decrease in MYC transcription (Zuber *et al.*,

2011). Dawson et al. (2011) showed that another BRD4 inhibitor, i-BET supressed oncoproteins such as MYC, BCL-2 and CDK6 (Dawson *et al.*, 2011). Although it is unlikely that these inhibitors directly affect MLL-fusion proteins, BET bromodomain inhibitors such as OTX-015 were successfully used in clinical trials, for the treatment of acute leukaemia patients (Berthon *et al.*, 2016). BRD4 is known to have an important role in AML maintenance. Previous studies identified two distinct isoforms of BRD4, BRD4s (short) and BRD4l (long). In their study, (Tzelepis *et al.*, 2018) show through SRPK1 inhibition that the tumor-supressor BRD4l isoform is upregulated and the tumour progressor BRD4s is downregulated in AML after SPHINX-31 treatment. To summarise, this thesis aims to demonstrate the efficacy of a known SRPK1 inhibitor, SPHINX-31. It introduces and demonstrates the efficacy of a new CLK1 inhibitor, Griffin 51 as well presents preliminary data from other potentially effective SRPK1 and CLK1 inhibitors: ET1126, ET1132, ET1055. The data presented also shows the effect of the aforementioned inhibitors via BRD4 splice change, namely SPHINX-31 and Griffin 51 switches the splicing of BRD4 (as an indirect target), from the short tumorigenic isoform to the tumour-suppressor long isoform.

## 1.25. SRPK1 inhibition in solid tumours

SRPK1 was found to trigger alternative splicing in solid tumour cell lines, such as the HT29 colorectal cells. 25μM SRPIN340 (an SRPK1 inhibitor) caused a decrease in Rac1b expression and a downregulation in SRSF1

phosphorylation (Goncalves et al., 2014). In breast cancer, high expression levels of SRPK1 correlated with poor prognosis. The same study identified that in *in vivo* models, SRPK1 knockdown supressed metastasis to lung and liver and inhibited focal adhesion reorganisation when tested in breast tumours (van Roosmalen *et al.*, 2015). Previous studies showed a link between SRPK1 inhibition and BRD4 splicing change in AML (Tzelepis *et al.*, 2018), which makes SRPK1 and BRD4 inhibition a potential drug target for hard to treat solid tumours, such as Glioblastoma Multiforme (GBM). Yang et al. (2021) showed in their study that BRD4 expression is significantly higher in gliomas, compared to the surrounding healthy tissue. They also show that BRD4 inhibitors such as JQ1, iBET151and iBET762 can pass through the Blood-Brain barrier, but in clinical trials were not successful and showed a lack of clinical efficacy (Yang *et al.*, 2021). More importantly, Akhtari et al. (2013) found that a significant percentage of Non-Hodgkin lymphoma patients (10% in their cohort), developed the disease as a side effect of radiotherapy-related myelodysplasia and had a life expectancy of less than 10 years (Akhtari *et al.*, 2013). GBM and AML share further similarities, they both predominantly occur in *de novo* form with only a small subset of a myelodysplastic syndrome or diffuse glioma. They are both characterised by aberrant RAS pathway, heightened BCL-2 expression, while their secondary counterparts have abnormalities in IDH expression (Goethe *et al.*, 2018). Dang et al. (2010) found that 70% of low-grade gliomas and secondary GBM samples had *IDH1 and IDH2* mutations, while they found the same mutations in 10% of AML samples (Dang *et al.*, 2010).

# 2. Chapter

# Aims and objectives

In Acute Myeloid Leukaemia (AML) drug resistance and relapse are very common events. Even in cases where patients respond well to therapy the side effects of chemotherapy drugs are very difficult to tolerate. Therefore, there is a clinical need to find and screen new inhibitors that can be effective and have minimal or no side effect to treat patient with AML. Tzelepis et al (2016) previously showed that knockout of SRPK1 was lethal in AML cells, and particularly those with MLL translocations. Moreover, it was shown that this acted through alternative splicing of BRD4, switching from a short isoform that drove HOXA9, MYC and BCL2 expression to a long isoform that repressed expression of those oncogenes in AML (Tzelepis *et al.*, 2016). Through our collaboration we had identified a number of potential small molecules that could have strong effect in inhibiting SRPK1 - in the nanomolar to micromolar range. In previous studies it had been shown that SPHINX-31 is a selective, highly potent SRPK1 inhibitor therefore I tested the hypothesis that SRPK1 inhibition by SPHINX-31 could switch splicing of BRD4 and expression of downstream oncogenic partners in both MLL translocated and MLL wildtype cells. Since SRPK1 is known to work in synergy with CLK1, I also tested a CLK1 selective inhibitor, Griffin 51 to see if I can recreate the same effect. Additionally, I also had access to a small selection of clinical samples from AML patients which we used to test SPHINX-31 and Griffin 51 in a colony forming unit study. SPHINX-31 and Griffin 51 was also tested in a solid tumour cell line, U87 to test if there is a similar effect that would reduce cell viability and the level of downstream targets.

# The hypotheses of this thesis:

a. SPHINX-31 is a highly selective and potent SRPK1 inhibitor that would cause an isoform change in BRD4 expression in AML both cell lines and in clinical samples. RT-PCR tests will show an isoform change, switching from BRD4 short to BRD4 long isoform.

b. Further to that SPHINX-31 can prevent cell proliferation in AML and Glioblastoma cells, which will be tested using a luminescence based ATP-uptake assay.

c. SPHINX-31 can decrease the expression of HOXA9, BCL2 and MYC, all known oncogenes that are highly expressed in AML, glioblastoma and in other types of cancers. Which will be tested using Digital Droplet PCR.

d. Griffin 51 a selective CLK1 inhibitor that would cause the same isoform to change in AML and U87 cells and therefore reduce the tumorigenic effect of all these cells. This will also be tested using RT-PCR.

e. Griffin 51 decreases HOXA9, BCL2 and MYC expression levels in AML cell and in Glioblastoma. This will be tested using Digital Droplet PCR.

g. SRPK1 and CLK1 inhibition halt cell viability in solid tumours.

# 3. Chapter

# Materials and methods

## 3.1. Acute Myeloid Leukaemia (AML) cell lines and clinical samples

The THP-1 and OCI-AML2 cell lines were purchased from DSMZ (Braunschweig, Germany). The other four AML cell lines used in this study was a kind gift from Dr Claire Seedhouse (University of Nottingham, UK). Clinical samples were provided by the Stamm Group from the Princess Maxima Hospital, Utrecht, The Netherlands. All cell lines and primary samples were kept and handled according to the University of Nottingham's and the Biodiscovery Institute's policies. The six AML cell lines were divided into two distinct groups; non-translocated (MLL-WT) and translocated (MLL-TL) cell line harbouring the MLL-AF6, MLL-AF9 or MLL-AF10 translocation.

### 3.1.1. OCI-AML2

OCI-AML2 is a translocated AML cell line MLL-R rearrangement, harbouring DNMT3A R635W mutation in addition to KMT2A-AFDN, MLL-MLLT4, MLL-AF6 gene fusions, purchased from DSMZ (Leibniz Institute DSMZ-German Collection of Microorganisms and Cell Cultures GmbH, Braunschweig, Germany, catalogue number: ACC 99). The cell line was stablished from the peripheral blood of a 65-year-old man with acute myeloid leukaemia (AML FAB M4) in 1986. Cells were described in the literature to express the retinoic acid receptor gene; (Klijn *et al.*, 2015)

### 3.1.2. THP-1

THP-1 is a translocated AML cell line MLL-R, with carries t(9;11)(p21;q23) leading to KMT2A-MLLT3 (MLL-MLLT3; MLL-AF9) translocation, purchased from DSMZ (Leibniz Institute DSMZ-German Collection of Microorganisms and Cell Cultures GmbH, Braunschweig, Germany, catalogue number: ACC 16) It was established from the peripheral blood of a 1-year-old boy with acute monocytic leukaemia (AML) at relapse in 1978; the cells were described in the literature to produce lysozyme and to be phagocytic.

### 3.1.3. MOLM-13

MOLM-13 is a translocated AML cell line MLL_R, with MLL-AF9 translocation and an internal tandem duplication of FLT43 was purchased from DSMZ (Leibniz Institute DSMZ-German Collection of Microorganisms and Cell Cultures GmbH, Braunschweig, Germany, catalogue number: ACC 554) and an aliquot was gifted to us by Dr Seedhouse (University of Nottingham, UK), at passage 8. It was established from the peripheral blood of a 20-year-old man with acute myeloid leukaemia AML FAB M5a at relapse in 1995 after initial myelodysplastic syndrome (MDS, refractory anaemia with excess of blasts, RAEB) (Matsuo *et al.*, 1997).

### 3.1.4. OCI-AML3

OCI-AML3 is a non-translocated AML cell line, however it consists of a NPM1 gene mutation (type A) and the DNMT3A R882C mutation. It was purchased

from DSMZ (Leibniz Institute DSMZ-German Collection of Microorganisms and Cell Cultures GmbH, Braunschweig, Germany, catalogue number: ACC 582) and an aliquot was gifted to us by Dr Seedhouse (University of Nottingham, UK), at passage 8. It was established from the peripheral blood of a 57-year-old man with acute myeloid leukaemia (AML FAB M4) at diagnosis in 1987.

### 3.1.5. HL60

HL-60 is a non-translocated AML cell line which carries an amplified MYC gene, it was purchased from DSMZ (Leibniz Institute DSMZ-German Collection of Microorganisms and Cell Cultures GmbH, Braunschweig, Germany, catalogue number: ACC 3) and an aliquot was gifted to us by Dr Seedhouse, at passage 12. It was established from the peripheral blood of a 35-year-old woman with acute myeloid leukaemia (AML FAB M2) in 1976. In the literature it was described in the literature to be responsive to DMSO, phorbol ester TPA and other reagents (e.g., expression of TNF alpha).

### 3.1.6. TF1a

TF1a is a non-translocated AML cell. This cell line has a constitutive activation of the MAP kinase and MEK proteins in TF-1a cells. Phenotypically, TF-1a cells are CD34 positive and CD38 negative. TF1-a cells are resistant to tumour necrosis factor alpha (TNF-alpha) induced apoptosis, they could be used as a model for studying human primitive myeloid progenitor cells and for

the process of progressive malignant transformation of myeloid cells. The cell line was purchased from ATCC (American Type Culture Collection, Manassas, Virginia, USA), catalogue number (ATCC CRL-2003) and an aliquot was gifted to us by Dr Seedhouse (University of Nottingham, UK), at passage 12. It was established from a 35-year-old man with an unknown diagnosis.

## 3.2. Non-AML cell lines:

### 3.2.1. HEK 293FT

HEK cells are a fast-growing, highly transfectable cell line. The HEK293FT has a clonal isolate derived from human embryonal kidney cells transformed with the SV40 large T antigen. This cell line is easy to grow and not too sensitive to manipulation. The distributor is unknown, we received it as a kind gift from Dr James Dixon's group (University of Nottingham, UK).

### 3.2.2. U87

U87 cells is a glioblastoma (astrocytoma) cell line, derived from a male patient. It is a hypodiploid human cell line with the modal chromosome number of 44 occurring in 48% of cells. The rate of higher ploidy is 5.9%. Twelve markers were common to all cells, including der(1)t(1;3) (p22;q21), der(16)t(1;16) (p22;p12), del(9) (p13) and nine others. The marker der(1) had

two copies in most cells. There was only one copy of normal X. N1, N6 and N9 were not found. The cells were a kind gift from Dr James Dixon's group (University of Nottingham, UK).

## 3.3. Growth conditions

AML cell lines were grown in Roswell Park Memorial Institute (RPMI) 1640 medium (Gibco, 31870074), except for the OCI-AML2 cells which were grown in Minimum Essential Medium Eagle (MEM, Sigma-Aldrich M8042) supplemented with L-Glutamine 1% (2mM) concentration (Sigma-Aldrich G7513). The media was supplemented with 10% serum (FBS), First Link, (Batch #5572). HEK293FT and U87 cells were maintained in DMEM, high glucose (Sigma-Aldrich D6429), supplemented with 10% serum (FBS) (Sigma-Aldrich F9665). Cells were incubated in a Sony HEPA filtered single chamber water jacketed incubator at 37°C in a humidified 5% $CO_2$ atmosphere.

## 3.4. Extraction of cortical astrocytes

Neonatal (P1-P5) Wistar rat pups (Charles River, UK) were culled by cervical dislocation and the brains were transferred to 5mL cell culture media (Dulbecco's Modified Eagle's Medium (DMEM, Sigma-Aldrich D6046) + Foetal Bovine Serum (FBS, Sigma-Aldrich, F4135) 10%, Penicillin/streptomycin 1% (Sigma-Aldrich, P4458)). The cerebellum, mid

brain and the optic nerves were discarded. The remaining tissue was finely chopped with a scalpel and dissociated with a 5mL serological pipette. The cells were digested in a papain solution (5mg/mL, LS003118, Worthington, USA) at 37°C, 5% $CO_2$ in a Sanyo cell culture incubator, for 40 minutes. After incubation, 0.5mL of DNase (Sigma-Aldrich, 11284932001) was added to the cell suspension. The cell suspension was then centrifuged at 182 x g for 3.5 minutes in 2mL media. The supernatant was removed, and the pellet was resuspended in fresh, 2 mL media and with an additional 0.5 mL DNase solution. The mixture was triturated and centrifuged again at 182 x g for 3.5 minutes. Finally, all the removed supernatant aliquots were collected and centrifuged in one universal tube for 5 minutes at 212 x g. The supernatant from the mixture was discarded and the final pellet was resuspended in 10mL media. The cell solution then was filtered through a 100μm and a 70μm cell strainer (Corning, 431751 and 431752). T75 cell culture flasks were coated with poly-D-lysine (10% dilution in PBS, Sigma-Aldrich, P7280) and the solution was divided between flasks (approximately 2 tissue sample/ flask). The following day the cell surface washed with PBS to remove dead cells and media refreshed. The flasks were then put on an orbital shaker in the incubator at 37°C, 5% $CO_2$ and gently moved horizontally at 200 RPM for 12 hours to remove microglia from the astrocyte layer. After 12 hours the media was refreshed again, and the cells were cultured for 7-10 days before starting and experiment. Media was changed every 3 days.

## 3.5. Primary brain pericytes and endothelial culture

5 week-old Wistar or Sprague-Dowley rats (mixed gender, Charles River, UK) were culled by $CO_2$ overdose (5% in raising concentration for 6 minutes) and brains were removed immediately and immersed in dissection buffer (HEPES 2 mL (Sigma-Aldrich H4034), Penicillin/streptomycin 1 mL (Sigma-Aldrich, P4458), Bovine serum albumin 30% (First Link Ltd., 43-30-850) 2 mL, and HBSS 95 mL (Sigma-Aldrich H6648)). Superficial vessels and meninges were carefully dissected under a dissection microscope. The midbrain, cerebellum and white matter parts were removed, and cortices were kept. The tissue was chopped up with a scalpel and further homogenized with a 20mL syringe. The mixture was then centrifuged at 380 x g for 3 minutes, then the supernatant was removed. 400μl DNase (Sigma-Aldrich, 11284932001) and 20μl TLCK ($N_\alpha$-Tosyl-L-lysine chloromethyl ketone hydrochloride, Sigma-Aldrich 90182) along with 20 mL Collagenase/dispase (Roche,10269638001). The mixture was then digested for 15 minutes at 37°C, 5% $CO_2$ in a cell culture incubator. After 15 minutes it was triturated with a cut end micro pipette tip (1000μl) and a regular pipette tip (1000μl). The now much more homogenous mixture was the incubated for 50 minutes at 37°C, 5% $CO_2$ in a cell culture incubator. The mixture was then triturated for the second time with a cut end and regular micropipette tip (1000μl), then centrifuged at 380 x g for 5 minutes. The supernatant was discarded and BSA solution added. (Bovine serum albumin (BSA) 30% 19mL, dissection buffer 11mL). The tube was shaken to

homogenize the content and the remaining 15mL dissection media was added to the tube. Then the mixture was centrifuged at 1490 x g for 15 minutes at 4°C, in a cooled centrifuge. After centrifugation the different concentration levels were separated, therefore the top myelin layer could be easily removed. The supernatant was transferred to another tube and triturated again, and the concentration dependent centrifugation repeated to maximize the number of collected cells. 1 mL of the dissection buffer was added to the cell pellet and the collagenase/dispase solution was added. The mixture was triturated with a cut end and regular micropipette tip (1000μl) and left to be incubated at 37°C, 5% $CO_2$ in a cell culture incubator for 2.5 hours. After the incubation the solution was centrifuged at 380 x g for 5 minutes. The supernatant was discarded and 2mL cell media was added to 1 previously coated (0.1mg/mL Type 1 Rat tail collagen, Sigma-Aldrich, C3867). 3mL cell media (DMEM, Sigma-Aldrich D6046) + FBS 10% Sigma-Aldrich, F4135, Penicillin/streptomycin 1% (Sigma-Aldrich, P4458) was added to each flask and the 1mL cell solution. Subsequently, 50μl (1mg/mL) puromycin (Sigma-Aldrich, P9620) was added to the flask containing endothelial cells. The media was changed on the next day and every 2 days after that.

### 3.5.1. Serum free media composites for primary cells

After the extraction of primary astrocytes, endothelial cells and pericytes, were cultured in serum rich media (as described above). The cell culture media

then was changed to a serum free composite after 5 days. Media for primary astrocytes: Advanced DMEM/F12 (Gibco, 12634010), G-5 Supplement 1 mL (Gibco, 17503012), 1% Penicilin/Streptomycin (Sigma-Aldrich, P4458), 1% L-Glutamine (Sigma-Aldrich G7513). Media for primary endothelial cells and pericytes: Advanced DMEM/F12, (Gibco, 12634010), bFGF 20ng/mL (Proteintech, HZ-1285), EGF 10ng/mL (Proteintech, HZ-1326), Fibronectin (Roche, 10838039001).

## 3.6. Detachment and passaging of adherent cells

Adherent cells were detached before experiments and for routine maintenance by using Trypsin-EDTA (0.25% Trypsin/0.53 mM EDTA) 1x solution (diluted from 10x Sigma-Aldrich 59418C in PBS). Flasks were incubated for 5-7 minutes in a regular cell culture incubator, then cell dissociation was facilitated by mechanical pipetting. Trypsin was neutralised with an equal volume of cell media with 10% serum. Then the solution was transferred to a 20mL universal tube (Sarstedt, Leicestershire, UK) and centrifuged at 400 x g for 5 minutes. The cell pellet was re-suspended in fresh media for the specific cell type.

## 3.7. Maintaining suspension cell lines

All six AML cell lines are suspension cells, therefore regular maintenance involved passaging the cell culture volume in 1:10 every 48 hours at approximately 90% confluency. To set up experiments, cells were withdrawn from the flask and either diluted or centrifuged at 400 x g for 5 minutes depending on the required cell number.

## 3.8. Culture vessels

For general maintenance of the AML cell lines T25 sterile tissue flasks were used with a ventilated cap. For the U87 and HEK 293FT cells T75 sterile tissue flasks were used from Corning (Loughborough, UK). For the specific assay different 96-well, 12-well and 6-well plates were used as it will be described later.

## 3.9. Cell counting

Cells were stained with Trypan Blue in a 1:1 ratio, then counted using a manual haemocytometer from Neubaurer (Paris, France). All 4 squares were accounted for and the average cell number was calculated (dead cells excluded) by the following calculation;

$$\frac{\text{(no. of cells) (dilution factor)} \times 1\text{x}10^4}{\text{(no. of squares)}} = \text{no. of cells/ml}$$

## 3.10. Cell viability assays

For the viability assays cells were seeded at a density of $1x10^4$/well cell suspension in 100 µL media at in 96 well-plate. All six AML cell line and the U87 cell line were tested in n=3, each biological replicate had 3 technical replicates. 5µl of the inhibitor solution was added to all appropriate wells to achieve the concentration of between 1nM to 10µM in an increasing dose. All the doses were plated in triplicates. A vehicle control (DMSO at 0.1%) was also included for baseline measurements.

Samples were incubated for 72 hours at 37 Celsius degree, 5% $CO_2$ atmosphere in a transparent cell culture plate. After 72 hours, the cell viability reagent, CellTiter-Glo 2.0 (Promega, Southampton, UK G9242) was added (30µl to each well). As this is a luminescence-based ATP production assay, the luminescence levels in all wells were read at 550nm excitation range on a FlexStation 2000 plate reader (Molecular Devices, Wokingham, UK).

## 3.11. Colony forming units (CFU)

To test the efficacy of SPHINX-31 and Griffin 51 clinical samples of AML were treated in a colony forming assay. Clinical samples were received from Dr Ron Stamm, from the Princess Maxima Hospital, Utrecht, The Netherlands. The samples were divided into two groups, the first group contains MLL-T cells, with known translocations and AF9, AF10, ENL and KIAA1524

oncogene. The second group contains the cells with other genetic mutations such as translocation but without the AF9 or AF10 oncogenes. Genetic data for all samples can be seen in Table 3.1.

Cells were suspended in a semi-solid media (MethoCult H4534, StemCell Technologies, Cambridge, UK) in the presence of either SPHINX-31 or Griffin 51 [300nM-3μM]. Samples ($1x10^5$ cells/1mL media) were incubated in a 24 well-plate (Starstedt, Leicester, UK) for 14 days in a cell culture incubator, at 37 Celsius degree, in 5% $CO_2$ atmosphere. After 14 days incubation, colonies were counted under a bright-field microscope (Nikon, Axio 10) and bright-field images were taken at 20x magnification. Colonies were defined as <100 cells in a tight formation. The AML cells were removed from the semi-solid media by adding cold (4° C) cell culture media (RPMI 1640, 31870074, Gibco, Paisley UK supplemented with 10% FCS (First Link, UK) and 2mM L-Glutamine, Sigma-Aldrich, G7513). The mixture was then centrifuged for 5 mins at 300 x g, the supernatant was removed, and the cell pellets were preserved and stored at -150°C for further processing.

| Lab ID | Karyotype | MLL status |
|---|---|---|
| 1584 | 47, XY, +6, t(11;19)(q23;p13), add(16)(q24), (add(22)(p1?2)) | ENL |
| 3206 | 46, XY, der(9)(p), der(10)t(10;11)(p12;q23q1?3), t(?,11)(?,q1?3)del(11)(q1?3); add(19)(p11) | AF10 |
| 4297 | 46, XY, t(9;11)(p22;q23) | AF9 |

| | | |
|---|---|---|
| 4790 | 46, XY, t(9;11) | AF9 |
| 6719 | 46, XY,a dd(3)(q?26),add(11)(q12)[18]/46,XY[1], na FISH: 46, XY?t(3;11)(q26;q12)inv(11)(q12q23) | AF10 |
| 7638 | 46, XX, t(3;11)(q12~13;q23)[20] | KIAA1524 |
| 672 | 46, XY, inv(16)(p13;q22) | |
| 2761 | 46, XX, t(15;17)(q22;q21) | |
| 5940 | t(16;16) | |
| 10349 | 46, XY, inv(16)(p13q22) | |
| 11367 | XY, t(8;21) | |
| 10347B | 45, XY, t(8;21)(q22;q22)[7] | |

***Table 3.1 Genetic data of AML samples with translocation and MLL-fused oncogenes.***

***List of primary human AML samples received from Stamm Group (Princess Maxima Hospital, The Netherlands). The first six samples carry an MLL fused AF9, AF10, ENL or KIAA1524 expression, (and therefore classed as MLL-TL), whereas samples in the last 6 rows have no detected expression levels of the AF9, AF10, ENL, KIAA1524 oncogenes and were classed as MLL-WT, although some translocations were detected. Question marks in the information sheet mark uncertain observations in the karyotype. Although karyotypes are common practice in haemato-oncology, as a way to identify genetic mutations, they are also complex and breakpoints often cannot be determined. These are depicted by question marks in the karyotypes. Sample 6719 has additional FISH (Fluorescence In Situ Hybridization) data, but it is inconclusive.***

# Molecular Biology Methods

## 3.12. Isolation of RNA

The extraction of DNA from cell lines was performed by using Tri-Reagent (Sigma-Aldrich T9424). $1x10^5$ cells/well were treated for 72 hours as described in paragraph 3.7 and 3.8 and centrifuged at 400 x g for 5 minutes than the cell pellet dissolved in 0.5mL Tri-reagent. After 5 minutes 0.1mL of chloroform was added to all samples, then vigorously shaken manually for 15 seconds, and left to stand for 5-10 minutes at RT (room temperature). The mix then were centrifuged at 12,000 x g for 15 minutes at 4°C. The RNA phase layer then was transferred to a fresh tube.

0.25mL of 2-propanol was added to the aqueous phase, and allowed to precipitate overnight at -20°C. The next day it was centrifuged at 12,000 x g for 20 minutes at 4°C to precipitate the RNA pellet. The pellets were washed with 0.5mL of 75% Ethanol, vortexed for 5 seconds and centrifuged at 7,500 x g for 5 minutes at 4°C. The RNA pellets were dried for 10 minutes at RT then the pellet was dissolved in DEPC water at room temperature.

## 3.13. RNA isolation from clinical samples

RNA extraction from clinical samples were performed by using the QIAShredder homogenisation kit (Qiagen 79656) and subsequently the QIAmp RNA Blood mini kit (Qiagen 52304) as per manufacturer's protocol. See Appendix, paragraph 12.3.

## 3.14. Quantification of nucleic acid and assessment of purity

The quality and quantity of RNA samples was measured by spectrophotometric analysis using the NanoDrop 2000 (ND2000) (Thermo Scientific, Abingdon, UK). 0.5μl of resuspended RNA sample was analysed, using NanoDrop. The ratio of absorbance is measured at 260nm and 280nm and this ratio (260/280) is used to assess the purity of the RNA. The acceptable purity level for RNA was set between 1.8-2.0.

## 3.15. cDNA synthesis

First strand cDNA synthesis was carried out from 1μg of RNA. For the synthesis PrimeScript RT-PCR kit (Takara, RR037A) was used, as per manufacturer's instructions. In brief, 1 μg of good quality (260/280 tolerance

between 1.8-2.0) total RNA was used for cDNA synthesis. To that end, 50 µM oligo dT and 100 µM Random hexamer was added in addition to the PrimeScript buffer and the mixture was incubated at 65°C for 10 minutes to melt and denature any secondary structures. Samples were snap frozen before the addition of PrimeScript RT enzyme. Samples were incubated at 25 °C for 10 minutes and 37°C for 75 minutes and stored at -20°C until required for RT-PCR.

### 3.15.1. Primer design

Genomic and cDNA sequences were obtained from the Ensemble genome browser (www.ensemble.org). All primers used throughout the study were purchased from Sigma-Aldrich. Primers were previously validated by Tzelepis *et al*. (2018).

### 3.15.2. Polymerase Chain Reaction (PCR)

Polymerase chain reaction (PCR) is an *in vitro* method of DNA synthesis (or cDNA in this case) that allows particular regions of DNA to be copied and amplified. The DNA template is first denaturated by incubating at high temperatures, then temperature is lowered and two oligonucleotide primers that flank the DNA fragment are annealed to their complementary sequences, target the sequence. The primers then extended by the Taq polymerase and

the sequence between the primers is synthesized. Multiple rounds of denaturation (cca. 35-40) annealing and extension allow for specific amplification of the sequence of interest.

## 3.16. Semi-Quantitative PCR

In reverse transcription (RT)-PCR, cDNA is used as a template in the semi quantitative PCR reaction. Primers are designed to amplify within the cDNA a copy of the mRNA sequence to be tested. That amplification is reflective of the gene expression at the transcript level. RT-PCR can be semi quantitative when equal amounts of cDNA template are used as starting material that is, in this case assessed by the ability to amplify an endogenous control gene with equal efficiencies across all of the samples. In this study, the endogenous control was Hypoxanthine-guanine phosphoribosyl transferase 1 or HPRT1 (See Appendix, paragraph 12.2) as this gene is stably expressed in leukaemia cells. Following approximate equalisation of the housekeeping gene cDNA, any observed difference between amplification of the target gene provided an indication of differences in the level of transcript expression.

Semi-quantitative (sq)RT-PCR amplification were carried out using Promega GoTaq G2 master mix containing a final reaction concentration of 10 mM Tris HCL (pH 9.0), 50 mM potassium chloride, and 0.1% Triton-X (Promega, Dorset, UK), 1.5 mM magnesium chloride, 200 µM each of dATP, dCTP, dGTP and dTTP (Promega, UK), 100 µM each of the forward and reverse primers and 1 unit of GoTaq polymerase. A master mix was prepared by

multiplying the volumes of the individual reagents required per reaction by the number of reactions being carried out. See Table 3.2.

| Name of reagent | Volumes per reaction (µL) |
|---|---|
| GoTaq B2 Mastermix | 12.5 |
| 100 µM Forward Primer | 1 |
| 100 µM Reverse Primer | 1 |
| cDNA | 1 |
| $ddH_2O$ | 9.5 |

***Table 3.2*** **PCR reagents per reaction**

Once prepared, 24 µL aliquots of the master mix were added to each reaction tube. Finally, 1 µL of the template cDNA or no template control ($ddH_2O$) was added to the appropriate universal tube giving the final reaction volume of 25 µL. Reaction cycles were carried out using BioRad QX100 thermal cycler. All sqRT-PCR amplification included a 120-minute denaturation stage at 96°C, followed by 35 cycles of denaturation, annealing and extension steps. A final extension of 15 minutes was included to terminate the reaction as shown in table 3.3. PCR products were electrophoresed on Agarose gels and visualised by ethidium bromide staining and compared to a known molecular size DNA ladder as described below.

| | Segment 1 | Segment 2 | Segment 3 |
|---|---|---|---|
| | Denaturation 96°C 10 minutes | Denaturation 96°C 30 sec | Final Elongation 72°C 15 minutes |
| | | Primer annealing 60-62°C 30 sec | |
| | | Elongation 72° 1 minute | |
| No of cycles | 1 | 35 | 1 |

*Table 3.3* ***Detailed description of the thermocycling steps for PCR***

## 3.17. Digital Droplet PCR

Digital Droplet PCR (ddPCR) is a more sensitive PCR method than qPCR or RT-PCR as the basis of the method is separating the PCR product into 20,000 water-in-oil droplets in each well (Chen et al., 2021). In every droplet, a PCR reaction is taking place, which is similar to most standard TaqMan based reactions but instead of the usual 40 cycle, in this case, it can measure 20,000 reactions. In each sample the sensor can detect the fraction of PCR positive and negative droplets, then the target DNA concentration can be calculated by Poisson distribution calculation.

The ddPCR mastermix was created by adding 10μl 2x Reaction Mix (Bio-Rad 186-3026) to 1μl probe (Life Technologies Hs00608023 BCL2 750rxn, Hs04931837 HOXA9 750rxn, Hs00153408 MYC 750rxn), 1μl cDNA (0.1μg)

and 8μl RNase free water. It was plated in single wells. 20μl of the ddPCR mastermix was transferred to the droplet generator cartridge (Bio-Rad 186-4109) and into the 'sample' row. 70μl of droplet generation oil (Bio-Rad, 186-3005) was added to the cartridge, into the 'oil' row. The cartridge was placed into the droplet generator (Bio-Rad QX200™ Droplet Generator 1864002). When finished, the content of the wells were transferred into a ddPCR plate (Bio-Rad, ddPCR™ 96-Well Plates 12001925) and sealed it with foil at 180°C for 6 seconds (Bio-Rad, Pierceable Foil Heat Seals 17005225). The plate then was transferred into a thermocycler and the following settings were used; 95°C for 10 minutes, 2.) 94°C for 30 seconds, 3.) 59°C for 1 second, 4.) step 2 for 40 cycles (on repeat) 5.) 98°C for 10 minutes, 6.) Hold at 4°C until next step. Once the PCR reaction was finished, the plate was read using the Digital Droplet Reader (Bio-Rad, QX100 Droplet Digital PCR System) provides an exact number for positive and negative hits, which then can be adjusted to the house keeping gene. After baseline calculations the number of positive hits will indicate the presence of the target gene in the sample.

## 3.18. Agarose gel electrophoresis

To enable visualisation of the products from sqPCR, gel electrophoresis was used with a 2% Agarose gel, prepared by melting 2g of Agarose (Sigma-Aldrich A9539) in 100mL of 1X TAE buffer (diluted from 50X, Merck LSKMTAE50) using a microwave oven on high power for 3 minutes or the total volume of Agarose was dissolved. The solution then was left to cool for

30 minutes, then Ethidium Bromide (Sigma-Aldrich E1385) was added at the concentration of 0.5μg/mL. The gel was then poured into a pre-prepared gel casting gel tray. A comb with the appropriate well sizes was immersed into the gel and left to fully cool at room temperature for 30 minutes for the gel to polymerise. After 30 minutes the comb was removed and the tray disassembled, the gel was immersed into a resolving tank containing 1X TAE buffer to cover the gel. 1μl of 6X loading dye was added to 5μl of nucleic acid samples, which were transferred to individual wells of the gel. Samples were subjected to electrophoresis in a Wide Mini-Sub Cell GT Cell (Bio-Rad, 1704405) attached to the appropriate power supply (Bio-Rad, PowerPac Universal Power Supply, 1645070). The process took 45 minutes at 100V to get from the negatively charged cathode to the positively charged anode, alongside 100 base pair DNA ladder (Invitrogen, 15628050) and nucleic acid fragments were detected and image by a Bio-Rad EZ Gel Doc (Bio-Rad, 1708270) system.

## 3.19. NanoBRET target engagement intracellular kinase assay

To eliminate any confounding variants, a target engagement assay was also used, which strictly focuses on a target protein and its inhibition in host cells. For CLK1, the K-5 NanoBRET™ TE Intracellular Kinase Assay (N2501, Promega, UK) was used. As there is no commercially available kit for the detection of SRPK1 levels, a new tracer (SRPKBNP-1) was developed by

Prof. Jonathan Morris (University of New South Wales) and optimised within this study.

HEK293FT cells were grown until 90% confluency in complete media (DMEM Sigma-Aldrich 6429 + 10% FCS Sigma-Aldrich F9665), detached and re-suspended in Assay media (OptiMEM™ 11058021 + 1% FCS). The cell density was adjusted to 2 x $10^5$/mL. and the DNA complex was created by mixing 9μg/mL of Transfection carrier DNA from the K-5 kit and 1μg/mL SRPK1-NanoLuc fusion vector (Custom made product from Promega, UK, the sequence is proprietary information belonging to Exonate Ltd., Cambridge, UK) or CLK-1 NanoLuc fusion vector (NV1131, Promega, UK, See plasmid map in Appendix, 12.3 Protocols) in 1mL of OptiMEM™ and mixed thoroughly. Then 30μl of FuGene® HD (E2311, Promega, UK) was added to the mixture and left to incubate for 20 mins at RT. Then 20mL of cell suspension was mixed with the 1mL DNA complex mix. 100μl cell suspension was added to each well in a white walled, clear bottom 96 well-plate (Thermo Scientific, 165306) and left to establish for 48 hours in a cell culture incubator (37°C with 5% $CO_2$).

After 48 hours the media was removed from the wells and replaced with 50μl of fresh assay media. Inhibitors were then added to the wells between 1nM to 10μM in linearly increasing concentrations. Then the appropriate tracer was diluted to 300nM final concentration in assay media supplemented with 0.1% DMSO (Sigma-Aldrich, D2650) then added to the wells. The plate was placed on an orbital shaker (Thermofisher 88882005) and incubated for 30 seconds at 100 x g. For the final incubation, the well-plate was transferred back to the

cell culture incubator and left for 2 hours. After 2 hours, 24μl NanoBRET-NanoGlo Substrate (part of the K-5 kit) was diluted in 3976μl assay media. 50μl of the diluted substrate was transferred to each well. The luminescence levels from each well were read with a FlexStation 3 (Molecular Devices, San Jose, CA, USA) plate reader at 460nm for acceptor emission and 610nm for donor emission.

The SRPKBNP-1 tracer was optimised using the same protocol only without the inhibitor treatment, the tracer concentration was between 1nM – 10μM that was added to transfected HEK 293FT cells and imaged with the appropriately diluted NanoBRET-NanoGlo substrate as per protocol. The optimal concentration of the tracer was decided based on the average mBU (BRET ratio) measurements.

# 4. Chapter

# SRPK1 inhibition in AML

## 4.1. Aims and objectives

SRPK1 has been shown to be a potentially good drug target for various drug resistant cancers. The aim of this chapter to prove the efficiency of SPHINX-31, a highly selective SRPK1 inhibitor in reducing common downstream targets such as MYC, HOXA9 and BCL-2 in AML. In addition, cell viability data is also presented to assess the efficacy of SPHINX-31 in reducing cell proliferation in response to treatment.

## 4.2. Introduction

Tzelepis et al. (2016) used a CRISPR knockout model to identify genetic vulnerabilities in AML. AML is a commonly drug resistant disease, which has a high relapse and mortality rate. They identified previously published drug targets such as DOT1L, BCL2 and MEN1 and showed that AML cell lines with an AF9 translocation (such as the OCI-AML2) were the most sensitive to inhibitor treatment and showed a down regulation of BCL2 (Tzelepis *et al.*, 2016). From then on, the same group (Tzelepis *et al.*, 2016) identified SRPK1 as a genetic vulnerability of AML, which then meant that a highly selective SRPK1 inhibitor was able to significantly decrease cell viability in *in vitro* studies and reduce tumour burden in *in vivo* experiments. As predicted, they also confirmed a genetic vulnerability for cell lines with MLL rearrangements (AF9 or AF6 oncogenes). The same study identified an isoform change of BRD4 as a result of SPHINX-31 treatment. BRD4 can be expressed as a pro-

tumourigenic short isoform (BRD4s) and as an anti-tumourigenic long isoform (BRD4l). The study compared known BRD4 inhibitors, such as iBET-151 to SPHINX-31 and showed that SPHINX-31 was equally successful in reducing colony forming efficiency in *in vitro* studies, in wild-type samples. The same research group later showed that cell lines with the AF9 oncogene were much more vulnerable to SPHINX-31 treatment than the AML cell lines without a translocation and the AF9 oncogene (Tzelepis *et al.*, 2018).

## 4.3. Downstream targets after SPHINX-31 treatment in AML cell lines

To determine whether SRPK1 inhibition was able to inhibit expression of downstream targets, AML cell lines were treated with SPHINX-31 for 72 hours in a cell culture incubator (37° C, 5% $CO_2$) in increasing levels (with 0.1% DMSO as a vehicle control in cell culture media). Cells then were harvested and the expression levels of MYC, HOXA9 and BCL2 were measured with ddPCR (See Fig. 4.1- 4.6). Expression levels were adjusted to the housekeeping gene, HPRT-1. Figure 4.1. (A) shows that SRPK1 inhibition significantly reduced MYC expression in THP1 cells ($IC_{50}$ 25.32 nM). Figure 4.1. (B) shows that SRPK1 inhibition reduced HOXA9 expression in THP1 cells ($IC_{50}$ 6.55 nM). These results indicate that S31 inhibits expression of downstream targets of BRD4 in THP1 cells. Fig. 4.1. (C) also shows that SPHINX-31 was successful in reducing the expression levels of BCL-2 in THP-1 cells ($IC_{50}$ 84.35 nM).

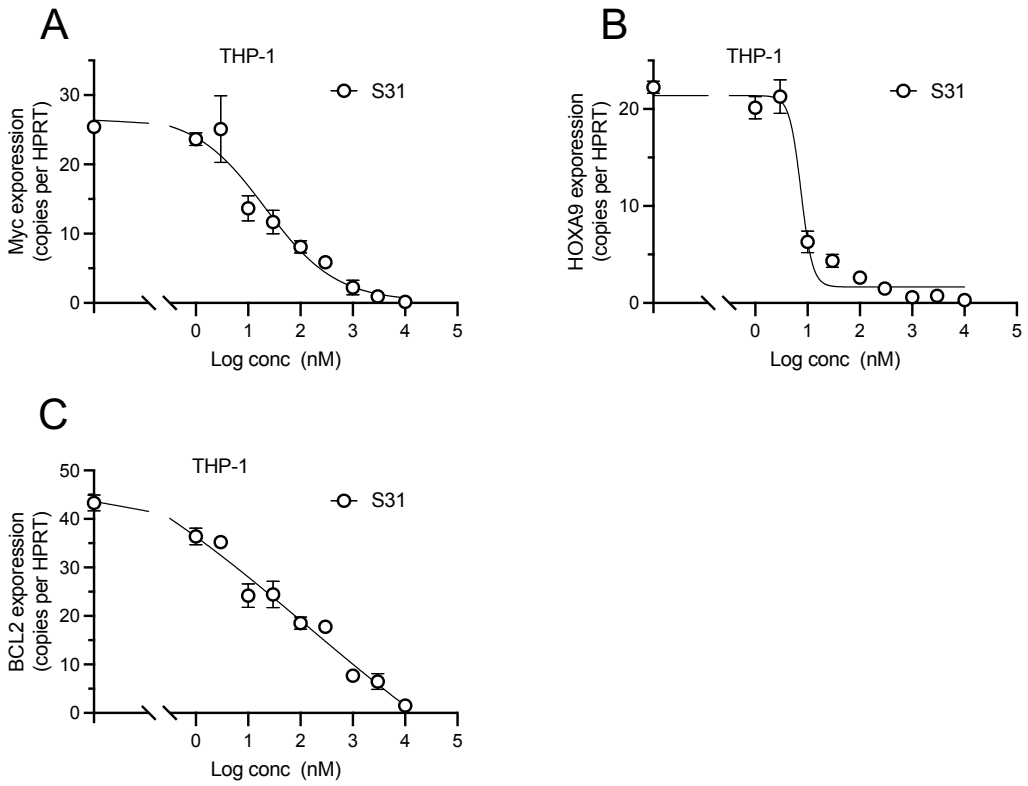



***Figure 4.1. Downstream target levels in THP-1 cells after SPHINX-31 treatment***

***Downstream target levels after 72 hours SPHINX-31 (S31) treatment in THP-1 cells, measured by assessing the MYC, BCL-2 and HOXA9 expression levels, using ddPCR. All measurements were normalised to HPRT-1 housekeeping gene. Data represents the average of three biological replicates (n=3), which each were measured from three technical repeats. 4.1.(A) MYC expression levels after 72 hours of SPHINX-31 treatment ($IC_{50}$ 25.32 nM), 4.1.(B) HOXA9 expression levels after 72 hours of SPHINX-31 treatment ($IC_{50}$ 6.548 nM), 4.1.(C) BCL-2 expression levels after 72 hours of SPHINX-31 treatment ($IC_{50}$ 84.35 nM).***

OCI-AML2 cells, also with an MLL translocation showed similar reduction in downstream targets as the THP-1 cells shown above. Fig.4.2. (A) shows that MYC levels are reduced in response to rising concentrations of S31 in OCI-AML2 cells ($IC_{50}$ 14.22 nM). Fig.4.2. (B) shows the reduced levels of HOXA9 in OCI-AML-2 in response to rising concentrations of S31 ($IC_{50}$ 3.783 nM). Finally, Fig.4.2. (C) shows the similarly reduced BCL-2 levels in the same cell line ($IC_{50}$ 0.4419 nM).

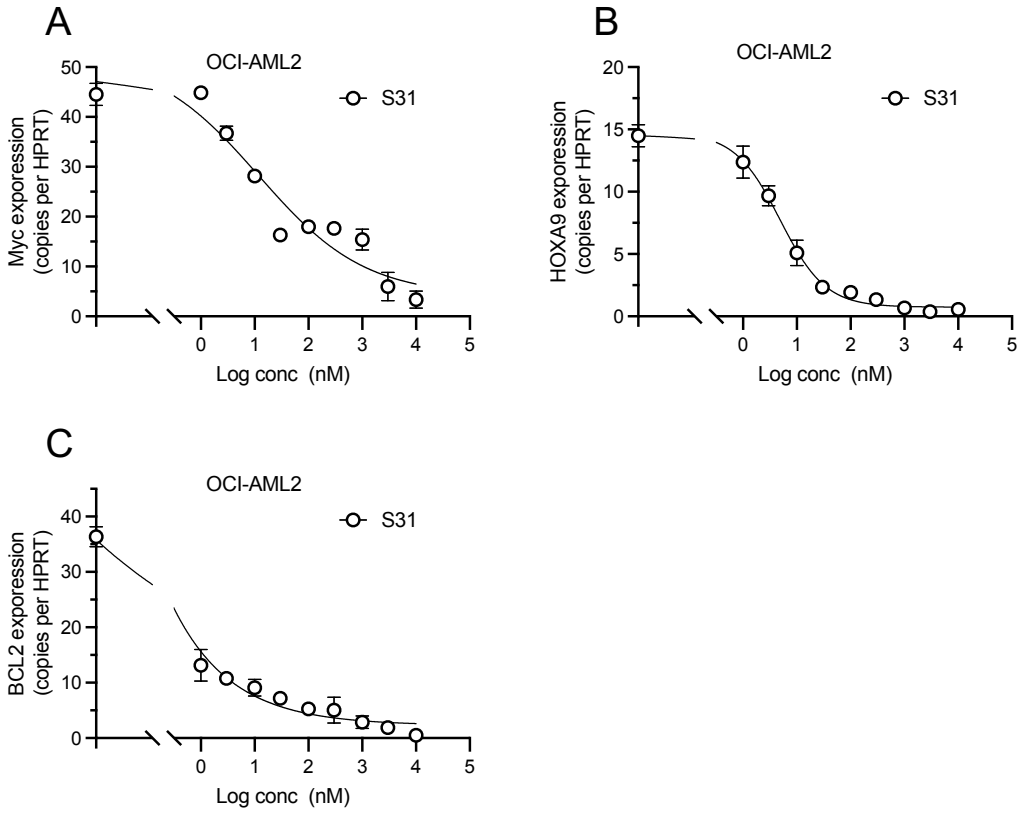



***Figure 4.2. Downstream target levels in OCI-AML2 cells after SPHINX-31 treatment***

***Downstream target levels after 72 hours SPHINX-31 (S31) treatment in OCI-AML2 cells, measured by assessing the MYC, BCL-2 and HOXA9 expression levels, using ddPCR. All measurements were normalised to HPRT-1 housekeeping gene. Data represents the average of three biological replicates (n=3), which each were measured from three technical repeats. 4.2.(A) MYC expression levels after 72 hours of SPHINX-31 treatment ($IC_{50}$ 14.22 nM). 4.2.(B) HOXA9 expression levels after 72 hours of SPHINX-31 treatment ($IC_{50}$ 3.783 nM). 4.2.(C) BCL-2 expression levels after 72 hours of SPHINX-31 treatment ($IC_{50}$ 0.4419 nM).***

Fig.4.3. (A) shows the reduced MYC expression levels in MOLM-13 ($IC_{50}$ 95.10 nM), the third translocated AML cell line. Fig.4.3. (B) shows a similarly sizeable reduction in HOXA9 levels ($IC_{50}$ 9.021 nM), whereas Fig.4.3. (C) demonstrates the decreased levels of BCL-2 in MOLM-13 cells ($IC_{50}$ 6.612 nM).

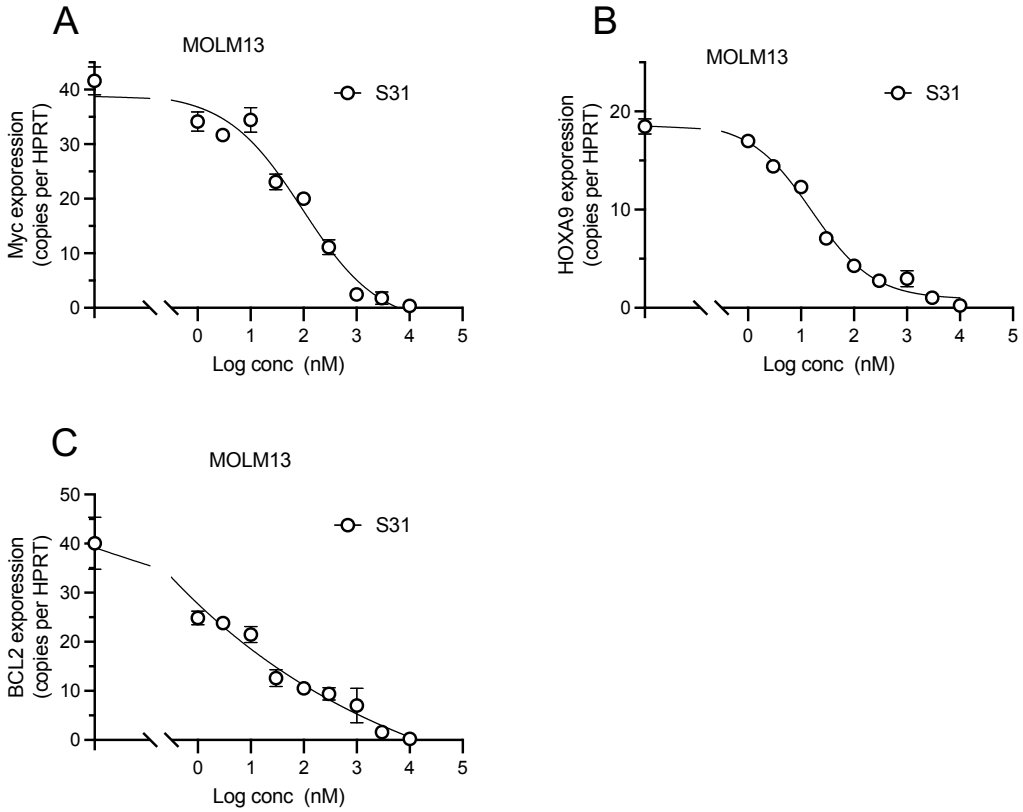



***Figure 4.3. Downstream target levels in MOLM-13 cells after SPHINX-31 treatment***

***Downstream target levels after 72 hours SPHINX-31 (S31) treatment in MOLM-13 cells, measured by assessing the MYC, BCL-2 and HOXA9 expression levels, using ddPCR. All measurements were normalised to HPRT-1 housekeeping gene. Data represents the average of three biological replicates (n=3), which each were measured from three technical repeats. 4.3.(A) MYC expression levels after 72 hours of SPHINX-31 treatment ($IC_{50}$ 95.10 nM). 4.3.(B) HOXA9 expression levels after 72 hours of SPHINX-31 treatment ($IC_{50}$ 9.021 nM), 4.3.(C) BCL-2 expression levels after 72 hours of SPHINX-31 treatment ($IC_{50}$ 6.612 nM).***

Fig.4.4. (A) demonstrates the effect of SPHINX-31 on MYC expression, in OCI-AML3 cells ($IC_{50}$ 240.2 nM), one of the non-translocated AML cell lines. Fig.4.4. (B) shows a similar reduction in HOXA9 levels in response to increasing levels of SPHINX-31 treatment ($IC_{50}$ 12.94 nM). Fig. 4.4. (C) demonstrated the levels of BCL-2 in OCI-AML3 cells after treatment ($IC_{50}$ 12.74 nM).

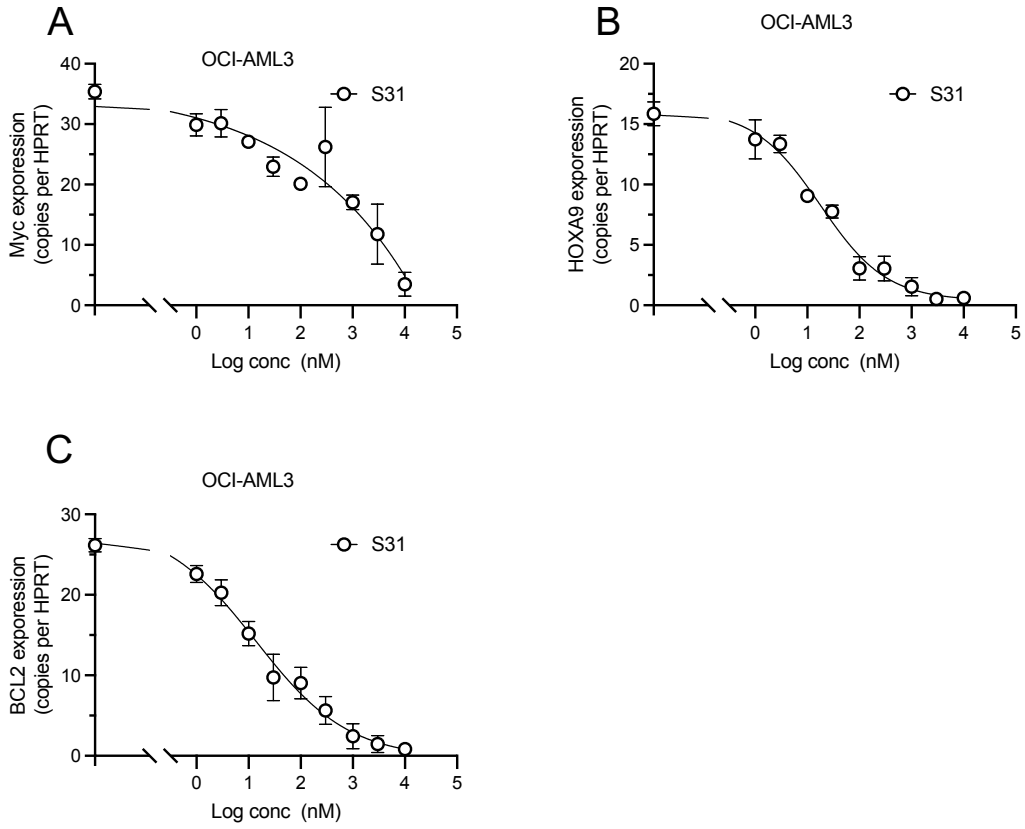



***Figure 4.4. Downstream target levels in OCI-AML3 cells after SPHINX-31 treatment***

***Downstream target levels after 72 hours SPHINX-31 (S31) treatment in OCI-AML3 cells, measured by assessing the MYC, BCL-2 and HOXA9 expression levels, using ddPCR. All measurements were normalised to HPRT-1 housekeeping gene. Data represents the average of three biological replicates (n=3), which each were measured from three technical repeats. 4.4.(A) MYC expression levels after 72 hours of SPHINX-31 treatment ($IC_{50}$ 240.2 nM). 4.4.(B) HOXA9 expression levels after 72 hours of SPHINX-31 treatment ($IC_{50}$ 12.94 nM). 4.4.(C) BCL-2 expression levels after 72 hours of SPHINX-31 treatment ($IC_{50}$ 12.74 nM).***

HL60, the next non-translocated AML cell line showed a very similar response than the OCI-AML3 cells, shown above. Fig.4.5. (A) represents the decreasing levels of MYC levels in HL60 cells ($IC_{50}$ 30.15 nM). Fig.4.5. (B) shows the reduction in HOXA9 levels after treatment ($IC_{50}$ 6.798 nM). And Fig.4.5. (C) demonstrated the decrease in BCL-2 levels after S31 treatment ($IC_{50}$ 16.75 nM).

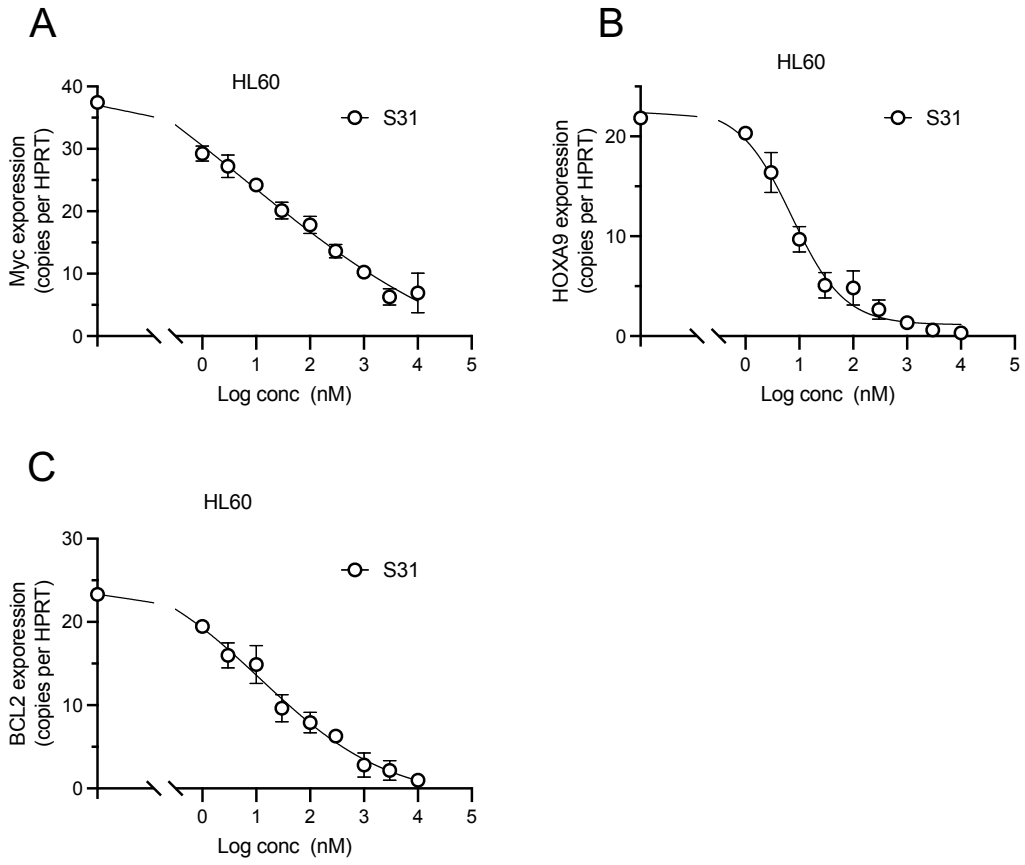



***Figure 4.5. Downstream target levels in HL60 cells after SPHINX-31 treatment***

***Downstream target levels after 72 hours SPHINX-31 (S31) treatment in HL60 cells, measured by assessing the MYC, BCL-2 and HOXA9 expression levels, using ddPCR. All measurements were normalised to HPRT-1 housekeeping gene. Data represents the average of three biological replicates (n=3), which each were measured from three technical repeats. 4.5.(A) MYC expression levels after 72 hours of SPHINX-31 treatment ($IC_{50}$ 30.15 nM). 4.5.(B) HOXA9 expression levels after 72 hours of SPHINX-31 treatment ($IC_{50}$ 6.798 nM. 4.5.(C) BCL-2 expression levels after 72 hours of SPHINX-31 treatment ($IC_{50}$ 16.75 nM).***

TF1a cells responded similarly to SPHINX-31 treatment as the other two non-translocated cell line, displaying a significant drop in MYC expression, as it is shown in Fig.4.6. (A) ($IC_{50}$ 9.425 nM). HOXA9 expression levels were also significantly reduced as it is shown in Fig.4.6. (B) ($IC_{50}$ 10.75 nM). BCL-2 expression levels were significantly reduced even in the nanomolar range ($IC_{50}$ 21.37 nM), as it can be seen in Fig.4.6. (C).

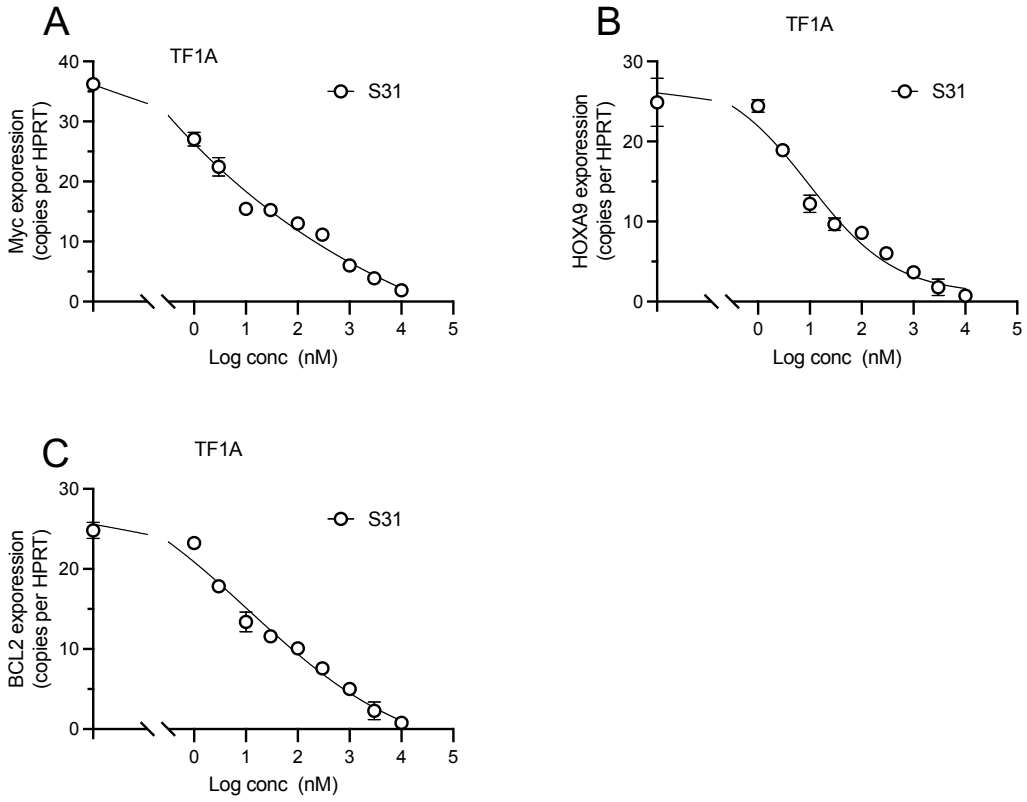



***Figure 4.6. Downstream target levels in TF1a cells after SPHINX-31 treatment***

***Downstream target levels after 72 hours SPHINX-31 (S31) treatment in TF1a cells, measured by assessing the MYC, BCL-2 and HOXA9 expression levels, using ddPCR. All measurements were normalised to HPRT-1 housekeeping gene. Data represents the average of three biological replicates (n=3), which each were measured from three technical repeats. 4.6.(A) MYC expression levels after 72 hours of SPHINX-31 treatment ($IC_{50}$ 9.425 nM). 4.6.(B) HOXA9 expression levels after 72 hours of SPHINX-31 treatment ($IC_{50}$ 10.75 nM. 4.6.(C) BCL-2 expression levels after 72 hours of SPHINX-31 treatment ($IC_{50}$ 21.37 nM).***

## 4.4. Cell viability assay

Following the successful treatment of AML cell lines with SPHINX-31 to reduce the levels of MYC, HOXA9, and BCL-2 expression, all 6 AML cell lines were treated with increasing levels of SPHINX-31 in regular *in vitro* conditions (37°C, 5% $CO_2$ atmosphere) for 72 hours. Then an ATP-based reagent, Cell-Titer Glo 2.0 was used to assess the viability levels. Fig.4.7. (A) shows that

SPHINX-31 did not have an obvious effect on cell viability in OCI-AML3 cells. Since all measurements were adjusted to the vehicle control, in some groups the viability levels increased above 100%, as it can be seen below. Fig.4.7. (B) shows the big variability in the viability levels of MOLM-13 cells, and the greatest effect in response to SPHINX-31 treatment. Fig.4.7. (C) shows no response to treatment in HL60 cells. Fig.4.7. (D) similarly demonstrates no effect to treatment in OCI-AML2 cells. Continuing with this trend, Fig.4.7. (E) shows that TF1a cells had no decrease in viability levels in response to treatment. In Fig.4.7. (F) it can be seen that THP-1 cells were not affected by treatment, although they displayed a significant standard error of mean (SEM). As a summary, 4.7. (G) shows the effect of SPHINX-31 in all the six different cell lines and that MOLM-13 cells are the most sensitive to S31 treatment ($IC_{50}$ 9753 nM). Due to viability levels increasing above 100% in some treatment groups, $IC_{50}$ values were not available for the other cell lines.

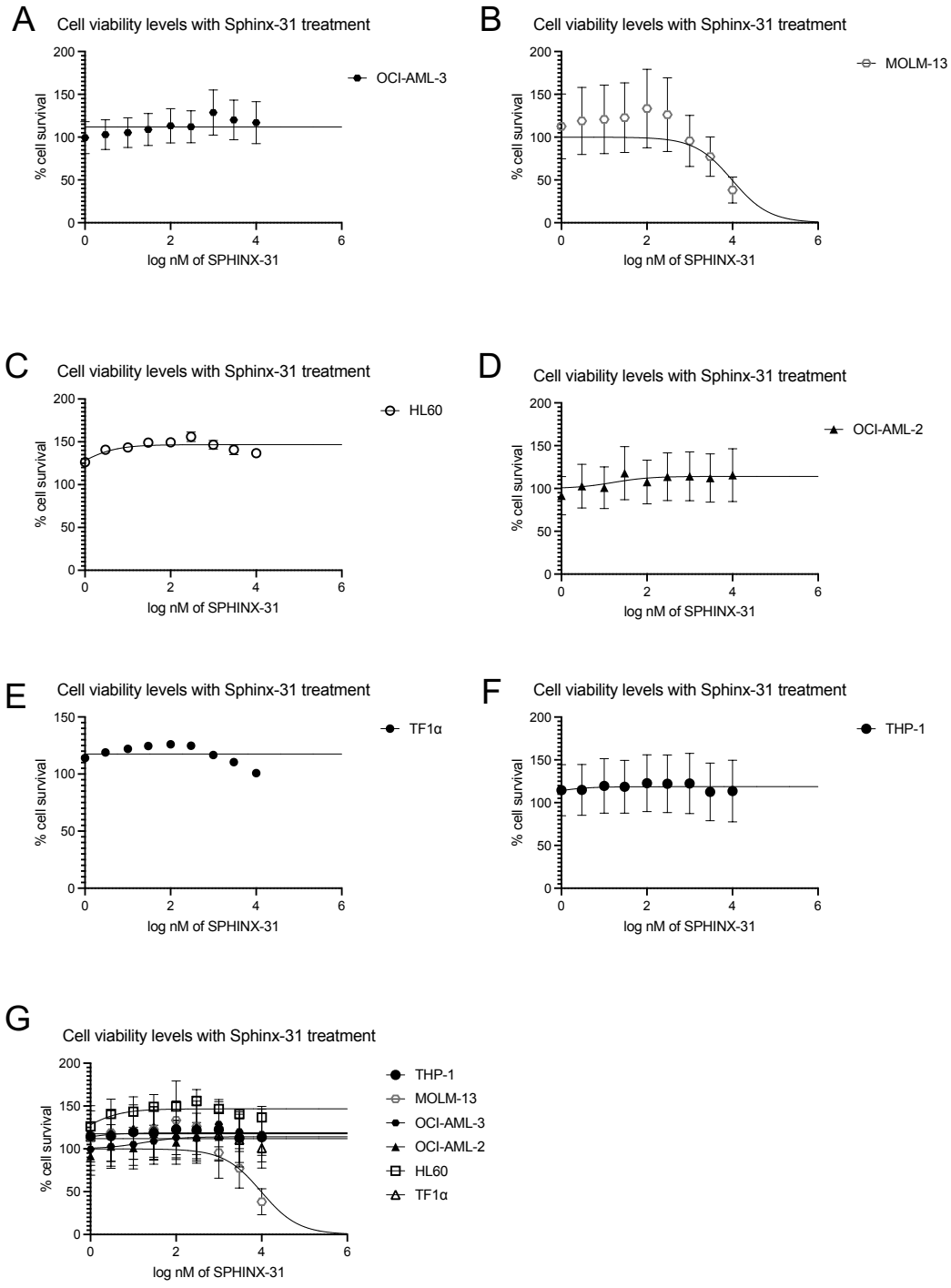



***Figure 4.7. Cell viability levels in AML cell lines after SPHINX -31 treatment***

***Fig. 4.7. (A) OCI-AML3 (MLL-WT ) cells after 72 hours SPHINX -31 treatment. 4.7. (B) MOLM-13 cells (MLL-TL) after SPHINX -31 treatment, ($IC_{50}$ 9753 nM). 4.7. (C) HL60 (MLL-WT ) cells after SPHINX -31 treatment. 4.7. (D) OCI-AML2 (MLL-TL)cells after SPHINX -31 treatment. 4.7. (E) Tf1a (MLL-WT ) cells after SPHINX -31 treatment. Error bars were calculated but cannot be displayed due to the lack of SEM. 4.7. (F) THP-1 (MLL-TL) cells after Sphinx-31 treatment. 4.7. (G) Summarised cell viability levels after Sphinx-31 treatment from in AML cell lines. All values were normalised to the vehicle control group (DMSO 0.1%), averages presented from three biological replicates (n=3) which each was calculated from three technical replicates.***

## 4.5. Discussion

SPRK1 has been established to be a potentially good therapeutic target for various cancers both in solid tumours and hard to treat cancers such as leukaemia. SRPK1 inhibition has been shown to have an anti-tumoural effect in prostate cancer, breast cancer, lung cancer and gliomas (Bullock and Oltean, 2017). SPHINX -31, a highly selective SRPK1 inhibitor proved to be an interesting drug candidate to target cancer cells. In a previous study (Tzelepis *et al.*, 2018) showed the vulnerability of AML cell lines and especially, the vulnerability of MOLM-13 cells to SPHINX -31 treatment. In contrast with the results published by Tzelepis *et al.* (2018), there was no difference in the effect of SPHINX-31 in the MLL-TL vs. MLL-WT group in this data presented here. It is worth noting that in their study they used a 6-day treatment regimen and a split back method which does not account for the dilution of compound by adding fresh media to the wells. In this study, a 3-day treatment was used, where the dosage of compound and number of cells can be strictly controlled.

In a study of PC-3 prostate cancer cells treated with SPHINX -31, a decreased tumour growth was observed in an *in vivo* model of PCa (Mavrou *et al.*, 2015) but did not affect cell viability. The same has been shown in melanoma cells (Gammons *et al.*, 2013). In endometrial carcinoma 5μM of SPHINX -31 treatment could not achieve a significant reduction in cell viability, but it was significantly more effective in combination with 1μM Lapatinib (GlaxoSmith Kline, $C_{29}H_{26}ClFN_4O_4S$) (Kurimchak *et al.*, 2020). In this study the effect of

SRPK1 inhibition is significant in AML cells, when compared to the control group. It significantly reduced BCL2, HOXA9 and MYC expression but it does not induce cell death. A similar result was observed in other studies, where SRPK1 inhibition alters gene expression (e.g. VEGF splicing) to reduce tumour growth but not necessarily induces cell death (Gammons *et al.*, 2013).

### 4.5.1. Downstream target levels after SPHINX-31 treatment

MYC, HOXA9 and BCL-2 are all known oncogenes that have high expression levels in cancer, and especially in haematological malignancies (Perini *et al.*, 2018). Previous studies showed that the inhibition of any or all of these oncogenes could be a therapeutic regimen for hard to treat types of cancers (Cerella *et al.*, 2017). The data presented here demonstrates that SPHINX-31 can significantly reduce the expression levels of MYC, HOXA9 and BCL-2 across all six AML cell lines, regardless of their translocation status. The fact that this could be done in both MLL translocated and non-translocated suggests that it is acting on a change in expression of a common upstream regulator, such as ATF4 (Wortel *et al.*, 2017).

### 4.5.2. Cell viability levels in response to treatment

In terms of cell viability, SPHINX-31 did not have a significant effect when adjusted to the vehicle control group. The cell line with the greatest drop in

viability was the MOLM-13 (MLL-TL) cell line ($IC_{50}$ 9753 nM), which is in line with previous findings (Tzelepis *et al.*, 2018). It should be noted that the treatment duration in this study was 3 days, whereas other studies used 6 day or longer treatments. We decided to treat for 3 days as it was the ideal length for the compound to have an effect but also to keep the number of cells in the wells at an optimal density. As other studies noted, after 3 days cells either need to be split back or the experiment to be terminated as the number of cells (especially in the control group) exceeds the volume capacity of the well and the lack of nutrients and oxygen triggers an artefact reaction. It is possible that in order to achieve a significant reduction in cell viability levels a 6-day treatment is required. We made a couple of attempts to create a 6-day treatment by systematically checking the number of cells in the wells and replenish the cell media with appropriate concentrations of treatment. However, the data did not support previous findings, and for the reasons mentioned above, the 3-day treatment regimen was implemented.

# 5. Chapter

# BRD4 Splice change in response to SPHINX-31 treatment

## 5.1. Aims and objectives

In this chapter the aim was to look at the splice change of BRD4 in response to inhibitor treatment. BRD4 isoform change in AML cell lines was reported in (Tzelepis *et al.*, 2018) in response to SPHINX-31. BRD4 has been found to have two isoforms, a short pro-oncogenic (BRD4s) and a long isoform (BRD4l), which is anti-angiogenic, which in turn provides a tumour suppressor function. By switching from BRD4s isoform to the BRD4l isoform, BRD4 splicing could become a drug target in AML. In other cancers the same change was observed; Wu et al. showed that BRD4s in breast cancer is oncogenic, whilst BRD4l is tumour-suppressive (Wu *et al.*, 2020).

## 5.2. Introduction

In this study, 6 AML cell lines were treated (w/o MLL translocation) with SPHINX-31 to trigger a splice change in BRD4. Expression of BRD4s, BRD4l and HPRT-1 was determined by RT-PCR and visualized on a 2% gel by agarose gel electrophoresis (Fig.5.1 - 5.6). The expected band sizes were 206 bp for BRD4s and 488 bp for BRD4l. HPRT-1 was used as a positive control for RNA extraction and cDNA generation, which produces a band at 101 bp. Optical density was measured using Image Studio (LI-COR Biotechnology, Cambridge, UK). Data from all 6 cell lines was collected and it shows a difference in intensity between the two BRD4 isoforms (BRD4s -

BRD4L) normalised to HPRT-1. Primer sequences can be found in the Appendix 12.1.

## 5.3. Results

RT-PCR data shows that with increasing concentration of SPHINX-31, the expression level of BRD4s decreases and the level of BRD4l increases in the treatment groups. Meanwhile, the housekeeping gene, HPRT-1 was unaffected. The data is presented according to the MLL translocation status of each cell line, starting from the MLL-translocated cell lines MOLM-13, THP-1, OCI-AML2, followed by the MLL-wildtype; OCI-AML3, HL60 and TF1a.

Fig.5.1. (A) below shows the effect of SPHINX-31 treatment on the BRD4 isoform change in MOLM-13 cells ($IC_{50}$ 133.1 nM). It can be seen that in the micromolar range the pro-tumourigenic BRD4s isoform was almost non-existent, and the tumour supressor BRD4l isoform is predominant. Fig.5.1. (B) shows the difference of the two isoforms in response to increasing levels of inhibitor treatment. Fig.5.1. (C) shows the normalised level of difference in the expression of the two isoform.

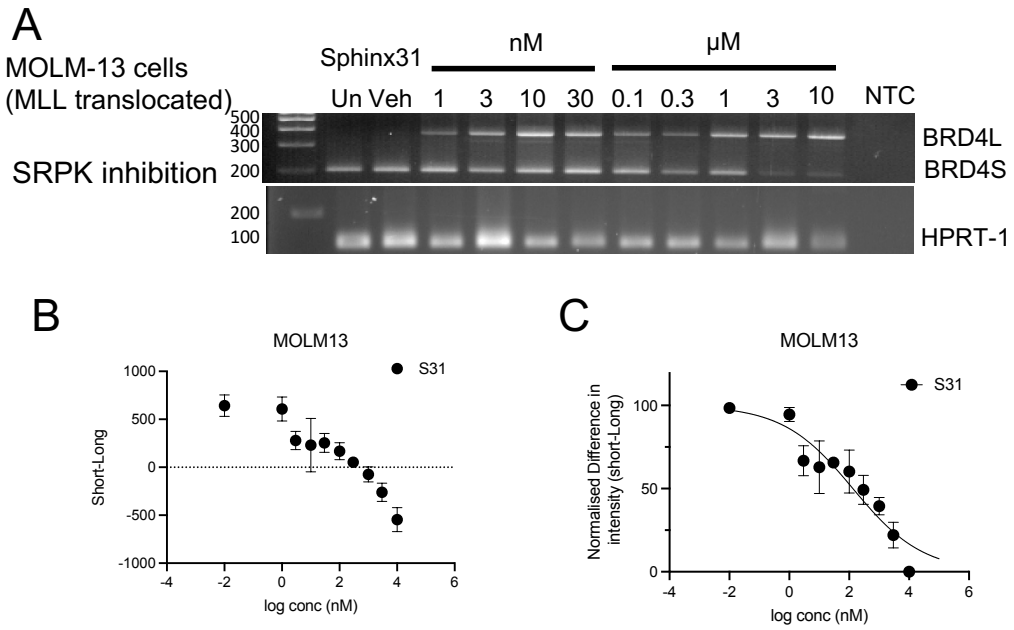



***Figure 5.1. BRD4 splice change in MOLM-13 cells after SPHINX31 treatment***

***Fig.5.1. (A) BRD4s, BRD4l and HPRT-1 expressions in MOLM-13 cells (MLL-TL), after 72 hours of SPHINX-31 treatment visualised on a 2% agarose gel ($IC_{50}$ 133.1 nM). Figure 5.1. (B) Difference in expression of BRD4s- BRD4l in MOLM-13 cells after 72 hours of SPHINX-31 treatment. Fig.5.1 (C) Normalised levels of expression between BRD4s-BRD4l isoform after 72 hours of SPHINX-31 treatment, the difference in expression was normalised to the vehicle control (i.e., 100% BRD4s) and the highest concentration (i.e. 100% BRD4L expression). Expressions of BRD4s, BRD4l and HPRT-1 in MOLM13 cell line was determined by RT-PCR and visualized on a 2% gel by agarose gel electrophoresis. The expected band sizes were, BRD4s: 206 bp and BRD4l: 488 bp, HPRT-1: 101 bp. The optical density was measured using Image Studio. All data points represent three biological replicates (n=3), which each were calculated using three technical replicates.***

In Fig.5.2 (A) THP-1, another MLL-translocated cell line shows a decreasing level of BRD4s as the SPHINX-31 concentration rises in the sample, ($IC_{50}$ 36.03 nM). Fig.5.2 (B) shows a decreasing level of Short:Long ratio, and in Fig.5.2 (C) can be seen that the normalized level of Short-Long isoform ratio displays a strong dose response curve.

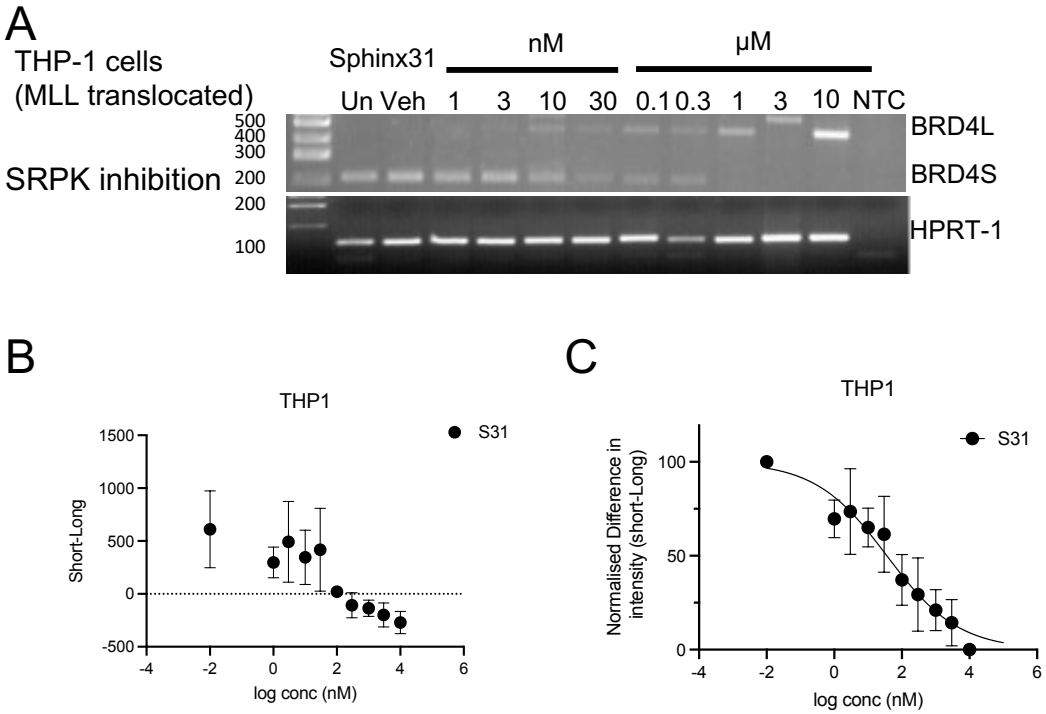



***Figure 5.2. BRD4 splice change in THP-1 cells after SPHINX31 treatment***

***Fig.5.2 (A) BRD4s, BRD4l and HPRT-1 expressions in THP-1 cells (MLL-TL), after 72 hours of SPHINX-31 treatment visualised on a 2% agarose gel ($IC_{50}$ 36.03 nM). Figure 5.2 (B) Difference in expression of BRD4s- BRD4l in THP-1 cells after 72 hours of SPHINX-31 treatment. Fig.5.2 (C) Normalised levels of expression between BRD4s-BRD4l isoform after 72 hours of SPHINX-31 treatment, the difference in expression was normalised to the vehicle control (i.e., 100% BRD4s) and the highest concentration (i.e. 100% BRD4L expression). Expressions of BRD4s, BRD4l and HPRT-1 in THP-1 cell line was determined by RT-PCR and visualized on a 2% gel by agarose gel electrophoresis. The expected band sizes were, BRD4s: 206 bp and BRD4l: 488 bp, HPRT-1: 101 bp. The optical density was measured using Image Studio. All data points represent three biological replicates (n=3), which each were calculated using three technical replicates.***

Fig.5.3 (A) shows that in OCI-AML2 cells, BRD4s does not disappear completely but gets significantly reduced in the μM range of treatment ($IC_{50}$ 54.42 nM). Fig.5.3 (B) shows that the ratio of Short vs. Long isoform reduces significantly and in Fig.5.3 (C) it can be seen that when the Short-Long isoforms were normalised to the base line, there is a strong response to inhibitor treatment.

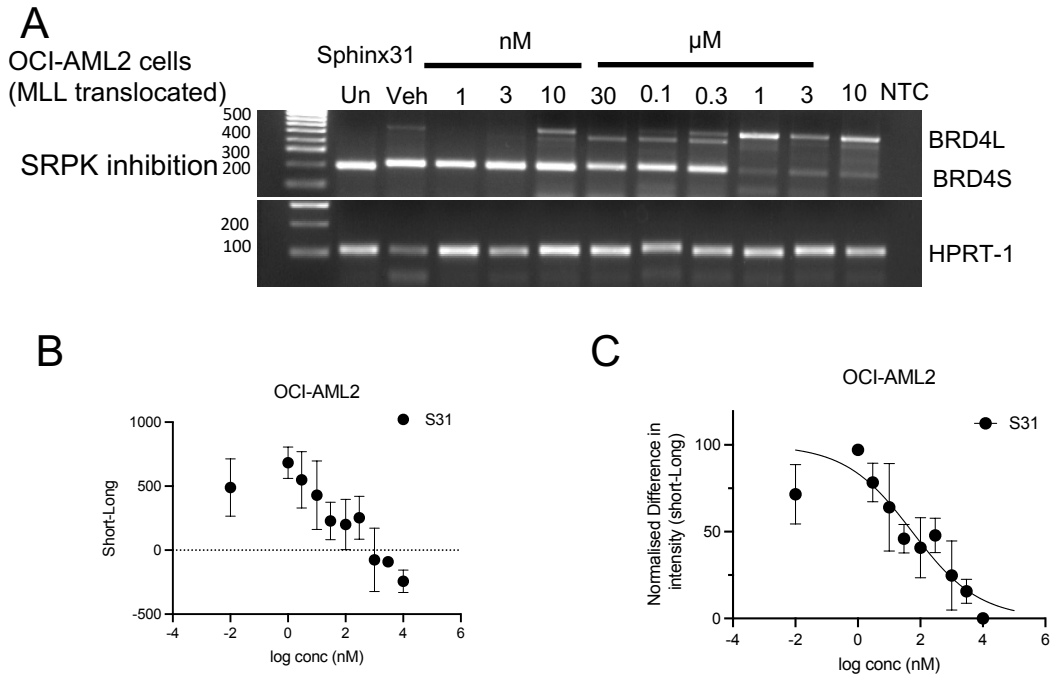



***Figure 5.3. BRD4 splice change in OCI-AML2 cells after SPHINX31 treatment***

***Fig.5.3 (A) BRD4s, BRD4l and HPRT-1 expressions in OCI-AML2 cells (MLL-TL), after 72 hours of SPHINX-31 treatment visualised on a 2% agarose gel ($IC_{50}$ 54.42 nM). Figure 5.3 (B) Difference in expression of BRD4s- BRD4l in OCI-AML2 cells after 72 hours of SPHINX-31 treatment. Fig.5.3 (C) Normalised levels of expression between BRD4s-BRD4l isoform after 72 hours of SPHINX-31 treatment, the difference in expression was normalised to the vehicle control (i.e., 100% BRD4s) and the highest concentration (i.e. 100% BRD4L expression). Expressions of BRD4s, BRD4l and HPRT-1 in OCI-AML2 cell line was determined by RT-PCR and visualized on a 2% gel by agarose gel electrophoresis. The expected band sizes were, BRD4s: 206 bp and BRD4l: 488 bp, HPRT-1: 101 bp. The optical density was measured using Image Studio. All data points represent three biological replicates (n=3), which each were calculated using three technical replicates.***

The splice change in the TF1a (MLL-WT) cells are not as pronounced as in the MLL-TL cells, as it can be seen from Fig.5.4 (A) ($IC_{50}$ 83.61 nM). It is clear that the ratio of Short:Long decreases in response to rising concentrations of S31 treatment, as it is shown in Fig.5.4 (B). Finally, Fig.5.4 (C) shows the full effect of inhibitor treatment after the Short-Long ratio was normalised to the baseline.

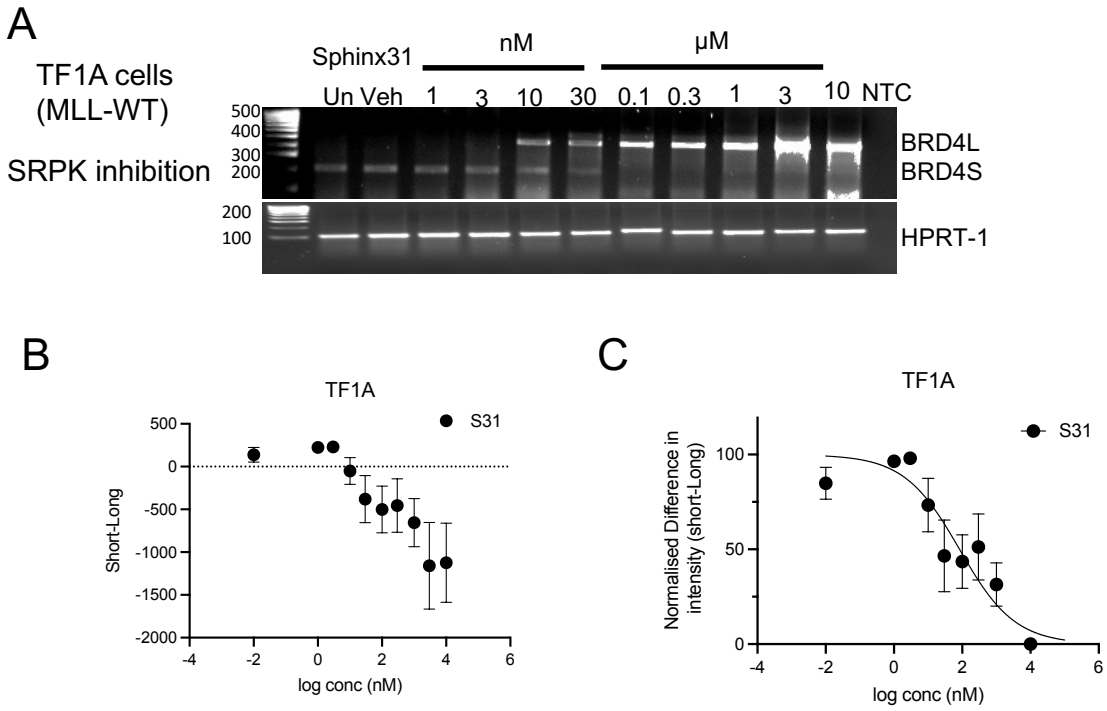



***Figure 5.4. BRD4 splice change in TF1a cells after SPHINX31 treatment***

***Fig.5.4 (A) BRD4s, BRD4l and HPRT-1 expressions in TF1a cells (MLL-WT), after 72 hours of SPHINX-31 treatment visualised on a 2% agarose gel ($IC_{50}$ 83.61 nM). Figure 5.4 (B) Difference in expression of BRD4s- BRD4l in TF1a cells after 72 hours of SPHINX-31 treatment. Fig.5.4 (C) Normalised levels of expression between BRD4s-BRD4l isoform after 72 hours of SPHINX-31 treatment, the difference in expression was normalised to the vehicle control (i.e., 100% BRD4s) and the highest concentration (i.e. 100% BRD4L expression). Expressions of BRD4s, BRD4l and HPRT-1 in Tf1a cell line was determined by RT-PCR and visualized on a 2% gel by agarose gel electrophoresis. The expected band sizes were, BRD4s: 206 bp and BRD4l: 488 bp, HPRT-1: 101 bp. The optical density was measured using Image Studio. All data points represent three biological replicates (n=3), which each were calculated using three technical replicates.***

The HL60 cell line that displayed double bands in the BRD4l expression levels, as it is shown in Fig.5.5 (A), with an $IC_{50}$ value of 20.61 nM, herefore the Short-Long ratio does not show a clear reduction but a reducing trend in response to treatment, as it can be seen from Fig.5.5 (B). Fig.5.5 (C) shows the normalised ratio of Short-Long isoform in response to increasing levels S31 treatment.

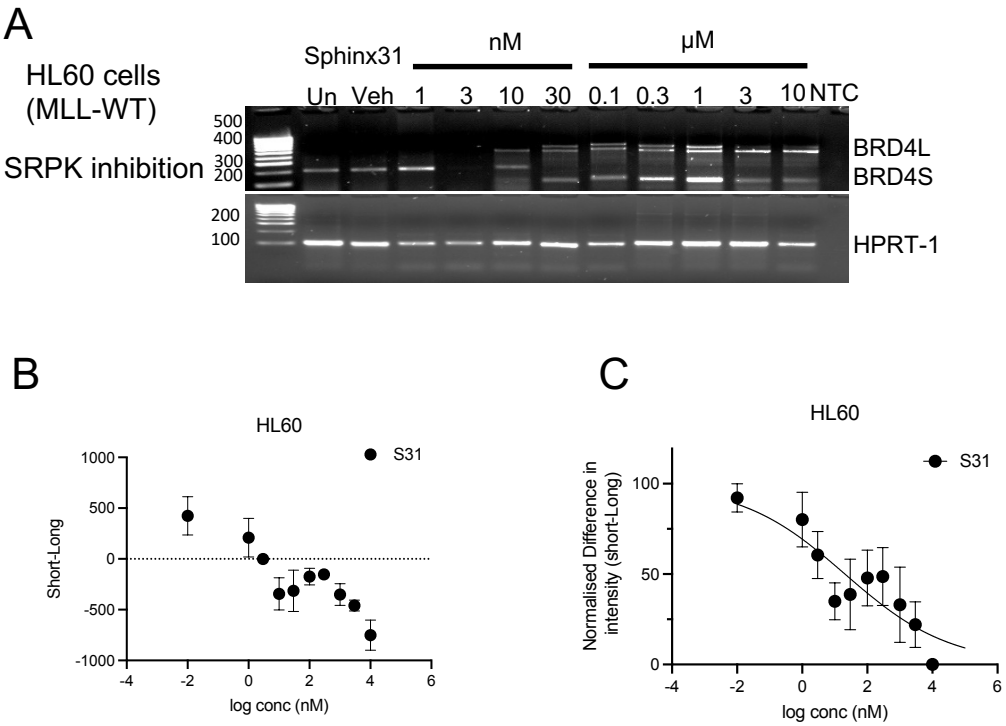



***Figure 5.5. BRD4 splice change in HL60 cells after SPHINX31 treatment***

***Fig.5.5. (A) BRD4s, BRD4l and HPRT-1 expressions in HL60 cells (MLL-WT), after 72 hours of SPHINX-31 treatment visualised on a 2% agarose gel ($IC_{50}$ 20.61 nM). Figure 5.5 (B) Difference in expression of BRD4s- BRD4l in HL60 cells after 72 hours of SPHINX-31 treatment. Fig.5.5 (C) Normalised levels of expression between BRD4s-BRD4l isoform after 72 hours of SPHINX-31 treatment, the difference in expression was normalised to the vehicle control (i.e., 100% BRD4s) and the highest concentration (i.e. 100% BRD4L expression). Expressions of BRD4s, BRD4l and HPRT-1 in HL60 cell line was determined by RT-PCR and visualized on a 2% gel by agarose gel electrophoresis. The expected band sizes were, BRD4s: 206 bp and BRD4l: 488 bp, HPRT-1: 101 bp. The optical density was measured using Image Studio. All data points represent three biological replicates (n=3), which each were calculated using three technical replicates.***

In the OCI-AML3 cells, the expression of BRD4s completely disappears in the 10μM treatment group as it is shown in Fig.5.6 (A) ($IC_{50}$ 40.39 nM). Fig.5.6 (B) shows the decreasing levels of Short-Long ratio in response to treatment, whereas Fig.5.6 (C) shows the normalised ratio of the Short-Long isoform ratio.

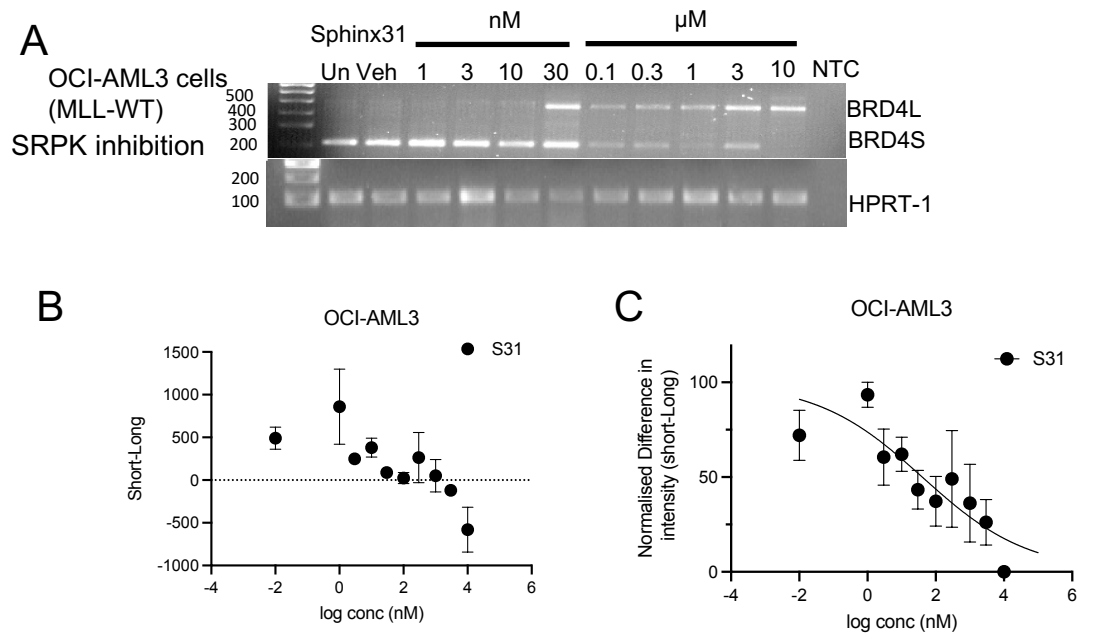



***Figure 5.6. BRD4 splice change in OCI-AML3 cells after SPHINX31 treatment***

***Fig.5.6 (A) BRD4s, BRD4l and HPRT-1 expressions in OCI-AML3 cells (MLL-WT), after 72 hours of SPHINX-31 treatment visualised on a 2% agarose gel ($IC_{50}$ 40.39 nM). Figure 5.6 (B) Difference in expression of BRD4s- BRD4l in OCI-AML3 cells after 72 hours of SPHINX-31 treatment. Fig.5.6 (C) Normalised levels of expression between BRD4s-BRD4l isoform after 72 hours of SPHINX-31 treatment, the difference in expression was normalised to the vehicle control (i.e., 100% BRD4s) and the highest concentration (i.e. 100% BRD4L expression). Expressions of BRD4s, BRD4l and HPRT-1 in OCI-AML3 cell line was determined by RT-PCR and visualized on a 2% gel by agarose gel electrophoresis. The expected band sizes were, BRD4s: 206 bp and BRD4l: 488 bp, HPRT-1: 101 bp. The optical density was measured using Image Studio. All data points represent three biological replicates (n=3), which each were calculated using three technical replicates.***

To compare the efficacy of SRPK1 inhibition of Wild type versus MLL translocated cells on BRD4 splicing, $IC_{50}$s for each dose response curve were calculated from all 6 cell lines. As it is shown in Figure 5.1 (C) - 5.6 (C). Figure 5.7. shows that there is no significant difference in the IC50s between MLL-WT and MLL-TL.

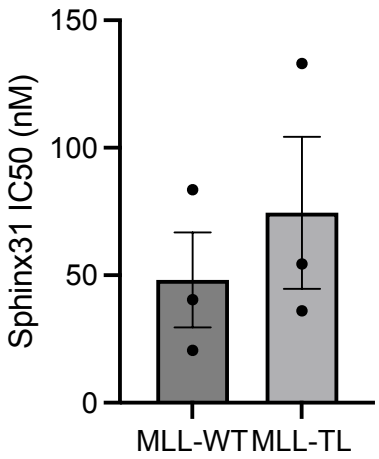



***Figure 5.7. IC50 values for SPHINX31 in MLL-WT and MLL-translocated cell lines for BRD4 splicing.***

***Fig.5.7. shows the difference between the $IC_{50}$ values of MLL-WT and MLL-TL. $IC_{50}$ values were calculated to show the effect of SPHINX-31 on BRD4 splice change. The MLL-WT cells were compared to the MLL-TL cells, using an unpaired T-test which had p=0.495 value, showing now significant difference between the two groups.***

## 5.4. Discussion and conclusion

### 5.4.1. BRD4 splice change in AML cell lines

BRD4 has been found to be critical for the disease maintenance in AML and BRD4 suppressors such as JQ1 had robust anti-leukaemic effects both *in vitro* and *in vivo.* The treatment with JQ1 has shown significant reduction in proliferation in THP-1, MOLM-13, and HL60, etc. cells after 72 hours of treatment with SPHINX-31 (Zuber *et al.*, 2011). Another study showed that when OCI-AML2 and OCI-AML3 cells were treated with JQ1, after 48 hours of treatment and with 200nM concentration it significantly reduced cell viability (Zhou *et al.*, 2018).

BRD4 splice change in THP-1 cells has been previously reported in (Tzelepis *et al.*, 2018) study and their preliminary results were replicated here in a much

wider data set, using 6 AML cell lines. The data shows that splice change occurs in all 6 AML cell lines, regardless of their rearrangement status. Furthermore, in our data set the treatment concentration ranges from 1nM to 10μM to show optimal treatment concentration. In the higher dose treatment groups, the long version of BRD4 significantly outweighs the short version. The only obvious sticking point in the data set is the double bands that appeared in the HL60 data, which likely were the result of unspecific binding.

### 5.4.2. Concluding remarks

The opportunity to change the splicing of BRD4 from the tumourigenic short to the anti-tumorigenic long form provides a great possibility of treatment for such notoriously therapy resistant cancers such as AML. As previous studies show, BRD4 inhibition (using a pan BRD4 inhibitor) can be very toxic and not sustainable for a long period of time, modulating the isoform could provide a solution and advance drug development. Therefore, a selective inhibitor such as SPHINX-31 could be used to switch the splicing of BRD4 isoforms to aid the anti-tumourigenic effect of BRD4l. In the future, short-read RNA-sequencing could be performed to calculate the percent splicing index which describes the proportion of reads that represent the inclusion isoform and includes transcriptions of all the exons of the specific gene.

# 6. Chapter

# Second generation inhibitor treatment in AML

## 6.1. Aims and objectives

In the previous chapters, it was shown that SPHINX-31 is successful in reducing downstream targets in AML cells, it can decrease cell viability in MOLM-13 cells and is able to switch the isoform of BRD4. ET1126, ET1132 and ET3002 are three new inhibitors that showed good results in SPRK1 inhibition in an in vitro kinase assays (Proprietary data- Emenda Therapeutics Ltd.). There was a need determine whether these were able to inhibit SRPK1 in cells using an Intracellular kinase target engagement assay and whether there was a change in SRPK1 expression in response to these new inhibitors. Since there is no SRPK1 tracer available on the market, a new tracer was developed by Prof. Jonathan Morris's group (University of New South Wales, Australia). Based on the data gathered from the SPHINX-31 treatment group, these inhibitors were tested to see if they would replicate previous results in reducing the expression levels of common oncogenes such as MYC, BCL-2 and HOXA9. The expression levels were measure using ddPCR in all 6 AML cell lines, after the validation of new SRPK1 inhibitors in the intracellular kinase target engagement assay.

## 6.2. Introduction

ET1126, ET1132 and ET3002 are second generation inhibitors that were developed by Prof. Jonathan Morris' group at the University of New South Wales. ET1126 and ET1132 have a Griffin-type structure, whereas ET3002

has an indole scaffold (See Figure 1.8). As these are all unpublished inhibitors, information on their efficacy is limited.

## 6.3. Intracellular kinase target engagement assay

Kinase signalling pathways have been successfully exploited to be therapy targets to inhibit cancer cell proliferation and angiogenesis. There are 484 kinases encoded in the human genome and every kinase has multiple ways for intervention (Ferguson and Gray, 2018). SPHINX-31 and other inhibitors used here have been tested to show specificity and selectivity in cell free assays. However, to determine whether an inhibitor that has shown to successfully target SRPK1 expression in *in vitro* (in a cell free environment) can work inside a cell, it needs to be tested further. To that end, a NanoBRET™ based intracellular kinase target engagement (TE) assay was used, which made it possible to test SPHINX-31 and other inhibitors within the intact cell but without any confounding factors. The advantage of this assay is that we could study the effect of the compound directly on the gene of interest under cellular conditions (physiological ATP, after uptake/diffusion into the cell, and in the right cell compartment). When the host cells are transfected with the NanoLuc-tagged target protein, then the test compound can be added for a short treatment with the cell-permeable tracer. After a couple of hours, the luminescent NanoBRET substrate is added, through bioluminescence resonance energy transfer (BRET) the level of nonradiative

transfer of luminescent energy determines how much effect the inhibitor had on the target protein and results in a dose dependent decrease in BRET. TE assays measure a blue-shifted donor signal and a red-shifted acceptor signal which result in a BRET ratio, or more commonly mBRET (mBU), which is calculated by the following formula:

$$\frac{\textbf{Acceptor emmission}}{\textbf{Donor emission}} \times \mathbf{1000} = \textbf{mBRET ratio}(\textbf{mBU})$$

### 6.3.1. SRPKBNP tracer optimisation

In order to use a NanoBRET™ based intracellular kinase target engagement (TE) assay to measure the inhibitory effect of various SRPK1 inhibitors, a specific SRPK1 tracer was developed. Similar to the commercially available NanoBRET tracers, this tracer was also covalently conjugated to a fluorescent dye which uses a small molecule ligand to bind to the target protein. The solubility and concentration of the tracer was optimised by using the same method as for the commercially available NanoBRET™ based intracellular kinase target engagement (TE) assay (Promega, N2501).

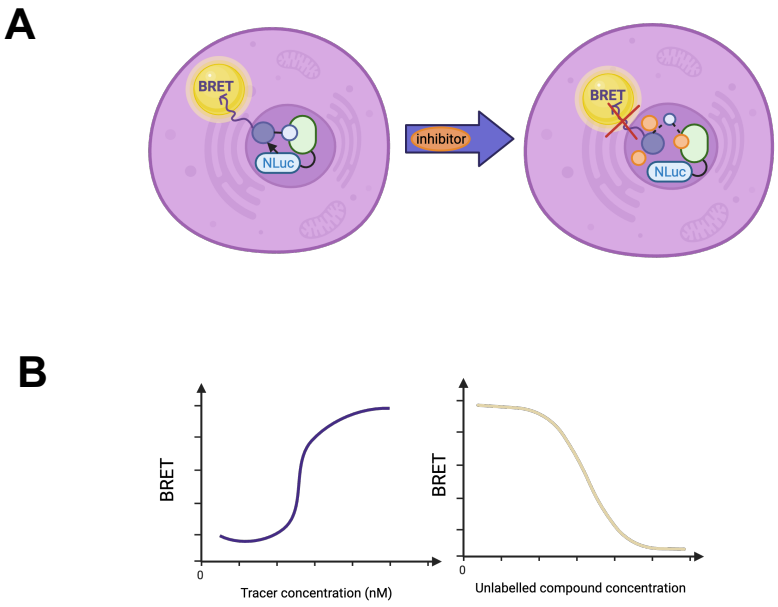



***Figure 6.1. Ilustration of the NanoBRET TE cell assay.***

**Panel A. shows the labelled NanoLuc vector within the cell (NLuc), the fluorescent tracer (purple circle) and the target protein (light blue circle) bound together in close proximity which then results in a BRET signal. It also shows the effect of a test compound (orange circle) which can inhibit the binding of target protein and fluorescent tracer (purple circle) which then results in very low or no BRET signal. Panel B. illustrates the predicted raising BRET signal in response to a rising concentration of fluorescent tracer. It also shows the predicted decreasing values (hypothetical presentation) of an effective compound. Graph based Manual TM598 (Property of Promega, UK), images created using BioRender Premium.**

Figure 6.2. shows the NanoBRET values measured at increasing concentrations of tracer. It shows that the SRPKBNP-1 tracer can achieve BRET values from ~9 mBU (mBRET unit) to 17 mBU from 300nM-1µM tracer concentration. As these values were in line with the manufacturer's recommendation for similar tracers, the SRPKBNP-1 tracer was used for all SRPK1 TE assays.

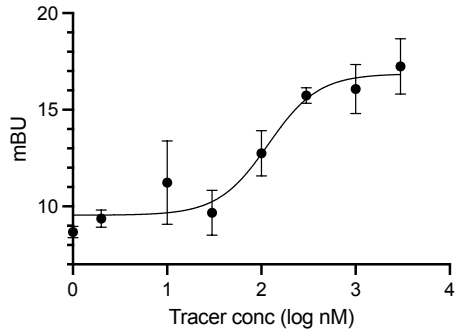



***Figure 6.2 Optimisation data for the newly developed SRPKBNP tracer for SRPK1***

***Fig. 6.2. shows the increasing levels of BRET signal (mBU) correlating with the increasing levels of tracer concentration(1nM – 10μM). Protocol is based on TM598 (Promega, UK) with modification and no inhibitor treatment. The luminescence levels were measured at 460nm for acceptor and 610nm for donor emission and mBU ratio were calculated based on the equation mentioned in paragraph 4.3. Data presented were calculated from one biological replicate which had three technical repeates.***

## 6.3.2. SRPK1 assays

Based on previous *in vitro and* enzyme data (Proprietary data commissioned by Emenda Therapeutics Ltd.) 3 inhibitors were pre-selected with high potential potency for SRPK1 inhibition. These are SPHINX-31 which has been used for other studies and two second generation inhibitors, ET1126 and ET1132. Figure 6.3. shows the inhibition of nanoBRET signal (in mBU) resulting from incubation with increasing concentration of SPHINX-31. From this it can be seen that SPHINX-31 trestment resulted in a dose dependent decrease in mBU with an $IC_{50}$ of 190nM.

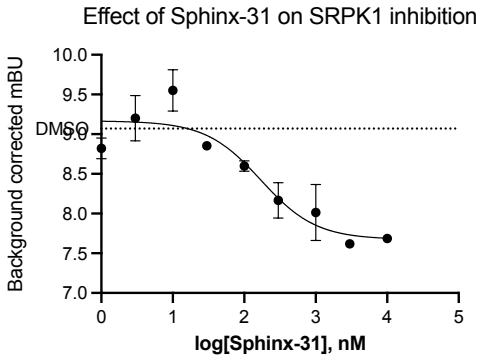



***Figure 6.3. SRPK1 inhibition after Sphinx-31 treatment measured via the NanoBRET Target Engagement assay.***

***Fig. 6.3. shows the decreasing levels of BRET signal (mBU) correlating with the increasing levels of SPHINX-31 treatment ($IC_{50}$ of 190nM). The mBU values were normalised to the vehicle control group (DMSO 0.1%).The luminescence levels were measured at 460nm for acceptor and 610nm for donor emission and mBU ratio were calculated based on the equation mentioned in paragraph 4.3.***

ET1126 and ET1132 are second generation SRPK1 selective inhibitors that have a Griffin-like scaffold. Figure 6.4. shows that ET1126 and ET1132 both resulted in a dose dependent decrease in mBU.

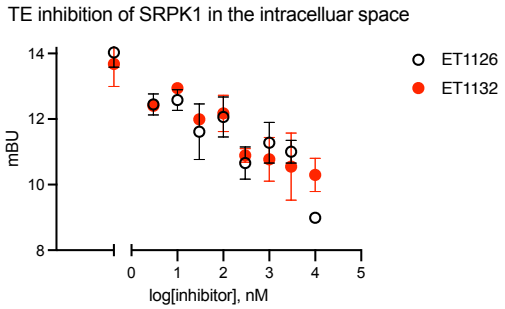



***Figure 6.4. SRPK1 inhibition after ET1126 and ET1132 treatment measured via the NanoBRET Target Engagement assay.***

***Fig. 6.4. shows the decreasing levels of BRET signal (mBU) correlating with the increasing levels of ET1126 and ET1132 treatment(1nM – 10$\mu$M). The mBU values were normalised to the vehicle control group (DMSO 0.1%).The luminescence levels were measured at 460nm for acceptor and 610nm for donor emission and mBU ratio were calculated based on the equation mentioned in paragraph 4.3.***

To determine an IC50 for each of these compounds the mBU were normalised to 100% (no compound) and 0% (maximum inhibition), all data was normalised to the vehicle control group (DMSO 0.1%). Figure 6.5. shows the effect of ET1126 on SRPK1 inhibition and that it has an $IC_{50}$ of 136 nM, lower than SPHINX31.

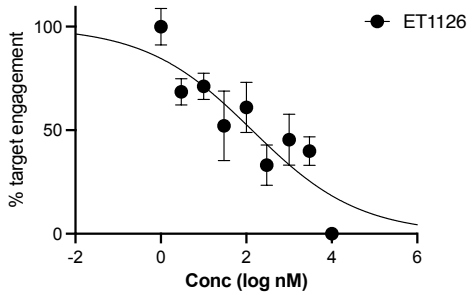



***Figure 6.5. SRPK1 inhibition after ET1126 treatment measured via the NanoBRET Target Engagement assay.***

***Fig. 6.5. shows the decreasing levels of BRET signal (mBU) correlating with the increasing levels of ET1126 treatment ($IC_{50}$ 136 nM ).The mBU values were normalised to the vehicle control group (DMSO 0.1%).The luminescence levels were measured at 460nm for acceptor and 610nm for donor emission and mBU ratio were calculated based on the equation mentioned in paragraph 4.3.***

Figure 6.6. shows the effect of ET1132, another second generation inhibitor on SRPK1 inhibition. It has an $IC_{50}$ of 46 nM, the most potent of all compounds tested. This compound has not been tested either in previous studies. It has a Griffin-type scaffold and although some optimisation is needed, it showed great potential for further tests.

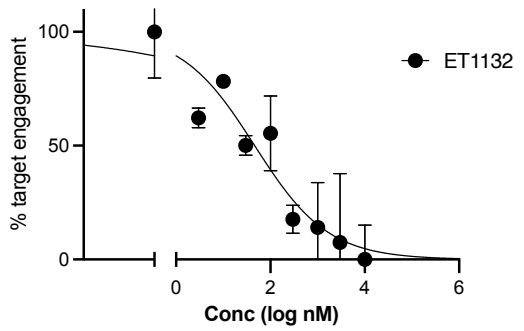



***Figure 6.6. SRPK1 inhibition after ET1132 treatment measured via the NanoBRET Target Engagement assay***

***Fig. 6.6. shows the decreasing levels of BRET signal (mBU) correlating with the increasing levels of ET1132 treatment ($IC_{50}$ 46 nM). The mBU values were normalised to the vehicle control group (DMSO 0.1%).The luminescence levels were measured at 460nm for acceptor and 610nm for donor emission and mBU ratio were calculated based on the equation mentioned in paragraph 4.3.***

## 6.4. Downstream target levels in response to ET1126 inhibitor treatment

As previously mentioned, BCL-2, HOX9 and MYC have been identified to be an interesting drug target in haematological malignancies (Perini *et al.*, 2018). To test if inhibitors ET1126, ET1132 and ET3002 would have a similar effect and reduce these downstream targets in AML cells, ddPCR was used to measure BCL-2, HOXA9 and MYC expression levels. This study shows that ET1126 was successful in reducing the level of BCL-2 expression in AML cell lines. Fig.6.7. (A) shows the effect of ET1126 in THP-1 cells and the reduction levels in MYC expression ($IC_{50}$ 29.51 nM). Fig.6.7. (B) shows the effect of ET1126 in THP-1 cells, in reducing HOXA9 expression levels ($IC_{50}$ 52.84 nM). In Fig.6.7. (C) the levels of BCL-2 can be seen in THP-1 cells, after ET1126 treatment ($IC_{50}$ 35.71 nM).

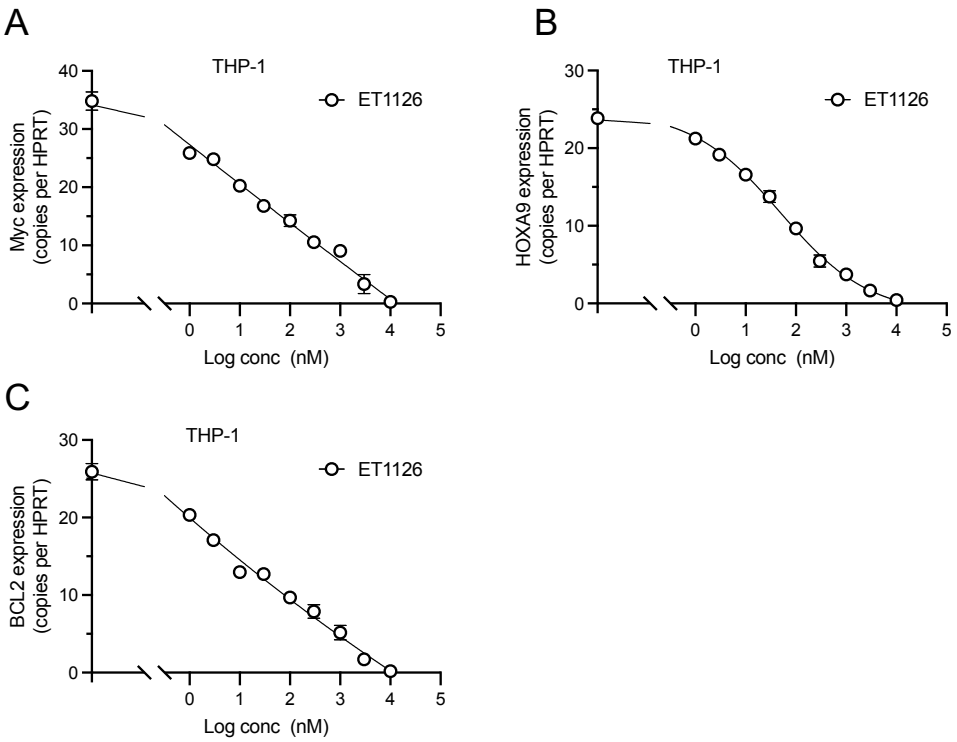



***Figure 6.7. Downstream target levels in THP-1 cells after ET1126 treatment.***

***Downstream target levels after 72 hours ET1126 treatment in THP-1 cells, measured by assessing the MYC, BCL-2 and HOXA9 expression levels, using ddPCR. All measurements were normalised to HPRT-1 housekeeping gene. Data represents the average of three biological replicates (n=3), which each were measured from three technical repeats. 6.7.(A) MYC expression levels after 72 hours of ET1126 treatment ($IC_{50}$ 29.51 nM). 6.7.(B) HOXA9 expression levels after 72 hours of ET1126 treatment ($IC_{50}$ 52.84 nM). 6.7.(C) BCL-2 expression levels after 72 hours of ET1126 treatment ($IC_{50}$ 35.71 nM).***

A similar effect can be observed in the MOLM-13 cell lines (as to what the data has shown in Fig. 6.7.) where all inhibitors significantly reduce the level of BCL-2, HOXA9 and MYC expression levels. Fig.6.8. (A) shows the reduction in MYC levels, in MOLM-13 cells in response to ET1126 treatment ($IC_{50}$ 16.43 nM). Fig. 6.8. (B) shows the reduction in HOXA9 in response to ET1126 treatment ($IC_{50}$ 26.85 nM). Fig.6.8. (C) shows the reductions in BCL-2 in response to ET1126 treatment ($IC_{50}$ 7.082 nM).

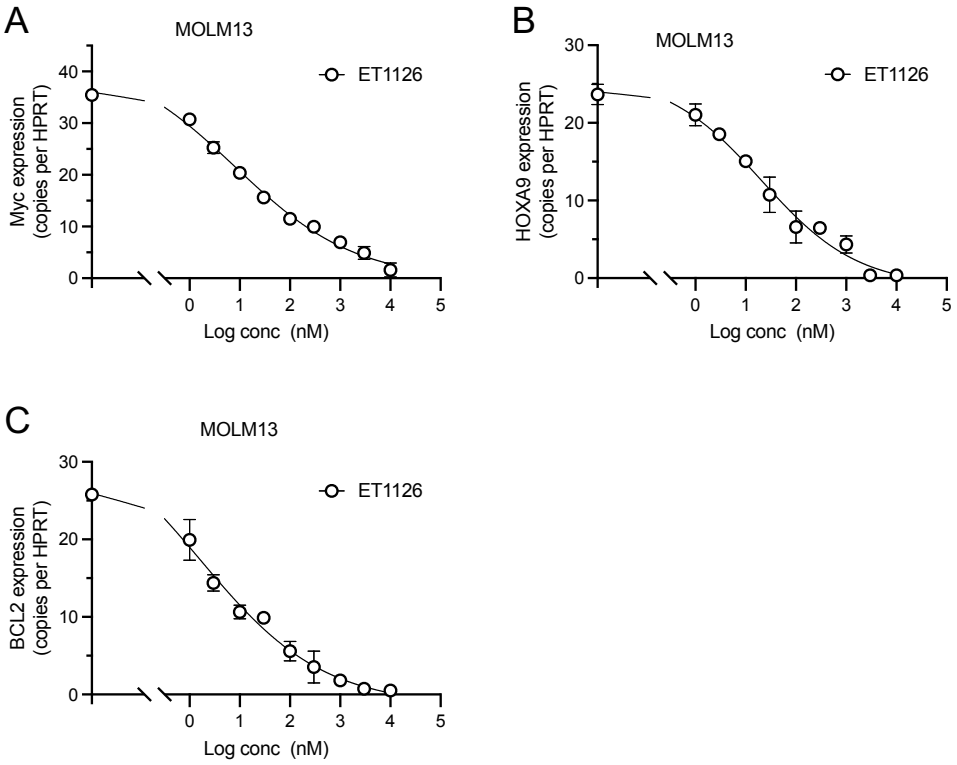



***Figure 6.8. Downstream target levels in MOLM-13 cells after ET1126 treatment.***

***Downstream target levels after 72 hours ET1126 treatment in MOLM-13 cells, measured by assessing the MYC, BCL-2 and HOXA9 expression levels, using ddPCR. All measurements were normalised to HPRT-1 housekeeping gene. Data represents the average of three biological replicates (n=3), which each were measured from three technical repeats. 6.8.(A) MYC expression levels after 72 hours of ET1126 treatment ($IC_{50}$ 16.43 nM). 6.8.(B) HOXA9 expression levels after 72 hours of ET1126 treatment ($IC_{50}$ 26.85 nM). 6.8.(C) BCL-2 expression levels after 72 hours of ET1126 treatment ($IC_{50}$ 7.082 nM).***

Fig.6.9. (A) shows the response to ET1126 treatment in OCI-AML2 in MYC expression levels ($IC_{50}$ 29.80 nM). Fig.6.9. (B) Shows the reduction in HOXA9 levels in OCI-AML2 cells after ET1126 treatment ($IC_{50}$ 46.24 nM). Whereas Fig.6.9. (C) shows the level of reduction in BCL-2 expressions in the same cells after ET1126 treatment ($IC_{50}$ 61.74 nM).

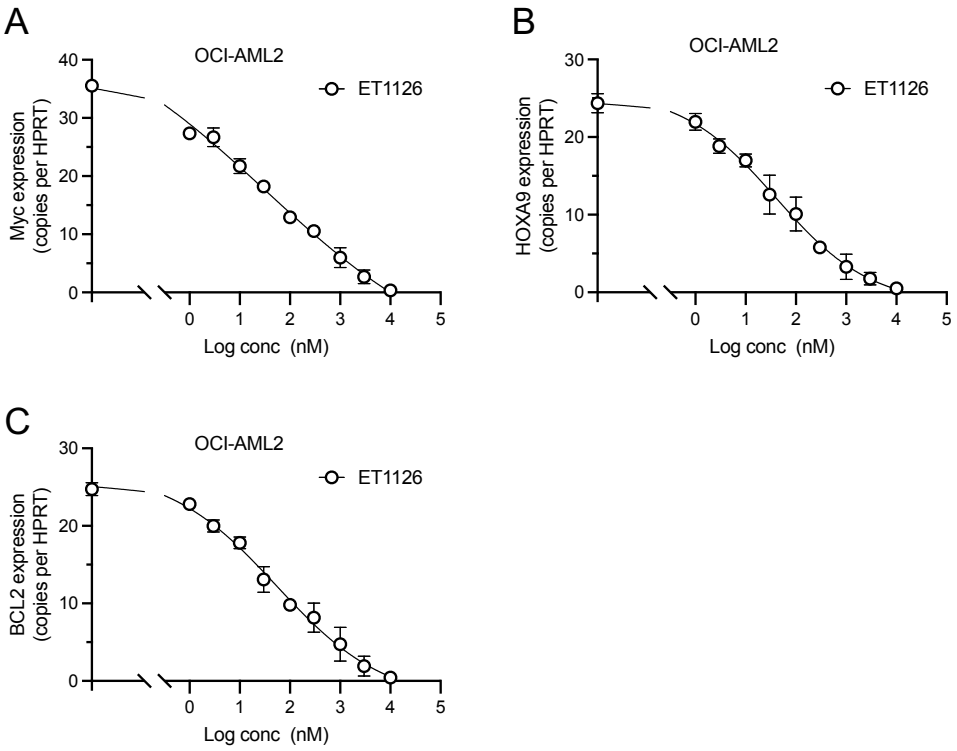



***Figure 6.9. Downstream target levels in OCI-AML2 cells after ET1126 treatment.***

***Downstream target levels after 72 hours ET1126 treatment in OCI-AML2 cells, measured by assessing the MYC, BCL-2 and HOXA9 expression levels, using ddPCR. All measurements were normalised to HPRT-1 housekeeping gene. Data represents the average of three biological replicates (n=3), which each were measured from three technical repeats. 6.9.(A) MYC expression levels after 72 hours of ET1126 treatment ($IC_{50}$ 29.80 nM). 6.9.(B) HOXA9 expression levels after 72 hours of ET1126 treatment ($IC_{50}$ 46.24 nM). 6.9.(C) BCL-2 expression levels after 72 hours of ET1126 treatment ($IC_{50}$ 61.74 nM).***

OCI-AML3 cells are a non-translocated AML cell line, but it shows the same response to inhibitor treatment. After ET1126 treatment, the level of MYC expression was significantly reduced as it can be seen in Fig.6.10. (A), ($IC_{50}$ 15.91 nM). The effect of ET1126 in reducing HOXA9 expression levels in OCI-AML3 cells can be seen in Fig.6.10. (B), ($IC_{50}$ 19.29 nM). Fig.6.10. (C) shows the effect in OCI-AML3 cells on BCL-2 expression levels in response to ET1126 inhibitor treatment ($IC_{50}$ 11.68 nM).

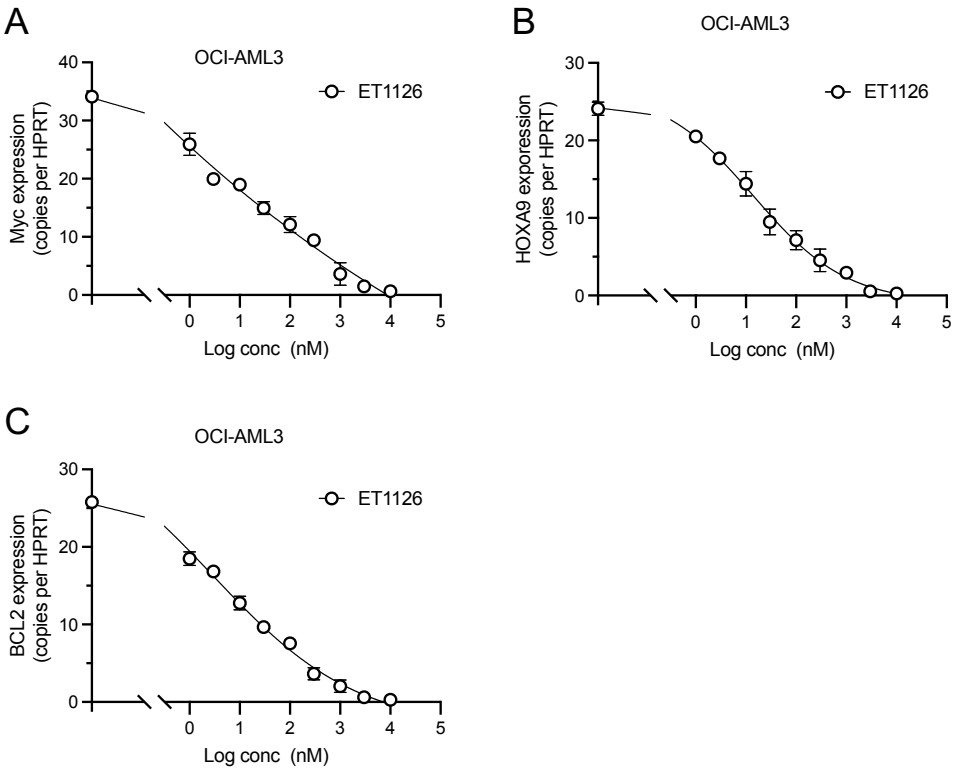



***Figure 6.10. Downstream target levels in OCI-AML3 cells after ET1126 treatment.***

***Downstream target levels after 72 hours ET1126 treatment in OCI-AML3 cells, measured by assessing the MYC, BCL-2 and HOXA9 expression levels, using ddPCR. All measurements were normalised to HPRT-1 housekeeping gene. Data represents the average of three biological replicates (n=3), which each were measured from three technical repeats. 6.10.(A) MYC expression levels after 72 hours of ET1126 treatment ($IC_{50}$ 15.91 nM). 6.10.(B) HOXA9 expression levels after 72 hours of ET1126 treatment ($IC_{50}$ 19.29 nM). 6.10.(C) BCL-2 expression levels after 72 hours of ET1126 treatment ($IC_{50}$ 11.68 nM).***

Fig.6.11. (A) shows the decrease in MYC levels in response to ET1126 treatment ($IC_{50}$ 16.53 nM). Fig.6.11. (B) shows the reduction in HOXA9 levels in TF1a cells after ET1126 treatment ($IC_{50}$ 21.45 nM). Fig.6.11. (C) shows that ET1126 was successful in reducing the expression levels of BCL-2 in TF1a cells ($IC_{50}$ 11.31 nM).

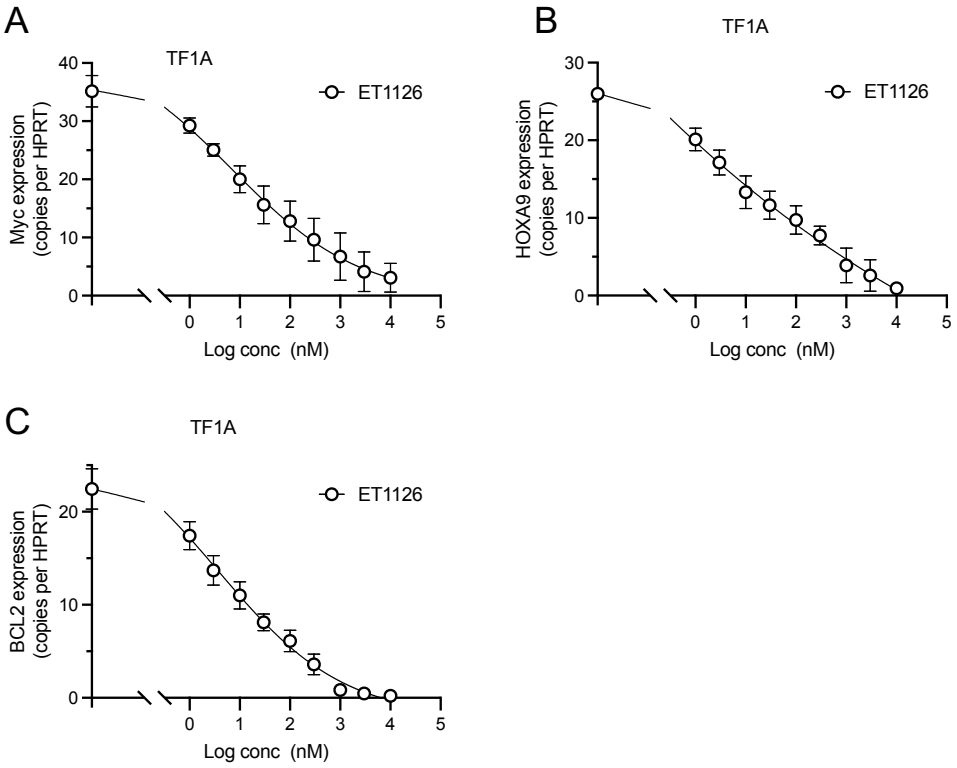



***Figure 6.11. Downstream target levels in TF1a cells after ET1126 treatment.***

***Downstream target levels after 72 hours ET1126 treatment in TF1a cells, measured by assessing the MYC, BCL-2 and HOXA9 expression levels, using ddPCR. All measurements were normalised to HPRT-1 housekeeping gene. Data represents the average of three biological replicates (n=3), which each were measured from three technical repeats. 6.11.(A) MYC expression levels after 72 hours of ET1126 treatment ($IC_{50}$ 16.53 nM). 6.11.(B) HOXA9 expression levels after 72 hours of ET1126 treatment ($IC_{50}$ 21.45 nM). 6.11.(C) BCL-2 expression levels after 72 hours of ET1126 treatment ($IC_{50}$ 11.31 nM).***

The HL60 cells demonstrated a similar response to inhibitor treatment as the TF1a cells (seen in Fig.11.). ET1126 caused a significant reduction in BCL-2 ($IC_{50}$ 12.78 nM), HOXA9 ($IC_{50}$ 8.39 nM) and MYC expression levels ($IC_{50}$ 11.92 nM) as it can be seen in Fig.6.12.

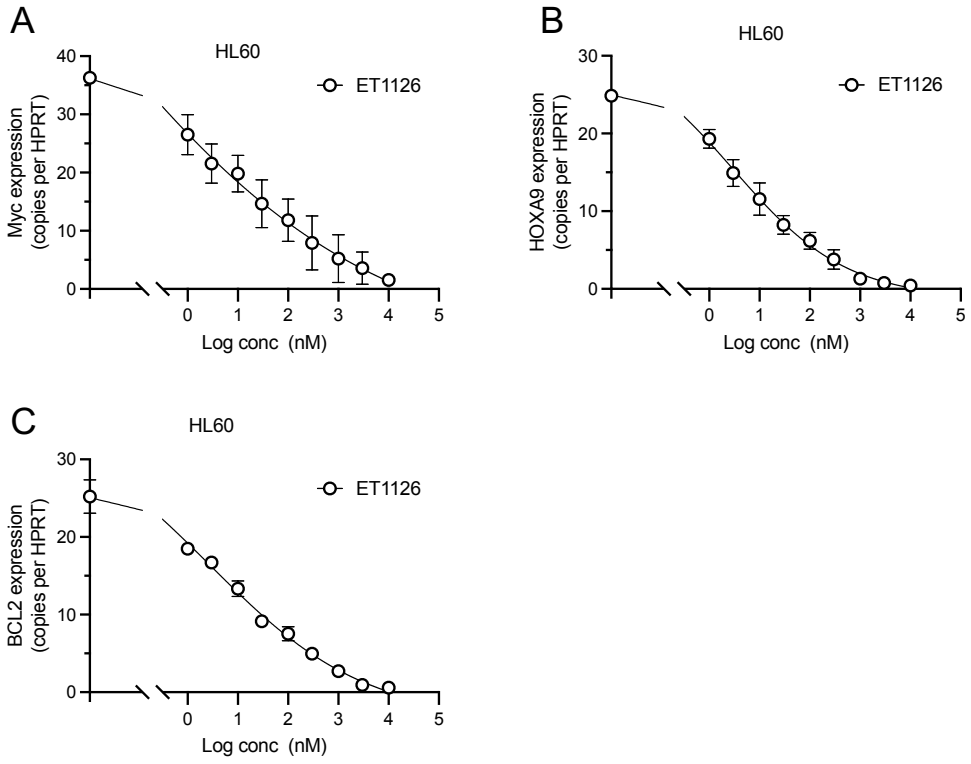



***Figure 6.12. Downstream target levels in HL60 cells after ET1126 treatment.***

***Downstream target levels after 72 hours ET1126 treatment in HL60 cells, measured by assessing the MYC, BCL-2 and HOXA9 expression levels, using ddPCR. All measurements were normalised to HPRT-1 housekeeping gene. Data represents the average of three biological replicates (n=3), which each were measured from three technical repeats. 6.12.(A) MYC expression levels after 72 hours of ET1126 treatment ($IC_{50}$ 11.92 nM). 6.12.(B) HOXA9 expression levels after 72 hours of ET1126 treatment ($IC_{50}$ 8.39 nM). 6.12.(C) BCL-2 expression levels after 72 hours of ET1126 treatment ($IC_{50}$ 12.78 nM).***

## 6.5. Downstream target levels in response to ET1132 inhibitor treatment

HOXA9 has been found to be overexpressed in AML and it is essential for maintaining leukaemic transformation. It has also been shown that higher levels of HOXA9 carries worse patient prognosis. Therefore reducing the expression levels of HOXA9 could be a successful treatment option in AML (Collins and Hess, 2016). Alongside with MYC and BCL-2, the reduction of

these downstream targets showed good potential to be drug candidates (Perini *et al.*, 2018). In this paragraph the data demonstrates the efficacy of another inhibitor, ET1132. The results are very similar to the ET1126 data;. Fig.6.13. (A) shows the reduction in MYC expression levels in response to increasing levels of ET1132 treatment ($IC_{50}$ 47.2 nM). Fig.6.13. (B) shows a similar effect, where the level of HOXA9 expression significantly decreases even in the nanomolar range of inhibitor treatment ($IC_{50}$ 10.23 nM). BCL-2 levels also significantly decreased in response to ET1132 treatment in THP-1 cells, as it can be seen in Fig.6.13. (C), ($IC_{50}$ 12.37 nM).

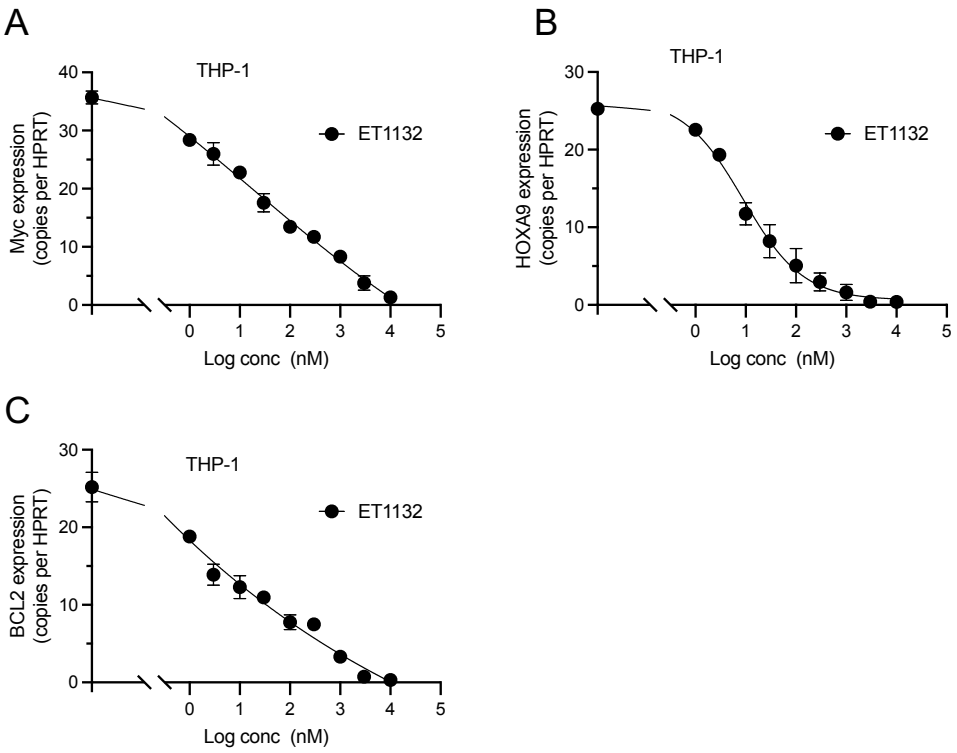



***Figure 6.13. Downstream target levels in THP-1 cells after ET1132 treatment.***

***Downstream target levels after 72 hours ET1132 treatment in THP-1 cells, measured by assessing the MYC, BCL-2 and HOXA9 expression levels, using ddPCR. All measurements were normalised to HPRT-1 housekeeping gene. Data represents the average of three biological replicates (n=3), which each were measured from three technical repeats. 6.13.(A) MYC expression levels after 72 hours of ET1132 treatment ($IC_{50}$ 47.2 nM). 6.13.(B) HOXA9 expression levels after 72 hours of ET1132 treatment ($IC_{50}$ 10.23 nM). 6.13.(C) BCL-2 expression levels after 72 hours of ET1132 treatment ($IC_{50}$ 12.37 nM).***

Similar results can be observed in the MOLM-13 cells, Fig.6.14. (A) shows the reduced levels of MYC in MOLM-13 cells in response to ET1132 treatment ($IC_{50}$ 27.43 nM). Fig. 6.14. (B) shows to response in MOLM-13 cells after ET1132 treatment, HOXA9 expression levels were significantly reduced ($IC_{50}$ 36.01 nM). Fig. 6.13. (C) shows the effect of ET1132 in MOLM-13 cells, which caused a significant reduction in BCL-2 levels.

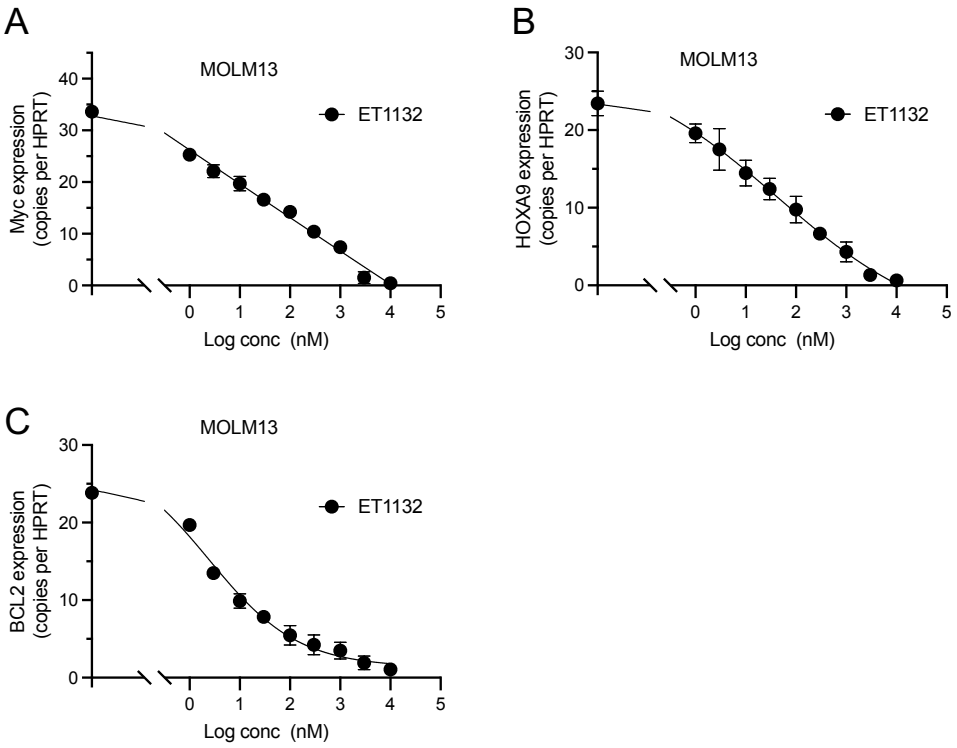



***Figure 6.14. Downstream target levels in MOLM-13 cells after ET1132 treatment.***

***Downstream target levels after 72 hours ET1132 treatment in MOLM-13 cells, measured by assessing the MYC, BCL-2 and HOXA9 expression levels, using ddPCR. All measurements were normalised to HPRT-1 housekeeping gene. Data represents the average of three biological replicates (n=3), which each were measured from three technical repeats. 6.14.(A) MYC expression levels after 72 hours of ET1132 treatment ($IC_{50}$ 27.43 nM). 6.14.(B) HOXA9 expression levels after 72 hours of ET1132 treatment ($IC_{50}$ 36.01 nM). 6.14.(C) BCL-2 expression levels after 72 hours of ET1132 treatment ($IC_{50}$ 5.12 nM).***

There were similar results observed in the OCI-AML2 cell line as in previous AML cells. Fig.6.15. (A) shows the effect of ET1132 inhibitor in MYC expression levels in OCI-AML2 cells ($IC_{50}$ 29.8 nM). Fig.6.15. (B) shows the

reduced levels of HOXA9 expression in OCI-AML2 cells after ET1132 treatment ($IC_{50}$ 32.21 nM). Fig. 6.15. (C) shows the effect of ET1132 in OCI-AML2 cells and finally in reducing BCL-2 expression levels ($IC_{50}$ 19.95 nM).

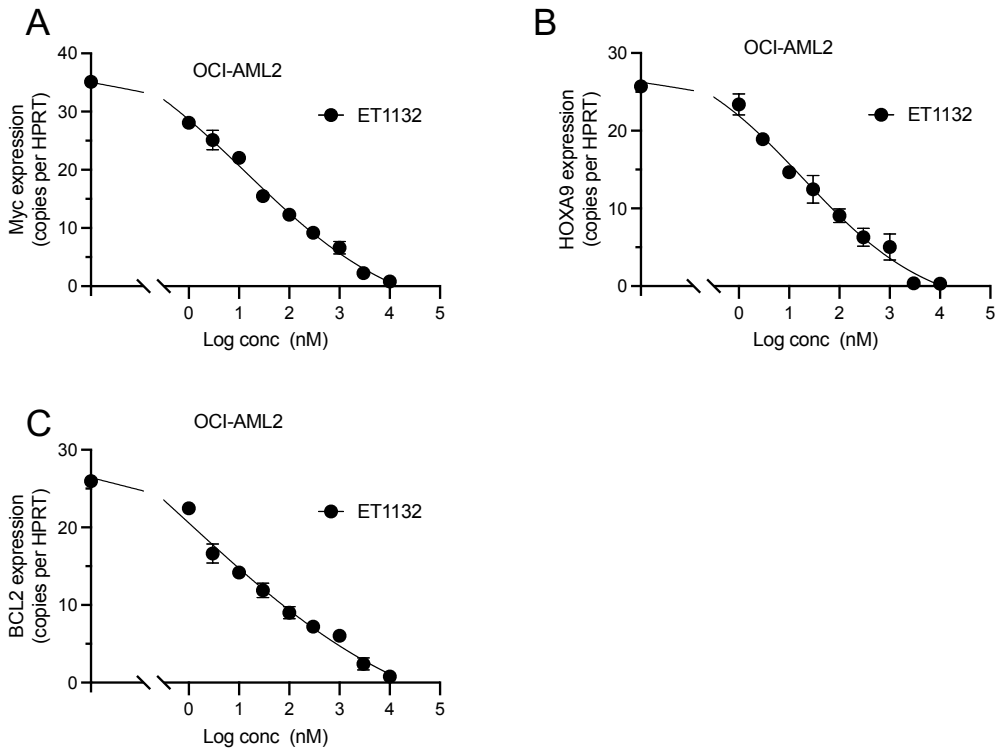



***Figure 6.15. Downstream target levels in OCI-AML2 cells after ET1132 treatment.***

***Downstream target levels after 72 hours ET1132 treatment in OCI-AML2 cells, measured by assessing the MYC, BCL-2 and HOXA9 expression levels, using ddPCR. All measurements were normalised to HPRT-1 housekeeping gene. Data represents the average of three biological replicates (n=3), which each were measured from three technical repeats. 6.15.(A) MYC expression levels after 72 hours of ET1132 treatment ($IC_{50}$ 29.8 nM). 6.15.(B) HOXA9 expression levels after 72 hours of ET1132 treatment ($IC_{50}$ 32.21 nM). 6.15.(C) BCL-2 expression levels after 72 hours of ET1132 treatment ($IC_{50}$ 19.95 nM).***

The OCI-AML3 cells are non-translocated AML cells, which showed similar response to inhibitor treatment. Fig.6.15. (A) shows the effect of ET1132 in OCI-AML3 cells, which significantly reduced the levels of MYC expression ($IC_{50}$ 29.45 nM). Fig.6.15. (B) shows the reduced HOXA9 levels in OCI-AML3 cells after ET1132 inhibitor treatment ($IC_{50}$ 22.96 nM). Fig.6.15. (C) shows the

reduced BCL-2 levels in OCI-AML3 cells after ET1132 inhibitor treatment ($IC_{50}$ 7.681 nM).

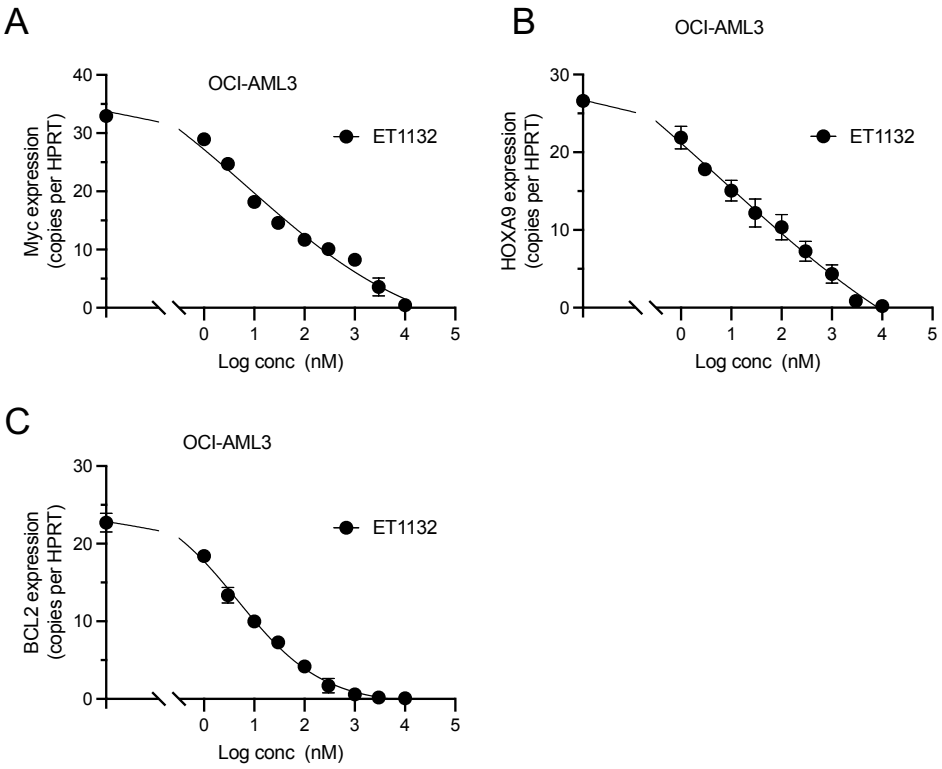



***Figure 6.16 Downstream target levels in OCI-AML3 cells after ET1132 treatment.***

***Downstream target levels after 72 hours ET1132 treatment in OCI-AML3 cells, measured by assessing the MYC, BCL-2 and HOXA9 expression levels, using ddPCR. All measurements were normalised to HPRT-1 housekeeping gene. Data represents the average of three biological replicates (n=3), which each were measured from three technical repeats. 6.16.(A) MYC expression levels after 72 hours of ET1132 treatment ($IC_{50}$ 29.45 nM). 6.16.(B) HOXA9 expression levels after 72 hours of ET1132 treatment ($IC_{50}$ 22.96 nM). 6.16.(C) BCL-2 expression levels after 72 hours of ET1132 treatment ($IC_{50}$ 7.681 nM).***

Downstream target expression levels were significantly reduced in TF1a cells after ET1132 inhibitor treatment. As it can be seen in Fig.6.17. (A) ET1132 was effective in reducing the MYC expression levels ($IC_{50}$ 9.378 nM). Fig.6.16. (B) shows the effect of ET1132 in reducing HOXA9 expression levels

in TF1a cells ($IC_{50}$ 48.83 nM). Fig. 6.17. (C) shows the reduction in BCL-2 levels in response to ET1132 treatment ($IC_{50}$ 13.94 nM).

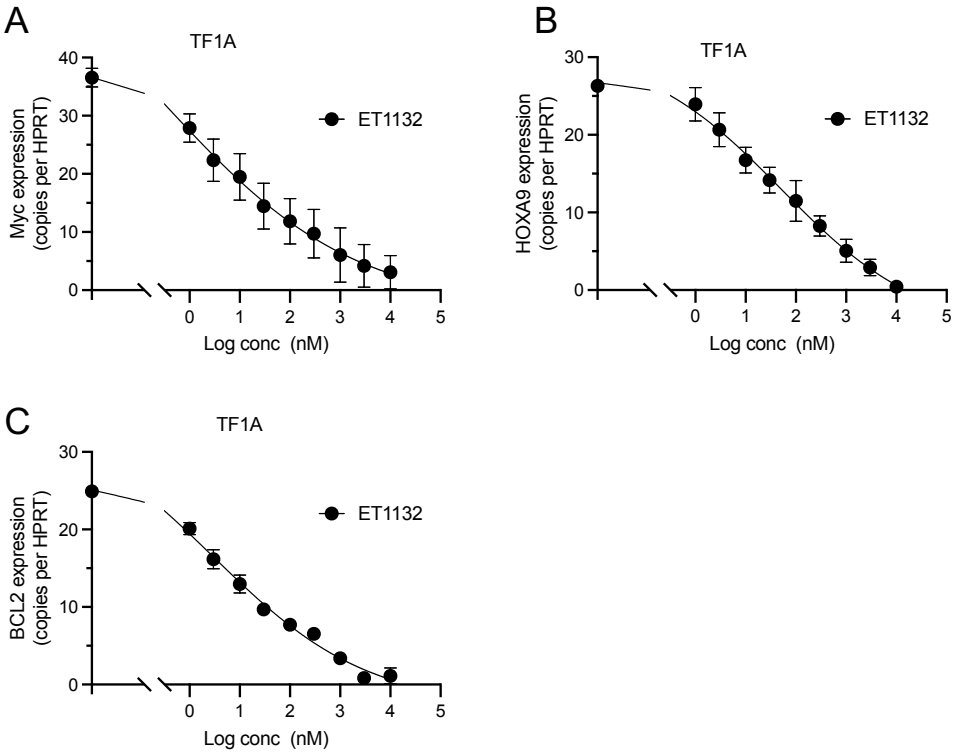



***Figure 6.17. Downstream target levels in TF1a cells after ET1132 treatment.***

***Downstream target levels after 72 hours ET1132 treatment in TF1a cells, measured by assessing the MYC, BCL-2 and HOXA9 expression levels, using ddPCR. All measurements were normalised to HPRT-1 housekeeping gene. Data represents the average of three biological replicates (n=3), which each were measured from three technical repeats. 6.17.(A) MYC expression levels after 72 hours of ET1132 treatment ($IC_{50}$ 9.378 nM). 6.17.(B) HOXA9 expression levels after 72 hours of ET1132 treatment ($IC_{50}$ 48.83 nM). 6.17.(C) BCL-2 expression levels after 72 hours of ET1132 treatment ($IC_{50}$ 13.94 nM).***

Fig.6.18. (A) shows the effect of ET1132 on HL60 cells, and the reduction in MYC expression levels ($IC_{50}$ 38.06 nM). Fig.6.17. (B) shows the effect of ET1132 on HOXA9 expression levels in HL60 cells ($IC_{50}$ 34.93 nM). Fig.6.17. (C) shows the effect of ET1132 on HL60 cells in reducing BCL-2 expression levels ($IC_{50}$ 9.773 nM).

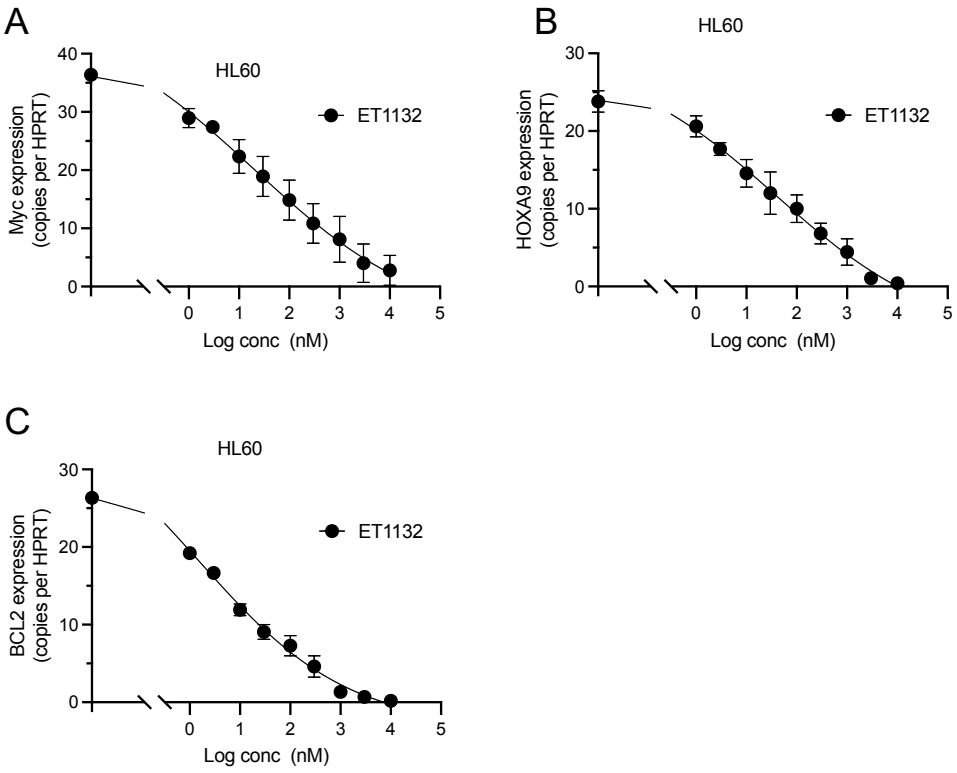



***Figure 6.18. Downstream target levels in HL60 cells after ET1132 treatment.***

***Downstream target levels after 72 hours ET1132 treatment in HL60 cells, measured by assessing the MYC, BCL-2 and HOXA9 expression levels, using ddPCR. All measurements were normalised to HPRT-1 housekeeping gene. Data represents the average of three biological replicates (n=3), which each were measured from three technical repeats. 6.18.(A) MYC expression levels after 72 hours of ET1132 treatment ($IC_{50}$ 38.06 nM). 6.18.(B) HOXA9 expression levels after 72 hours of ET1132 treatment ($IC_{50}$ 34.93 nM). 6.18.(C) BCL-2 expression levels after 72 hours of ET1132 treatment ($IC_{50}$ 9.773 nM).***

## 6.6. Downstream target levels in response to ET3002 treatment

ET3002 is another second generation inhibitor that showed great results in enzyme data. Data presented here shows that ET3002 was succesfull in reducing all downstream targets, albeit not as successfully as the ET1126 and ET1132 inhibitors. Fig.6.19. (A) shows the reduced levels of MYC expression levels after ET1132 treatment ($IC_{50}$ 330.7 nM). Fig.6.19. (B) shows the reduced HOXA9 expression levels in THP-1 cells after ET3002 treatment ($IC_{50}$ 229.5 nM) and Fig.6.19.C shows the effect of ET1132 in THP-1 cells in terms of BCL-2 expression levels ($IC_{50}$ 243.0 nM).

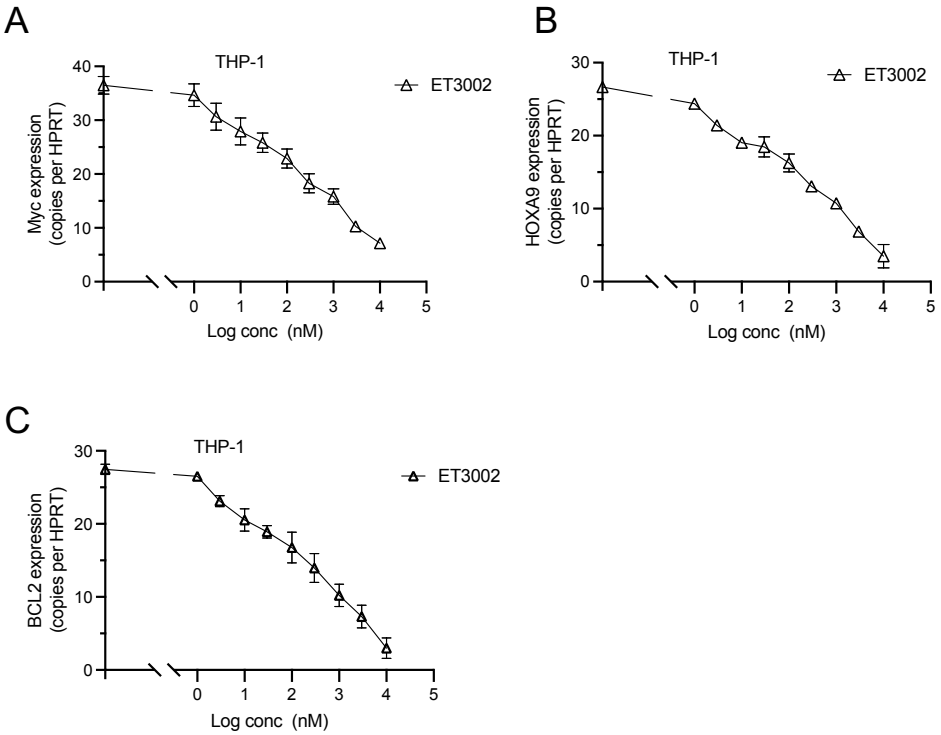



***Figure 6.19. Downstream target levels in THP-1 cells after ET3002 treatment.***

***Downstream target levels after 72 hours ET3002 treatment in THP-1 cells (MLL-TL), measured by assessing the MYC, BCL-2 and HOXA9 expression levels, using ddPCR. All measurements were normalised to HPRT-1 housekeeping gene. Data represents the average of three biological replicates (n=3), which each were measured from three technical repeats. 6.19.(A) MYC expression levels after 72 hours of ET3002 treatment ($IC_{50}$ 330.7 nM). 6.19.(B) HOXA9 expression levels after 72 hours of ET3002 treatment ($IC_{50}$ 229.5 nM). 6.19.(C) BCL-2 expression levels after 72 hours of ET3002 treatment ($IC_{50}$ 243.0 nM).***

MOLM-13 cells showed a similar dose response curve in response to inhibitor treatment with ET3002. Fig.6.20. (A) shows the effect of the ET3002 inhibitor in terms of MYC expression level reduction ($IC_{50}$ 475.7 nM). Fig.6.20. (B) shows the reduced expression levels of HOXA9 in MOLM-13 cells after ET3002 treatment ($IC_{50}$ 203.3 nM). Fig.6.20. (C) shows the decrease in BCL-2 levels in MOLM-13 cells after ET3002 treatment ($IC_{50}$ 710.7 nM).

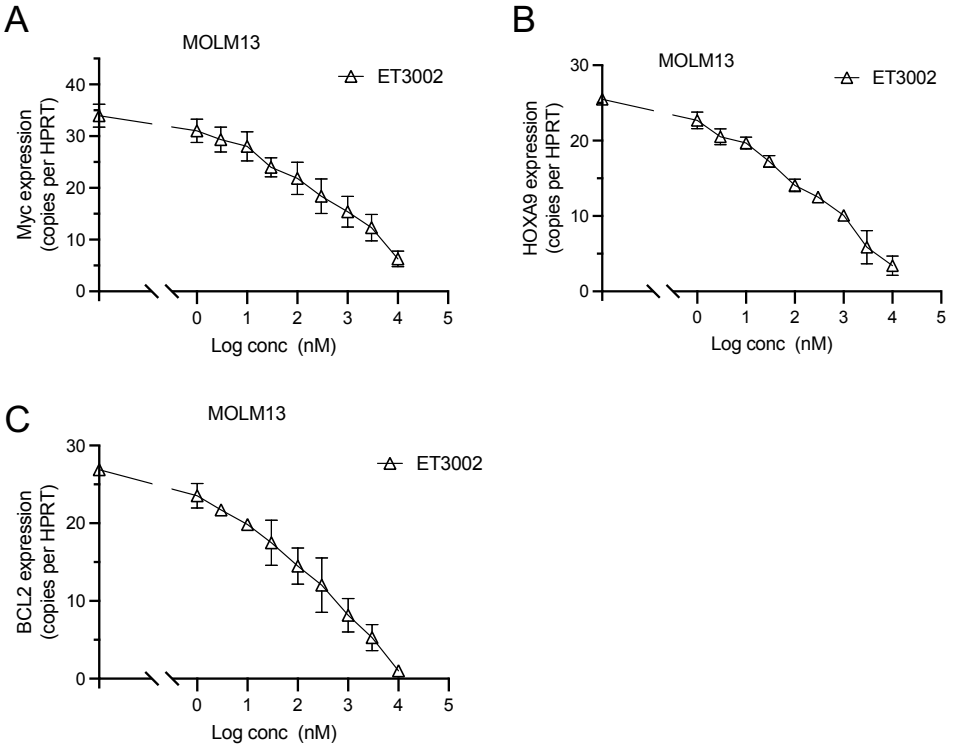



***Figure 6.20. Downstream target levels in MOLM-13 cells after ET3002 treatment.***

***Downstream target levels after 72 hours ET3002 treatment in MOLM-13 (MLL-TL) cells, measured by assessing the MYC, BCL-2 and HOXA9 expression levels, using ddPCR. All measurements were normalised to HPRT-1 housekeeping gene. Data represents the average of three biological replicates (n=3), which each were measured from three technical repeats. 6.20.(A) MYC expression levels after 72 hours of ET3002 treatment ($IC_{50}$ 475.7 nM). 6.20.(B) HOXA9 expression levels after 72 hours of ET3002 treatment ($IC_{50}$ 203.3 nM). 6.20.(C) BCL-2 expression levels after 72 hours of ET3002 treatment ($IC_{50}$ 710.7 nM).***

The OCI-AML2 cells had a very similar response then the MOLM-13 cells (Fig. 20). All the inhibitors triggered a significant reduction, Fig.6.21. (A) demonstrates the effect of ET3002 on MYC expression levels in OCI-AML2 cells ($IC_{50}$ 330.0 nM). Fig.6.21. (B) demonstrates the reduced expression levels of HOXA9 in OCI-AML2 cells after ET3002 treatment ($IC_{50}$ 256.6 nM). Fig.6.21. (C) shows the reduced levels of BCL-2 expression in OCI-AML2 cells after ET3002 treatment ($IC_{50}$ 187.0 nM).

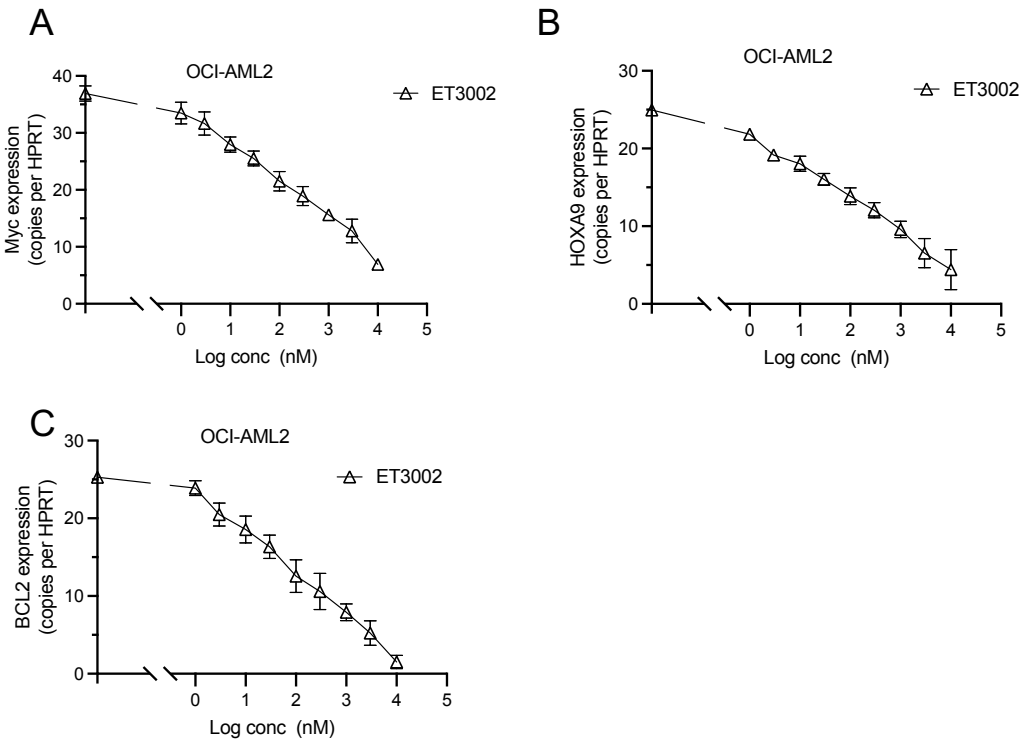



***Figure 6.21. Downstream target levels in OCI-AML2 cells after ET3002 treatment.***

***Downstream target levels after 72 hours ET3002 treatment in OCI-AML2 (MLL-TL) cells, measured by assessing the MYC, BCL-2 and HOXA9 expression levels, using ddPCR. All measurements were normalised to HPRT-1 housekeeping gene. Data represents the average of three biological replicates (n=3), which each were measured from three technical repeats. 6.21.(A) MYC expression levels after 72 hours of ET3002 treatment ($IC_{50}$ 330.0 nM). 6.21.(B) HOXA9 expression levels after 72 hours of ET3002 treatment ($IC_{50}$ 256.6 nM). 6.21.(C) BCL-2 expression levels after 72 hours of ET3002 treatment ($IC_{50}$ 187.0 nM).***

The OCI-AML3 (MLL-WT) cells had a similar response to the inhibitor treatment, regardless of their MLL translocation status. Fig.6.22. (A) shows the effect of ET3002 on OCI-AML3 cells in terms of MYC expression ($IC_{50}$ 76.78 nM). Fig.6.22. (B) shows the reduced HOXA9 expression levels in OCI-AML3 cells after ET3002 treatment ($IC_{50}$ 93.87 nM). And Fig.6.22. (C) depicts the reduction of BCL-2 expression levels in OCI-AML3 cells after ET3002 treatment ($IC_{50}$ 133.0 nM).

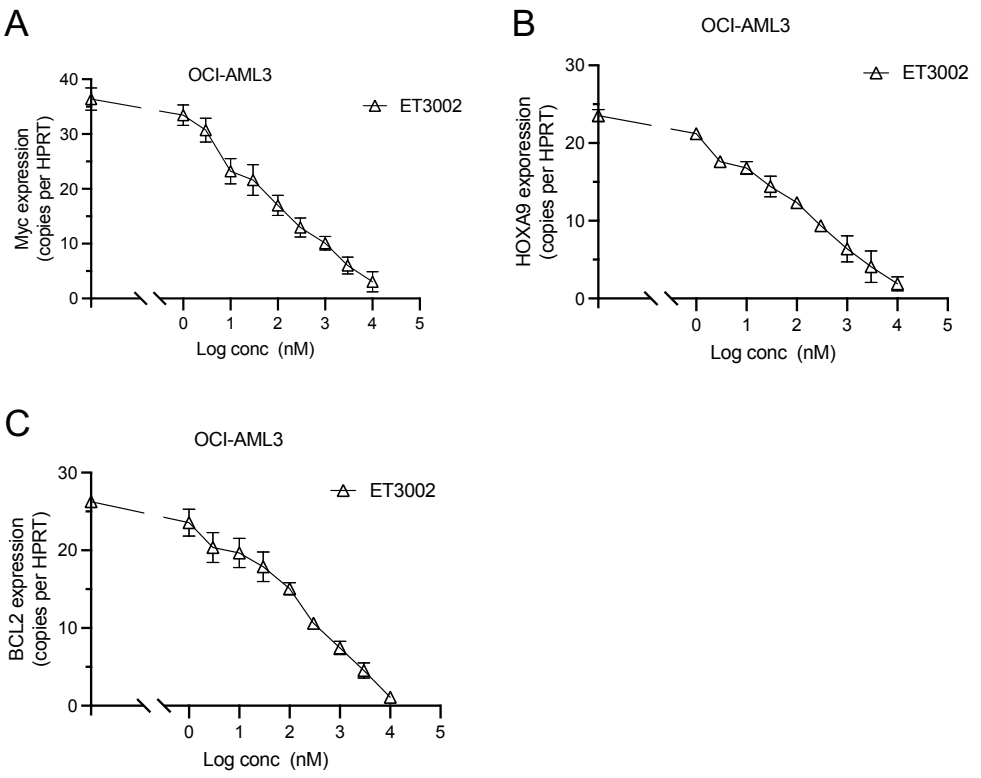



***Figure 6.22. Downstream target levels in OCI-AML3 cells after ET3002 treatment.***

***Downstream target levels after 72 hours ET3002 treatment in OCI-AML3 (MLL-WT) cells, measured by assessing the MYC, BCL-2 and HOXA9 expression levels, using ddPCR. All measurements were normalised to HPRT-1 housekeeping gene. Data represents the average of three biological replicates (n=3), which each were measured from three technical repeats. 6.22.(A) MYC expression levels after 72 hours of ET3002 treatment ($IC_{50}$ 76.78 nM). 6.22.(B) HOXA9 expression levels after 72 hours of ET3002 treatment ($IC_{50}$ 93.87 nM). 6.22.(C) BCL-2 expression levels after 72 hours of ET3002 treatment ($IC_{50}$ 133.0 nM).***

TF1a cells had a similarly robust response to inhibitor treatment, Fig.6.23. (A) shows the reduced MYC expression levels in response to increasing levels of ET3002 treatment ($IC_{50}$ 184.0 nM). Fig.6.23. (B) shows a strong dose response curve to ET3002 in HOXA9 expression in TF1a cells ($IC_{50}$ 322.7 nM). Fig.6.23. (C) shows the effect of ET3002 on TF1a cells on BCL-2 expression levels ($IC_{50}$ 223.0 nM).

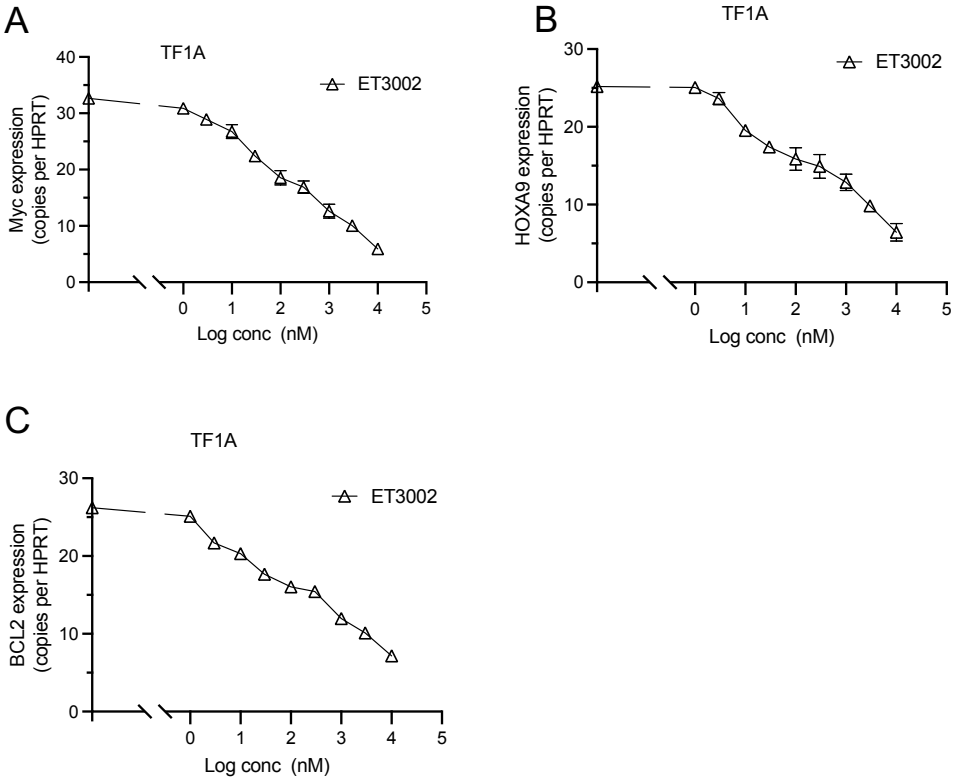



***Figure 6.23. Downstream target levels in TF1a cells after ET3002 treatment.***

***Downstream target levels after 72 hours ET3002 treatment in TF1a (MLL-WT) cells, measured by assessing the MYC, BCL-2 and HOXA9 expression levels, using ddPCR. All measurements were normalised to HPRT-1 housekeeping gene. Data represents the average of three biological replicates (n=3), which each were measured from three technical repeats. 6.23.(A) MYC expression levels after 72 hours of ET3002 treatment ($IC_{50}$ 184.0 nM). 6.23.(B) HOXA9 expression levels after 72 hours of ET3002 treatment ($IC_{50}$ 322.7 nM). 6.23.(C) BCL-2 expression levels after 72 hours of ET3002 treatment ($IC_{50}$ 223.0 nM).***

HL60 cells had a very similar response to the inhibitor treatment as the TF1a cells (Fig.23.), both displaying a significant reduction in all of the studied gene expression levels. Specifically, Fig.6.24. (A) shows the decreased levels of MYC expression in HL60 cells after ET3002 treatment ($IC_{50}$ 333.6 nM). Fig.6.24. (B) shows the effect of ET3002 in HL60 cells on HOXA9 expression levels ($IC_{50}$ 294.7 nM). Fig.6.24. (C) shows the decrease in BCL-2 expression levels after ET3002 treatment ($IC_{50}$ 485.6 nM).

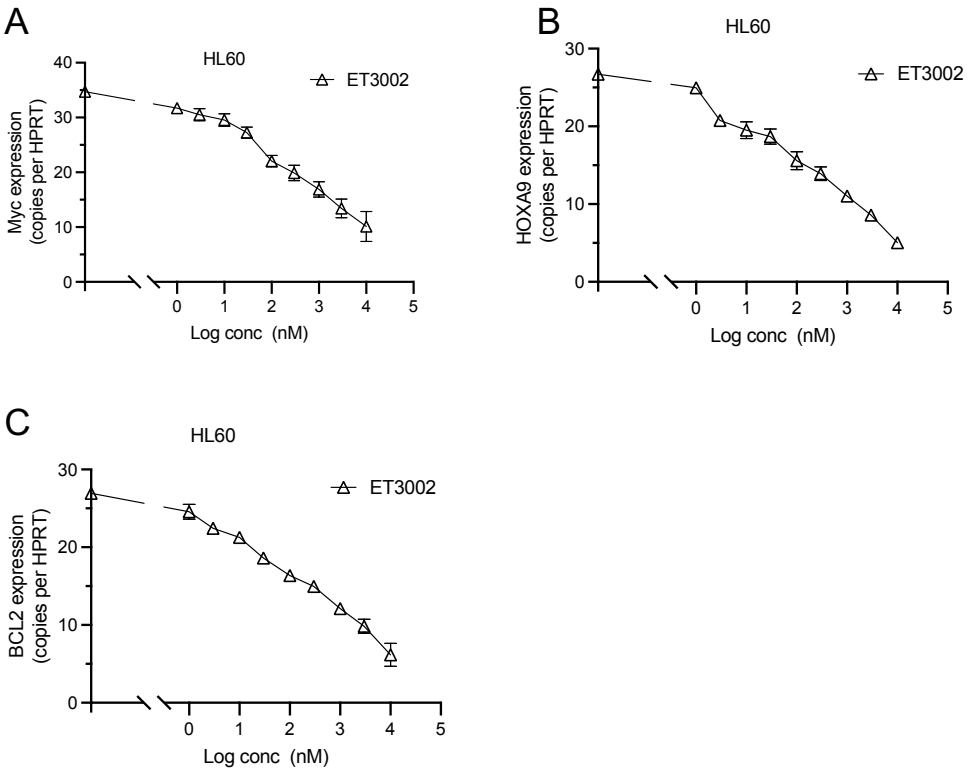



***Figure 6.24. Downstream target levels in HL60 cells after ET3002 treatment.***

***Downstream target levels after 72 hours ET3002 treatment in HL60 (MLL-WT) cells, measured by assessing the MYC, BCL-2 and HOXA9 expression levels, using ddPCR. All measurements were normalised to HPRT-1 housekeeping gene. Data represents the average of three biological replicates (n=3), which each were measured from three technical repeats. 6.24.(A) MYC expression levels after 72 hours of ET3002 treatment ($IC_{50}$ 333.6 nM). 6.24.(B) HOXA9 expression levels after 72 hours of ET3002 treatment ($IC_{50}$ 294.7 nM). 6.24.(C) BCL-2 expression levels after 72 hours of ET3002 treatment ($IC_{50}$ 485.6 nM).***

To determine whether any of these inhibitors were more or less potent the $IC_{50}$ values for each compound were plotted for each expression marker. Figure 6.25. shows that there was a significant difference in potency between the three new generation inhibitors and SPHINX31 when MYC expression levels are compared (p=0.0115).

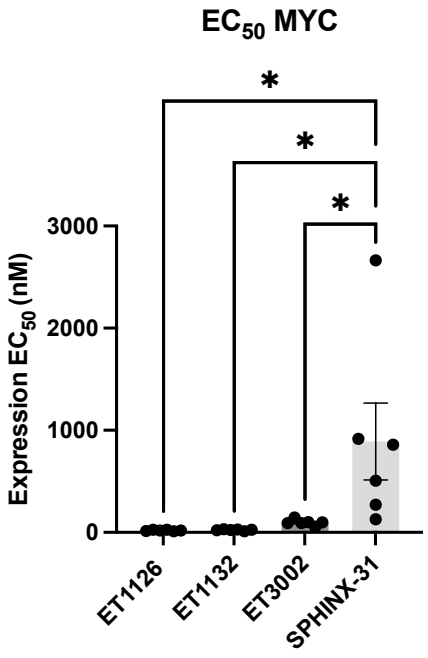



***Figure 6.25. $EC_{50}$ data of ET1126, ET1132 and ET3002 compared to SPHINX-31on MYC expression levels***

**Fig.6.25. shows the $EC_{50}$ data on the expression level changes in MYC, after ET1126, ET1132, ET3002 and SPHINX-31 treatment, respectively. ET1126, ET1132, ET3002 are second generation, inhibitors that were selected for their high potency for SRPK1 inhibition but never tested before. SPHINX-31 is a known compound that proved to be a worthy candidate in in vitro and in vivo conditions to inhibit SRPK1 expression and therefore used to be as a drug target. $EC_{50}$ values were calculated using data from all six AML cell lines, nine treatment conditions [1nM-10μM], three biological replicates (n=3), which each had three technical repeats. *P=0.0115.**

Fig.6.26. shows the data on HOXA9 levels and the efficacy of ET1126, ET1132, ET3002 inhibitors compared to the published, SPHINX-31 compound.

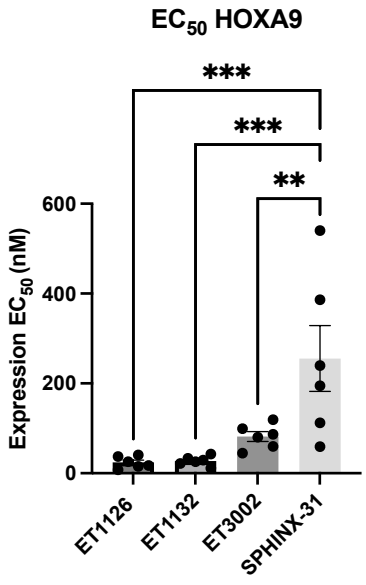



***Figure 6.26. $EC_{50}$ data of ET1126, ET1132 and ET3002 compared to SPHINX-31on HOXA9 expression levels***

**Fig.6.26. shows the $EC_{50}$ data on the expression level changes in HOXA9, after ET1126, ET1132, ET3002 and SPHINX-31 treatment, respectively. ET1126, ET1132, ET3002 are second generation inhibitors that were selected for their high potency for SRPK1 inhibition but were never tested before. SPHINX-31 is a published compound that proved to be a worthy candidate in in vitro and in vivo conditions to inhibit SRPK1 expression and therefore used to be as a drug target. $EC_{50}$ values were calculated using data from all six AML cell lines, nine treatment conditions [1nM-10μM], three biological replicates (n=3), which each had three technical repeats **P=0.0036, ***P=0.0008.**

Fig.6.27. shows the effect of ET1126, ET1132, ET3002 and SPHINX-31 in terms of BCL-2 expression levels. The graph shows the significant difference between the inhibitors, ET1126, ET1132, ET3002 and SPHINX-31. It also depicts how these second generation inhibitors are significantly more effective in reducing SPRK1 levels in the assay. Which makes these inhibitor potentially effective drug candidates.

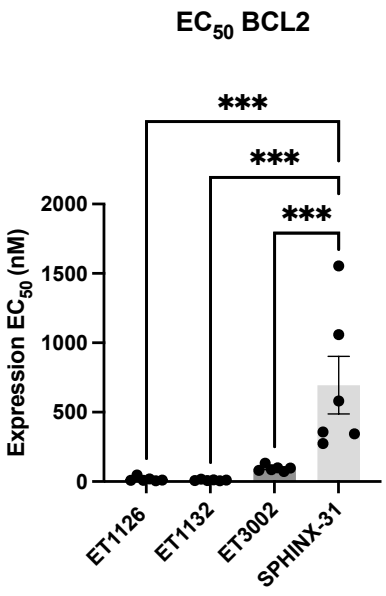



***Figure 6.27. $EC_{50}$ data of ET1126, ET1132 and ET3002 compared to SPHINX-31on BCL-2 expression levels***

**Fig.6.27. shows the $EC_{50}$ data on the expression level changes in BCL-2, after ET1126, ET1132, ET3002 and SPHINX-31 treatment, respectively. ET1126, ET1132, ET3002 are second generation, unpublished inhibitors that were selected for their high potency for SRPK1 inhibition. SPHINX-31 is a published compound that proved to be a worthy candidate in in vitro and in vivo conditions to inhibit SRPK1 expression and therefore used to be as a drug target.***P=0.0005, 0.0006. n=3, 3 experimental replicates were used when calculating the SEM, in each experimental round 3 technical replicates were used for each condition.**

## 6.7. Discussion

A robust dataset is shown here to present the reduction of common downstream targets such as MYC, HOXA9 and BCL2 expression levels in six AML cell lines in response to inhibitor treatment. All six AML cell line showed a significant reduction in response to inhibitor treatment, ET1126 and ET1132 being the most effective. ET3002 also showed a significant reduction and a very clear dose response curve in MYC, HOXA9 and BCL2 expressions when adjusted to the housekeeping gene. As oncogenes are known to be upregulated in cancer, any significant reduction in their expression level is a valuable result and could be a potential drug target.

### 6.7.1. Intracellular target engagement assay

Within the intracellular target engagement assay, it was shown that SRPK1 inhibition is present after SPHINX-31, ET1126, ET1132 and ET3002 treatment, which indicates that these inhibitors are highly selective for SRPK1 and the other inhibitory effect in different assays are a direct result of SRPK1 inhibition. The optimisation step for a new SRPK1 tracer which has not been used or tested before is also shown here. The BRET levels (mBU) measured in these assays are in line with previous publications (Yang *et al.*, 2023) and show reliable results that can be used in further screening of new inhibitors.

### 6.7.2. Downstream targets after ET1126 inhibitor treatment

BCL-2 expression in AML has been a longstanding drug target, as BCL-2 expression strongly correlates with resistance to therapy and apoptotic cell death. In their study (Cerella *et al.*, 2017) tested the UNBS1450 glycoside, venetoclax and BH3 mimetic and their combinations in a colony formation assay, using primary AML cells in a zebrafish xenograft. They found promising results which could make UNBS1450 a good candidate, however high $IC_{50}$ values could cause potential toxicity issues in the future which limits the translation capability of the model (Cerella *et al.*, 2017). Data presented here shows promising results in all AML cells when treated with ET1126. BCL-2 expression levels were reduced signficantly where the highest $IC_{50}$ value was 61.74 nM in the MOLM-13 cells, and the lowest was 7.082 nM in the OCI-

AML2 cells. In their study, Lillico *et al*., (2018) tested MOLM-13 cells (w/MLL-F9 translocation), to measure the efficacy of DOT1L (EPZ5676), LSD1 (GSK2879552), and HDAC (mocetinostat) inhibitors. Each of the compounds achieved reduced cell viability but only DOT1L induced apoptosis. DOT1L was also the most effective compound to reduce HOXA9 expression to about 30% (corrected to vehicle control) (Lillico *et al.*, 2018). In their study, Koo *et al.*, (2022) demonstrated that a CDK7 inhibitor, YPN-005 can not only reduce viability in OCI-AML2 cells but also significantly reduce MYC expression levels even in the nM range, after a 24 hour treatment (Koo *et al.*, 2022). In a similar study, AG490 inhibited IL-5-mediated c-Myc induction and promoter activity in TF1 cells (Lee *et al.*, 2009). The Liu *et al.,* (2022) study also looked at HL60 cells (MLL-WT) and showed that MYC is severely inhibited after only 6 hours (most significant difference after a 24-hour treatment) after AZD5991 treatment (Liu *et al.*, 2022). Data shown here demonstrates that all AML cell lines displayed a significant reduction in MYC expression levels as well as all other downstream target levels (in the nM range) in response to ET1126 treatment, regardless of their MLL status.

### 6.7.3. Downstream target levels after ET1132 treatment

In the OCI-AML3 cell line, the same study by Koo *et al.* (2022) found that BCL-2 expression was not altered even after the lentiviral downregulation of MCL-1, via an shRNA system, as they hypothesized that MCL-1 downregulation could sensitize OCI-AML3 cells to ABT-199. Their data only showed a

relevant reduction in BCL-2 levels at around 1μM concentration (Koo *et al.*, 2022). Our data here shows that ET1132 was successful in reducing BCL-2 expression levels in MOLM-13 cells, where the $IC_{50}$ value was 5.12 nM. The highest $IC_{50}$ value was measured in the OCI-AML2 cells (19.95 nM), significantly below the μM range. Slack and Yu (1998) presented similar results in their study when they treated TF1 cells with All-trans retinoic acid (ATRA) and showed a similar reduction in BCL-2 expression than what we found in the similar TF1a cells (Slack and Yu, 1998) Our data shows an $IC_{50}$ value of 19.94 nM for TF1a cells after ET1132 treatment. Another study found that the HL60 cells were the most sensitive to ABT-199 (venetoclax) treatment in terms of BCL-2 expression levels (Ishizawa *et al.*, 2015), similarly to what is shown here. In a previously published study, Sonoda et al. (2021) tested a synthetic HOXA9 inhibitor, DB818 which was able to reduce the HOXA9 expression in THP-1 cells as well as supress growth and induce apoptosis (Sonoda *et al.*, 2021). A similar outcome was presented in this study, in response to the second-generation inhibitor ET1132. HOXA9 expression levels are reduced in all cell lines, even in the nM range ($IC_{50}$ 10.23 nM). AZD5991, a selective MCL-1 inhibitor has been found to lower MYC expression levels in AML cell lines. Liu et al. (2022) found that AZD5991 is the most efficient after a 24-hour treatment. In this study it is shown that after a 72-hour treatment, MYC is virtually undetectable in the THP-1 samples in the highest treatment concentration which is set at 10μM. The same study looked at the effect of AZD5991 in MOLM-13 cells. They found that MOLM-13 cells were even more sensitive to the AZD5991 treatment (Liu *et al.*, 2022).

This study shows that ET1132 treatment reduces the level of MYC expression levels in MOLM-13 cells effectively with an $IC_{50}$ value 27.43 nM.

### 6.7.4. Downstream target levels after ET3002 inhibitor treatment

In their study, Koo et al., (2022) demonstrated that a CDK7 inhibitor, YPN-005 can not only reduce viability in OCI-AML2 cells but also significantly reduce MYC expression levels even in the nM range, after a 24 hour treatment (Koo *et al.*, 2022). In a similar study, AG490 inhibited IL-5-mediated c-Myc induction and promoter activity in TF1 cells (Lee *et al.*, 2009). The Liu et al. study also looked at HL60 cells (MLL-WT) and showed that MYC is severely inhibited after only 6 hours (most significant difference after a 24-hour treatment) of AZD5991 treatment (Liu *et al.*, 2022). We show here that all AML cell lines displayed a significant reduction in MYC expression levels in the nM range, after ET3002 treatment regardless of their MLL status. As previously described by Wu et al. (2022), MOLM-13 cells respond well to treatments such as AZD5991, gilterinib, MRX-2843 or their combination. Concentrations above 50nM resulted in a significantly higher (2-4-fold difference, ranging from cca. 20%-80%) value in apoptotic cells than in the control group or, in fact in the lower concentration treatment groups (Wu *et al.*, 2022). In this study similar results are presented, after 72 hours of ET3002, the levels of BCL-2 expression reduced significantly even in the nM range of treatment groups. The lowest $IC_{50}$ value was measured in OCI-AML3 cells; 133.0 nM. Similar results were published in a study by (Ishizawa *et al.*, 2015) where in OCI-

AML2 cells, they found a significantly reduced BCL-2 levels after a 48-hour treatment of ABT-199 (BCL-2 selective inhibitor). Another study looked at the effect of USF1 and USF2 compounds in the OCI-AML2 cell lines, which carries the MLL-AF6 translocation. A slight decrease in HOXA9 expression in each treatment group was observed but the biggest effect was achieved in the combined treatment group, that reduced the expression level to about 50% (Zhang *et al.*, 2020). Tzelepis *et. al.,* (2016) show that HOXA9 expressions in OCI-AML3 cells reduces in response to MB-3 which is a drug regulating the GCN5/PGC-1α pathway (Tzelepis *et al.*, 2016). A similar reduction is shown here, in HOXA9 levels in OCI-AML3 cells ($IC_{50}$ 93.87 nM), after a 72-hour of ET3002 treatment. In HL60 cells, a previous study found that in response to arsenic trioxide ($As_2O_3$) and ATRA (all trans retinoic acid) HOXA9 expression goes down significantly after a 12-hour treatment (Chen *et al.*, 2017).

Overall ET1126, ET1132 and ET3002 displayed a very strong efficacy to decrease the level of all downstream targets in AML cell lines, median $IC_{50}$ value roughly 10nM for ET1126 and ET1132 inhibitors, whereas ET3002 was not as effective. This data suggests that ET1126 and ET1132 could be a worthy drug candidate for solo regimen or for combination treatment.

# 7. Chapter

# CLK 1 activity in AML cells

## 7.1. Aims and objectives

In their study, (Iwai *et al.*, 2018) demonstrated that a pan-CLK inhibitor, T-025 has a tumour suppressor effect in an AML cell line (MV4-11) and in PDX (Patient derived xenograft) models. They also show that CLK inhibition downregulates *c-myc*-driven cancers and acts as a splicing modulator. In this study, a highly selective CLK1 inhibitor, Griffin 51 was tested to see if by CLK1 inhibition treatment, a down regulation in MYC can be seen. Other common oncogene levels such as HOXA9 and BCL-2 were also measured to test if Griffin 51 would have the same or similar effect on AML cells as SPHINX-31 (significant reduction in MYC, HOXA9 and BCL-2). To that end, cell viability levels in six different cell lines were measured and gauged if there is a similar effect on the BRD4 isoforms that can be used as a druggable target.

## 7.2. Introduction

CDC Like Kinase 1 (CLK1) plays an important role in pre-mRNA splicing by regulating serine-arginine-rich (SR) proteins. When phosphorylated, SR proteins transfer from nuclear speckles to the spliceosome. CLK1 enables the release of phosphorylated SR proteins by interacting with the RS-like domain in the N-terminus. By modulating the pre-mRNA splicing, many cancer cells can be rendered vulnerable to growth suppression and later to cell death. In their study, Iwai *et al.* (2018) showed that CLK inhibition functions as a pre-mRNA splicing modulator in MYC driven cancers and that T-025, a selective CLK inhibitor can be successfully used to reduce tumour burden *in vivo* which makes T-025 a worthy drug candidate for clinical use (Iwai *et al.*, 2018). Based

on this study and on the fact that CLK1 has a unique, symbiotic relationship with SRPK1, it was the logical next step to test if the same effect could be achieved.

## 7.3. Griffin 51 treatment on AML cell lines

As a highly selective CLK1 inhibitor, Griffin 51 was expected to reduce cell viability in AML cells as a previous study showed that CLK1 inhibition can be effective in reducing viability in T cell acute lymphoblastic leukaemia (Cordo *et al.*, 2022). A CRISPR based screening study identified that combining a CLK1 inhibitor with the clinically approved Venetoclax provides the best outcome for survival as it overcomes BCL-2 resistance. Although SM09419 is a pan-CLK pan-DYRK inhibitor, a separate target engagement assay showed that it is most effective in inhibiting CLK1 and CLK4 with an $IC_{50}$ value of 1nM (Wang *et al.*, 2022).

## 7.4. CLK1 intracellular TE assays

To assess the efficacy of these inhibitors without any potential confounding factors an Intracellular Kinase Target Engagement assay (K-5) was used with Griffin 51, ET1055, Thiii27 and ET1008, which all showed significant reduction in CLK-1 levels. For the ease of vector delivery, HEK293FT cells were used which were cultured as described in Chapter 3., paragraph 3.2.1.

Fig.7.1. shows a significant reduction in CLK1 ($IC_{50}$ 106.3 nM) after a 2-hour treatment of Griffin-51, a highly selective CLK1 inhibitor. The inhibitor

treatment successfully reduced CLK1 levels akin to a normal state which indicates that Griffin 51 could be a good drug candidate, with lesser side effects.

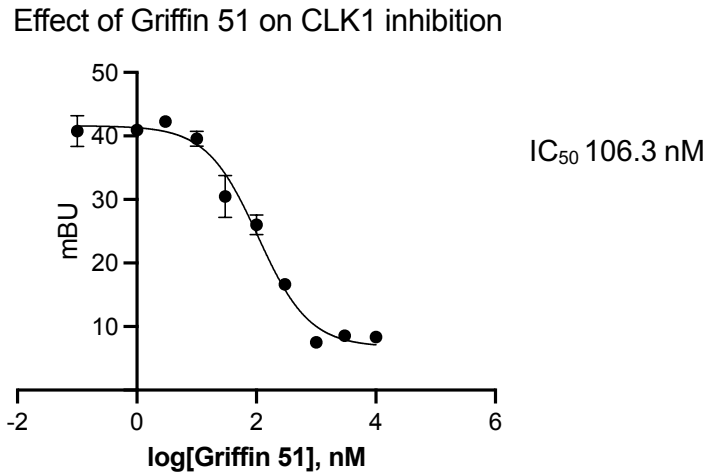



***Figure 7.1. CLK1 inhibition after Griffin 51 treatment measured via the NanoBRET Target Engagement assay***

***Fig. 7.1. shows the decreasing levels of BRET signal (mBU) correlating with the increasing levels of Griffin 51 treatment(1nM – 10$\mu$M). The mBU values were normalised to the vehicle control group (DMSO 0.1%). $IC_{50}$ value 106.3 nM The luminescence levels were measured at 460nm for acceptor and 610nm for donor emission and mBU ratio were calculated based on the equation mentioned in paragraph 4.3. Data presented were calculated from one biological replicate which had three technical repeates.***

ET1055 is a dual CLK1 and SRPK1 inhibitor that showed a significant reduction in CLK1 expression in this intracellular target engagement assay. With an $IC_{50}$ value of 142.6 nM it proved to be a worthy candidate to be further tested. Due to its dual inhibition quality (Based on previous data, proprietary information, Emenda Therapeutics, Gloucester, UK) ET1055 could have a synergistic effect on CLK1 and SRPK1 in supressing cell growth in AML (vs. when compared to single treatment) and other types of cancer. Fig.7.2. shows the effect of ET1055 on CLK1 inhibition after a 2 hour treatment.

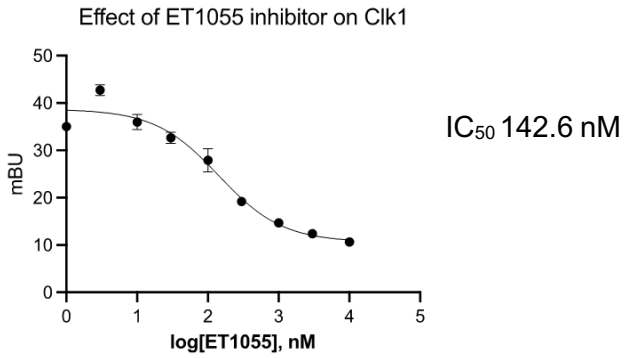



***Figure 7.2. CLK1 inhibition after ET1055 treatment measured via the NanoBRET Target Engagement assay***

***Fig. 7.2. shows the decreasing levels of BRET signal (mBU) correlating with the increasing levels of ET1055 treatment(1nM – 10$\mu$M). The mBU values were normalised to the vehicle control group (DMSO 0.1%). $IC_{50}$ value 142.6 nM The luminescence levels were measured at 460nm for acceptor and 610nm for donor emission and mBU ratio were calculated based on the equation mentioned in paragraph 4.3. Data presented were calculated from one biological replicate which had three technical repeates.***

Thiii27 is CLK1 inhibitor that showed great potential in this study but failed to achieve meaningful effect when tested in cell viability assays (data not shown). Fig.7.3. shows the effect of Thiii27, a selective CLK1 inhibitor's effect after a 2-hour treatment.

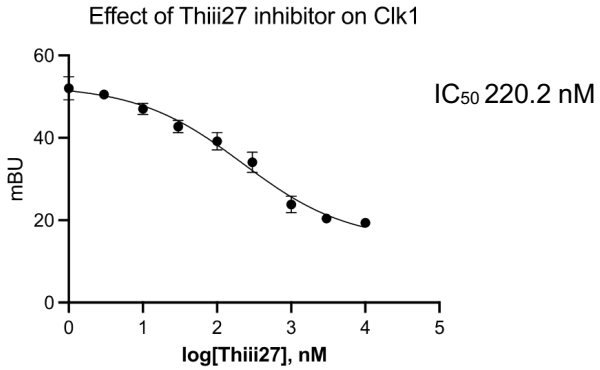



***Figure 7.3. CLK1 inhibition after Thiii27 treatment measured via the NanoBRET Target Engagement assay***

***Fig. 7.3. shows the decreasing levels of BRET signal (mBU) correlating with the increasing levels of Thiii27 treatment(1nM – 10$\mu$M). The mBU values were normalised to the vehicle control group (DMSO 0.1%). $IC_{50}$ value 220.2 nM. The luminescence levels were measured at 460nm for acceptor and 610nm for donor emission and mBU ratio were calculated based on the equation mentioned in paragraph 4.3. Data presented were calculated from one biological replicate which had three technical repeates.***

ET1008 is another CLK1 inhibitor that showed great potential in this assay and is yet to be tested in other assays to see if it is capable of achieving meaningful CLK1 inhibition in AML or other types of cancers. Fig.7.4. shows the effect of ET1008 on CLK1 inhibition in the cellular kinase target engagement assay, after a 2 hour incubation period with ET1008.

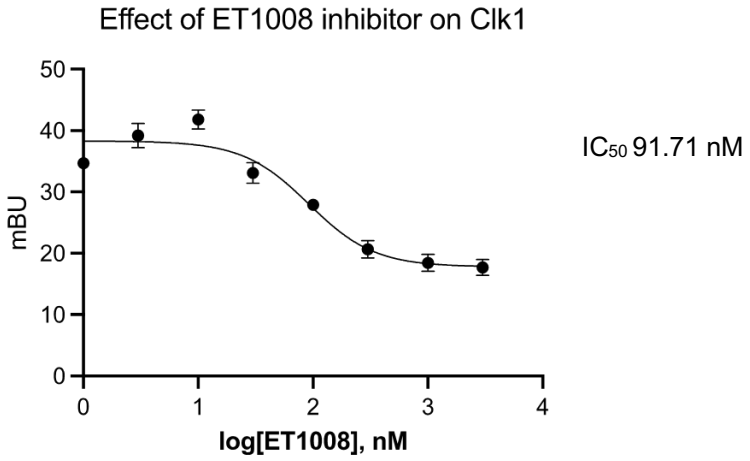



***Figure 7.4. CLK1 inhibition after ET1008 treatment measured via the NanoBRET Target Engagement assay***

***Fig. 7.4 shows the decreasing levels of BRET signal (mBU) correlating with the increasing levels of ET1008 treatment(1nM – 10$\mu$M). The mBU values were normalised to the vehicle control group (DMSO 0.1%).$IC_{50}$ value 91.71 nM.The luminescence levels were measured at 460nm for acceptor and 610nm for donor emission and mBU ratio were calculated based on the equation mentioned in paragraph 4.3. Data presented were calculated from one biological replicate which had three technical repeates.***

### 7.4.1. Cell viability assays after Griffin 51 treatment

Griffin 51, the most effective CLK1 inhibitor was selected to be tested for cell viability assays. all six AML cell lines (three with an MLL translocation and three without an MLL translocation or wild type) were tested to see if CLK1 inhibition would cause reduction in cell viability levels. In Fig. 7.5. the cell lines without MLL translocation can be found on the left hand side (figures 7.5. A, C, E) and cell lines with an MLL translocation (7.5. B, D, F) can be found on the right hand side. A compilation of all the data can be seen in Fig 7.5. (G).

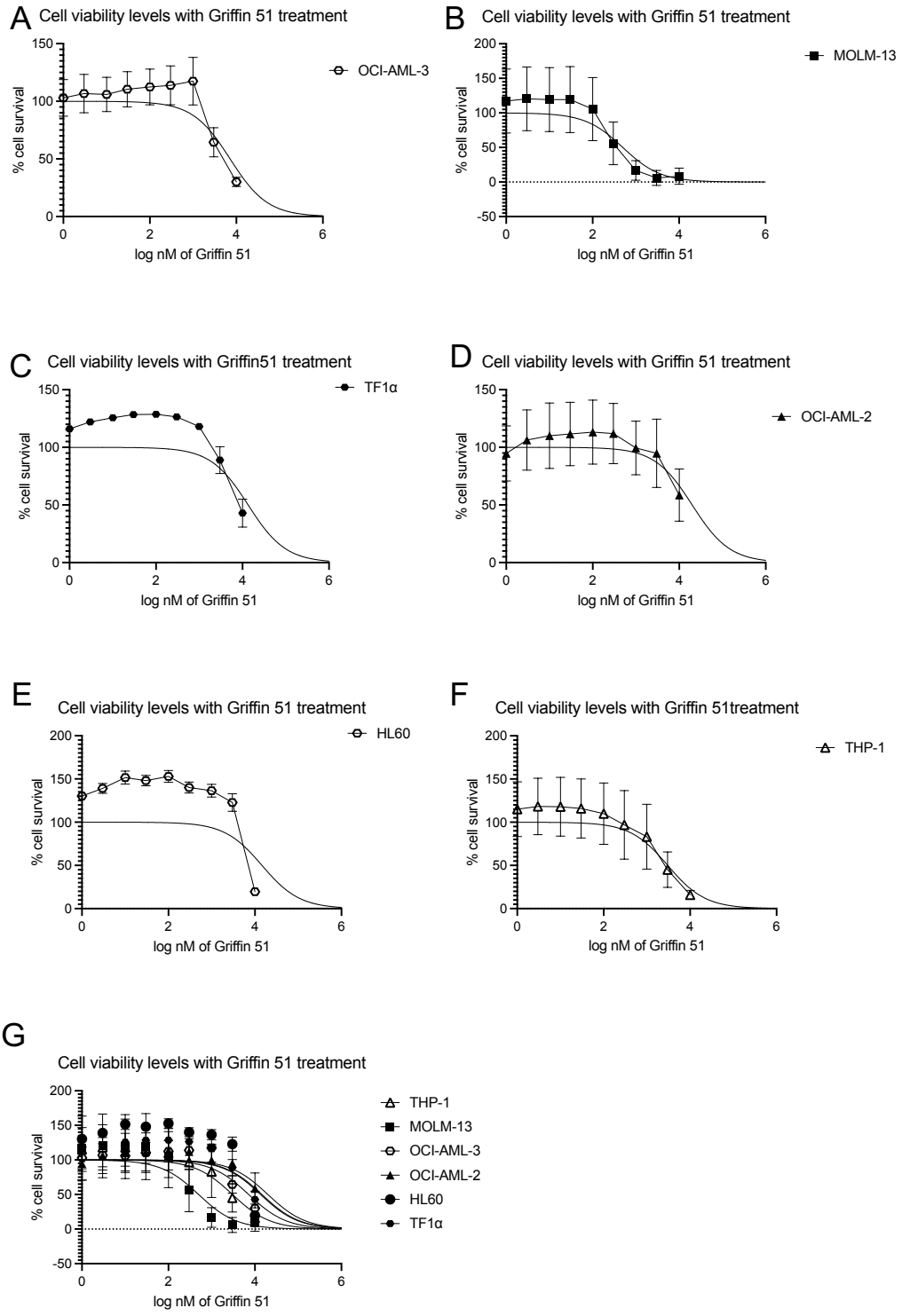



***Figure 7.5. AML Cell viability levels after Griffin 51 treatment***

***Fig. 7.5. (A) OCI-AML3 cells (MLL-WT) after 72 hours of Griffin 51 treatment, cell viability measured with Cell Titer Glo 2.0 ($IC_{50}$ 7181 nM). 7.5. (B) MOLM-13 cells (MLL-TL) after 72 hours of Griffin 51 treatment, ($IC_{50}$ 499.0 nM). 7.5. (C) TF1a cells (MLL-WT) after 72 hours of Griffin51 treatment. 7.5. (D) OCI-AML2 cells (MLL-TL) after 72 hours of Griffin 51 treatment. 7.5. (E) HL60 cells (MLL-WT) after 72 hours of Griffin 51 treatment. 7.5. (F) THP-1 (MLL-TL) cells after 72 hours of Griffin 51 treatment($IC_{50}$ 3034 nM). 7.5. (G) Summarised cell viability levels after Griffin 51 treatment in six different AML cell lines. All values were normalised to the vehicle control group***

***(DMSO 0.1%), averages presented from three biological replicates (n=3) which each was calculated from three technical replicates. Due to the high baseline the model was unable to calculate the $IC_{50}$ values for the OCI-AML2, HL60 and TF1a cell lines, the predicted range would be between 13-19$\mu$M.***

## 7.5. Downstream targets after Griffin 51 treatment in AML cell lines

As it was shown previously that CLK1 inhibition can be a successful drug target in MYC driven cancers. Griffin 51, a selective CLK1 inhibitor was tested in six different AML cell lines. Fig. 7.6. demonstrates that Griffin 51 was successful in significantly reducing the expression levels of MYC, HOXA9 and BCL-2 in all the six AML cell lines, even in nanomolar range. Fig.7.6. (A) shows the reduced levels of MYC expression in response to Griffin 51 treatment in THP-1 cells ($IC_{50}$ 41.29 nM). Fig.7.6. (B) shows the effect of Griffin 51 on BCL-2 levels in THP-1 cells ($IC_{50}$ 14.34 nM). Fig.7.6. (C) shows the effect of Griffin 51 on HOXA9 expression in THP-1 cells ($IC_{50}$ 68.60 nM).

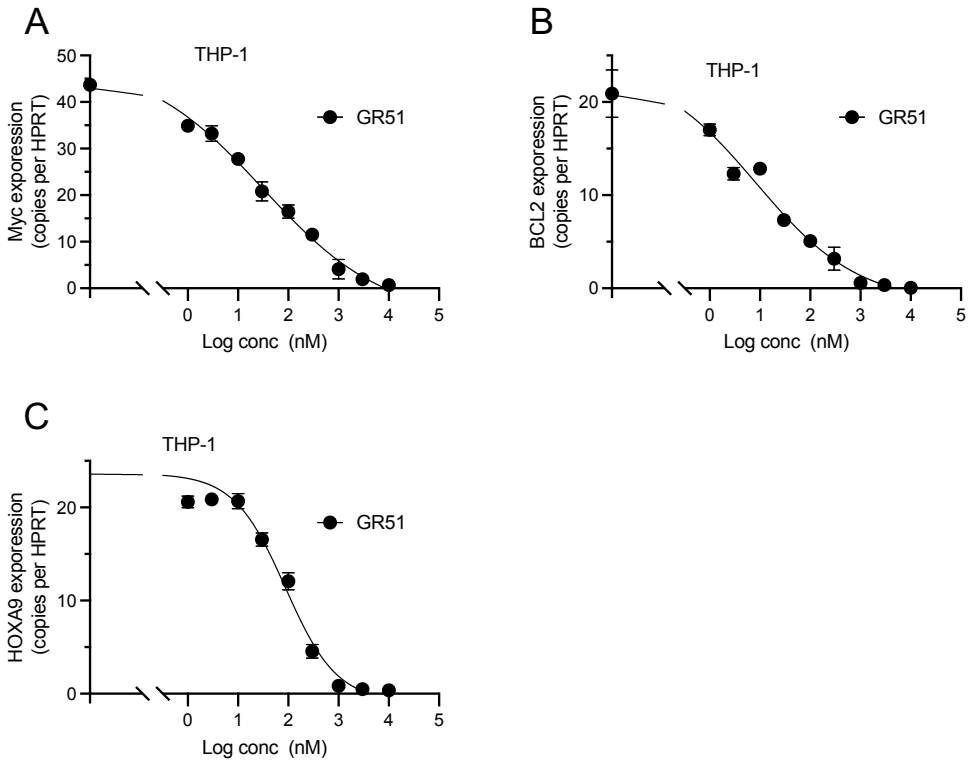



***Figure 7.6. Downstream target levels in THP-1 cells after Griffin 51 treatment.***

***Downstream target levels after 72 hours Griffin 51(GR51) treatment in THP-1 cells, measured by assessing the MYC, BCL-2 and HOXA9 expression levels, using ddPCR. All measurements were normalised to HPRT-1 housekeeping gene. Data represents the average of three biological replicates (n=3), which each were measured from three technical repeats. 7.6.(A) MYC expression levels after 72 hours of Griffin 51 treatment ($IC_{50}$ 41.29 nM). 7.6.(B) BCL-2 expression levels after 72 hours of Griffin 51 treatment ($IC_{50}$ 14.34 nM). 7.6.(C) HOXA9 expression levels after 72 hours of Griffin 51 treatment ($IC_{50}$ 68.60 nM).***

OCI-AML2, an MLL-TL cell line showed similar results to the THP-1 cells (Fig. 7.6.) where the reduction in MYC expression level was significantly reduces as it is shown in Fig.7.7. (A), ($IC_{50}$ 45.86 nM). HOXA9 expression level were similarly successful with an $IC_{50}$ value of 10.47 nM, as it is presented in Fig.7.7. (B). BCL-2 levels were also considerably reduced even in the nanomolar range, as it is demonstrated in Fig.7.7. (C), ($IC_{50}$ 0.7619 nM), making Griffin 51 the most effective inhibitor candidate for BCL-2 driven cancers.

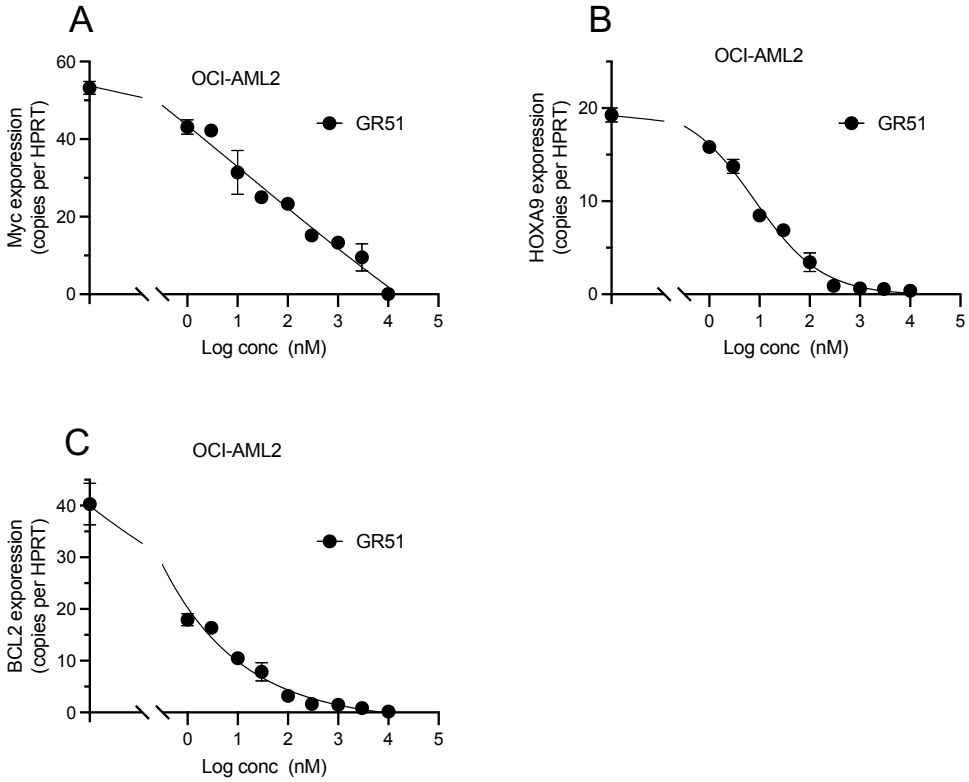



***Figure 7.7. Downstream target levels in OCI-AML2 cells after Griffin 51 treatment.***

***Downstream target levels after 72 hours Griffin 51(GR51) treatment in OCI-AML2 cells, measured by assessing the MYC, BCL-2 and HOXA9 expression levels, using ddPCR. All measurements were normalised to HPRT-1 housekeeping gene. Data represents the average of three biological replicates (n=3), which each were measured from three technical repeats. 7.7.(A) MYC expression levels after 72 hours of Griffin 51 treatment ($IC_{50}$ 45.86 nM). 7.7.(B) HOXA9 expression levels after 72 hours of Griffin 51 treatment ($IC_{50}$ 10.47 nM). 7.7.(C) BCL-2 expression levels after 72 hours of Griffin 51 treatment ($IC_{50}$ 0.7619 nM).***

MOLM-13 cells showed a significant reduction in MYC expression level as it can be seen in Fig.7.8. (A), $IC_{50}$ 6.569 nM, as well as in HOXA9 expression levels (as shown in Fig.7.8. (B), $IC_{50}$ 2.28 nM) and BCL-2 expression levels (as shown in Fig.7.8. (C), $IC_{50}$ 4.178 nM) expression levels. It showed similar results when compared to the previous two AML cell lines.

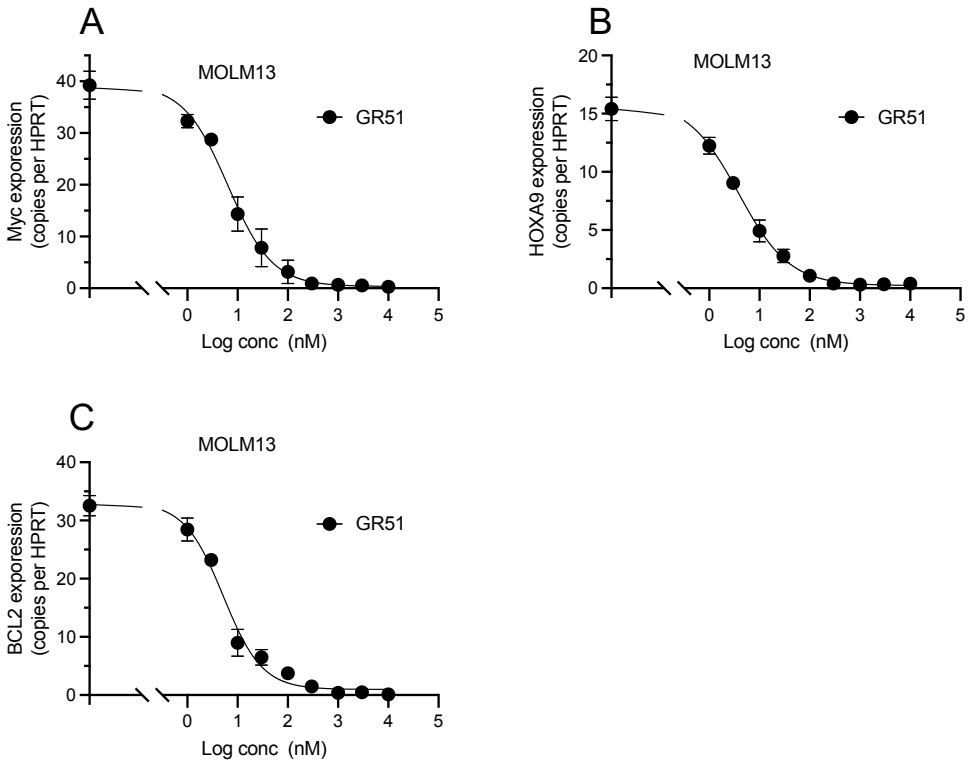



***Figure 7.8. Downstream target levels in MOLM-13 cells after Griffin 51 treatment***

***Downstream target levels after 72 hours Griffin 51(GR51) treatment in MOLM1-3 cells, measured by assessing the MYC, BCL-2 and HOXA9 expression levels, using ddPCR. All measurements were normalised to HPRT-1 housekeeping gene. Data represents the average of three biological replicates (n=3), which each were measured from three technical repeats. 7.8.(A) MYC expression levels after 72 hours of Griffin 51 treatment ($IC_{50}$ 6.569 nM). 7.8.(B) HOXA9 expression levels after 72 hours of Griffin 51 treatment ($IC_{50}$ 2.28 nM). 7.8.(C) BCL-2 expression levels after 72 hours of Griffin 51 treatment ($IC_{50}$ 4.178 nM).***

OCI-AML3, an AML-WT cell line showed very similar reduction in all three downstream targets as the MLL-translocated cells. The expression level of MYC was significantly reduced as it is shown in Fig.7.9. (A), $IC_{50}$ 7.158 nM. HOXA9 and BCL-2 levels were also significantly reduced in the nanomolar treatment range. The decrease in HOXA9 expression levels in response to Griffin 51 treatment can be seen in Fig.7.9. (B), ($IC_{50}$ 3.307 nM). Whereas the reduction in BCL-2 expression in OCI-AML3 cells is shown in Fig.7.9. (C),

($IC_{50}$ 0.84 nM), which is very similar to the level of BCL-2 reduction in the OCI-AML2, making this the second biggest inhibitor effect on BCL-2 expression.

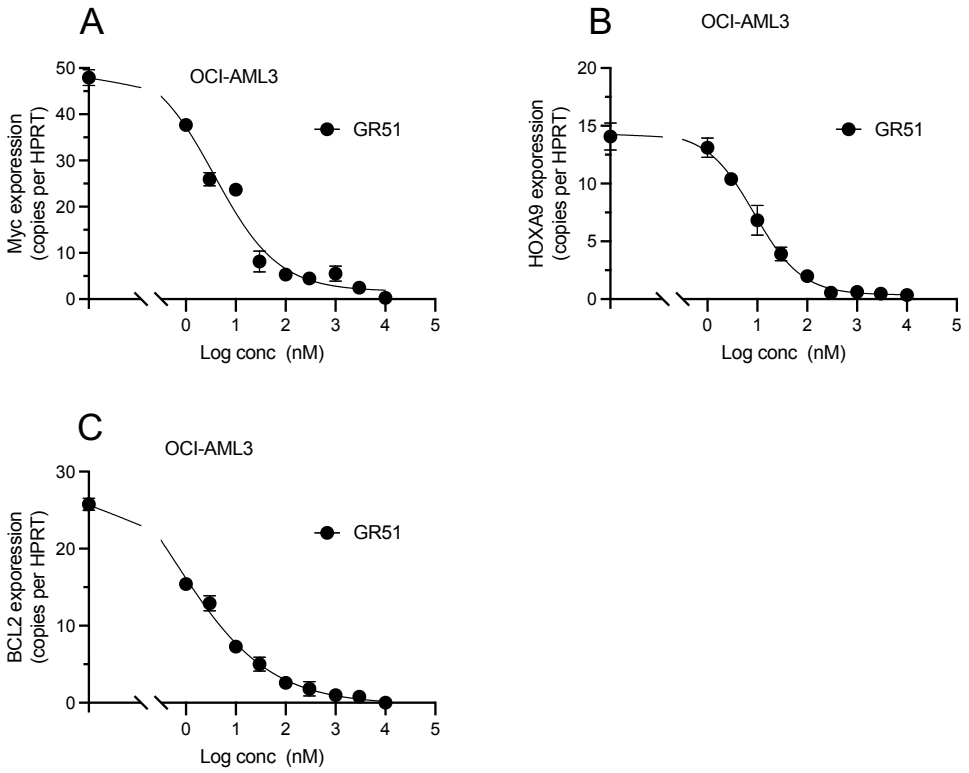



***Figure 7.9. Downstream target levels in OCI-AML3 cells after Griffin 51 treatment***

***Downstream target levels after 72 hours Griffin 51(GR51) treatment in OCI-AML3 cells, measured by assessing the MYC, BCL-2 and HOXA9 expression levels, using ddPCR. All measurements were normalised to HPRT-1 housekeeping gene. Data represents the average of three biological replicates (n=3), which each were measured from three technical repeats. 7.9.(A) MYC expression levels after 72 hours of Griffin 51 treatment ($IC_{50}$ 7.158 nM). 7.9.(B) HOXA9 expression levels after 72 hours of Griffin 51 treatment ($IC_{50}$ 3.307 nM). 7.9.(C) BCL-2 expression levels after 72 hours of Griffin 51 treatment ($IC_{50}$ 0.84 nM).***

All cell lines, including the HL60 cells showed a significant reduction in all downstream targets. As with the previous cell lines, the highest level of baseline expression was measured from MYC and similar levels of expressions were measured from HOXA9 and BCL-2, which all responded well to Griffin 51 treatment. The reduction in MYC expression levels in response to Griffin 51 treatment in shown in Fig.7.10. (A), ($IC_{50}$ 9.222 nM) The

decreased HOXA9 levels in HL60 cells is shown in Fig.7.10 (B), ($IC_{50}$ 18.30 nM). And the level of BCL-2 expression in HL60 cells is shown in Fig.7.10. (C), ($IC_{50}$ 5.429 nM).

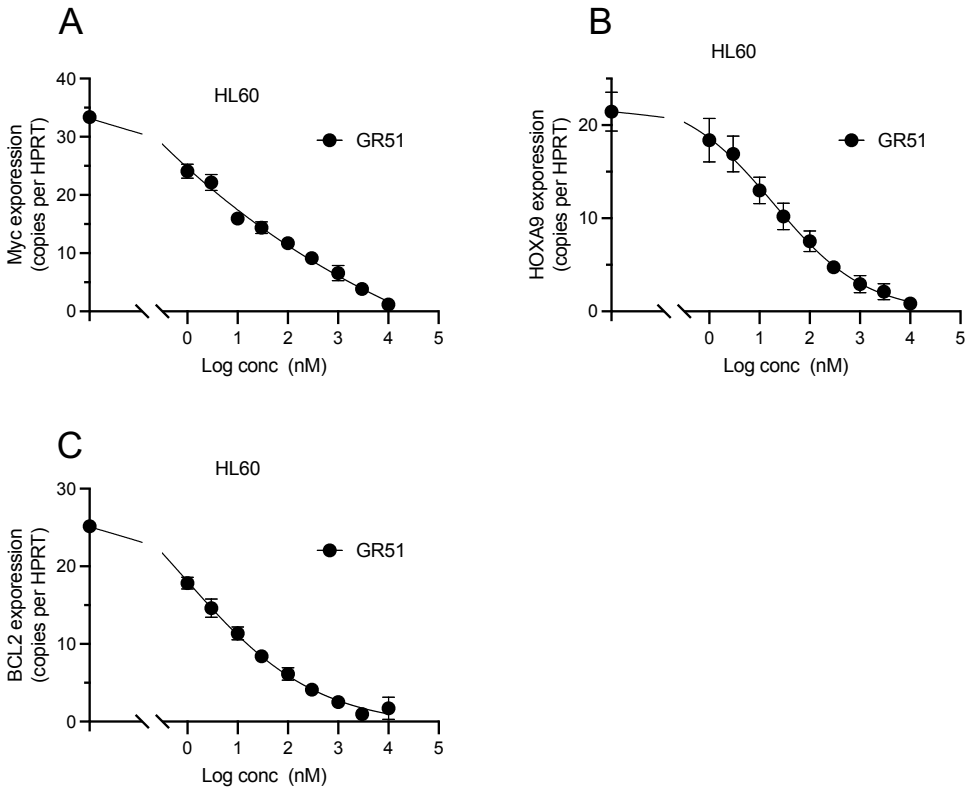



***Figure 7.10. Downstream target levels in HL60 cells after Griffin 51 treatment***

***Downstream target levels after 72 hours Griffin 51(GR51) treatment in HL60 cells, measured by assessing the MYC, BCL-2 and HOXA9 expression levels, using ddPCR. All measurements were normalised to HPRT-1 housekeeping gene. Data represents the average of three biological replicates (n=3), which each were measured from three technical repeats. 7.10.(A) MYC expression levels after 72 hours of Griffin 51 treatment ($IC_{50}$ 9.222 nM). 7.10.(B) HOXA9 expression levels after 72 hours of Griffin 51 treatment ($IC_{50}$ 18.30 nM). 7.10.(C) BCL-2 expression levels after 72 hours of Griffin 51 treatment ($IC_{50}$ 5.429 nM).***

TF1a, the last cell line without the MLL-translocation expressed similar levels of MYC, HOXA9 and BCL-2 as the previous cell lines, regardless of their MLL status. The highest level of baseline expression was measured in the MYC group as shown in Fig.7.11. (A), which was significantly reduced by Griffin 51

treatment, ($IC_{50}$ 7.139 nM). Moderate baseline expression levels were measured in HOXA9 (as it is shown in Fig.7.11. (B), $IC_{50}$ 43.26 nM) and BCL-2 (as it is shown in Fig.7.11. (C), ($IC_{50}$ 12.03 nM).

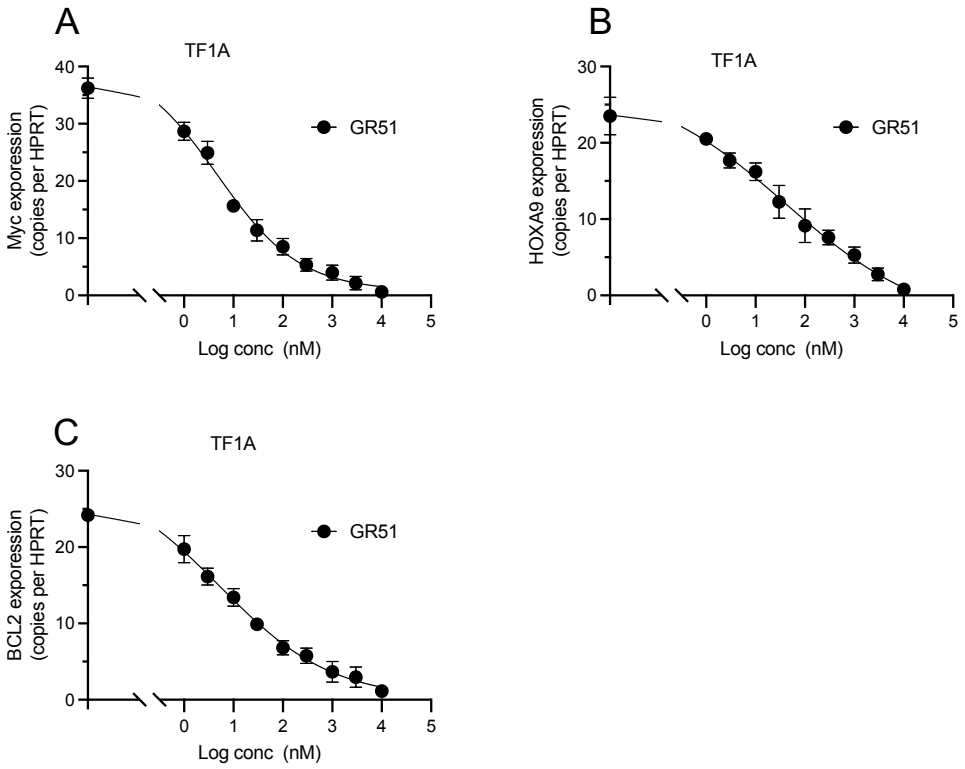



***Figure 7.11. Downstream target levels in TF1a cells after Griffin 51 treatment***

***Downstream target levels after 72 hours Griffin 51(GR51) treatment in TF1a (MLL-WT) cells, measured by assessing the MYC, BCL-2 and HOXA9 expression levels, using ddPCR. All measurements were normalised to HPRT-1 housekeeping gene. Data represents the average of three biological replicates (n=3), which each were measured from three technical repeats. 7.11.(A) MYC expression levels after 72 hours of Griffin 51 treatment ($IC_{50}$ 7.139 nM). 7.11.(B) HOXA9 expression levels after 72 hours of Griffin 51 treatment ($IC_{50}$ 43.26 nM). 7.11.(C) BCL-2 expression levels after 72 hours of Griffin 51 treatment ($IC_{50}$ 12.03 nM).***

## 7.6. IC50 values of different AML cells after SPHINX-31 and Griffin 51 treatment

To sum up the inhibitory effect of SPHINX-31 and Griffin 51 on the expression of MYC, HOXA9 and BCL-2, ddPCR data is shown below with averages $IC_{50}$ data for all six AML cell lines, separated by their MLL-status. In terms of reducing the MYC protein levels, SPHINX-31 and Griffin 51 seemed to have no difference, with MOLM-13 cells being the most vulnerable to Griffin 51 treatment and HL60 cells to be most affected by SPHINX-31 treatment. The different $IC_{50}$ values are shown in Fig.7.12 below.

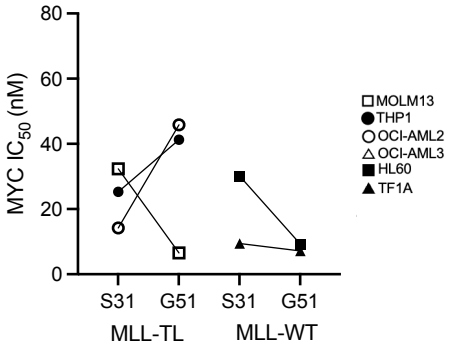



***Figure 7.12. Comparison of IC50 values of MYC levels in AML cells***

***$IC_{50}$ values were plotted and compared based of the MYC level measurements presented in the above figures. The MYC levels were measure after a 72 hour treatment in the 6 AML cell lines. The figure shows the effects of SPHINX-31 and Griffin 51 treatment in reducing MYC levels in AML cell lines. No significant difference was found (p=0.356) between the efficacy of the two inhibitors.***

The biggest effect could be seen in HOXA9 levels in MOLM-13 cells, after Griffin 51 treatment and in OCI-AML2 cell line, which was the most susceptible to SPHINX-31 treatment, as it is shown in Fig.7.13. below.

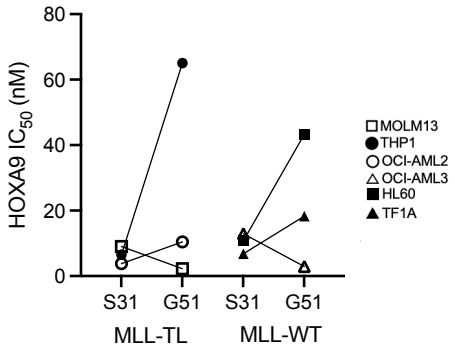



***Figure 7.13. Comparison of IC50 values of HOXA9 levels in AML cells***

***$IC_{50}$ values were plotted and compared based on the HOXA9 level measurements presented in the above figures. The HOXA9 levels were measure after a 72 hour treatment in the 6 AML cell lines. The figure shows the effects of SPHINX-31 and Griffin 51 treatment.***

Levels of BCL-2 expression showed similar results, HL60 cells were most effected by Griffin 51 treatment and THP-1 cells turned out to be most vulnerable to SPHINX-31 treatment. Data shown below in Fig.7.14.

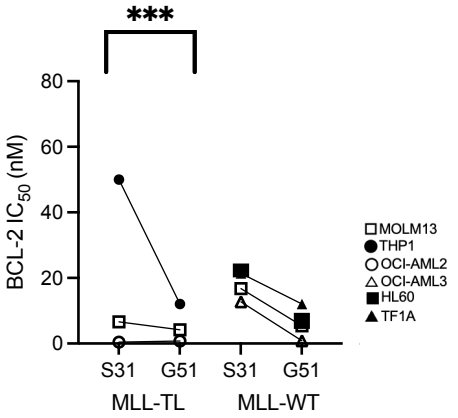



***Figure 7.14. Comparison of IC50 values of BCL2 levels in AML cells***

***$IC_{50}$ values were plotted and compared based on the BCL-2 level measurements presented in the above figures. The BCL-2 levels were measure after a 72 hour treatment in the 6 AML cell lines. The figure shows the effects of SPHINX-31 and Griffin 51 treatment. ***p=0.0004, calculated by one way ANOVA, comparing the MLL-TL and MLL-WT groups and cell lines within***

## 7.7. BRD4 splice change after Griffin 51 treatment in AML cell lines

Given the effect that was achieved using SPHINX-31 in modulating the BRD4 isoform change, CLK1 inhibition was also tested to see if, Griffin 51 a selective CLK1 inhibitor could trigger the same effect. A somewhat similar study tested T-025, a pan CLK inhibitor for the treatment of MYC driven breast cancer cells, MDA-MB-468, which showed significant reduction in *in vitro* cell proliferation and in *in vivo* xenograft size. Since it has been shown that T-025 works through the modulation of pre-mRNA splicing, the next logical step was to look at other targets which can influence alternative splicing and use it as a druggable target for treatment (Iwai *et al.*, 2018).

MOLM-13 cells were treated with Griffin 51 with increasing concentrations and tested via RT-PCR, using BRD4s and BRD4l primers. Fig.7.15. (A) demonstrates the changes in band intensity; with the increasing concentration level of Griffin 51 the anti-tumourigenic BRD4l isoform becomes more profound, $IC_{50}$ 166.0 nM. In the gel, there are signs of double bands which could be due to unspecific primer annealing but the overall picture shows that BRD4s practically disappears in the highest treatment group. Fig.7.15. (B) shows the ratio of BRD4s-BRD4l from the raw data. And Fig.7.15. (C) shows the normalised values of the BRD4s-BRD4l values in the different treatment groups.

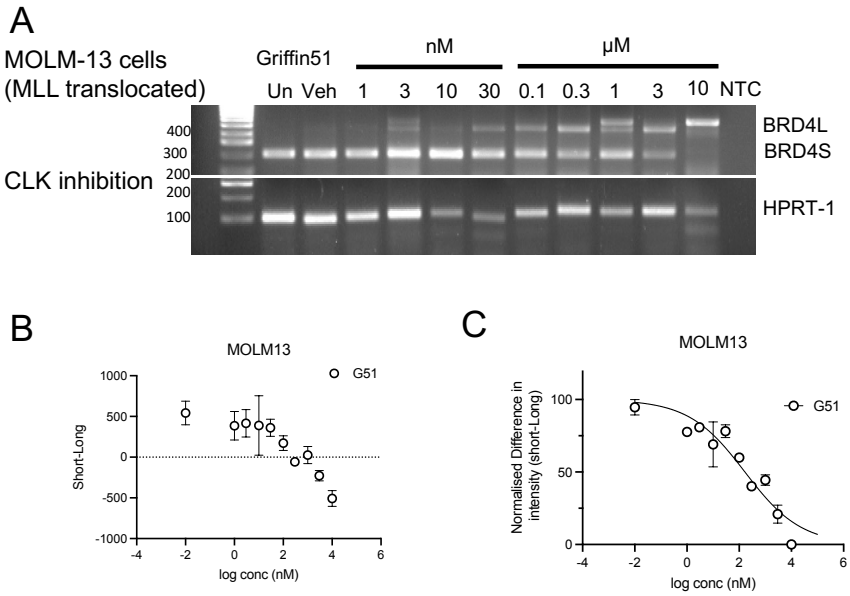



***Figure 7.15. BRD4 splice change in MOLM-13 cells after Griffin 51 treatment***

***Fig.7.15. (A) Expression levels of HPRT-1, BRD4s and BRD4l isoforms are shown on 2% agarose gel in MOLM-13 (MLL-TL) cells, after 72 hours of Griffin 51 treatment, $IC_{50}$ 166.0 nM. Expression of the housekeeping gene HPRT1 was not altered by Griffin 51 treatment. Figure 7.15 (B)shows the difference in expression of the two isoforms with increasing concentration of Griffin51. Fig. 7.15. (C) To obtain the sensitivity of the MOLM13 cells to these inhibitors the difference in expression was normalised to the vehicle control (i.e., 100% BRD4s) and the highest concentration (i.e. 100% BRD4L expression). Expression of BRD4s, BRD4l and HPRT-1 in MOLM13 cell line was determined by RT-PCR and visualized on a 2% gel by agarose gel electrophoresis. The expected band sizes were, BRD4s 206 bp and BRD4l: 488 bp, HPRT-1: 101 bp. The optical density was measured using Image Studio. All data points represent three biological replicates (n=3), which each were calculated using three technical replicates.***

OCI-AML2 cells, also an MLL-translocated cell line showed an even more robust response to treatment. Where the short isoform visibly disappeared from 300nM concentration as it can be seen in Fig.7.16. (A). Here, double bands (that could signal some unspecific binding) also appear but the isoform change is definitive in the sample, $IC_{50}$ 182.7 nM. Fig.7.16. (B) shows the difference in short-long isoform, whereas Fig.7.16. (C) demonstrates the response curve in OCI-AML2 cells, normalised to the baseline.

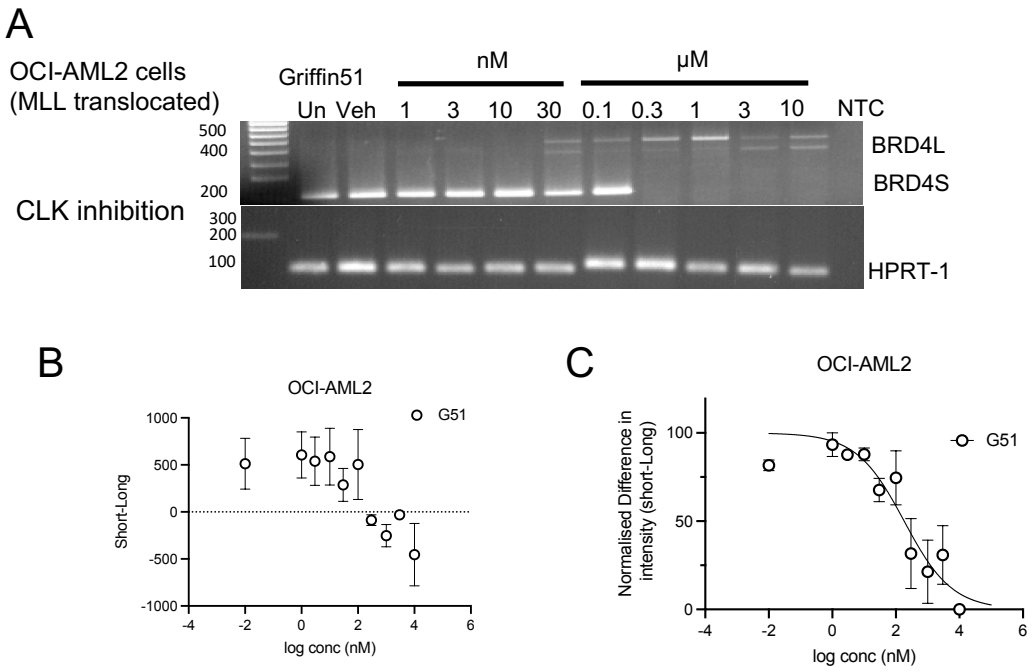



***Figure 7.16. BRD4 splice change in OCI-AML2 cells after Griffin 51 treatment***

***Fig.7.16. (A) Expression levels of BRD4s and BRD4l isoforms are shown on agarose gel in OCI-AML2 (MLL-TL) cells, after 72 hours of Griffin 51 treatment $IC_{50}$ 182.7 nM. Expression of the housekeeping gene HPRT1 was not altered by Griffin 51 treatment. Figure 7.16 (B)shows the difference in expression of the two isoforms with increasing concentration of Griffin51. Fig. 7.16. (C) To obtain the sensitivity of the OCI-AML2 cells to these inhibitors the difference in expression was normalised to the vehicle control (i.e., 100% BRD4s) and the highest concentration (i.e. 100% BRD4L expression). Expression of BRD4s, BRD4l and HPRT-1 in OCI-AML2 cell line was determined by RT-PCR and visualized on a 2% gel by agarose gel electrophoresis. The expected band sizes were, BRD4s 206 bp and BRD4l: 488 bp, HPRT-1: 101 bp. The optical density was measured using Image Studio. All data points represent three biological replicates (n=3), which each were calculated using three technical replicates.***

THP-1 cells showed a similar dose response to Griffin 51 treatment, with multiple bands appearing in same of the samples, as it can be seen in Fig.7.17. (A). However, the short isoforms visibly disappear in the micromolar range and that the long isoform is well presented from 300nM concentration $IC_{50}$ 227.9 nM. In Fig.7.17. (B) the difference between the short and long isoform is shown in response to increasing concentration of inhibitor treatment. Fig.7.17. (C) shows the dose response curve (in response to Griffin 51 treatment in THP-1 cells) normalised to the baseline.

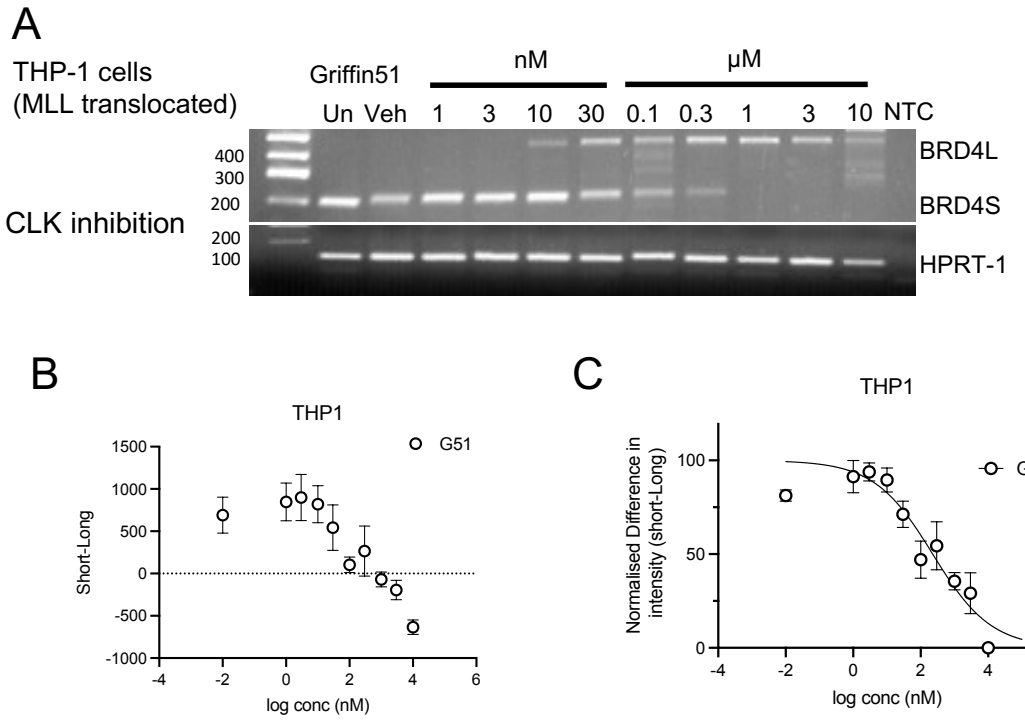



***Figure 7.17. BRD4 splice change in THP-1 cells after Griffin 51 treatment***

***Fig.7.17. (A) Expression levels of BRD4s and BRD4l isoforms are shown on agarose gel in THP-1 (MLL-TL) cells, after 72 hours of Griffin 51 treatment, $IC_{50}$ 227.9 nM. Expression of the housekeeping gene HPRT1 was not altered by Griffin 51 treatment. Figure 7.17 (B)shows the difference in expression of the two isoforms with increasing concentration of Griffin51. Fig. 7.17. (C) To obtain the sensitivity of the THP-1 cells to these inhibitors the difference in expression was normalised to the vehicle control (i.e., 100% BRD4s) and the highest concentration (i.e. 100% BRD4L expression). Expression of BRD4s, BRD4l and HPRT-1 in THP-1 cell line was determined by RT-PCR and visualized on a 2% gel by agarose gel electrophoresis. The expected band sizes were, BRD4s 206 bp and BRD4l: 488 bp, HPRT-1: 101 bp. The optical density was measured using Image Studio. All data points represent three biological replicates (n=3), which each were calculated using three technical replicates.***

Results from TF1a cells are less clear than from the previous cell lines. BRD4s expression disappears after 100nM of Griffin 51 treatment but a shadow can be seen (these are likely to be unannealed primers) in all the higher treatment groups, as it is shown in Fig.7.18. (A), $IC_{50}$ 11.24 nM. Fig.7.18. (B) shows the difference of the short and long isoforms in the different treatment groups. Fig.7.19. (C) shows to dose response curve (in response to increasing levels of Griffin 51 treatment in TF1a cells) normalised to the baseline.

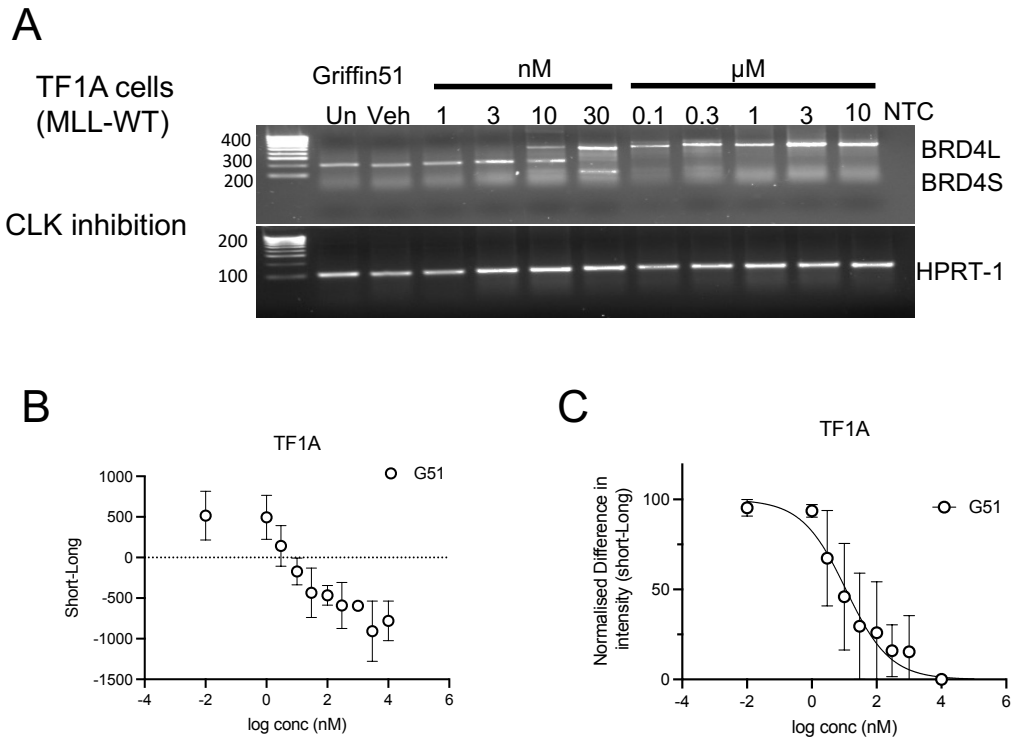



***Figure 7.18. BRD4 splice change in TF1a cells after Griffin 51 treatment***

***Fig.7.18. (A) Expression levels of BRD4s and BRD4l isoforms are shown on agarose gel in TF1a (MLL-WT) cells, after 72 hours of Griffin 51 treatment $IC_{50}$ 11.24 nM. Expression of the housekeeping gene HPRT1 was not altered by Griffin 51 treatment. Figure 7.18. (B)shows the difference in expression of the two isoforms with increasing concentration of Griffin51. Fig. 7.18. (C) To obtain the sensitivity of the TF1a cells to these inhibitors the difference in expression was normalised to the vehicle control (i.e., 100% BRD4s) and the highest concentration (i.e. 100% BRD4L expression). Expression of BRD4s, BRD4l and HPRT-1 in TF1a cell line was determined by RT-PCR and visualized on a 2% gel by agarose gel electrophoresis. The expected band sizes were, BRD4s 206 bp and BRD4l: 488 bp, HPRT-1: 101 bp. The optical density was measured using Image Studio. All data points represent three biological replicates (n=3), which each were calculated using three technical replicates.***

Similar to the TF1a cells (Fig.7.18.), the HL60 cells also showed a less clear expression of the two different BRD4 isoform. The BRD4s isoform visibly disappears from the 300nM treatment group but a background shadow can be seen in all the treatment groups as it is shown in Fig.7.19. (A), $IC_{50}$ 40.76 nM . The BRD4l isoform appears from 30nM treatment group, with the splice change seemingly complete in the 300nM treatment group. Fig.7.19. (B) shows the difference between the short and long isoforms. Fig.7.19. (C)

shows the dose response curve in HL60 cells, which is normalised to the baseline.

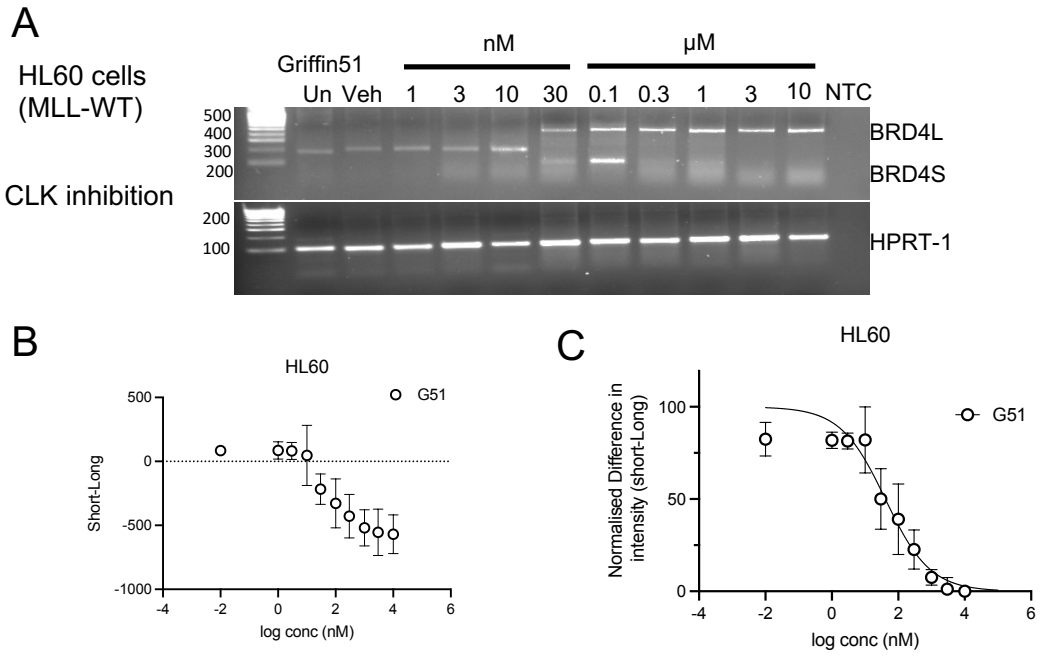



***Figure 7.19. BRD4 splice change in HL60 cells after Griffin 51 treatment***

***Fig.7.19. (A) Expression levels of BRD4s and BRD4l isoforms are shown on agarose gel in HL60 (MLL-WT) cells, after 72 hours of Griffin 51 treatment $IC_{50}$ 40.76 nM. Expression of the housekeeping gene HPRT1 was not altered by Griffin 51 treatment. Figure 7.19. (B) shows the difference in expression of the two isoforms with increasing concentration of Griffin51. Fig. 7.19. (C) To obtain the sensitivity of the HL60 cells to these inhibitors the difference in expression was normalised to the vehicle control (i.e., 100% BRD4s) and the highest concentration (i.e. 100% BRD4L expression). Expression of BRD4s, BRD4l and HPRT-1 in HL60 cell line was determined by RT-PCR and visualized on a 2% gel by agarose gel electrophoresis. The expected band sizes were, BRD4s 206 bp and BRD4l: 488 bp, HPRT-1: 101 bp. The optical density was measured using Image Studio. All data points represent three biological replicates (n=3), which each were calculated using three technical replicates.***

OCI-AML3 cells also showed a strong response to Griffin 51 treatment. Fig.7.20. (A) demonstrates the isoform change from BRD4s (more pronounced in the lower concentration groups) to BRD4l which is more pronounced in the higher concentration groups, $IC_{50}$ 42.79 nM. There are also double bands which can indicate non-specific annealing. Fig.7.20. (B) shows the difference between the short and long isoform of BRD4 in the different

treatment groups. Fig.7.20. (C) shows the normalised response curve in OCI-AML3 cells.

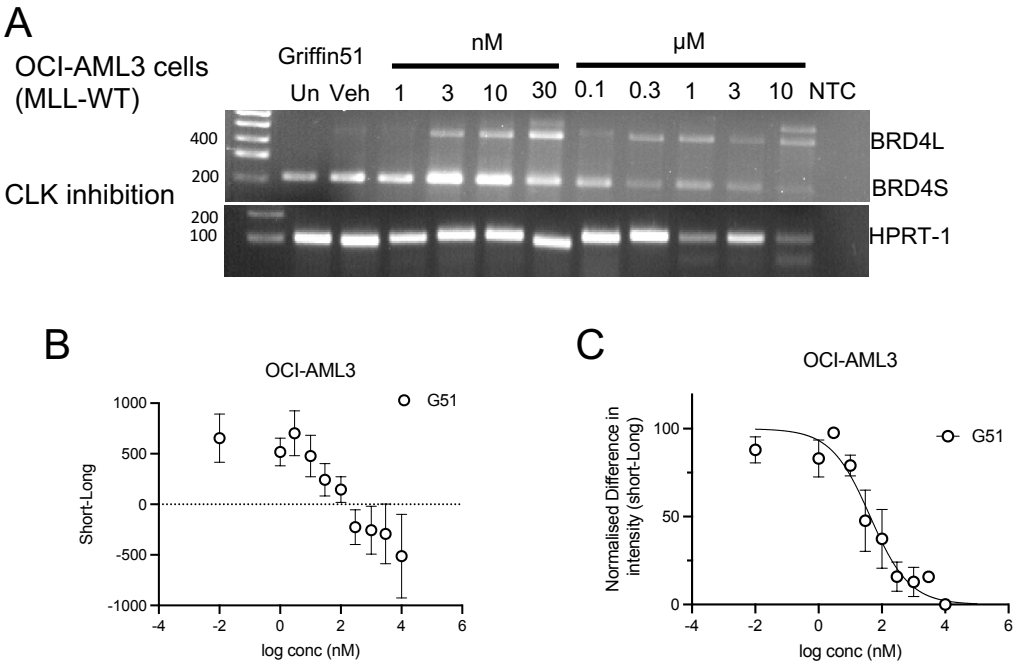



***Figure 7.20. BRD4 splice change in OCI-AML3 cells after Griffin 51 treatment***

***Fig.7.20. (A) Expression levels of BRD4s and BRD4l isoforms are shown on agarose gel in OCI-AML3 (MLL-WT) cells, after 72 hours of Griffin 51 treatment $IC_{50}$ 42.79 nM. Expression of the housekeeping gene HPRT1 was not altered by Griffin 51 treatment. Figure 7.20. (B)shows the difference in expression of the two isoforms with increasing concentration of Griffin51. Fig. 7.20. (C) To obtain the sensitivity of the OCI-AML3 cells to these inhibitors the difference in expression was normalised to the vehicle control (i.e., 100% BRD4s) and the highest concentration (i.e. 100% BRD4L expression). Expression of BRD4s, BRD4l and HPRT-1 in OCI-AML3 cell line was determined by RT-PCR and visualized on a 2% gel by agarose gel electrophoresis. The expected band sizes were, BRD4s 206 bp and BRD4l: 488 bp, HPRT-1: 101 bp. The optical density was measured using Image Studio. All data points represent three biological replicates (n=3), which each were calculated using three technical replicates.***

## 7.8. $IC_{50}$ data for BRD4 splice change in AML cells

A compilation of $IC_{50}$ data shows that SPHINX-31 (S31) was more successful in initiating a splice change in BRD4 expression than Griffin 51 (GR51) in the AML cell lines where there is a MLL translocation present. However, the statistical analysis did not show significant differences due to large SEM values. In the AML cell lines without the MLL translocation, a smaller effect can be seen and the difference between the SPHINX-31 and Griffin 51 treatment is not significant. Fig.7.21. shows the difference between the $IC_{50}$ data of SPHINX-31 and Griffin 51. Datapoints are separated into two groups, representing the three cell lines with translocations (MLL-TL) and the cells lines without a translocation (MLL-WT).

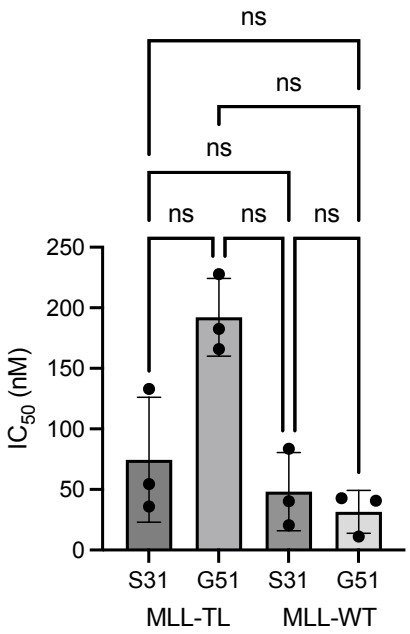



***Figure 7.21. IC50 data for BRD4 splice change in AML cells***

***Fig 7.21 shows the effect of SPHINX-31 and Griffin 51 treatment on the isoform change of BRD4. Data was gathered from six different AML cell lines with or without an MLL translocation. It can be seen that SPHINX-31 was a lot more effective in both MLL-TL and MLL-WT groups, whereas Griffin 51 had little effect in the MLL-TL group. Overall, the tested inhibitors achieved a robust effect in switching the expression of BRD4s to the favourable BRD4l in small dosage whit $IC_{50}$ values well below the micromolar range. Statistical analysis was done by using a paired t-test, p=0.125.***

## 7.9. Discussion and conclusion

In previous studies, cells with low expression of CLK1 such as T47D (breast carcinoma) and THP-1 (monocytic leukaemia) were tested with developmental inhibitors and compared to high expression level CLK1 cell lines such as T24 (urinary bladder carcinoma), MDA-MB-231 (breast adenocarcinoma) and HepG2 (hepatocellular carcinoma). The most sensitive cell lines were those with higher CLK1 levels; T24 and HepG2 with 0.6μM and 2.8μM $GI_{50}$ values respectively. The low level CLK1 cell lines were considerably less affected, such as THP-1 and T47D, and the cell line with moderate expression levels of CLK1 was only mildly affected ($GI_{50}$ 9.6 μM) (ElHady *et al.*, 2017). Other studies showed similar effects, when gastric cancer cell lines: SNU-1, SNU-5, SNU-16, KATO-III and AGS were treated with TG003 and CLK1 siRNA. Silencing CLK1 in these cell lines resulted in decreased cell viability, proliferation and the lack of invasion and migration capability, which usually is present. These results were later replicated in patient derived xenografts (PDX) (Babu *et al.*, 2020). In other cancer types, such as lung cancer, hypoxia stimulated the expression of alternatively spliced isoform of tissue factor (asTF) which is highly expressed in the A549 cell lines, whereas in normoxia they express the full-length tissue factor (flTF). They also found that alongside asTF CLK1 is also highly expressed and by using siRNA the effect can be reversed (Eisenreich *et al.*, 2013).

Previous work showed that CLK1 can be a good drug target for hard to treat cancers such as AML. Iwai *et al.* (2018) tested T-025 which caused a

modulation in pre-mRNA splicing, which reduced the CLK dependent phosphorylation, resulting in skipped exons, cell death and suppression in cell growth both *in vitro* and in *in vivo* models. They found that the biggest effect was observed in CLK2 (0.096 $K_d$ nmol/L) inhibition but T-025 also reduced MYC expression which had a synergistic effect with CLK inhibitors. In a MYC-driven breast cancer (MBA-MD468) *in vivo* model, T-025 achieved a significant reduction in tumour progression and was well tolerated through oral administration (Iwai *et al.*, 2018). However, T-025 is not CLK selective as it has an inhibitory effect on the DYRK kinase group (for instance DYRK1A 0.074 $K_d$ nmol/L). Therefore, we cannot be certain if the positive effects of the inhibitor were a result of CLK1 inhibition or inhibiting other protein kinases.

### 7.9.1. Intracellular target engagement assay

Very recently an effective benzothiophene-based hydrazides CLK1 inhibitor on a 5-methoxybenzothiophene scaffold was published, which was effective in reducing CLK1 levels in T24 cells (El-Gamil *et al.*, 2023). In our study, we show similar results, namely that Griffin 51 had a similarly strong effect on CLK1 inhibition in transfected HEK cells only after 2 hour treatment vs. the 6.4 hour treatment used in the El-Gamil et. al (2023) study. See Fig.7.1.

### 7.9.2. Cell viability assays

A previous study showed that CLK inhibition results in reduced viability levels in various cancer cells such as MDA-MB-468, SW620, HCT-116, etc. (Araki *et al.*, 2015). It is shown in our data that Griffin 51 was successful in significantly reducing cell viability levels in AML cells in the micromolar range, regardless of their MLL status. A drop in viability levels can be seen from 1μM inhibitor concentration with most cell lines displaying the greatest effect in the highest treatment group (10μM).

### 7.9.3. BRD4 splice change in response to Griffin 51 treatment

Previously, Tzelepis et al. (2018) showed that SPHINX-31 can initiate a splice change in BRD4 in AML cells. Here, it is shown that Griffin 51 is equally successful in initiating a splice change in BRD4 in the MLL-WT cells and slightly less successful in the MLL-TLL cells. None of the results are however significantly different due to large SEM. This is due to a couple of outlier data points, especially in the MOLM-13 and TF1a cell line data. See. Fig.7.21.

### 7.9.4. Downstream target levels after inhibitor treatments

Another study found high MYC expression levels to correlate with higher chances of relapse in amongst untreated AML patients. It was also associated with a significantly lower median survival (24 vs. 13 months) and a lesser chance of a relapse free survival (25 vs. 12 months), (Ohanian *et al.*, 2019). When looking at AML cell lines, (Brondfield *et al.*, 2015) found that JQ1, a BRD4 selective inhibitor can indirectly reduce the MYC expression levels in the MOLM-14, MV4-11, HL60, FKH-1, OCI-AML5, AP1060, MUTZ-2 AML cell lines even in nanomolar range. AZD5991, a selective MCL-1 inhibitor was able to downregulate the expression levels of MYC in MOLM-13 cells. The study by (Wu *et al.*, 2022) show similar results to the ones presented here, with the slight difference that their focus was on specifically testing inhibitors against FLT3-mutated AML cells such as MOLM-13 and MV4-11.

OCI-AML2 cells overexpress BCL-2, which can be inhibited with only 100nM of Venetoclax with only a 2-hour treatment. Venetoclax is an FDA approved BCL-2 selective inhibitor (Zhang *et al.*, 2022). It is shown here that very low doses of Griffin 51 can have the same effect within the same period.

In their study, (Wu *et al.*, 2015) noted the heightened expression of BCL-2 in the HL-60 cell line but they were able to reduce the expression rate alongside with inducing apoptosis just by treating the cells with a naturally occurring compound, asiatic acid. This study demonstrates here that HL-60 cells were similarly sensitive to Griffin 51 treatment, where even small doses of them caused a significant reduction on BCL-2 levels of expression. A treatment with

all-transretinoic acid in TF1 cells, similar to TF1a cells, except for $CD34^{+}/CD38^{+}$ status whereas TF1a are $CD34^{+}/CD38^{-,}$ showed that BCL-2 expression can be decreased, and programmed cell death can be induced (Slack and Yu, 1998). Our data indicate that TF1a cells have a mass reduction in BCL-2 even after small doses of Griffin 51 treatment.

HOXA9 has been long known as an 'undruggable' target in AML, although high expression levels were shown in many studies. In recent years there have been two approaches to combat high HOXA9 expression levels, as they are also associated with poor prognosis and heightened aggressiveness. The two approaches are the following: a) at epigenetic level, through indirect inhibition of its expression and b) directly, through inhibition of its transcription factors, which would block the protein:protein and protein:DNA interactions (Lambert *et al.*, 2019). In the Sonoda et al. (2021) study, they found that HOXA9 is also reduced in the OCI-AML3 cell line, regardless of its MLL-status (Sonoda *et al.*, 2021). Similar results are presented here, namely that Griffin-51 significantly reduces HOXA9 expressions even in low concentrations. Just like in clinical AML, AML cell lines also overexpress oncogenes such as HOXA9. In THP-1 cells, (Sonoda *et al.*, 2021) found that DB818, a HOXA9 inhibitor supressed growth, induced apoptosis and successfully reduced the expression of HOXA9. They found the same effect when looked at the levels of MYC and BCL-2.

## 7.10. Concluding remarks

In their study, Wang et. al (2022) found that the pan-CLK and pan-DYRK inhibitor SM09419 inhibits CLK 1-4 and DYRK1A-B and DYRK2 even in small concentrations ($IC_{50}$ 1-77nM, the lowest being CLK1 and CLK4, the highest is DYRK1B) (Wang *et al.*, 2022). They found that the compound was very effective in *in vitro* and in *in vivo* studies and did not cause cytotoxicity. However, due to its blanket effect, it is not the most ideal drug candidate. In this chapter it has been demonstrated that CLK1 could be a worthy drug target in hard to treat cancers such as AML. Within the CLK1 intracellular target engagement assay, it is shown that CLK1 inhibition can be achieved at low doses ($IC_{50}$ values 90-142nM) which means that Griffin 51, ET1055, Thiii27 and ET1008 are all proved to be good candidates for *in vivo* studies and further testing. It is also shown here the efficacy of Griffin 51 in reducing the expression of well-known oncogenes such as HOXA9, BCL-2 and MYC. The first set of experiments include six AML cell lines, three with an MLL-translocation and three without an MLL-translocation. We found significant reductions in all six AML cell lines in terms of oncogene expressions but could not identify a distinct vulnerability in cells with an MLL translocation as it was suggested before in the study conducted by (Tzelepis *et al.*, 2016).

# 8. Chapter

# The effect of SRPK1 and CLK1 inhibition in primary AML cells

## 8.1. Inhibitor treatment on AML primary samples

Following the successful inhibitor treatment of SPHINX-31 and Griffin 51 in AML cell lines and to test the translational capabilities of these inhibitors, it was reasonable to extend the data by testing primary AML cells with the same methods to see if the inhibitors would have the same effect as in the cell lines. In this chapter, the data presented here shows the expression levels of MYC, BCL-2 and HOXA9 oncogenes which all showed a reduction after SPHINX-31 and Griffin 51 treatment in cell lines. The effect of SPHINX-31 and Griffin 51 treatment was also tested to see it they would trigger the same BRD4 splice change in AML cells as it did for AML cell lines.

Finally, results from the colony forming unit (CFU) experiment is also displayed after 14 days of SPRK1 and CLK1 inhibition treatment in AML cells with or without an MLL-translocation.

## 8.2. SRPK1 inhibition in AML primary cells

To extend the dataset that was obtained from AML cell lines, clinical samples of AML was used to test the effect of SRPK1 and CLK1 inhibition. Below data is shown from three AML samples AML11367, AML5940 and AML10349 (MLL-WT). These samples were treated for 14 days in the previously described CFU assay (See chapter 3., paragraph 3.10) with SPHINX-31 and Griffin 51 (300nM-3μM concentration). The samples were set up in the CFU

assay, imaged then collected and prepared for further processing. Figure 8.1. below show the MYC, HOXA9 and BCL-2 expression levels in the vehicle treatment group and in the SPHINX-31 treatment groups between 300nM to 3μM. Sample 5940 show a significant reduction in all three downstream targets, when adjusted to the housekeeping gene (HPRT-1). The data is somewhat inconclusive, but there is a definitive dose response in BCL-2 expression levels. Fig.8.1. (A) shows the reduced expression levels of MYC in the clinical sample AML 5940 in response to increasing levels of SPHINX-31 treatment. Fig.8.1 (B) shows the effect of SPHINX-31 on the clinical sample AML 5940 in terms of HOXA9 expression levels. Fig.8.1. (C) demonstrates the effect of SPHINX-31 on the sample AML 5940 in terms of BCL-2 expression levels. In some samples, the data points did not form a clear dose response, therefore these data points could not be fitted to a curve. Where curve fitting was possible, the data points are lined up to the curve.

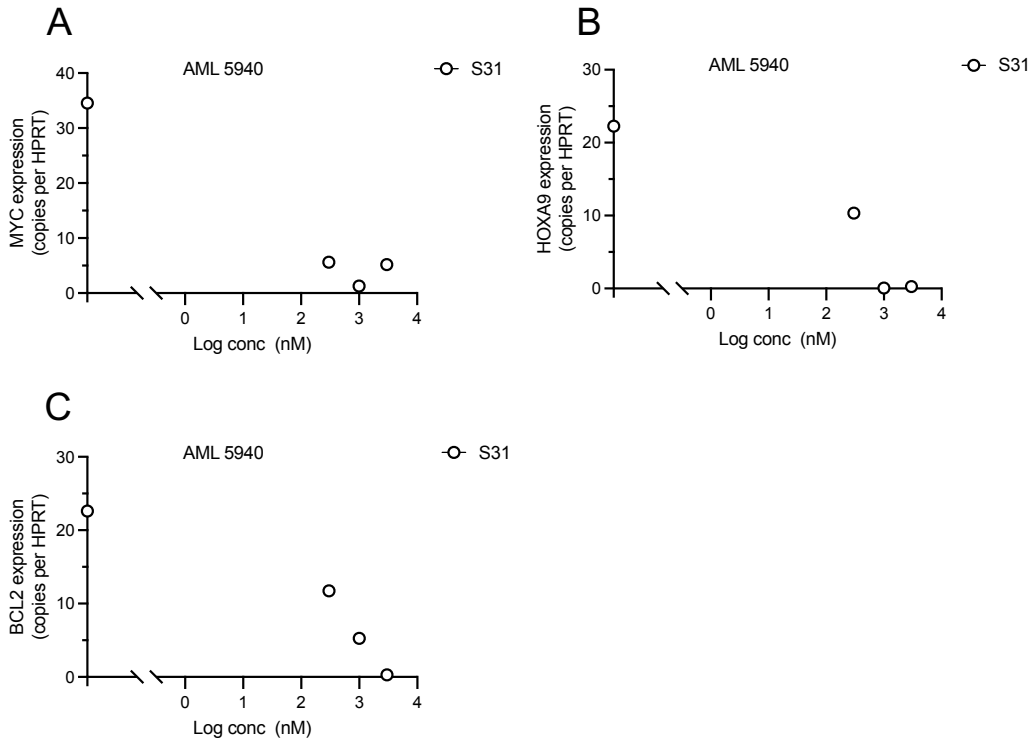



***Figure 8.1. Downstream targets in AML 5940 sample after SPHINX-31 treatment***

***Figure 8.1. (A) shows the effect of SPHINX-31 in sample AML 5940 on MYC expression ($IC_{50}$ 235.8 nM). Figure 8.1.(B) show the effect of SPHINX-31 in sample AML 5940 on HOXA9 expression levels ($IC_{50}$ 299.9 nM), whereas Figure 8.1.(C) show the reduction BCL-2 levels in sample AML 5940 after SPHINX-31 treatment ($IC_{50}$ 370.9 nM). Cells were treated for 14 days SPHINX-31 (300nM-3$\mu$M) in a colony forming unit and processed afterwards. Data presented here represents one donor (n=1), MYC, HOXA9 and BCL-2 expression levels were calculated from three technical replicates.***

Sample AML 11367 showed similar response to SPHINX-31, with decreasing levels of MYC that can be observed, however there is no clear dose response as it is shown in Fig.8.2. (A). HOXA9 and BCL-2 expression levels are also reduced, as it is shown in Fig.8.2. (B) and Fig.8.2. (C). A clear dose response could only be observed in the BCL-2 expression levels.

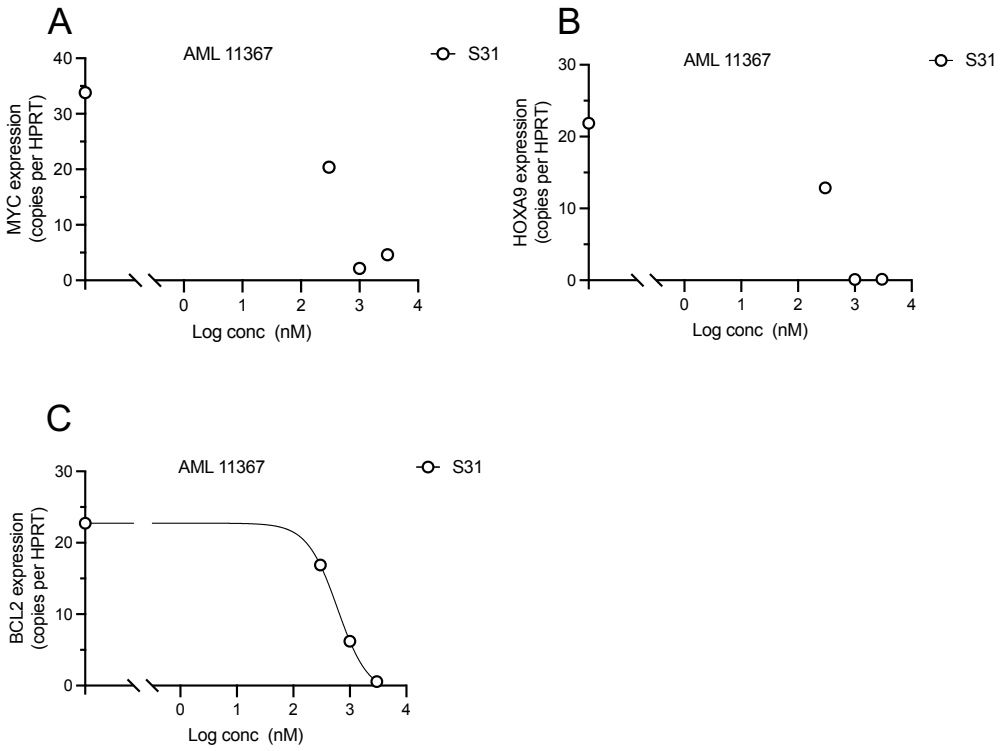



***Figure 8.2. Downstream targets in AML 11367 sample after SPHINX-31 treatment***

***Figure 8.2. (A) shows the effect of SPHINX-31 in sample AML 11367 on MYC expression ($IC_{50}$ 305.7 nM). Figure 8.2. (B) show the effect of SPHINX-31 in sample AML 11367 on HOXA9 expression levels ($IC_{50}$ 314.3 nM), whereas Figure 8.2. (C) show the reduction BCL-2 levels in sample AML 11367 after SPHINX-31 treatment ($IC_{50}$ 592.4 nM). Cells were treated for 14 days SPHINX-31 (300nM-3$\mu$M) in a colony forming unit, and processed afterwards. Data presented here represents one donor (n=1), MYC, HOXA9 and BCL-2 expression levels were calculated from three technical replicates.***

In the sample AML 10349, there were clear dose response curves in all expression levels, Fig.8.3. (A) shows the reduction in MYC expression levels, Fig.8.3. (B) shows the reduced expression levels of HOXA9 in response to SPHINX-31 treatment. And Fig.8.3. (C) shows the dose response curve in terms of BCL-2 expression levels.

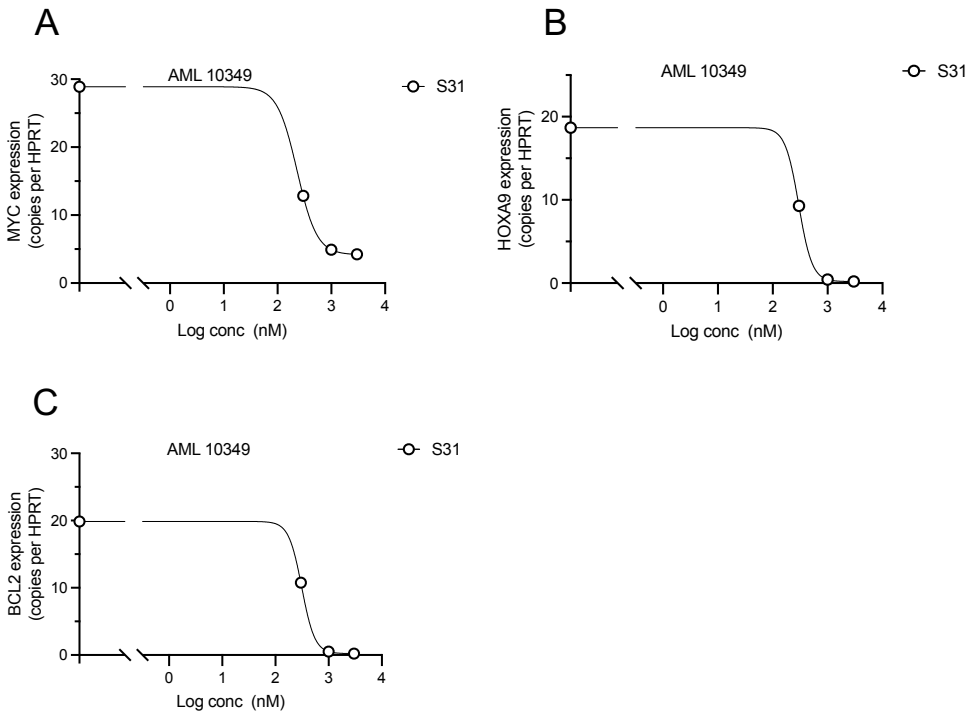



***Figure 8.3. Downstream targets in AML 10349 sample after SPHINX-31 treatment***

***Figure 8.3. (A) shows the effect of SPHINX-31 in sample AML 10349 on MYC expression ($IC_{50}$ 212.9 nM). Figure 8.3.(B) show the effect of SPHINX-31 in sample AML 10349 on HOXA9 expression levels ($IC_{50}$ 285.2 nM), whereas Figure 8.3. (C) show the reduction BCL-2 levels in sample AML 10349 after SPHINX-31 treatment ($IC_{50}$ 301.8 nM). Cells were treated for 14 days SPHINX-31 (300nM-3$\mu$M) in a colony forming unit and processed afterwards. Data presented here represents one donor (n=1), MYC, HOXA9 and BCL-2 expression levels were calculated from three technical replicates.***

The same samples were treated with Griffin 51 for the same period of time (14 days) and in the same concentration of inhibitors to see if there is a similar or more robust response to CLK1 inhibition.

# 8.3. CLK1 inhibition in primary AML cells

Seeing the successful effect of Griffin 51 in AML cell lines, it was reasonable to test if the same effect could be achieved in primary AML samples. For that reason, the primary AML cells that were used for the CFU assay were extracted from the CFU model, to measure the levels of MYC, HOXA9 and BCL-2 oncogenes. Figure 8.4. (A) below shows the results from sample AML 5940 in terms of MYC expression levels. Fig.8.3. (B) shows the level of HOXA9 expression in the different treatment groups. Fig.8.3. (C) shows the levels of BCL-2 expression levels in response to increasing level of Griffin 51 treatment.

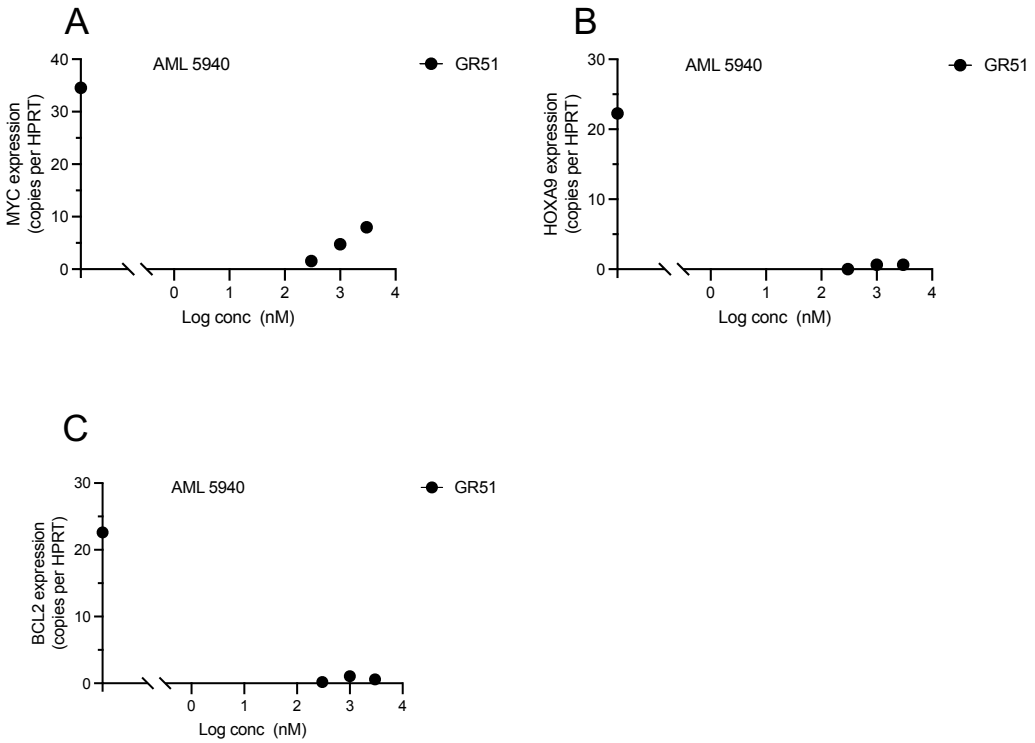



***Figure 8.4. Downstream targets in AML 5940 sample after Griffin 51 treatment***

***Figure 8.4. (A) shows the effect of Griffin 51 in sample AML 5940 on MYC expression. Figure 8.4. (B) show the effect of Griffin 51 in sample AML 5940 on HOXA9 expression levels, whereas Figure 8.4.(C) show the reduction BCL-2 levels in sample AML 5940 after Griffin 51 treatment. Cells were treated for 14 days Griffin51 (300nM-3$\mu$M) in a colony forming unit and processed afterwards. Data presented here represents one donor (n=1), MYC, HOXA9 and BCL-2 expression levels were calculated from three technical replicates. Due to irregularities in the data, it was not possible to calculate $IC_{50}$ values for this sample.***

Sample AML 11367 displayed very similar, unusual expression levels of MYC, HOXA9 and in BCL-2. Fig.8.5. (A) shows the expression levels of MYC in response to Griffin 51 treatment. Fig.8.5. (B0 shows the different expression levels of HOXA9 in response to inhibitor treatment. Fig.8.5. (C) shows the different expression levels of BCL-2 in response to treatment.

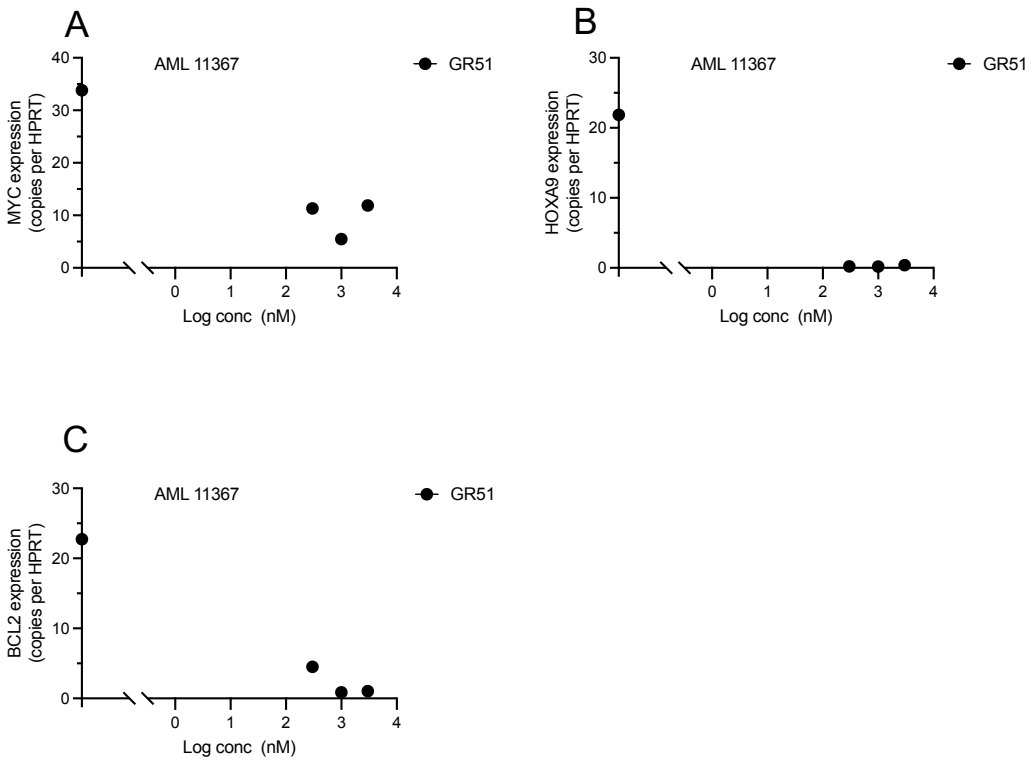



***Figure 8.15. Downstream targets in AML 11367 sample after Griffin 51 treatment***

***Figure 8.5. (A) shows the effect of Griffin 51 in sample AML 11367 on MYC expression ($IC_{50}$ 245.2 nM). Figure 8.5. (B) show the effect of Griffin 51 in sample AML 11367 on HOXA9 expression levels, whereas Figure 8.5.(C) show the reduction BCL-2 levels in sample AML 11367 after Griffin 51 treatment ($IC_{50}$ 258.9 nM). All expression levels were significantly reduced compared to the vehicle control group, but there is no obvious dose response curve, although there is a statistical trend in the BCL-2 dataset. $IC_{50}$ values could not be calculated for the HOXA9 expression level.***

In the AML 10349 sample, there was a uniform response to Griffin 51 treatment; there is a clear reduction in MYC, HOXA9 and BCL-2 expression levels compared to the vehicle control group, but the concentration of the inhibitor did not seem to make a reasonable difference in the measured expression levels. Fig.8.6. (A) shows the reduced levels of MYC in response to treatment. Fig.8.6. (B) shows the different levels of HOXA9 expression in response to treatment. And Fig.8.5. (C) shows the expression levels of BCL-2 in response to increasing levels Griffin 51 treatment.

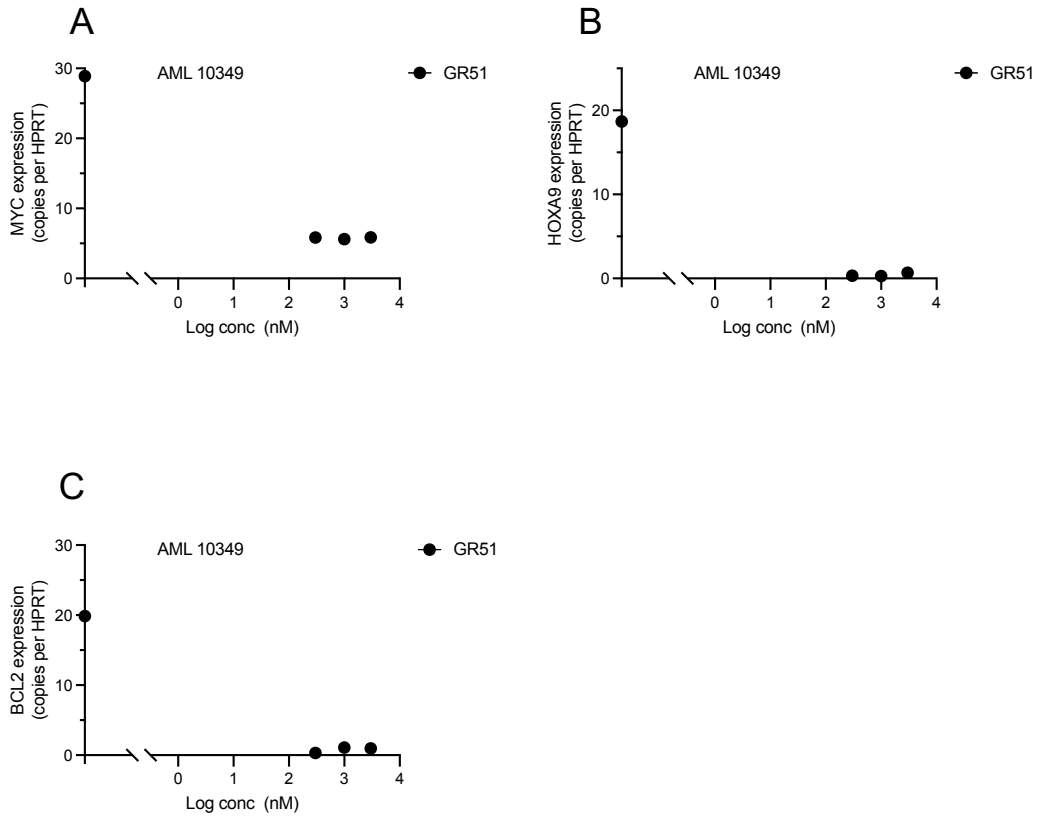



***Figure 8.16. Downstream targets in AML 10349 sample after Griffin 51 treatment***

***Figure 8.6. (A) shows the effect of Griffin 51 in sample AML 10349 on MYC expression. Figure 8.6. (B) show the effect of Griffin 51 in sample AML 10349 on HOXA9 expression levels, whereas Figure 8.6. (C) show the reduction BCL-2 levels in sample AML 10349 after Griffin 51 treatment. All expression levels were significantly reduced compared to the vehicle control group, but there is no obvious dose response curve. Due to irregularities in the data, it was not possible to calculate $IC_{50}$ values for this sample.***

# 8.4. BRD4 isoform change in AML clinical samples

The following dataset shows the effect of SPHINX-31 and Griffin 51 in BRD4 splice change. Three primary AML cell samples were tested to see if the same isoform change could be achieved as reported previously in AML cell lines. Figure 8.7. (A) shows the effect SPHINX-31 in sample AML 5940. In the lower concentration treatment groups, the pro-tumourigenic BRD4s isoform is more prominent, but it shows a decrease in response to increasing concentrations of inhibitor treatment. Fig.8.7. (B) shows the difference between the BRD4s-BRD4l isoform.

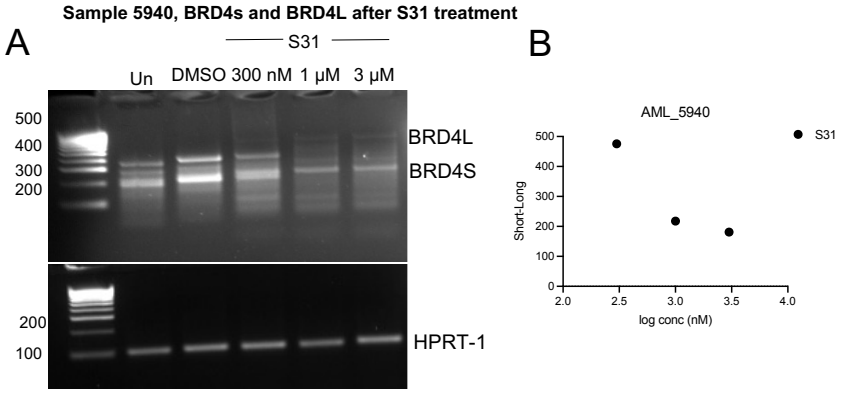



***Figure 8.17. BRD4 splice change in sample 5940 after SPHINX31 treatment***

***Fig.8.7. (A) BRD4s and BRD4l expression levels in sample AML5940 visualised on a 2% agarose gel after 14 days of SPHINX-31 treatment in a CFU ($IC_{50}$ 909.8 nM). Expression of the housekeeping gene HPRT1 was not altered by SPHINX-31 treatment. Figure 8.7. (B) Difference between the BRD4s and BRD4l values after 14 days of SPHINX-31 treatment. Expression of BRD4s, BRD4l and HPRT-1 in sample 5940 was determined by RT-PCR and visualized on a 2% gel by agarose gel electrophoresis. The expected band sizes were, BRD4s 206 bp and BRD4l: 488 bp, HPRT-1: 101 bp. The optical density was measured using Image Studio. Sample AML 5940 represents one donor (n=1).***

Fig.8.8. (A) demonstrates the expression levels of the two different BRD4 isoform in sample AML 10349. From the image, it can be seen that there is a double banding issue in the 300nM treatment group which made it impossible to calculate the splice change via subtracting the levels of the short isoform from the long isoform. The response to treatment in the 1μM and 3μM groups are presented below in Fig.8.8.(B).

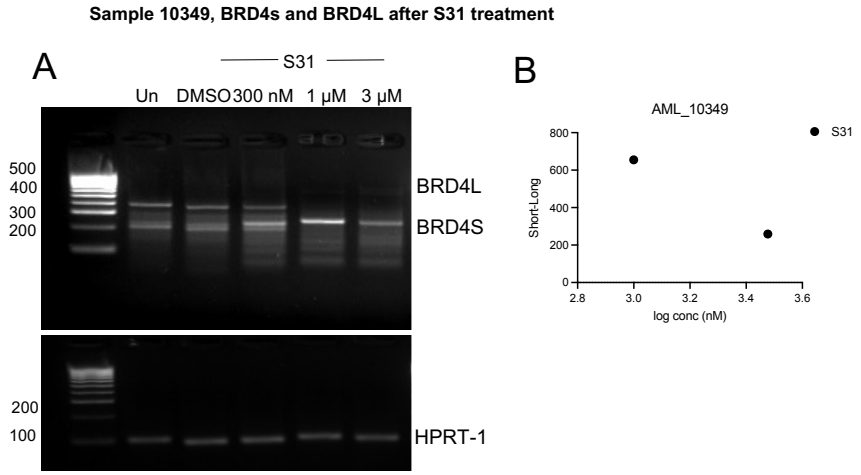



***Figure 8.18. BRD4 splice change in sample 10349 after SPHINX-31 treatment***

***Fig.8.8. (A) BRD4s and BRD4l expression levels in sample AML10349 visualised on a 2% agarose gel after 14 days of SPHINX-31 treatment in a CFU ($IC_{50}$ 1520 nM). Expression of the housekeeping gene HPRT1 was not altered by SPHINX-31 treatment. Figure 8.8. (B) Difference between the BRD4s and BRD4l values after 14 days of SPHINX-31 treatment. Expression of BRD4s, BRD4l and HPRT-1 in sample 10349 was determined by RT-PCR and visualized on a 2% gel by agarose gel electrophoresis. The expected band sizes were, BRD4s 206 bp and BRD4l: 488 bp, HPRT-1: 101 bp. The optical density was measured using Image Studio. Sample AML 10349 represents one donor (n=1).***

Finally, sample AML 11367 is shown here after SPHINX-31 treatment in terms of BRD4 isoform change.Fig.8.9. (A) shows the different levels of expression of BRD4s and BRD4l. Fig.8.9. (B) shows the difference between the BRD4s and BRD4l isoforms.

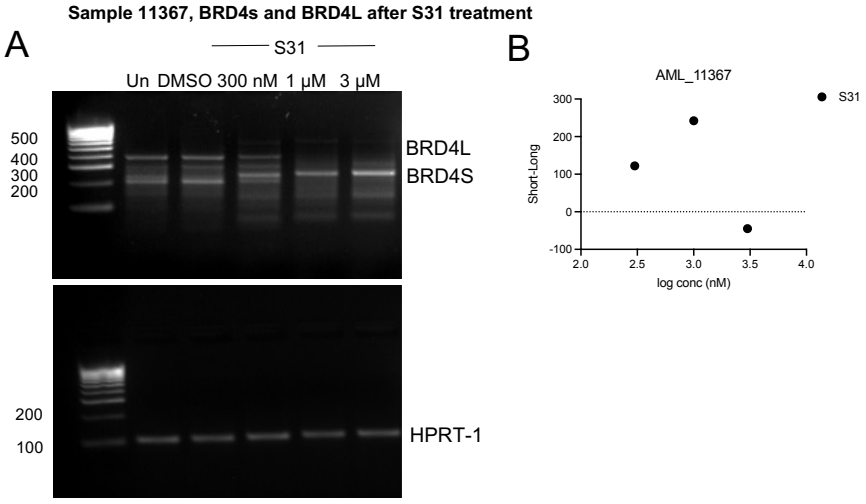



***Figure 8.19. BRD4 splice change in sample 11367 after SPHINX31 treatment***

***Fig.8.9. (A) BRD4s and BRD4l expression levels in sample AML11367 visualised on a 2% agarose gel after 14 days of SPHINX-31 treatment in a CFU ($IC_{50}$ 1730.0 nM). Expression of the housekeeping gene HPRT1 was not altered by SPHINX-31 treatment. Figure 8.7. (B) Difference between the BRD4s and BRD4l values after 14 days of SPHINX-31 treatment. Expression of BRD4s, BRD4l and HPRT-1 in sample 11367 was determined by RT-PCR and visualized on a 2% gel by agarose gel electrophoresis. The expected band sizes were, BRD4s 206 bp and BRD4l: 488 bp, HPRT-1: 101 bp. The optical density was measured using Image Studio. Sample AML 11367 represents one donor (n=1).***

Sample AML 10349 was also treated with Griffin 51 to see if a CLK1 selective inhibitor could reduce the expression levels of BRD4s and switch the BRD4 isoform to the tumour-supressor BRD4l. Figure 8.10. (A0 demonstrates the effect of Griffin 51 on primary AML cells in terms of BRD4 splice change. Fig.8.10. (B0 shows the data from the 300nM and 3μM treatment group, as there was no meaningful data available from BRD4l at 1μM concentration.

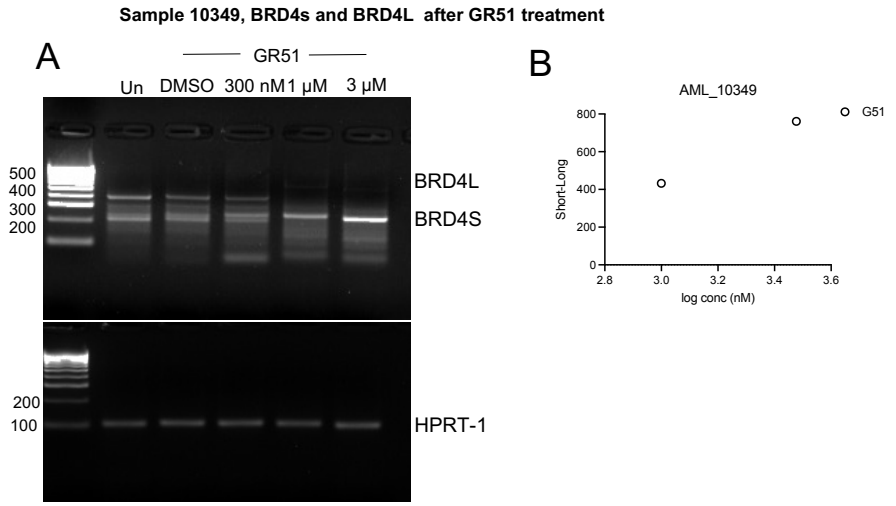



***Figure 8.110. BRD4 splice change in sample 10349 after Griffin 51 treatment***

***Fig.8.10. (A) BRD4s and BRD4l expression levels in sample AML10349 visualised on a 2% agarose gel after 14 days of Griffin 51 treatment in a CFU ($IC_{50}$ 1974.0 nM). Expression of the housekeeping gene HPRT1 was not altered by Griffin 51 treatment. Figure 8.7. (B) Difference between the BRD4s and BRD4l values after 14 days of Griffin 51 treatment. Expression of BRD4s, BRD4l and HPRT-1 in sample 10349 was determined by RT-PCR and visualized on a 2% gel by agarose gel electrophoresis. The expected band sizes were, BRD4s 206 bp and BRD4l: 488 bp, HPRT-1: 101 bp. The optical density was measured using Image Studio. Sample AML 10349 represents one donor (n=1).***

The following sample AML 11367 show a very slight reduction in the BRD4s-BRD4l ratio with increasing levels of Griffin 51 treatment, but the short isoform remains pronounced in all the treatment groups as it can be seen in Fig.8.11. (A). Fig.8.11. (B) shows a slight reduction in the BRD4s:BRD4l ratio in response to increasing levels of inhibitor treatment.

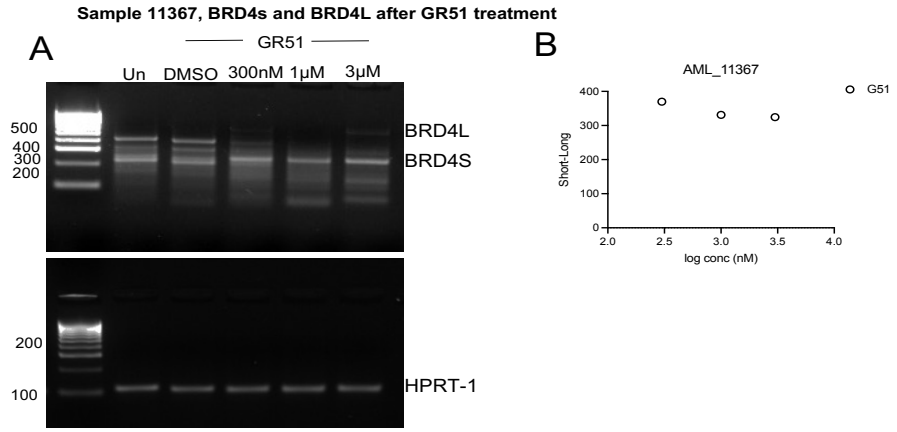



***Figure 8.111. BRD4 splice change in sample 11367 after Griffin 51 treatment***

***Fig.8.11. (A) BRD4s and BRD4l expression levels in sample AML11367 visualised on a 2% agarose gel after 14 days of Griffin 51 treatment in a CFU ($IC_{50}$ 918.0 nM). Expression of the housekeeping gene HPRT1 was not altered by Griffin 51 treatment. Figure 8.7. (B) Difference between the BRD4s and BRD4l values after 14 days of Griffin 51 treatment. Expression of BRD4s, BRD4l and HPRT-1 in sample 11367 was determined by RT-PCR and visualized on a 2% gel by agarose gel electrophoresis. The expected band sizes were, BRD4s 206 bp and BRD4l: 488 bp, HPRT-1: 101 bp. The optical density was measured using Image Studio. Sample AML 11367 represents one donor (n=1).***

Sample AML 5940 showed an unexpected response to increasing levels of inhibitor treatment where there was not a clear response curve. Fig.8.12. (A) shows a mix result gel where there is no clear response curve. Fig.8.12. (B) shows variable levels of data when calculated the BRD4s:BRD4l ratio.

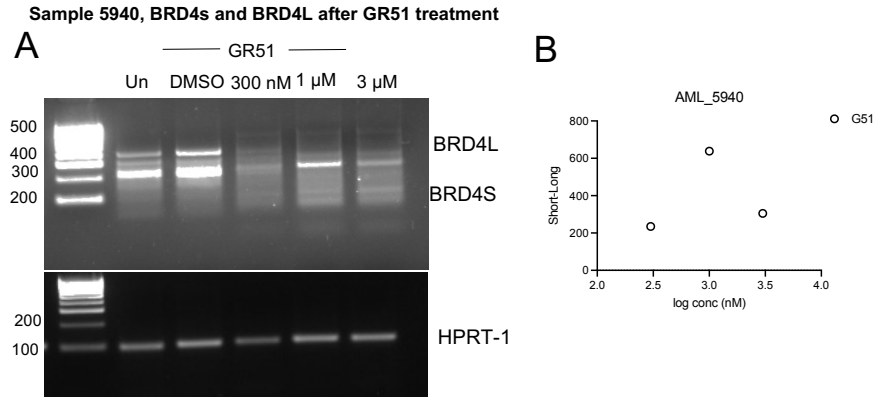



***Figure 8.112. BRD4 splice change in sample 5940 after Griffin 51 treatment***

***Fig.8.12. (A) BRD4s and BRD4l expression levels in sample AML5940 visualised on a 2% agarose gel after 14 days of Griffin 51 treatment in a CFU ($IC_{50}$ 4182 nM), however the data does not follow the level of inhibitor concentration. Expression of the housekeeping gene HPRT1 was not altered by Griffin 51 treatment. Figure 8.7. (B) Difference between the BRD4s and BRD4l values after 14 days of Griffin 51 treatment. Expression of BRD4s, BRD4l and HPRT-1 in sample 5940 was determined by RT-PCR and visualized on a 2% gel by agarose gel electrophoresis. The expected band sizes were, BRD4s 206 bp and BRD4l: 488 bp, HPRT-1: 101 bp. The optical density was measured using Image Studio. Sample AML 5940 represents one donor (n=1).***

### 8.4.1. Colony forming units

Colony forming units (CFU) are used to establish long term treatment options for freshly extracted or cryopreserved cells *in vitro.* Sutherland and *et al.* (2001) evaluated the best combination of serum rich and serum free medium with or without cytokines and found that blood cells grow well in all conditions, regardless of their origin (bone or marrow). They also optimised the length of treatment and found that cells could be cultured long-term, between 2-8 weeks which allows for establishing long-term treatment models (Sutherland *et al.*, 2001).

In this study the effects of SRPK1 and CLK1 inhibition were tested in a colony forming unit (CFU) using primary AML cells. The primary AML cells were a kind gift from the Stamm group from Utrecht, the Netherlands. All samples were handled in accordance with international and local regulations. By establishing primary cells in a colony forming unit (CFU) it was possible to add inhibitor treatment for a longer period of time (14 days vs. 3 days) to see if it would cause a higher level of apoptosis (if any) that can be observed in a semi-solid media, as well as self-assembling capabilities, proliferation rate and basic morphology. In Figure 8.13 the number of colonies are shown as it was recorded on day 14 in the different treatment groups. In each treatment group, the number of colonies were recorded by visual observation, under a brightfield microscope, using a 10x magnification lens, from the three AML samples with a translocation and (MLL-TL) and the number of colonies from three AML samples without a translocation (MLL-WT).

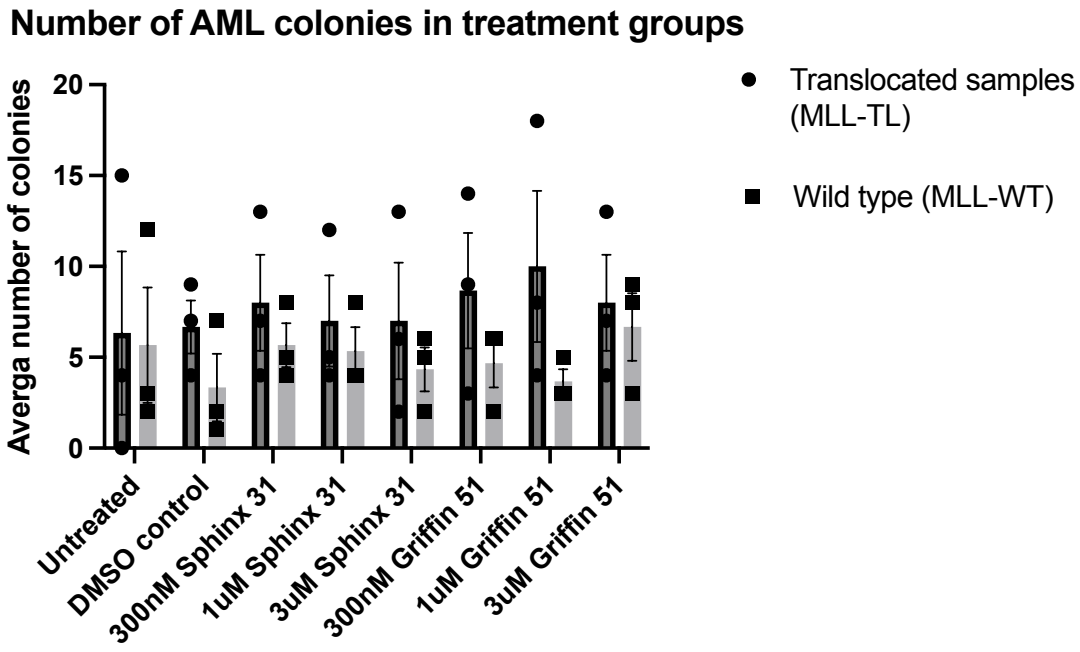



***Figure 8.113. Number of colonies in CFUs in response to long term inhibitor treatment***

***Fig. 8.13. Shows the number of colonies in the translocated and wildtype AML clinical samples. Data divided by the translocation status of samples (n=3 in each group). Translocated samples represent the cohort with a AF10 or AF9 translocation. The Wild-type group represent a cohort of cells without a translocation with AF10 or AF10 fusion genes. All cells were set up and treated in the CFU assay for 14 days in a cell culture incubator. The number of colonies were assessed by counting under a brightfield microscope on day 14. No significant difference was found between the MLL-TL and MLL-WT groups (p=0.5893) and neither SPHINX-31 nor Griffin 51 had a significant effect on the number of colonies. Averages were calculated from n=3 in each group.***

The next graph (Figure 8.14) represents the average number of colonies in each treatment group. There is a significant difference between Translocated group (MLL-TL) and Wild type (MLL-WT). Statistical analysis was performed by using a two-way ANOVA with Geisser-Greenhouse correction, $p<0.001$.

Fig.8.14. shows the average number of colonies in each treatment groups. MLL-WT group consistently had lower number of colonies than the MLL-TL group, meaning that the MLL-WT group was more sensitive to inhibitor treatment, on average. There was no significant difference between the MLL-TL and MLL-WT group, $p=0.4180$.

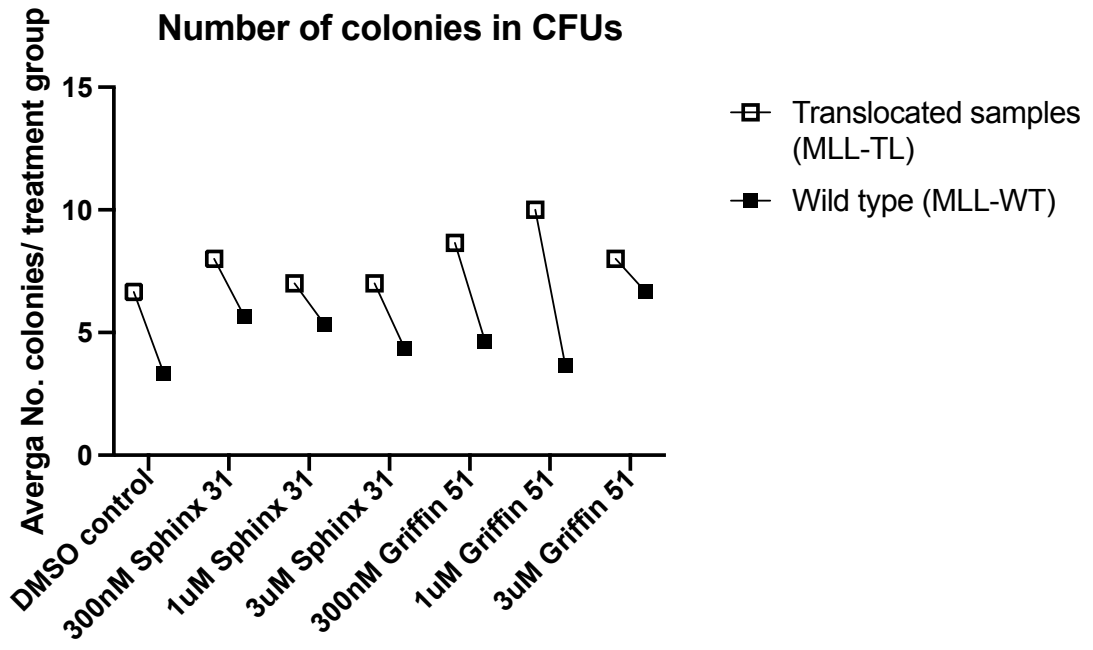



***Figure 8.114. Average number of colonies in CFUs in response to long term inhibitor treatment***

***The average number of colonies in each treatment group, recorded on day 14 of the long term treatment. Colonies were established and maintained in a semi-solid media and counted under a bright-field microscope on the last day of treatment. It can be seen that the cells without an MLL translocation (MLL-WT) were more sensitive to treatment than the cells with the translocation (MLL-TL). The type of treatment did not seem to make a difference, e.g. the number of colonies did not significantly differ in the SPHINX-31 and Griffin 51 treatment group (p=0.4180).***

## 8.4.2. CFU assay images- MLL-WT

Below images are shown of a randomly selected sample from the MLL-WT group on day 14. Images were taken using a camera system attached to a brightfield microscope. Below, Fig.8.15. shows a randomly selected sample from the MLL-WT group. Each image represents a well/treatment group that depicts a randomly selected colony formation. Each sample were treated in one technical replicate, due to the low number of cells available (which in usual and accepted in primary cell research).

Sample 5940 wild type (without a translocation) treated with S31 and G51

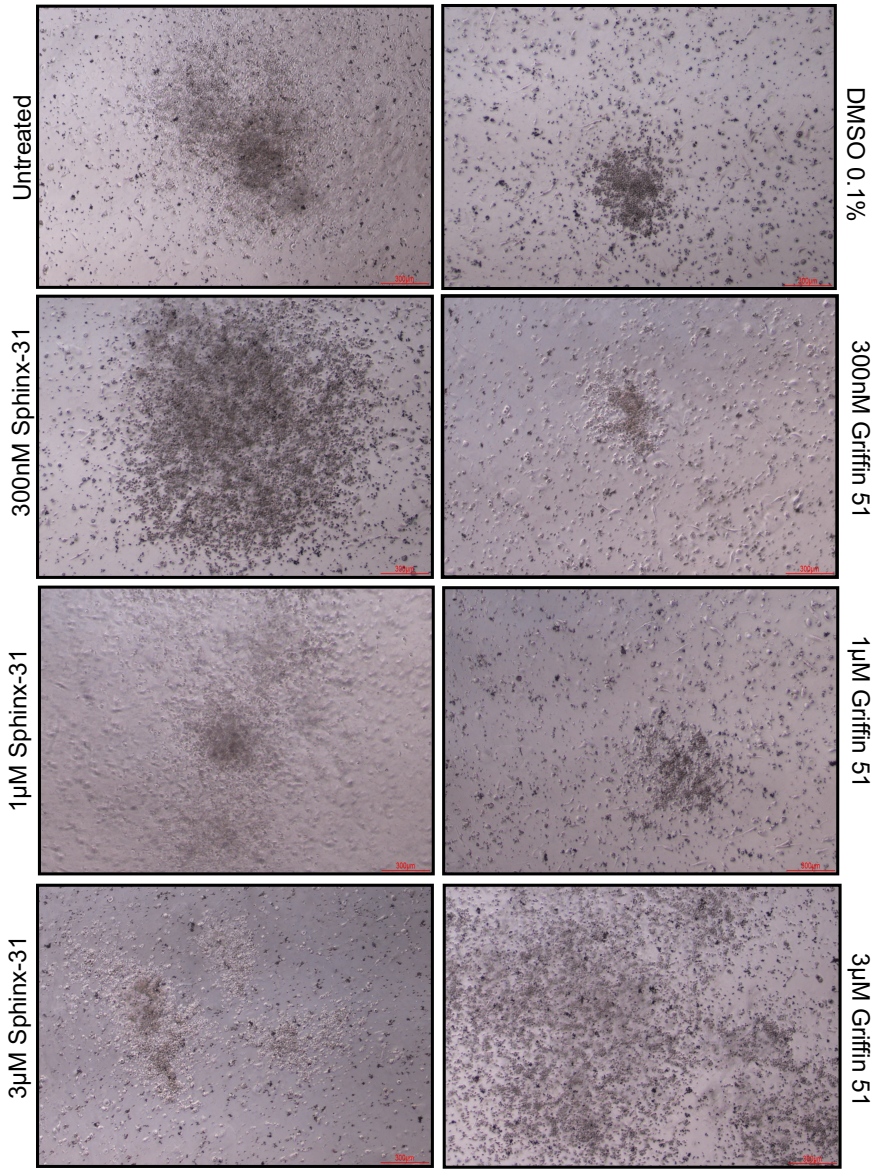



***Figure 8.115. Randomly selected images of sample 5940 (MLL-WT) in CFUs***

***Primary AML cells in CFUs, imaged on day 14 under a brightfield microscope, each image represents a randomly selected colony from each treatment group. Sample 5940 was randomly selected from the AML MLL-WT group, e.g. cells without an MLL translocation. Cells were set up and maintained in a semi-solid media, then harvested after treatment and imaging for further processing.***

## 8.4.3. CFU images- MLL-TL

Fig. 8.16 depicts a randomly selected sample; 6719 (MLL-TL). Each image represents a colony formation from a treatment group, as labelled below.

Sample 6719 with AF10 translocation after S31 and GR51 treatment

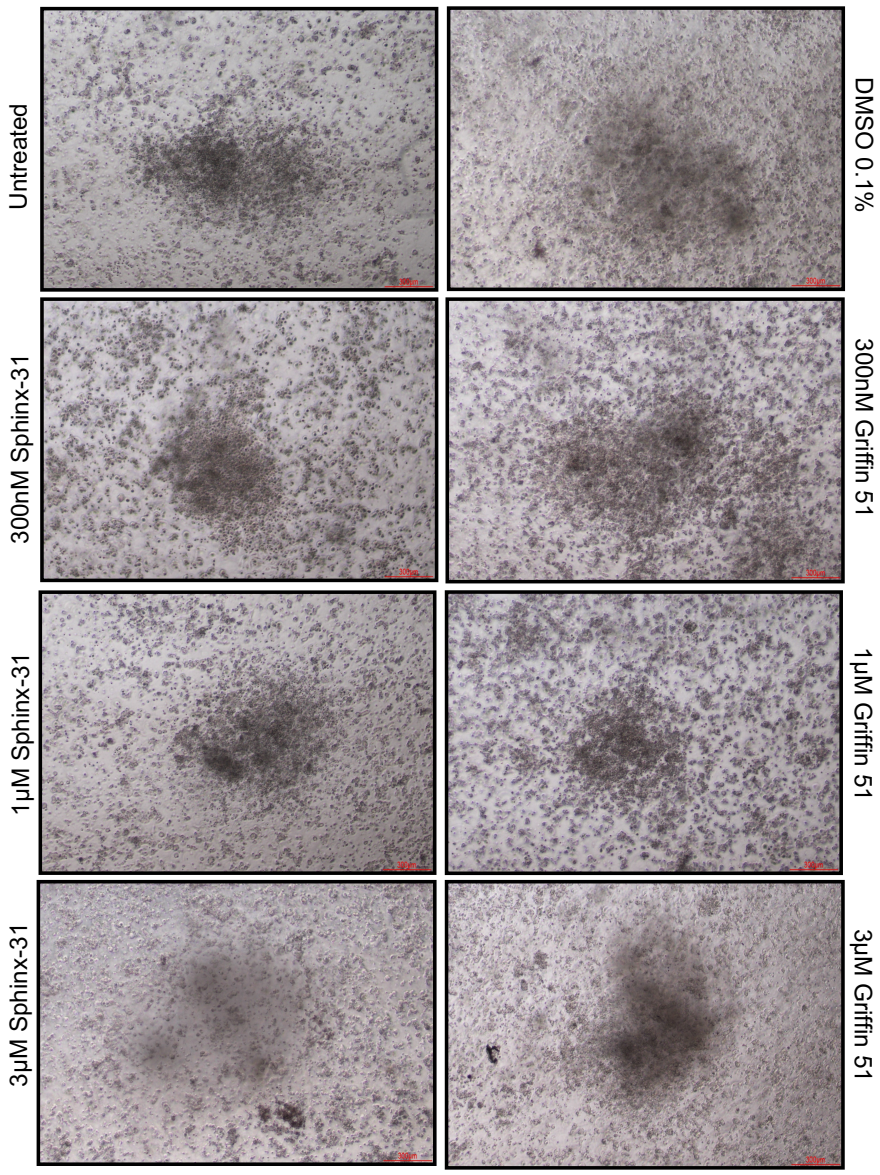



***Figure 8.16. Randomly selected images of sample 6719 (MLL-TL) in CFUs.***

***Primary AML cells in CFUs, imaged on day 14 under a brightfield microscope, each image represents a randomly selected colony from each treatment group. Sample 6719 was randomly selected from the AML MLL-TL group, e.g. cells with an MLL translocation and AF10 mutation. Cells were set up and maintained in a semi-solid media, then harvested after treatment and imaging for further processing.***

## 8.5. Discussion and Conclusion

### 8.5.1. SRPK1 and CLK1 inhibition in primary AML cells

In a previous clinical study, where MYC levels of AML patients were tested, they found that high levels of MYC correlated with poor patient outcomes. Although patients with low MYC levels did not have a significant advantage in terms of clinical outcomes, their overall survival rate was longer (median 42.3 vs. 17.5 months) (Yun *et al.*, 2019). It is shown here that SPHINX-31 and Griffin 51 were successful in reducing the levels of MYC, HOXA9 and BCL-2 expression levels in all samples. It must be noted that in some samples the data is inconclusive and only a few samples show a clear dose response to increasing concentration of treatment The least amount of reduction can be seen in sample AML5940 (HOXA9 and BCL-2 levels) and AML11367 (MYC, HOXA9 and BCL-2). There was no clear reason as to why the results would be different but it would certainly be beneficial to extend the database to a larger number of primary samples (>50).

### 8.5.2. BRD4 splice change in AML clinical samples

Previous studies have shown that JQ1, a BRD4 pan-inhibitor can induce major growth inhibition and even apoptosis in primary human AML stem and

progenitor cells, with an $IC_{50}$ value of 0.005-0.5μM (Herrmann *et al.*, 2012). However, BRD4 splice change is not a well-researched subject and there was no available publication that would describe BRD4 splice change in primary AML at the time of writing. One similar study looked at BRD4 splice change after JQ1 treatment and similarly found that the BRD4s isoform to promote breast cancer growth and metastasis (Wu *et al.*, 2020). Whereas BRD4l inhibits tumour progression and metastatic capabilities. Based on the data presented here, it can be said that the BRD4s isoform is clearly present in all samples but the BRD4l isoform is only very vaguely expressed, if expressed at all. These results are not in line with my previous findings in AML cell lines presented in paragraph 5.3 and 7.7. It should be noted that results from the primary AML samples are very low in numbers which could cause a difference in results. A larger database would provide a statistically more robust result. It is also a concern that primary AML samples are genetically much more diverse than cell lines, therefore the results can vary from one database to another. It could also be hypothesised that a shorter treatment would show a different result, rather than a pro-longed treatment in CFUs as it was the case here, and of course perhaps a higher dosage would be necessary for primary cells than for immortalised cell lines.

## 8.6. Colony forming units (CFU)

When using HSPCs to model de novo leukemogenesis, Schneidawind *et al.* (2018) found that by editing the genome of these blood cells, they can induce AML with MLL-AF9 translocation in a mouse model. They also found that cells with this specific translocation have an increased ability to form colonies (Schneidawind *et al.*, 2018). In this study, there was no difference between the number of colonies in the translocated group (MLL-TL) and the non-translocated (MLL-WT) group. The difference in results could be explained by the heterogeneity of the different samples and the low number of samples which does not provide a robust base for data analysis. The type of treatment whether it was SPHINX-31 or Griffin 51 did not make a significant difference,in response to treatment but the non-translocated cells (MLL-WT) seemed to form a lower number of colonies than the cells with a translocation (MLL-TL). The difference was not statistically significant ($p=0.418$).

# 9. Chapter

# SRPK1 and CLK1 inhibition in astrocyte derived cancer cells and in primary glia cells

## 9.1. Aims and Objectives

SRPK1 has also been found to be a main contributor to the growth, metastasis and drug sensitivity in gliomas. Wu *et al.* (2013) found that by silencing SRPK1 in glioma cells such as U251, U87 inhibited tumour cell growth, invasion and migration (Wu *et al.*, 2013). Based on this finding, it was the next logical step to test a highly selective SRPK1 inhibitor, such as SPHINX-31, to see if the viability levels in U87 cells can be reduced. CLK1 inhibition has been found to be a drug target in pancreatic cancer (Chen *et al.*, 2021) and in gastric cancer (Babu *et al.*, 2020). High expression levels of CLK1 have been associated with poor prognosis in gliomas (Zhang *et al.*, 2017). Therefore, a CLK1 selective inhibitor, Griffin 51 was applied to U87 cells to test its efficacy in reducing cell viability and expression levels of MYC, HOXA9 and BCL-2.

## 9.2. Introduction

This chapter focuses on the effect of SPHINX-31 and Griffin 51 in a glioblastoma cell line, studying cell viability and common downstream targets such as HOXA9, BCL-2 and MYC. According to previous data high expressions of CLK1 and CLK2 were associated in poor prognosis for patients diagnosed with Glioblastoma (GBM) (Naro *et al.*, 2021). However, modulation of specific splice variants (FOXO3a) impaired growth and metastatic properties. CLK inhibition have been found to favour the cytoplasmic isoform of oestrogen related receptor $\beta$, which inhibits tumour cell growth and

migration (Park *et al.*, 2016). Sigala et al. (2016) showed that glioblastoma cell lines express an aberrant form of SRPK1 and that the knockdown of SRPK1 with siRNA does not influence the cell viability in these GBM cell lines, nor does it enhance the effect of approved drugs such as cisplatin (Sigala *et al.*, 2016). The effects of both SRPK1 and CLK1 inhibition are shown below in Fig. 9.1. after a 72 hour treatment of SPHINX-31 and Griffin 51 in U87 cells, respectively. Fig.9.1. (A) demonstrates the cell viability levels measured in U87 cells in response to increasing levels of Griffin 51 treatment. Fig.9.1. (B) demonstrated the viability levels in U87 cells after SPHINX-31 treatment.

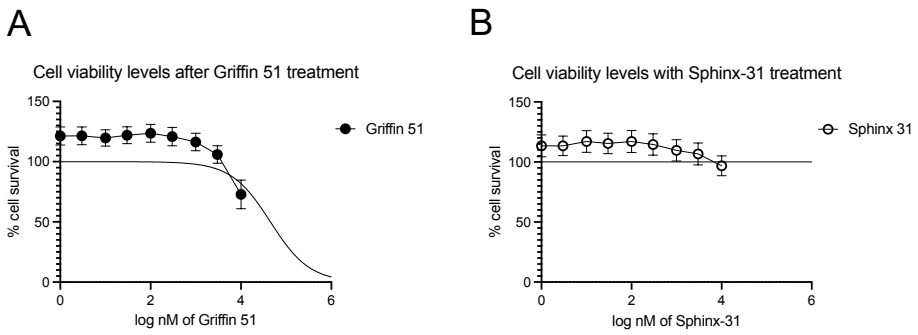



***Figure 9.1. Cell viability of U87 cells after Griffin 51 and SPHINX-31 treatment***

***Fig. 9.1. (A) shows the cell viability levels of U87 cells after 72 hours of Griffin 51 treatment in increasing concentrations [1nM -10$\mu$M]. Fig. 9.1. (B) shows the cell viability levels of U87 cells after 72 hours of SPHINX-31 treatment in increasing concentration [1nM -10$\mu$M]. All data points were corrected to the vehicle control (0.1% DMSO), and values were recorded from three biological replicates (n=3), which each had three technical replicates. Due to high levels of baseline, the model could not calculate $IC_{50}$ values.***

## 9.3. Downstream targets after SPHINX-31 and Griffin 51 treatment in U87 cells

Given the clinical relevance of the highly expressed CLK1 and SRPK1 in gliomas, the next logical step was to test SPHINX-31 and Griffin 51 to see if the same effect can be observed in Glioblastoma cells (GBM) as in the AML cell lines. According to their study, (Fels *et al.*, 2000) found that BCL-2 is overexpressed in high-grade gliomas, which are usually therapy resistant. Therefore, any inhibitor that reduces the levels of BCL-2 expression could be beneficial for treatment. Within patients diagnosed with Grade IV Glioblastoma, BCL-2 negative patients have a significantly longer survival rate than patients with positive BCL-2 tumours. Which indicates that reduction in BCL-2 can be a future drug target. Below in Figure 9.2., the effect of SPHINX-31 and Griffin 51 is shown in reducing the levels of MYC, HOXA9 and BCL-2 in the U87 cell line. Fig. 9.2. (A) shows the decrease in BCL-2 expression levels in response to SPHINX-31(S31) treatment in U87 cells, ($IC_{50}$ 34.47 nM). Fig.9.2. (B) shows the decreasing levels of BCL-2 levels in response to Griffin 51(GR51) treatment, ($IC_{50}$ 32.07 nM). Fig.9.2. (C) shows the decrease in MYC expression in response to S31 treatment, ($IC_{50}$ 17.16 nM). Fig.9.2. (D) shows the decreasing levels of MYC expression in response to GR51 treatment, ($IC_{50}$ 6.986 nM). Fig.9.2. (E) shows the decrease in HOXA9 expression levels in response to S31 treatment, ($IC_{50}$ 3.303 nM). Fig.9.2. (F) shows the decreasing levels of HOXA9 levels in response to GR51 treatment ($IC_{50}$ 2.801 nM).

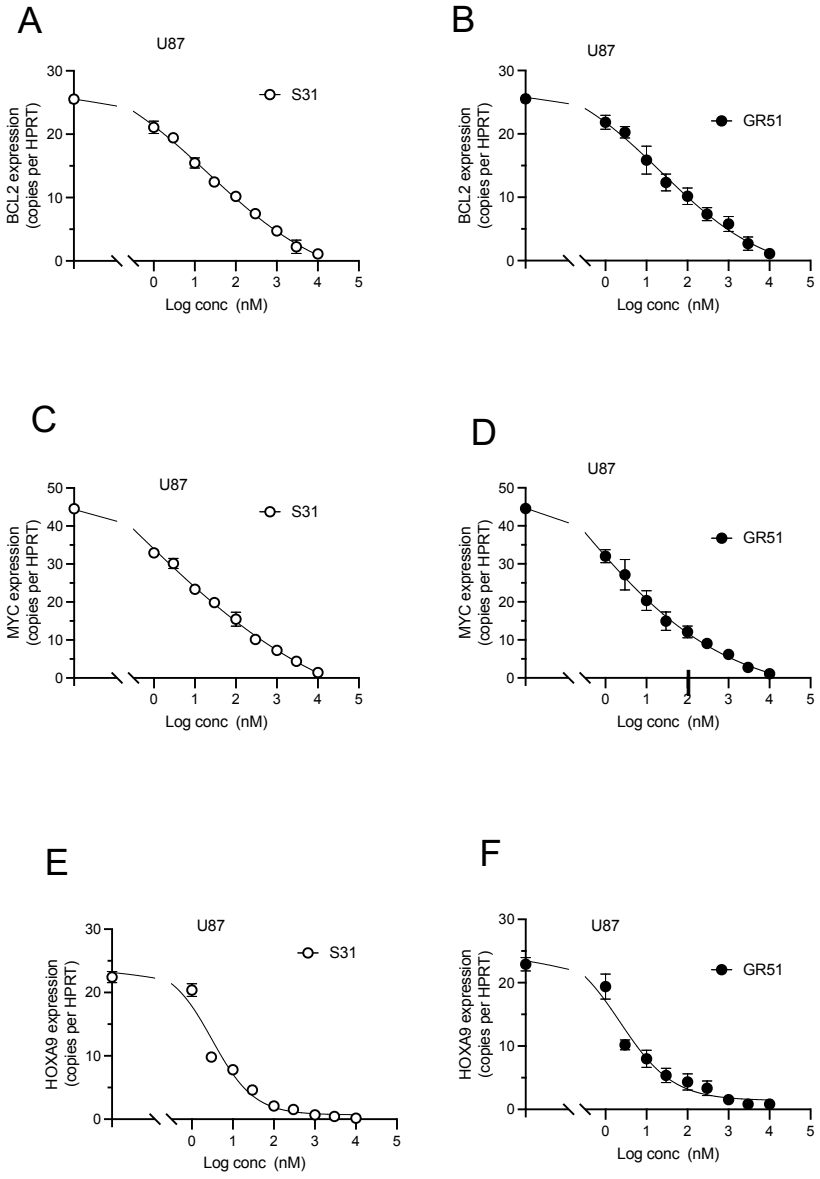



***Figure 9.2. BCL2, HOXA9 and MYC levels in U87 cells.***

***BCL2, HOXA9 and MYC expression levels measured with ddPCR from U87 samples. (A) BCL2 expression in U87cells after SPHINX-31 treatment ($IC_{50}$ 34.47 nM), (B) BCL2 expression in U87 cells after Griffin-51 treatment, ($IC_{50}$ 32.07 nM). (C) MYC expression in U87 cells after SPHINX-31 treatment, ($IC_{50}$ 17.16 nM), (D) MYC expression in U87cells after Griffin-51 treatment. ($IC_{50}$ 6.986 nM), (E) HOXA9 expression in U87 cells after SPHINX-31 treatment, ($IC_{50}$ 3.303 nM). (F) HOXA9 expression in U87 cells after Griffin 51 treatment ($IC_{50}$ 2.801 nM).***

## 9.4. The role of the BBB in Glioblastoma therapy

Glioblastoma Multiforme (GBM) remains the most common and aggressive primary brain tumour which is associated with high resistance to radiotherapy and chemotherapy. The median survival rate of GBM patients is still between 12-15 months, with less than 5% of patients surviving longer than 5 years (Ostrom *et al.*, 2014). One of the main challenges in delivering effective treatment for GBM is the Blood-Brain Barrier (BBB), which is in healthy state serves as a barrier protecting the central nervous system from harmful substances. The BBB is composed of brain endothelial cells, pericytes, cortical astrocytes, neurons, microglia and oligodendrocytes which are tightly packed together to form the neurovascular unit (Abbott *et al.*, 2006). See Fig. 9.3. below.

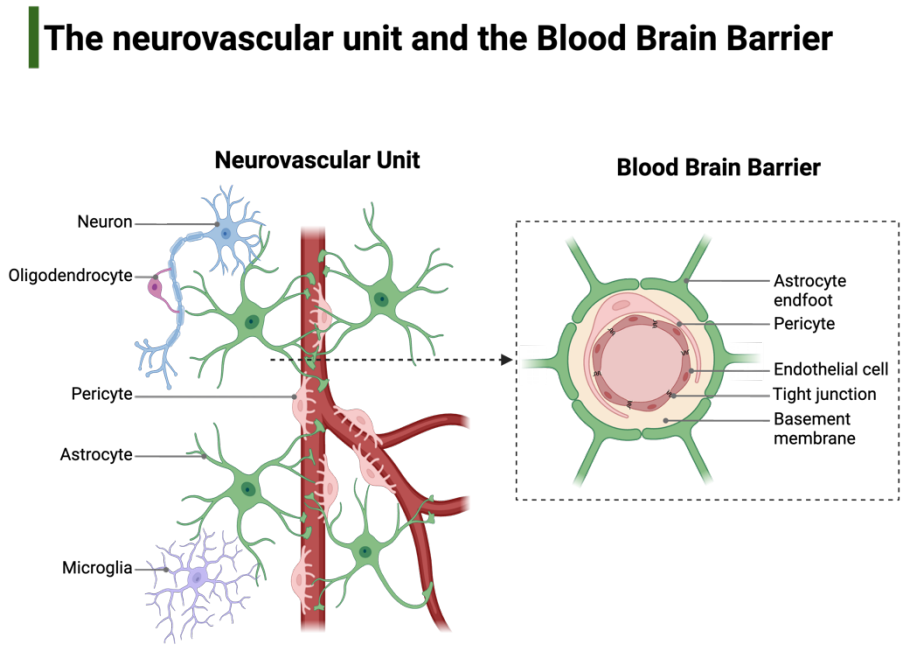



***Figure 9.3. The neurovascular unit and the Blood Brain Barrier***

**Figure 9.3. represents the Blood Brain Barrier (BBB) and the neurovascular unit in healthy state, with all the different cell types; cortical neurons, oligodendrocytes, pericytes, cortical astrocytes and microglia. Image created by Bio Render Premium, based on Jiang, X., *et al.* (2018). Blood-brain barrier dysfunction and recovery after ischemic stroke. Prog Neurobiol. 163-164:144-171**

Most molecules, specifically a large number of cancer drugs cannot cross the BBB, due to active efflux transporters such as P-glycoproteins (Demeule *et al.*, 2002). The other important factor is the Blood-Brain Tumour Barrier (BBTB), which is created due to the malignant alterations caused by penetrating tumour cells. The BBTB is characterised by excessive vascularisation and enhanced BBB permeability (Wang *et al.*, 2019). This caused by the overexpression of VEGF and other pro-angiogenic factors such as cytokines (Oberoi *et al.*, 2016). To study the effect of GBM in the breakdown of the BBB, a 3D spheroid of the BBB was created from primary cells (See paragraph 3.4 and 3.5 ) and treated with cytokines. To eliminate

any confounding effects in the cytokine treatment a serum free media composite was also developed to use for the spheroid model.

## 9.5. Serum free cell media

It has been noted in numerous studies that commonly used Foetal calf serum (FCS) in cell media can greatly influence the results. Ben Haim et al. (2015) noted that FCS triggers an activation in astrocytes in regular *in vitro* culture which then pushes them into a reactive state. In previous studies, they found that serum in the media appears to irreversibly alter the morphology and transcriptome of glia cells which means that they create false positive or false negative results (Foo *et al.*, 2011). In their study Zhang *et al.* (2016) found that human astrocytes drastically change their morphology when they are exposed to serum, whereas immunopanned astrocytes in serum free condition represent the shape that we can observe in intact tissue (Zhang *et al.*, 2016). For details of the serum free media composite, please see paragraph 3.5.1.

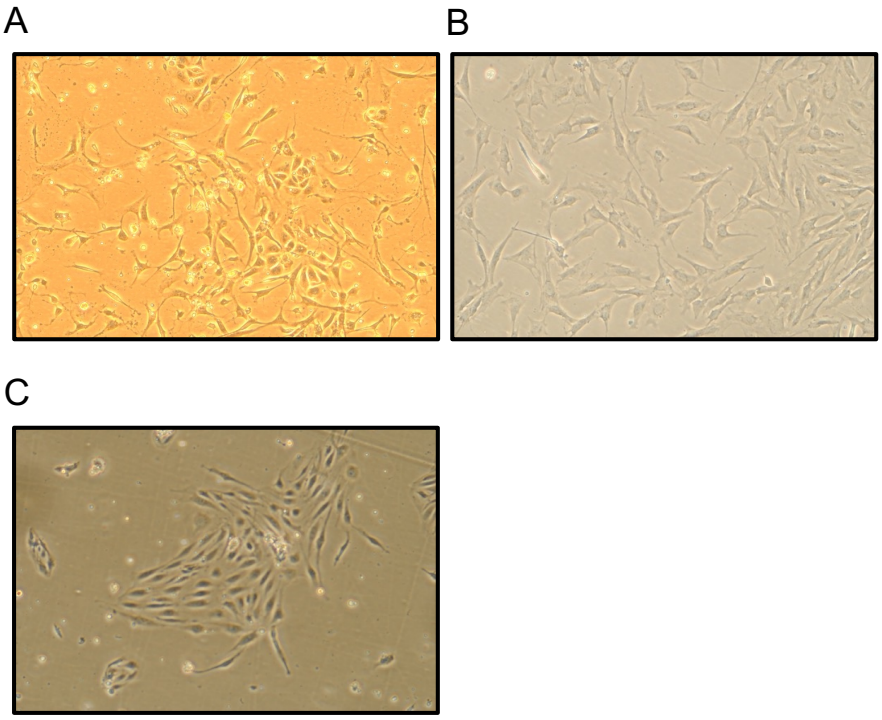



***Figure 9.4. Primary glia cells in serum free media***

***(A) primary cortical astrocytes 48 hours after extraction in a serum free media, magnification 20x. (B) primary cortical pericytes 8 days after extraction in a serum free media, magnification 20x. (C) brain endothelial cells***

## 9.6. Cytokine treatment on primary astrocytes

For the cytokine treatment, primary astrocytes were plated in regular 6 well-plates, in regular *in vitro* conditions (37°C, 5% $CO_2$), $10^6$ cells/well in serum free media, and treated for 6 hours in different conditions. Astrocytes were stained against GFAP, and DAPI to confirm morphology and cell density. Fig.9.5. (A) shows a randomly selected image of an astrocyte which is fixed and stained against GFAP (green) with no treatment applied. Fig.9.5. (B) shows a second randomly selected image of and astrocyte, fixed and stained against GFAP (green), nuclei stained with DAPI.

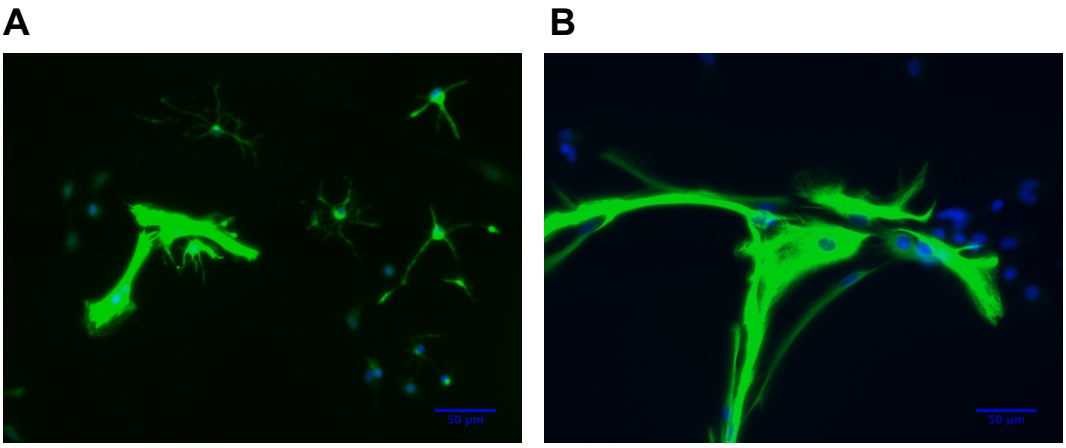



***Figure 9.5. Astrocytes after 6 hours in the no treatment group.***

***Astrocytes were stained against GFAP (in green) and as secondary antibody, Alexa488 was used. DAPI was used for staining the nuclei (blue). Images were captured on a Zeiss 100 epifluorescent microscope at 20x magnification. Astrocyte monocultures might contain other glia cells.***

Fig.9.6. (A) shows a randomly selected image of an astrocyte culture after 6 hours of 50ng/mL IL-1β treatment. Fig.9.5. (B) shows another randomly selected astrocyte image from the same treatment group. Astrocytes stained against GFAP (green), nuclei stained against DAPI (blue).

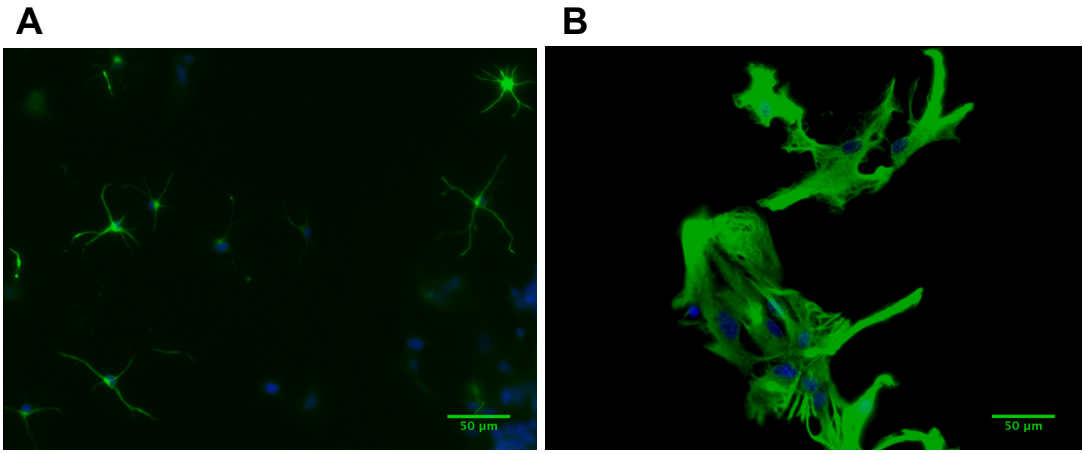



***Figure 9.6 Primary cortical astrocytes after 6 hours of 50ng/mL IL-1b treatment***

***Primary astrocytes were extracted, cultured and fixed on a cover slip after 6 hours of 50ng/mL IL-1β direct treatment. ICC: Primary antibody GFAP (in green) and nuclei stained with DAPI, shown in blue. Images were captured on a Zeiss 100 epifluorescent microscope at 20x magnification.***

Figure 9.7. (A) shows the effect of a 6-hour treatment of 25ng/mL IL-1β on astrocytes and the slight morphological changes. 9.7. (B) is another randomly selected image from the 25ng/mL treatment group.

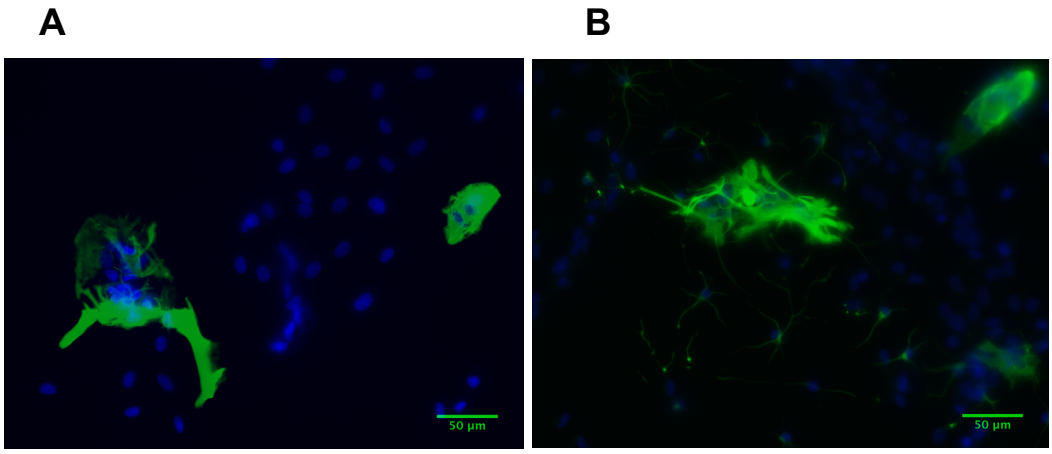



***Figure 9.7 Primary cortical astrocytes after 6 hours of 25ng/mL IL-1b treatment***

***Primary astrocytes were extracted, grown and fixed on a cover slip after 6 hours of 25ng/mL IL-1b direct treatment. ICC: Primary antibody GFAP (in green) and nuclei stained with DAPI, shown in blue. Stained nuclei, where the body of the cell is not stained are likely to be other glia cells. Images were captured on a Zeiss 100 epifluorescent microscope at 20x magnification.***

In Figure 9.8. the combined effect of IL-1β and TNF-α on astrocyte cultures is shown. Fig.9.8. (A) is a randomly selected image of an astrocyte culture stained against GFAP (green) and DAPI (blue). Fig.9.8. (B) shows a second randomly selected image of the treatment group of 25ng/mL IL-1β and 20ng/mL TNF-α treatment.

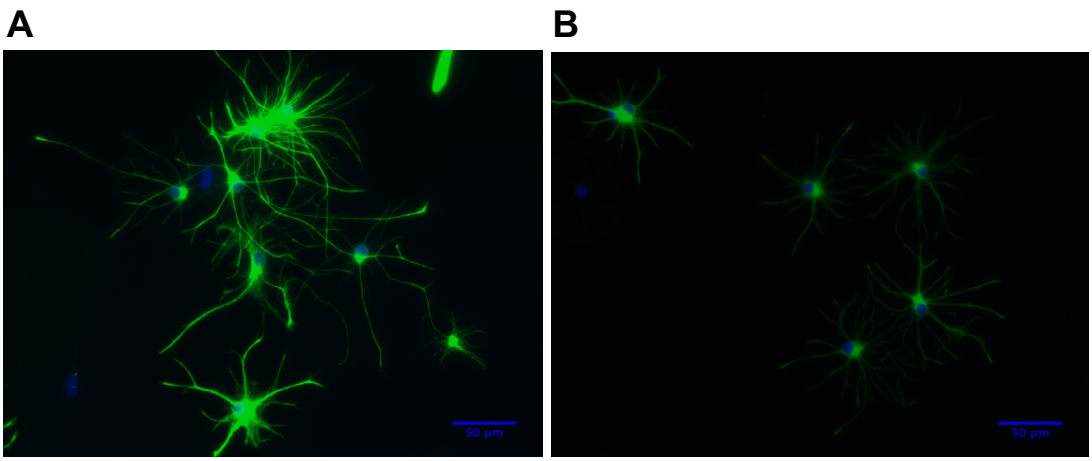



***Figure 9.8 Primary cortical astrocytes after 6 hours of 25ng/mL IL-1b and 20ng/mL TNF-α treatment***

***Primary astrocytes were extracted, grown and fixed on a cover slip after 6 hours of 25ng/mL IL-1b and 20ng/mL TNf-alpha direct treatment. ICC: Primary antibody GFAP (in green) and nuclei stained with DAPI, shown in blue. Images were captured on a Zeiss 100 epifluorescent microscope at 20x magnification. Images shown from two different cultures.***

Figure 9.9. (A) shows the effect of a 6-hour treatment of TNF-α on astrocyte culture. A random image has been selected to represent the treatment group. Astrocytes stained against GFAP (green), cytokines stained against STAT3-CY3 (red) and DAPI (blue). STAT3 is the most multifaceted member of the signal transducer and activator of transcription (STAT) family of transcription factors and mediates pivotal responses for cytokines. STAT3-CY3 was used to detect any potential cytokine activity in the culture that could have been triggered by the TNF-α treatment. Due to the merging of images, DAPI may appear as purple.

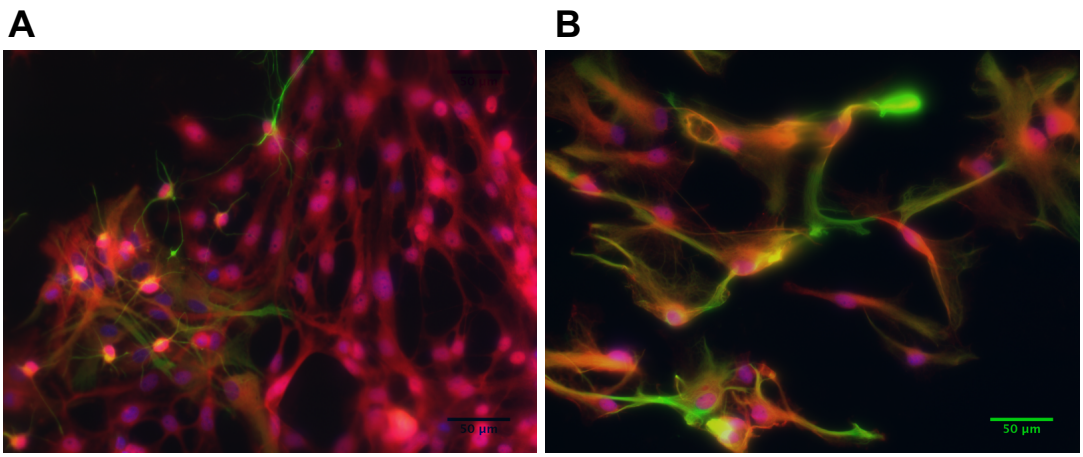



***Figure 9.9 Primary cortical astrocytes after 6 hours 20ng/mL TNF-α treatment***

***Primary astrocytes were extracted, cultured and fixed on a cover slip after 6 hours of 20ng/mL TNF-alpha direct treatment. ICC: Primary antibody GFAP (in green), STAT3-CY3 (red) to detect the likely presence of cytokines such as IL-6. Images were captured on a Zeiss 100 epifluorescent microscope at 20x magnification.***

Finally, Figure 9.10. shows the effect of 100ng/mL of TNF-α treatment on astrocytes. Fig.9.10. (A) represents a randomly chosen image from the treatment group, where astrocytes stained against GFAP(green), cytokines against STAT3-CY3 (red) and against DAPI (blue). Fig.9.10. (B) shows a second randomly selected image from the same treatment group, with the same staining conditions. DAPI might appear as purple in the images due to the merging of channels.

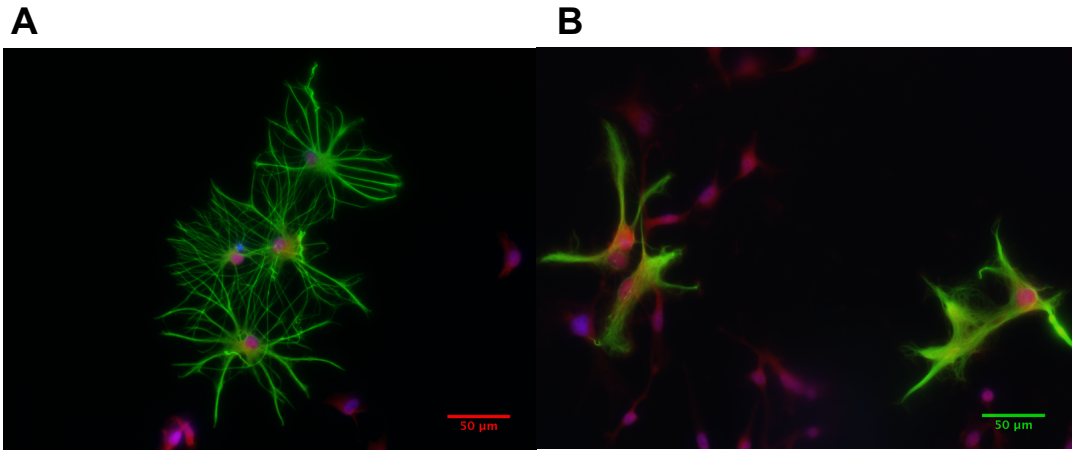



***Figure 9.10 Primary cortical astrocytes after 6 hours 100ng/mL TNF-α treatment***

***Primary astrocytes were extracted, cultured and fixed on a cover slip after 6 hours of 100ng/mL TNf-alpha direct treatment. ICC: Primary antibody GFAP (in green), STAT3-CY3 (red) to detect***

***the presence of cytokines such as IL-6. Images were captured on a Zeiss 100 epifluorescent microscope at 20x magnification. Images taken from two different cultures (same treatment group).***

## 9.7. Spheroid cultures

To create the 3D model of glia cells, a protocol was adapted from (Leek *et al.*, 2016), where freshly extracted astrocytes were plated in a low-adherent 96 well-plate with a Matrigel (Corning, #11543550) that acted as a scaffold for the cells to attach. After attachment, cells were stained to confirm their location and morphology in the co-culture. Fig.9.11. shows a randomly selected image of an astrocyte spheroid monoculture stained against GFAP (red) and DAPI (blue).

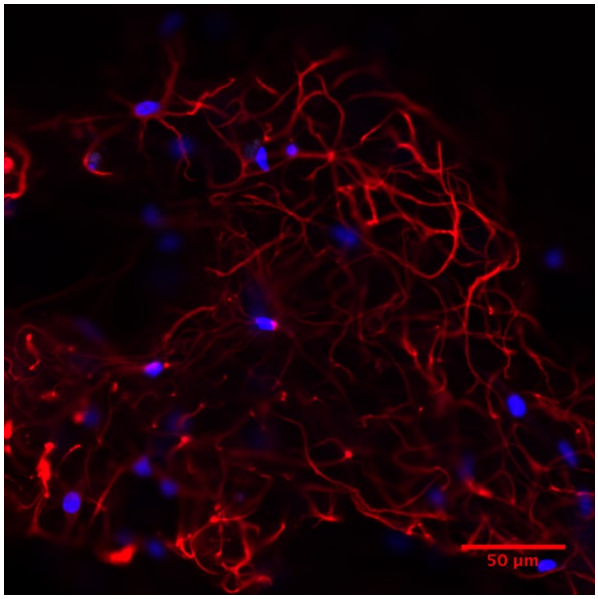



***Figure 9.11. Primary astrocytes in a 3D spheroid culture***

***Astrocytes in the control group were fixed on day 10 and stained against GFAP with Rhodamine X (in red) and DAPI for nuclei (in blue). 3D spheroids were established using Matrigel. Images were captured on a Zeiss 100 epifluorescent microscope at 10x magnification.***

Following image shows the full scale and shape of the spheroids, depicting the expected self-assembling pattern. Figure 9.11. shows a spheroid monoculture of astrocytes, stained against GFAP (orange) and DAPI (blue).

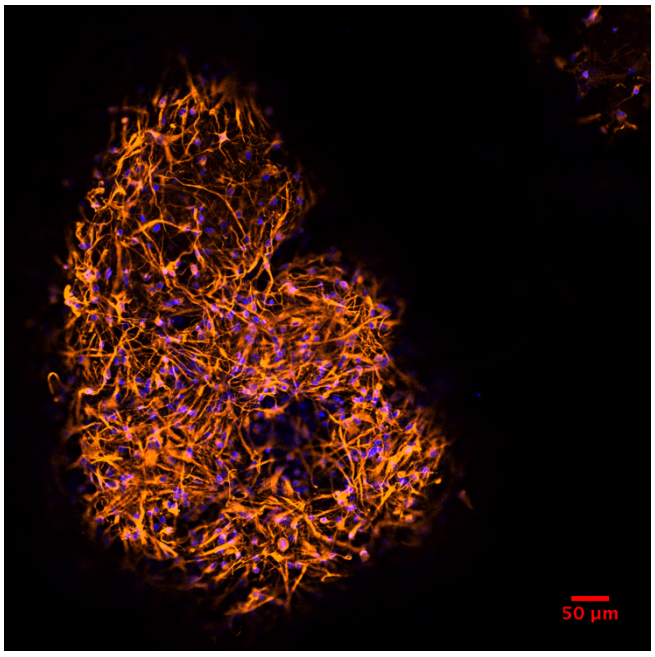



***Figure 9.12. Primary astrocytes in a 3D spheroid culture***

***Astrocytes in the control group were fixed on day 10 and stained against GFAP with Alexa 566 (in orange) and DAPI for nuclei in blue. 3D spheroid cultures were established using Matrigel. Images were captured on a Zeiss 100 epifluorescent microscope at 10x magnification.***

Brain endothelial cells (BECS) were extracted based on a protocol by (Abbott *et al.*, 2012), then similarly to astrocytes, cultured and established in a low adherent plate with the addition of a Matrigel™ to act as a scaffold. Fig.9.13. shows a monoculture of BECS stained against VE-Cadherin (green) and DAPI (blue), on day 10 of the culture.

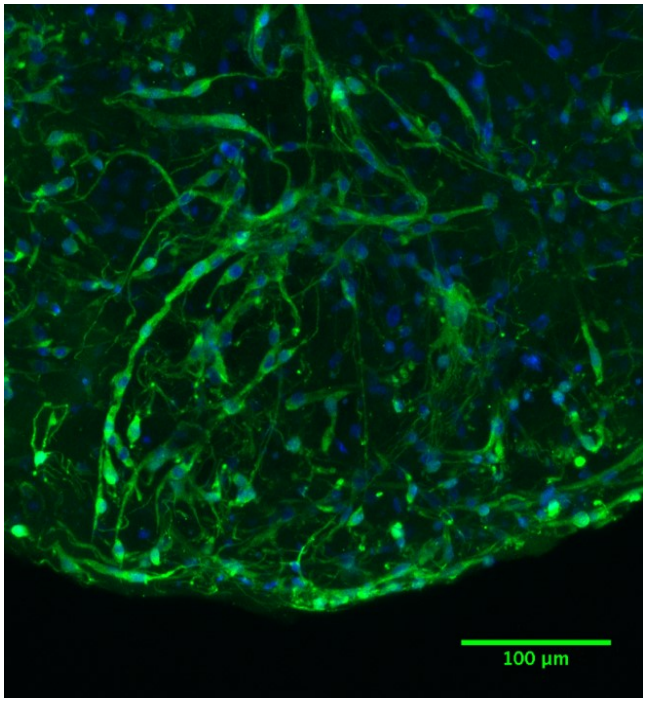



***Figure 9.13. Primary brain endothelial cells (BECS) in a 3D spheroid model.***

***BECS were stained against VE-Cadherin with Alexa 488 (in green) DAPI for nuclei (in blue), cells were fixed and stained on day 10. Images were captured on a Zeiss 100 epifluorescent microscope at 10x magnification.***

To create a monoculture of cortical pericytes the same method was used as for BECS. Pericytes were also cultured in the same conditions as BECS and

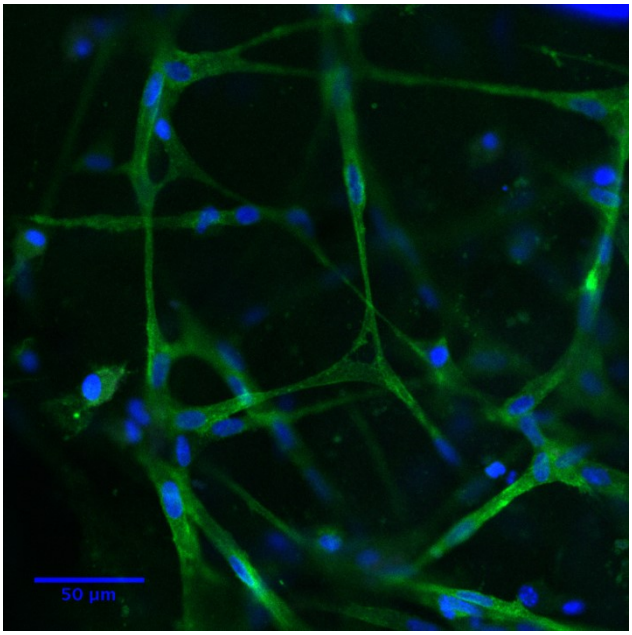



***Figure 9.14. Primary pericytes in a 3D spheroid model.***

***Pericytes were fixed on Day 10 after removing the Matrigel scaffold, stained against PDGFR-β with Alexa 488 (green), DAPI for nuclei (in blue). Images were captured on a Zeiss 100 epifluorescent microscope at 20x magnification.***

established in a spheroid model in a low adherent plate. Fig.9.14. shows a monoculture of pericytes, stained against PDGFR-β (green) and DAPI (blue).

Finally, a co-culture of primary brain endothelial cells, astrocytes and pericytes is shown here, in a 3D spheroid model. Fig.9.15. represents a randomly selected image of a co-culture of astrocytes, BECS and pericytes. Tight junctions stained against ZO-1 (red) and DAPI (blue).

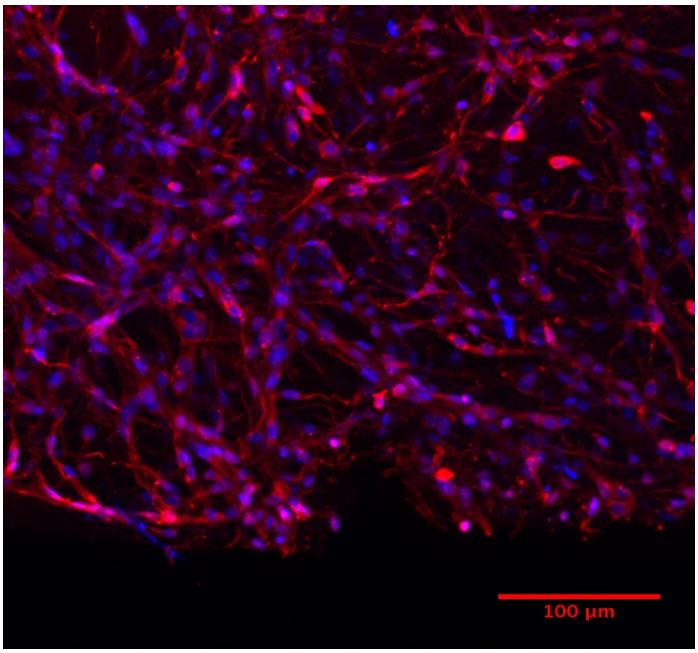



***Figure 9.15. Co-culture of primary astrocytes, endothelial cells and pericytes.***

***Stained against ZO-1 and Rhodamine X (in red), DAPI for nuclei (in blue). Images were captured on a Zeiss 100 epifluorescent microscope at 10x magnification.***

The next image shows a co-culture of astrocytes, pericytes, and brain endothelial cells in a spheroid model. Fig.9.16. represents a second randomly selected image of a spheroid co-culture, consisting of astrocytes shown in yellow and nuclei stained against DAPI (in blue).

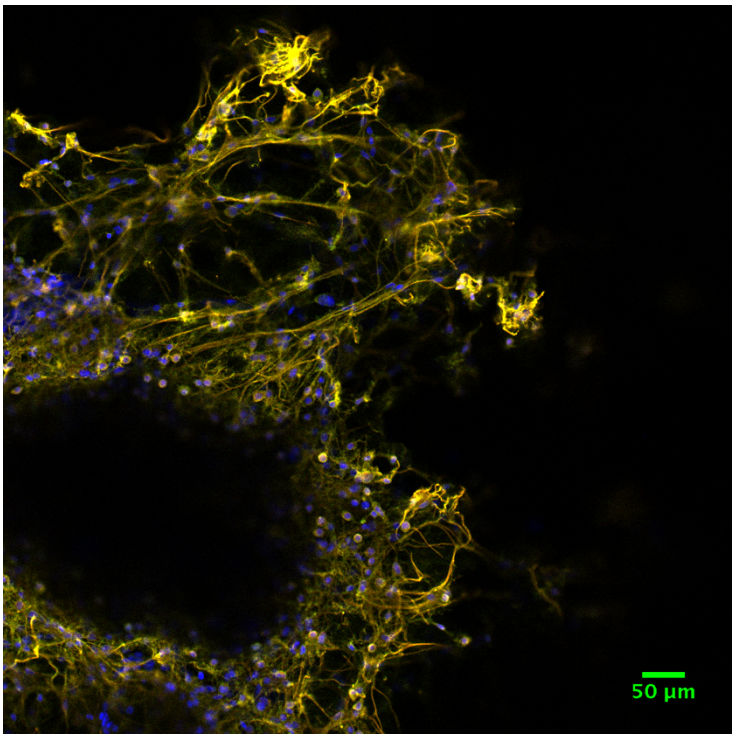



***Figure 9.16 Co-culture of primary astrocytes, brain endothelial cells and pericytes in a 3D spheroid.***

***Astrocytes were fixed after the removal of the Matrigel scaffold, stained against GFAP and Alexa 566 (yellow), DAPI for nuclei (in blue). Images were captured on a Zeiss 100 epifluorescent microscope at 4x magnification. The middle of the spheroid represents the hypoxic core which firms up and does not allow for cell proliferation.***

## 9.8. Discussion and conclusions

U87 cells showed a drop in viability levels after SPHINX-31 and Griffin 51 treatment in the highest concentration treatment group (10μM), however $IC_{50}$ values could not be calculated due to high baseline measurements. This results somewhat supports the previous findings of (Wu *et al.*, 2013) in which they found that using siSRPK1 in glioma cells can inhibit tumour cell growth, invasion and migration, although future studies are required to definitely prove the inhibitory effects of these inhibitors. CLK1 inhibition in glioblastoma cells caused a significant reduction in viability, migration and invasion (Zhou *et al.*, 2017b). In this study, only the highest concentration [10μM] treatment could achive a visible drop in viability levels, and therefore this needs further investigation. On the other hand, even low concentrations of SPHINX-31 and Griffin 51 caused a significant drop in downstream targets. MYC, HOXA9 and BCL-2 levels were significantly reduced with $IC_{50}$ values of [3nM- 35nM] across treatment groups. The 3D spheroid model was created to test the application of the small molecule inhibitors and their ability to cross the BBB in GBM. The cytokine treatment showed no adverse effect on the model, however the final stage of the development and the application of the inhibitors remain outstanding which could greatly contribute to this study in the future.

# 10. Chapter

# Conclusion and future work

# Conclusion

Acute Myeloid Leukaemia is still one of the most aggressive types of cancer. It is caused by the abnormal proliferation of haematopoietic cells that underwent a genetic mutation, which means they have an abnormal growth rate and are irresponsive to normal cell signalling. Many advances have been made in the past to develop subset-specific treatments, for instance, FLT3 and IDH1/2 inhibitors but these have not been approved for clinical use (Dang *et al.*, 2010). The current drug regime for any de novo AML is still general chemotherapy with venetoclax (selective BCL-2 inhibitor) and either azacitidine (DNA methyltransferase blocker) or low dose cytarabine (pyrimidine nucleoside analogue) (Roloff *et al.*, 2022) and (NICE, 2022 TA787). Relapse within 5 years is still very common (in 95% of cases), therefore there is a real clinical need for selective drugs to be used, especially for patients who are unsuitable for high-dose chemotherapy (Wang *et al.*, 2019).

SRPK1 is a key splicing regulator, which phosphorylates specific amino acids of protein rich serine/arginine repeats such as SRSF1. The SRPK1 in normal circumstances overexpressed in the pancreas and testicular germ cells and interestingly, under expressed in healthy glia cells. Through alternative splicing, SRPK1 regulates RNA maturation, cell cycle progression, and immune responses. However, the aberrant version of alternative splicing is a key factor in carcinogenesis and a hallmark of cancer. SRPK1 has been found to be overexpressed in many types of cancers, and its downregulation in preclinical models causes tumour-suppression. (Nikas *et al.*, 2019). In Acute

Myeloid Leukaemia, SRPK1 inhibition showed a significant reduction in cell viability (tested in AML cell lines) (Tzelepis *et al.*, 2018) and also in extranodal natural killer/T-cell lymphoma (ENKTL), a very aggressive subtype of non-Hodgkin lymphoma. The same study showed that SPHINX-31 and SRPIN340 (both are highly selective SRPK1 inhibitors) have the same effect on peripheral blood lymphocytes (PBLs) that were isolated from samples from ENKTL patients (He *et al.*, 2022). In glia originated cancer cells, such as gliomas or glioblastomas, SRPK1 has been found to be highly overexpressed, which is the opposite of their normal state. Furthermore, the level of SRPK1 expression also has a significant role in predicting patient survival, wherein the higher the expression level is, the lower the survival rate (Sigala *et al.*, 2016).

## 10.1. SRPK1 inhibition in AML

SRPK1 has been known to be a relevant drug target in AML (Siqueira *et al.*, 2020) and various SRPK1 inhibitors showed good results in reducing cell viability and proliferation (Tzelepis *et al.*, 2016). Here is shown that SPHINX-31 can significantly reduce common downstream targets such as BCL-2, HOXA9 and MYC (Perini *et al.*, 2018, Collins and Hess, 2016, Salvatori *et al.*, 2011) even in the nanomolar range. However, the findings of the Tzelepis et al. (2016) study could not be replicated, in terms of cell viability. When adjusted to the vehicle control group, it was not possible to show a dose response curve or in fact, a response to treatment.

## 10.2. BRD4 splice change in AML

BRD4 has long been considered to be a worthy drug candidate in AML (Roe and Vakoc, 2016), however it has also been understood that pan BRD4 inhibitors such as iBET151 have great issues with toxicity which became clear in clinical trials. It has been recently proposed that instead of trying to utilise pan BRD4 inhibitors, other inhibitors can be used that trigger an effect in the BRD4 splice change (Alsarraj *et al.*, 2011). This study demonstrates that both SPHINX-31 and Griffin 51 trigger an isoform change in AML, which caused the tumourigenic BRD4s isoform to be reduced and the BRD4l, tumour suppressor isoform to be increased in response to rising concentrations of inhibitor treatment. The data in small molecule inhibitors that affect the isoform of BRD4 is limited but the results here show a promising opportunity to test the efficacy of SPHINX-31 and Griffin 51 in reducing tumour burden further. The obvious improvement that needs to be made is the further optimisation of primer sequences to avoid double banding that appeared in some gels during RT-PCR visualisation.

## 10.3. New generation SRPK1 inhibitors

In Chapter 6. the effect of three new generation inhibitors, ET1126, ET1132, ET3002 is shown. All three inhibitors caused a significant reduction in common downstream targets such as BCL-2, HOXA9 and MYC. Data from

other inhibitors from the Intracellular Kinase Target Engagement assay are also presented, that showed promising results in SRPK1 inhibition. These have yet to be tested further, however, from the data it is clear that the new SRPKBNP-1 tracer produces reliable measuring capabilities of the BRET activity and therefore is a good starting point for further testing. When compared to SPHINX-31, it can be seen that the second-generation inhibitors are significantly more potent and therefore are worthy candidates to be tested further. See Fig. 6.25., 6.26., 6.27.

## 10.4. CLK1 inhibition in AML

Due to its synergistic relationship with SRPK1 (Aubol *et al.*, 2016) (as described in Chapter 7.) A highly selective CLK1 inhibitor was also tested, which has not been published yet. Griffin 51 showed great results in reducing cell viability levels in AML cells, in fact, it displayed a greater effect than SPHINX-31. It also significantly reduced the expression levels of HOXA9, BCL-2 and MYC. It triggered a BRD4 splice change (similarly to SPHINX-31) and promoted the tumour-suppressor BRD4l isoform, especially in the higher concentration treatment. Overall, it proved to be a good candidate to be tested further.

## 10.5. SRPK1 and CLK1 inhibition in astrocyte derived cancer models

In this chapter, a similar effect in U87 cells after SPHINX-31 and Griffin 51 treatment was observed as in the AML cell lines. In terms of downstream targets, SPHINX-31 and Griffin 51 were able to significantly reduce the expression levels of MYC, HOXA9 and BCL-2, even in the nanomolar range. To test these inhibitors further, a 3D model from primary cells was created to study the effect of GBM on the BBB. The application of the mentioned inhibitors are outstanding but the data obtained from U87 cells shows a promising result.

## 10.6. Future Work

Glioblastoma and Acute Myeloid Leukaemia are still some of the most treatment resistant types of cancers. AML carries an especially poor prognosis in children and elderly (De Kouchkovsky and Abdul-Hay, 2016). The treatment regime for AML has not changed for some twenty years now and not all patients can tolerate the usual treatments that consists of chemo and radiotherapy. As AML is a highly heterogenous disease which carries many variations, therefore an appropriate targeted treatment can be much beneficial. Here is presented how the tested inhibitors are effective in inhibiting SRPK1 expression in all AML cell lines. Griffin 51 a highly selective

CLK1 inhibitor was effective across all studies in CLK1 inhibition, and the data showed that both SPHINX-31 and Griffin 51 trigger a splice change in AML cells, causing the upregulation of the tumour-suppressor BRD4l isoform in response to increasing concentration of inhibitor treatment. Levels of downstream targets such as MYC, HOXA9 and BCL-2 showed that these inhibitors can cause a significant reduction at very low concentrations.

In the future, the continuation of this work is going to be to screen new inhibitors similar to Griffin 51 (e.g. those with the Griffin scaffold). *In vivo* studies are currently taking place to further test the potency of SPHINX-31 and Griffin 51, which will be extended to ET1126, ET1132 and ET3002 to measure their effect on SRPK1 and CLK1 inhibition in *in vivo* rat models of leukaemia. We are also expanding the scope of this research to other types of cancer, such as cholangiocarcinoma and will continue using U87 cell line for glioblastoma models.

# 11. REFERENCES


ABBOTT, N. J., DOLMAN, D. E., DRNDARSKI, S. & FREDRIKSSON, S. M. 2012. An improved in vitro blood-brain barrier model: rat brain endothelial cells co-cultured with astrocytes. *Methods Mol Biol,* 814**,** 415-30.

ABBOTT, N. J., RONNBACK, L. & HANSSON, E. 2006. Astrocyte-endothelial interactions at the blood-brain barrier. *Nat Rev Neurosci,* 7**,** 41-53.

AKHTARI, M., BHATT, V. R., TANDRA, P. K., KRISHNAMURTHY, J., HORSTMAN, H., DREESSEN, A., CHEN, P. X. & ARMITAGE, J. O. 2013. Therapy-related myeloid neoplasms after autologous hematopoietic stem cell transplantation in lymphoma patients. *Cancer Biol Ther,* 14**,** 1077-88.

ALSARRAJ, J., WALKER, R. C., WEBSTER, J. D., GEIGER, T. R., CRAWFORD, N. P., SIMPSON, R. M., OZATO, K. & HUNTER, K. W. 2011. Deletion of the proline-rich region of the murine metastasis susceptibility gene Brd4 promotes epithelial-to-mesenchymal transition- and stem cell-like conversion. *Cancer Res,* 71**,** 3121-31.

ARAKI, S., DAIRIKI, R., NAKAYAMA, Y., MURAI, A., MIYASHITA, R., IWATANI, M., NOMURA, T. & NAKANISHI, O. 2015. Inhibitors of CLK protein kinases suppress cell growth and induce apoptosis by modulating pre-mRNA splicing. *PLoS One,* 10**,** e0116929.

ARBER, D. A., ORAZI, A., HASSERJIAN, R., THIELE, J., BOROWITZ, M. J., LE BEAU, M. M., BLOOMFIELD, C. D., CAZZOLA, M. & VARDIMAN, J. W. 2016. The 2016 revision to the World Health Organization classification of myeloid neoplasms and acute leukemia. *Blood,* 127**,** 2391-405.

AUBOL, B. E., WU, G., KESHWANI, M. M., MOVASSAT, M., FATTET, L., HERTEL, K. J., FU, X. D. & ADAMS, J. A. 2016. Release of SR Proteins from CLK1 by SRPK1: A Symbiotic Kinase System for Phosphorylation Control of Pre-mRNA Splicing. *Mol Cell,* 63**,** 218-228.

BABU, N., PINTO, S. M., BISWAS, M., SUBBANNAYYA, T., RAJAPPA, M., MOHAN, S. V., ADVANI, J., RAJAGOPALAN, P., SATHE, G., SYED, N., RADHAKRISHNA, V. D., MUTHUSAMY, O., NAVANI, S., KUMAR, R. V., GOPISETTY, G., RAJKUMAR, T., RADHAKRISHNAN, P., THIYAGARAJAN, S., PANDEY, A., GOWDA, H., MAJUMDER, P. & CHATTERJEE, A. 2020. Phosphoproteomic analysis identifies CLK1 as a novel therapeutic target in gastric cancer. *Gastric Cancer,* 23**,** 796-810.

BARNARD, D. R., KALOUSEK, D. K., WIERSMA, S. R., LANGE, B. J., BENJAMIN, D. R., ARTHUR, D. C., BUCKLEY, J. D., KOBRINSKY, N., NEUDORF, S., SANDERS, J., MILLER, L. P., SHINA, D. C., HAMMOND, G. D. & WOODS, W. G. 1996. Morphologic, immunologic, and cytogenetic classification of acute myeloid leukemia and

myelodysplastic syndrome in childhood: a report from the Childrens Cancer Group. *Leukemia,* 10**,** 5-12.

BATSON, J., TOOP, H. D., REDONDO, C., BABAEI-JADIDI, R., CHAIKUAD, A., WEARMOUTH, S. F., GIBBONS, B., ALLEN, C., TALLANT, C., ZHANG, J., DU, C., HANCOX, J. C., HAWTREY, T., DA ROCHA, J., GRIFFITH, R., KNAPP, S., BATES, D. O. & MORRIS, J. C. 2017. Development of Potent, Selective SRPK1 Inhibitors as Potential Topical Therapeutics for Neovascular Eye Disease. *ACS Chem Biol,* 12**,** 825-832.

BERGSMA, A. J., VAN DER WAL, E., BROEDERS, M., VAN DER PLOEG, A. T. & PIM PIJNAPPEL, W. W. M. 2018. Alternative Splicing in Genetic Diseases: Improved Diagnosis and Novel Treatment Options. *Int Rev Cell Mol Biol,* 335**,** 85-141.

BERTHON, C., RAFFOUX, E., THOMAS, X., VEY, N., GOMEZ-ROCA, C., YEE, K., TAUSSIG, D. C., REZAI, K., ROUMIER, C., HERAIT, P., KAHATT, C., QUESNEL, B., MICHALLET, M., RECHER, C., LOKIEC, F., PREUDHOMME, C. & DOMBRET, H. 2016. Bromodomain inhibitor OTX015 in patients with acute leukaemia: a dose-escalation, phase 1 study. *Lancet Haematol,* 3**,** e186-95.

BOURGEOIS, C. F., LEJEUNE, F. & STEVENIN, J. 2004. Broad specificity of SR (serine/arginine) proteins in the regulation of alternative splicing of pre-messenger RNA. *Prog Nucleic Acid Res Mol Biol,* 78**,** 37-88.

BOZIC, T., FROBEL, J., RAIC, A., TICCONI, F., KUO, C. C., HEILMANN-HEIMBACH, S., GOECKE, T. W., ZENKE, M., JOST, E., COSTA, I. G. & WAGNER, W. 2018. Variants of DNMT3A cause transcript-specific DNA methylation patterns and affect hematopoiesis. *Life Sci Alliance,* 1**,** e201800153.

BRADLEY, T., COOK, M. E. & BLANCHETTE, M. 2015. SR proteins control a complex network of RNA-processing events. *RNA,* 21**,** 75-92.

BRONDFIELD, S., UMESH, S., CORELLA, A., ZUBER, J., RAPPAPORT, A. R., GAILLARD, C., LOWE, S. W., GOGA, A. & KOGAN, S. C. 2015. Direct and indirect targeting of MYC to treat acute myeloid leukemia. *Cancer Chemother Pharmacol,* 76**,** 35-46.

BULLOCK, N. & OLTEAN, S. 2017. The many faces of SRPK1. *J Pathol,* 241**,** 437-440.

BUSH, S. J., CHEN, L., TOVAR-CORONA, J. M. & URRUTIA, A. O. 2017. Alternative splicing and the evolution of phenotypic novelty. *Philos Trans R Soc Lond B Biol Sci,* 372.

CAZALLA, D., ZHU, J., MANCHE, L., HUBER, E., KRAINER, A. R. & CACERES, J. F. 2002. Nuclear export and retention signals in the RS domain of SR proteins. *Mol Cell Biol,* 22**,** 6871-82.

CERELLA, C., GAIGNEAUX, A., MAZUMDER, A., LEE, J. Y., SALAND, E., RADOGNA, F., FARGE, T., VERGEZ, F., RECHER, C., SARRY, J. E., KIM, K. W., SHIN, H. Y., DICATO, M. & DIEDERICH, M. 2017. Bcl-2 protein family expression pattern determines synergistic pro-apoptotic

effects of BH3 mimetics with hemisynthetic cardiac glycoside UNBS1450 in acute myeloid leukemia. *Leukemia,* 31**,** 755-759.

CHASIN, L. A. 2007. Searching for splicing motifs. *Adv Exp Med Biol,* 623**,** 85-106.

CHEN, S., YANG, C., WANG, Z. W., HU, J. F., PAN, J. J., LIAO, C. Y., ZHANG, J. Q., CHEN, J. Z., HUANG, Y., HUANG, L., ZHAN, Q., TIAN, Y. F., SHEN, B. Y. & WANG, Y. D. 2021. CLK1/SRSF5 pathway induces aberrant exon skipping of METTL14 and Cyclin L2 and promotes growth and metastasis of pancreatic cancer. *J Hematol Oncol,* 14**,** 60.

CHEN, S., YU, J., LV, X. & ZHANG, L. 2017. HOXA9 is critical in the proliferation, differentiation, and malignancy of leukaemia cells both in vitro and in vivo. *Cell Biochem Funct,* 35**,** 433-440.

CHEUNG, H. C., BAGGERLY, K. A., TSAVACHIDIS, S., BACHINSKI, L. L., NEUBAUER, V. L., NIXON, T. J., ALDAPE, K. D., COTE, G. J. & KRAHE, R. 2008. Global analysis of aberrant pre-mRNA splicing in glioblastoma using exon expression arrays. *BMC Genomics,* 9**,** 216.

COLLINS, C. T. & HESS, J. L. 2016. Role of HOXA9 in leukemia: dysregulation, cofactors and essential targets. *Oncogene,* 35**,** 1090-8.

COLWILL, K., FENG, L. L., YEAKLEY, J. M., GISH, G. D., CACERES, J. F., PAWSON, T. & FU, X. D. 1996. SRPK1 and Clk/Sty protein kinases show distinct substrate specificities for serine/arginine-rich splicing factors. *J Biol Chem,* 271**,** 24569-75.

CORDO, V., MEIJER, M. T., HAGELAAR, R., DE GOEIJ-DE HAAS, R. R., POORT, V. M., HENNEMAN, A. A., PIERSMA, S. R., PHAM, T. V., OSHIMA, K., FERRANDO, A. A., ZAMAN, G. J. R., JIMENEZ, C. R. & MEIJERINK, J. P. P. 2022. Phosphoproteomic profiling of T cell acute lymphoblastic leukemia reveals targetable kinases and combination treatment strategies. *Nat Commun,* 13**,** 1048.

CSIZMAR, C. M., KIM, D. H. & SACHS, Z. 2016. The role of the proteasome in AML. *Blood Cancer J,* 6**,** e503.

DANG, L., JIN, S. & SU, S. M. 2010. IDH mutations in glioma and acute myeloid leukemia. *Trends Mol Med,* 16**,** 387-97.

DAWSON, M. A., PRINJHA, R. K., DITTMANN, A., GIOTOPOULOS, G., BANTSCHEFF, M., CHAN, W. I., ROBSON, S. C., CHUNG, C. W., HOPF, C., SAVITSKI, M. M., HUTHMACHER, C., GUDGIN, E., LUGO, D., BEINKE, S., CHAPMAN, T. D., ROBERTS, E. J., SODEN, P. E., AUGER, K. R., MIRGUET, O., DOEHNER, K., DELWEL, R., BURNETT, A. K., JEFFREY, P., DREWES, G., LEE, K., HUNTLY, B. J. & KOUZARIDES, T. 2011. Inhibition of BET recruitment to chromatin as an effective treatment for MLL-fusion leukaemia. *Nature,* 478**,** 529-33.

DE KOUCHKOVSKY, I. & ABDUL-HAY, M. 2016. 'Acute myeloid leukemia: a comprehensive review and 2016 update'. *Blood Cancer J,* 6**,** e441.

DEMEULE, M., REGINA, A., JODOIN, J., LAPLANTE, A., DAGENAIS, C., BERTHELET, F., MOGHRABI, A. & BELIVEAU, R. 2002. Drug transport to the brain: key roles for the efflux pump P-glycoprotein in the blood-brain barrier. *Vascul Pharmacol,* 38**,** 339-48.

DIABA-NUHOHO, P. 2023. Plant homeodomain-finger protein 5A: A key player in cancer progression. *Biomed Pharmacother,* 169**,** 115857.

DING, F. & ELOWITZ, M. B. 2019. Constitutive splicing and economies of scale in gene expression. *Nat Struct Mol Biol,* 26**,** 424-432.

DOHNER, H., ESTEY, E., GRIMWADE, D., AMADORI, S., APPELBAUM, F. R., BUCHNER, T., DOMBRET, H., EBERT, B. L., FENAUX, P., LARSON, R. A., LEVINE, R. L., LO-COCO, F., NAOE, T., NIEDERWIESER, D., OSSENKOPPELE, G. J., SANZ, M., SIERRA, J., TALLMAN, M. S., TIEN, H. F., WEI, A. H., LOWENBERG, B. & BLOOMFIELD, C. D. 2017. Diagnosis and management of AML in adults: 2017 ELN recommendations from an international expert panel. *Blood,* 129**,** 424-447.

DUGGAN, W. P., O'CONNELL, E., PREHN, J. H. M. & BURKE, J. P. 2022. Serine-Arginine Protein Kinase 1 (SRPK1): a systematic review of its multimodal role in oncogenesis. *Mol Cell Biochem*.

EISENREICH, A., ZAKRZEWICZ, A., HUBER, K., THIERBACH, H., PEPKE, W., GOLDIN-LANG, P., SCHULTHEISS, H. P., PRIES, A. & RAUCH, U. 2013. Regulation of pro-angiogenic tissue factor expression in hypoxia-induced human lung cancer cells. *Oncol Rep,* 30**,** 462-70.

EL MARABTI, E. & YOUNIS, I. 2018. The Cancer Spliceome: Reprograming of Alternative Splicing in Cancer. *Front Mol Biosci,* 5**,** 80.

EL-GAMIL, D. S., ELHADY, A. K., CHEN, P. J., HWANG, T. L., ABADI, A. H., ABDEL-HALIM, M. & ENGEL, M. 2023. Discovery of novel 5-methoxybenzothiophene hydrazides as metabolically stable Clk1 inhibitors with high potency and unprecedented Clk1 isoenzyme selectivity. *Eur J Med Chem,* 247**,** 115019.

ELHADY, A. K., ABDEL-HALIM, M., ABADI, A. H. & ENGEL, M. 2017. Development of Selective Clk1 and -4 Inhibitors for Cellular Depletion of Cancer-Relevant Proteins. *J Med Chem,* 60**,** 5377-5391.

ESTEY, E. H., GALE, R. P. & SEKERES, M. A. 2018. New drugs in AML: uses and abuses. *Leukemia,* 32**,** 1479-1481.

FAIRBROTHER, W. G., YEH, R. F., SHARP, P. A. & BURGE, C. B. 2002. Predictive identification of exonic splicing enhancers in human genes. *Science,* 297**,** 1007-13.

FEDOROV, O., HUBER, K., EISENREICH, A., FILIPPAKOPOULOS, P., KING, O., BULLOCK, A. N., SZKLARCZYK, D., JENSEN, L. J., FABBRO, D., TRAPPE, J., RAUCH, U., BRACHER, F. & KNAPP, S. 2011. Specific CLK inhibitors from a novel chemotype for regulation of alternative splicing. *Chem Biol,* 18**,** 67-76.

FELS, C., SCHAFER, C., HUPPE, B., BAHN, H., HEIDECKE, V., KRAMM, C. M., LAUTENSCHLAGER, C. & RAINOV, N. G. 2000. Bcl-2 expression

in higher-grade human glioma: a clinical and experimental study. *J Neurooncol,* 48**,** 207-16.

FENG, Y., VALLEY, M. T., LAZAR, J., YANG, A. L., BRONSON, R. T., FIRESTEIN, S., COETZEE, W. A. & MANLEY, J. L. 2009. SRp38 regulates alternative splicing and is required for Ca(2+) handling in the embryonic heart. *Dev Cell,* 16**,** 528-38.

FERGUSON, F. M. & GRAY, N. S. 2018. Kinase inhibitors: the road ahead. *Nat Rev Drug Discov,* 17**,** 353-377.

FOO, L. C., ALLEN, N. J., BUSHONG, E. A., VENTURA, P. B., CHUNG, W. S., ZHOU, L., CAHOY, J. D., DANEMAN, R., ZONG, H., ELLISMAN, M. H. & BARRES, B. A. 2011. Development of a method for the purification and culture of rodent astrocytes. *Neuron,* 71**,** 799-811.

FOX-WALSH, K. L., DOU, Y., LAM, B. J., HUNG, S. P., BALDI, P. F. & HERTEL, K. J. 2005. The architecture of pre-mRNAs affects mechanisms of splice-site pairing. *Proc Natl Acad Sci U S A,* 102**,** 16176-81.

GAMMONS, M. V., FEDOROV, O., IVISON, D., DU, C., CLARK, T., HOPKINS, C., HAGIWARA, M., DICK, A. D., COX, R., HARPER, S. J., HANCOX, J. C., KNAPP, S. & BATES, D. O. 2013. Topical antiangiogenic SRPK1 inhibitors reduce choroidal neovascularization in rodent models of exudative AMD. *Invest Ophthalmol Vis Sci,* 54**,** 6052-62.

GAMMONS, M. V., LUCAS, R., DEAN, R., COUPLAND, S. E., OLTEAN, S. & BATES, D. O. 2014. Targeting SRPK1 to control VEGF-mediated tumour angiogenesis in metastatic melanoma. *Br J Cancer,* 111**,** 477-85.

GHOSH, G. & ADAMS, J. A. 2011. Phosphorylation mechanism and structure of serine-arginine protein kinases. *FEBS J,* 278**,** 587-97.

GIANNAKOUROS, T., NIKOLAKAKI, E., MYLONIS, I. & GEORGATSOU, E. 2011. Serine-arginine protein kinases: a small protein kinase family with a large cellular presence. *FEBS J,* 278**,** 570-86.

GOETHE, E., CARTER, B. Z., RAO, G. & PEMMARAJU, N. 2018. Glioblastoma and acute myeloid leukemia: malignancies with striking similarities. *J Neurooncol,* 136**,** 223-231.

GONCALVES, V., HENRIQUES, A. F., PEREIRA, J. F., NEVES COSTA, A., MOYER, M. P., MOITA, L. F., GAMA-CARVALHO, M., MATOS, P. & JORDAN, P. 2014. Phosphorylation of SRSF1 by SRPK1 regulates alternative splicing of tumor-related Rac1b in colorectal cells. *RNA,* 20**,** 474-82.

GOUT, S., BRAMBILLA, E., BOUDRIA, A., DRISSI, R., LANTUEJOUL, S., GAZZERI, S. & EYMIN, B. 2012. Abnormal expression of the pre-mRNA splicing regulators SRSF1, SRSF2, SRPK1 and SRPK2 in non small cell lung carcinoma. *PLoS One,* 7**,** e46539.

GRIGOROPOULOS, N. F., PETTER, R., VAN 'T VEER, M. B., SCOTT, M. A. & FOLLOWS, G. A. 2013. Leukaemia update. Part 1: diagnosis and management. *BMJ,* 346**,** f1660.

GUI, J. F., TRONCHERE, H., CHANDLER, S. D. & FU, X. D. 1994. Purification and characterization of a kinase specific for the serine- and arginine-rich pre-mRNA splicing factors. *Proc Natl Acad Sci U S A,* 91**,** 10824-8.

HACKER, I., SANDER, B., GOLAS, M. M., WOLF, E., KARAGOZ, E., KASTNER, B., STARK, H., FABRIZIO, P. & LUHRMANN, R. 2008. Localization of Prp8, Brr2, Snu114 and U4/U6 proteins in the yeast tri-snRNP by electron microscopy. *Nat Struct Mol Biol,* 15**,** 1206-12.

HAGOPIAN, J. C., MA, C. T., MEADE, B. R., ALBUQUERQUE, C. P., NGO, J. C., GHOSH, G., JENNINGS, P. A., FU, X. D. & ADAMS, J. A. 2008. Adaptable molecular interactions guide phosphorylation of the SR protein ASF/SF2 by SRPK1. *J Mol Biol,* 382**,** 894-909.

HANAHAN, D. & WEINBERG, R. A. 2000. The hallmarks of cancer. *Cell,* 100**,** 57-70.

HATCHER, J. M., WU, G., ZENG, C., ZHU, J., MENG, F., PATEL, S., WANG, W., FICARRO, S. B., LEGGETT, A. L., POWELL, C. E., MARTO, J. A., ZHANG, K., KI NGO, J. C., FU, X. D., ZHANG, T. & GRAY, N. S. 2018. SRPKIN-1: A Covalent SRPK1/2 Inhibitor that Potently Converts VEGF from Pro-angiogenic to Anti-angiogenic Isoform. *Cell Chem Biol,* 25**,** 460-470 e6.

HE, C., LIU, B., WANG, H. Y., WU, L., ZHAO, G., HUANG, C., LIU, Y., SHAN, B. & LIU, L. 2022. Inhibition of SRPK1, a key splicing regulator, exhibits antitumor and chemotherapeutic-sensitizing effects on extranodal NK/T-cell lymphoma cells. *BMC Cancer,* 22**,** 1100.

HERRMANN, H., BLATT, K., SHI, J., GLEIXNER, K. V., CERNY-REITERER, S., MULLAUER, L., VAKOC, C. R., SPERR, W. R., HORNY, H. P., BRADNER, J. E., ZUBER, J. & VALENT, P. 2012. Small-molecule inhibition of BRD4 as a new potent approach to eliminate leukemic stem- and progenitor cells in acute myeloid leukemia AML. *Oncotarget,* 3**,** 1588-99.

HUANG, H. T. & FIGUEROA, M. E. 2021. Epigenetic deregulation in myeloid malignancies. *Blood,* 138**,** 613-624.

ISHIZAWA, J., KOJIMA, K., MCQUEEN, T., RUVOLO, V., CHACHAD, D., NOGUERAS-GONZALEZ, G. M., HUANG, X., PIERCEALL, W. E., DETTMAN, E. J., CARDONE, M. H., SHACHAM, S., KONOPLEVA, M. & ANDREEFF, M. 2015. Mitochondrial Profiling of Acute Myeloid Leukemia in the Assessment of Response to Apoptosis Modulating Drugs. *PLoS One,* 10**,** e0138377.

IWAI, K., YAGUCHI, M., NISHIMURA, K., YAMAMOTO, Y., TAMURA, T., NAKATA, D., DAIRIKI, R., KAWAKITA, Y., MIZOJIRI, R., ITO, Y., ASANO, M., MAEZAKI, H., NAKAYAMA, Y., KAISHIMA, M., HAYASHI, K., TERATANI, M., MIYAKAWA, S., IWATANI, M., MIYAMOTO, M., KLEIN, M. G., LANE, W., SNELL, G., TJHEN, R., HE,

X., PULUKURI, S. & NOMURA, T. 2018. Anti-tumor efficacy of a novel CLK inhibitor via targeting RNA splicing and MYC-dependent vulnerability. *EMBO Mol Med,* 10.

IWAKIRI, R., OHTA, M., MIKOSHIBA, M., TSUTSUMI, H., KUMAKAWA, T. & MORI, M. 2002. Prognosis of elderly patients with acute myelogenous leukemia: analysis of 126 AML cases. *Int J Hematol,* 75**,** 45-50.

JUMAA, H., WOLLSCHEID, B., MITTERER, M., WIENANDS, J., RETH, M. & NIELSEN, P. J. 1999. Abnormal development and function of B lymphocytes in mice deficient for the signaling adaptor protein SLP-65. *Immunity,* 11**,** 547-54.

KLIJN, C., DURINCK, S., STAWISKI, E. W., HAVERTY, P. M., JIANG, Z., LIU, H., DEGENHARDT, J., MAYBA, O., GNAD, F., LIU, J., PAU, G., REEDER, J., CAO, Y., MUKHYALA, K., SELVARAJ, S. K., YU, M., ZYNDA, G. J., BRAUER, M. J., WU, T. D., GENTLEMAN, R. C., MANNING, G., YAUCH, R. L., BOURGON, R., STOKOE, D., MODRUSAN, Z., NEVE, R. M., DE SAUVAGE, F. J., SETTLEMAN, J., SESHAGIRI, S. & ZHANG, Z. 2015. A comprehensive transcriptional portrait of human cancer cell lines. *Nat Biotechnol,* 33**,** 306-12.

KONOPLEVA, M. Y. 2021. Mechanisms for resistance in AML insights into molecular pathways mediating resistance to venetoclax. *Best Pract Res Clin Haematol,* 34**,** 101251.

KOO, B. K., CHOI, E. J., HUR, E. H., MOON, J. H., KIM, J. Y., PARK, H. S., CHOI, Y., LEE, J. H., LEE, K. H., CHOI, E. K., KIM, J. & LEE, J. H. 2022. Antileukemic activity of YPN-005, a CDK7 inhibitor, inducing apoptosis through c-MYC and FLT3 suppression in acute myeloid leukemia. *Heliyon,* 8**,** e11004.

KRAINER, A. R., CONWAY, G. C. & KOZAK, D. 1990. The essential pre-mRNA splicing factor SF2 influences 5' splice site selection by activating proximal sites. *Cell,* 62**,** 35-42.

KUMAR, C. C. 2011. Genetic abnormalities and challenges in the treatment of acute myeloid leukemia. *Genes Cancer,* 2**,** 95-107.

KURIMCHAK, A. M., KUMAR, V., HERRERA-MONTAVEZ, C., JOHNSON, K. J., SRIVASTAVA, N., DAVARAJAN, K., PERI, S., CAI, K. Q., MANTIA-SMALDONE, G. M. & DUNCAN, J. S. 2020. Kinome Profiling of Primary Endometrial Tumors Using Multiplexed Inhibitor Beads and Mass Spectrometry Identifies SRPK1 as Candidate Therapeutic Target. *Mol Cell Proteomics,* 19**,** 2068-2090.

KUYKENDALL, A., DUPLOYEZ, N., BOISSEL, N., LANCET, J. E. & WELCH, J. S. 2018. Acute Myeloid Leukemia: The Good, the Bad, and the Ugly. *Am Soc Clin Oncol Educ Book,* 38**,** 555-573.

LAI, A. Y. & KONDO, M. 2008. T and B lymphocyte differentiation from hematopoietic stem cell. *Semin Immunol,* 20**,** 207-12.

LAI, J., LIU, Z., ZHAO, Y., MA, C. & HUANG, H. 2021. Anticancer Effects of I-BET151, an Inhibitor of Bromodomain and Extra-Terminal Domain Proteins. *Front Oncol,* 11**,** 716830.

LAMBERT, M., ALIOUI, M., JAMBON, S., DEPAUW, S., VAN SEUNINGEN, I. & DAVID-CORDONNIER, M. H. 2019. Direct and Indirect Targeting of HOXA9 Transcription Factor in Acute Myeloid Leukemia. *Cancers (Basel),* 11.

LAN, Q., ZHANG, L., LI, G., VERMEULEN, R., WEINBERG, R. S., DOSEMECI, M., RAPPAPORT, S. M., SHEN, M., ALTER, B. P., WU, Y., KOPP, W., WAIDYANATHA, S., RABKIN, C., GUO, W., CHANOCK, S., HAYES, R. B., LINET, M., KIM, S., YIN, S., ROTHMAN, N. & SMITH, M. T. 2004. Hematotoxicity in workers exposed to low levels of benzene. *Science,* 306**,** 1774-6.

LARIBI, K., SOBH, M., GHEZ, D. & BAUGIER DE MATERRE, A. 2021. Impact of age, functional status, and comorbidities on quality of life and outcomes in elderly patients with AML: review. *Ann Hematol,* 100**,** 1359-1376.

LEE, J. Y. & HONG, S. H. 2020. Hematopoietic Stem Cells and Their Roles in Tissue Regeneration. *Int J Stem Cells,* 13**,** 1-12.

LEE, W. H., LIU, F. H., LIN, J. Y., HUANG, S. Y., LIN, H., LIAO, W. J. & HUANG, H. M. 2009. JAK pathway induction of c-Myc critical to IL-5 stimulation of cell proliferation and inhibition of apoptosis. *J Cell Biochem,* 106**,** 929-36.

LEEK, R., GRIMES, D. R., HARRIS, A. L. & MCINTYRE, A. 2016. Methods: Using Three-Dimensional Culture (Spheroids) as an In Vitro Model of Tumour Hypoxia. *Adv Exp Med Biol,* 899**,** 167-96.

LI, X. & MANLEY, J. L. 2005. Inactivation of the SR protein splicing factor ASF/SF2 results in genomic instability. *Cell,* 122**,** 365-78.

LILLICO, R., LAWRENCE, C. K. & LAKOWSKI, T. M. 2018. Selective DOT1L, LSD1, and HDAC Class I Inhibitors Reduce HOXA9 Expression in MLL-AF9 Rearranged Leukemia Cells, But Dysregulate the Expression of Many Histone-Modifying Enzymes. *J Proteome Res,* 17**,** 2657-2667.

LIU, S., QIAO, X., WU, S., GAI, Y., SU, Y., EDWARDS, H., WANG, Y., LIN, H., TAUB, J. W., WANG, G. & GE, Y. 2022. c-Myc plays a critical role in the antileukemic activity of the Mcl-1-selective inhibitor AZD5991 in acute myeloid leukemia. *Apoptosis,* 27**,** 913-928.

MA, C. T., VELAZQUEZ-DONES, A., HAGOPIAN, J. C., GHOSH, G., FU, X. D. & ADAMS, J. A. 2008. Ordered multi-site phosphorylation of the splicing factor ASF/SF2 by SRPK1. *J Mol Biol,* 376**,** 55-68.

MAKAROV, E. M., MAKAROVA, O. V., URLAUB, H., GENTZEL, M., WILL, C. L., WILM, M. & LUHRMANN, R. 2002. Small nuclear ribonucleoprotein remodeling during catalytic activation of the spliceosome. *Science,* 298**,** 2205-8.

MARTIN MOYANO, P., NEMEC, V. & PARUCH, K. 2020. Cdc-Like Kinases (CLKs): Biology, Chemical Probes, and Therapeutic Potential. *Int J Mol Sci,* 21.

MATSUO, Y., MACLEOD, R. A., UPHOFF, C. C., DREXLER, H. G., NISHIZAKI, C., KATAYAMA, Y., KIMURA, G., FUJII, N., OMOTO, E.,

HARADA, M. & ORITA, K. 1997. Two acute monocytic leukemia (AML-M5a) cell lines (MOLM-13 and MOLM-14) with interclonal phenotypic heterogeneity showing MLL-AF9 fusion resulting from an occult chromosome insertion, ins(11;9)(q23;p22p23). *Leukemia,* 11**,** 1469-77.

MAVROU, A., BRAKSPEAR, K., HAMDOLLAH-ZADEH, M., DAMODARAN, G., BABAEI-JADIDI, R., OXLEY, J., GILLATT, D. A., LADOMERY, M. R., HARPER, S. J., BATES, D. O. & OLTEAN, S. 2015. Serine-arginine protein kinase 1 (SRPK1) inhibition as a potential novel targeted therapeutic strategy in prostate cancer. *Oncogene,* 34**,** 4311-9.

MEDEIROS, B. C., SATRAM-HOANG, S., HURST, D., HOANG, K. Q., MOMIN, F. & REYES, C. 2015. Big data analysis of treatment patterns and outcomes among elderly acute myeloid leukemia patients in the United States. *Ann Hematol,* 94**,** 1127-38.

MURAKI, M., OHKAWARA, B., HOSOYA, T., ONOGI, H., KOIZUMI, J., KOIZUMI, T., SUMI, K., YOMODA, J., MURRAY, M. V., KIMURA, H., FURUICHI, K., SHIBUYA, H., KRAINER, A. R., SUZUKI, M. & HAGIWARA, M. 2004. Manipulation of alternative splicing by a newly developed inhibitor of Clks. *J Biol Chem,* 279**,** 24246-54.

MURPHY, T. & YEE, K. W. L. 2017. Cytarabine and daunorubicin for the treatment of acute myeloid leukemia. *Expert Opin Pharmacother,* 18**,** 1765-1780.

NARO, C., BIELLI, P. & SETTE, C. 2021. Oncogenic dysregulation of pre-mRNA processing by protein kinases: challenges and therapeutic opportunities. *FEBS J,* 288**,** 6250-6272.

NATELSON, E. A. & PYATT, D. 2010. Temozolomide-induced myelodysplasia. *Adv Hematol,* 2010**,** 760402.

NIKAS, I. P., THEMISTOCLEOUS, S. C., PASCHOU, S. A., TSAMIS, K. I. & RYU, H. S. 2019. Serine-Arginine Protein Kinase 1 (SRPK1) as a Prognostic Factor and Potential Therapeutic Target in Cancer: Current Evidence and Future Perspectives. *Cells,* 9.

O'CONNOR, O. A., WRIGHT, J., MOSKOWITZ, C., MUZZY, J., MACGREGOR-CORTELLI, B., STUBBLEFIELD, M., STRAUS, D., PORTLOCK, C., HAMLIN, P., CHOI, E., DUMETRESCU, O., ESSELTINE, D., TREHU, E., ADAMS, J., SCHENKEIN, D. & ZELENETZ, A. D. 2005. Phase II clinical experience with the novel proteasome inhibitor bortezomib in patients with indolent non-Hodgkin's lymphoma and mantle cell lymphoma. *J Clin Oncol,* 23**,** 676-84.

OBEROI, R. K., PARRISH, K. E., SIO, T. T., MITTAPALLI, R. K., ELMQUIST, W. F. & SARKARIA, J. N. 2016. Strategies to improve delivery of anticancer drugs across the blood-brain barrier to treat glioblastoma. *Neuro Oncol,* 18**,** 27-36.

OHANIAN, M., ROZOVSKI, U., KANAGAL-SHAMANNA, R., ABRUZZO, L. V., LOGHAVI, S., KADIA, T., FUTREAL, A., BHALLA, K., ZUO, Z., HUH, Y. O., POST, S. M., RUVOLO, P., GARCIA-MANERO, G.,

ANDREEFF, M., KORNBLAU, S., BORTHAKUR, G., HU, P., MEDEIROS, L. J., TAKAHASHI, K., HORNBAKER, M. J., ZHANG, J., NOGUERAS-GONZALEZ, G. M., HUANG, X., VERSTOVSEK, S., ESTROV, Z., PIERCE, S., RAVANDI, F., KANTARJIAN, H. M., BUESO-RAMOS, C. E. & CORTES, J. E. 2019. MYC protein expression is an important prognostic factor in acute myeloid leukemia. *Leuk Lymphoma,* 60**,** 37-48.

OSTROM, Q. T., GITTLEMAN, H., LIAO, P., ROUSE, C., CHEN, Y., DOWLING, J., WOLINSKY, Y., KRUCHKO, C. & BARNHOLTZ-SLOAN, J. 2014. CBTRUS statistical report: primary brain and central nervous system tumors diagnosed in the United States in 2007-2011. *Neuro Oncol,* 16 Suppl 4**,** iv1-63.

OWEN, C. J., TOZE, C. L., KOOCHIN, A., FORREST, D. L., SMITH, C. A., STEVENS, J. M., JACKSON, S. C., POON, M. C., SINCLAIR, G. D., LEBER, B., JOHNSON, P. R., MACHETA, A., YIN, J. A., BARNETT, M. J., LISTER, T. A. & FITZGIBBON, J. 2008. Five new pedigrees with inherited RUNX1 mutations causing familial platelet disorder with propensity to myeloid malignancy. *Blood,* 112**,** 4639-45.

PARK, S. Y., PIAO, Y., THOMAS, C., FULLER, G. N. & DE GROOT, J. F. 2016. Cdc2-like kinase 2 is a key regulator of the cell cycle via FOXO3a/p27 in glioblastoma. *Oncotarget,* 7**,** 26793-805.

PERINI, G. F., RIBEIRO, G. N., PINTO NETO, J. V., CAMPOS, L. T. & HAMERSCHLAK, N. 2018. BCL-2 as therapeutic target for hematological malignancies. *J Hematol Oncol,* 11**,** 65.

PLOCINIK, R. M., LI, S., LIU, T., HAILEY, K. L., WHITESIDES, J., MA, C. T., FU, X. D., GOSH, G., WOODS, V. L., JR., JENNINGS, P. A. & ADAMS, J. A. 2011. Regulating SR protein phosphorylation through regions outside the kinase domain of SRPK1. *J Mol Biol,* 410**,** 131-45.

QAZI, S. & UCKUN, F. M. 2010. Gene expression profiles of infant acute lymphoblastic leukaemia and its prognostically distinct subsets. *Br J Haematol,* 149**,** 865-73.

RAMACHANDRAN, P., MORCUS, R., TAHIR, M., ONUKOGU, I., SPINOWITZ, B. & WANG, J. C. 2018. Alectinib (Alecensa)-induced reversible grade IV nephrotoxicity: a case report and review of the literature. *J Med Case Rep,* 12**,** 303.

REARICK, D., PRAKASH, A., MCSWEENY, A., SHEPARD, S. S., FEDOROVA, L. & FEDOROV, A. 2011. Critical association of ncRNA with introns. *Nucleic Acids Res,* 39**,** 2357-66.

ROE, J. S. & VAKOC, C. R. 2016. The Essential Transcriptional Function of BRD4 in Acute Myeloid Leukemia. *Cold Spring Harb Symp Quant Biol,* 81**,** 61-66.

ROLOFF, G. W., ODENIKE, O., BAJEL, A., WEI, A. H., FOLEY, N. & UY, G. L. 2022. Contemporary Approach to Acute Myeloid Leukemia Therapy in 2022. *Am Soc Clin Oncol Educ Book,* 42**,** 1-16.

ROSE, D., HAFERLACH, T., SCHNITTGER, S., PERGLEROVA, K., KERN, W. & HAFERLACH, C. 2017. Subtype-specific patterns of molecular mutations in acute myeloid leukemia. *Leukemia,* 31**,** 11-17.

ROTH, M. B., ZAHLER, A. M. & STOLK, J. A. 1991. A conserved family of nuclear phosphoproteins localized to sites of polymerase II transcription. *J Cell Biol,* 115**,** 587-96.

SALVATORI, B., IOSUE, I., DJODJI DAMAS, N., MANGIAVACCHI, A., CHIARETTI, S., MESSINA, M., PADULA, F., GUARINI, A., BOZZONI, I., FAZI, F. & FATICA, A. 2011. Critical Role of c-Myc in Acute Myeloid Leukemia Involving Direct Regulation of miR-26a and Histone Methyltransferase EZH2. *Genes Cancer,* 2**,** 585-92.

SANIDAS, I., KOTOULA, V., RITOU, E., DAANS, J., LENZ, C., MAIRHOFER, M., DANIILIDOU, M., KOLBUS, A., KRUFT, V., PONSAERTS, P. & NIKOLAKAKI, E. 2010. The ratio of SRPK1/SRPK1a regulates erythroid differentiation in K562 leukaemic cells. *Biochim Biophys Acta,* 1803**,** 1319-31.

SCHNEIDAWIND, C., JEONG, J., SCHNEIDAWIND, D., KIM, I. S., DUQUE-AFONSO, J., WONG, S. H. K., IWASAKI, M., BREESE, E. H., ZEHNDER, J. L., PORTEUS, M. & CLEARY, M. L. 2018. MLL leukemia induction by t(9;11) chromosomal translocation in human hematopoietic stem cells using genome editing. *Blood Adv,* 2**,** 832-845.

SHAO, C., YANG, B., WU, T., HUANG, J., TANG, P., ZHOU, Y., ZHOU, J., QIU, J., JIANG, L., LI, H., CHEN, G., SUN, H., ZHANG, Y., DENISE, A., ZHANG, D. E. & FU, X. D. 2014. Mechanisms for U2AF to define 3' splice sites and regulate alternative splicing in the human genome. *Nat Struct Mol Biol,* 21**,** 997-1005.

SHORT, N. J., KONOPLEVA, M., KADIA, T. M., BORTHAKUR, G., RAVANDI, F., DINARDO, C. D. & DAVER, N. 2020. Advances in the Treatment of Acute Myeloid Leukemia: New Drugs and New Challenges. *Cancer Discov,* 10**,** 506-525.

SIGALA, I., KOUTROUMANI, M., KOUKIALI, A., GIANNAKOUROS, T. & NIKOLAKAKI, E. 2021. Nuclear Translocation of SRPKs Is Associated with 5-FU and Cisplatin Sensitivity in HeLa and T24 Cells. *Cells,* 10.

SIGALA, I., TSAMIS, K. I., GOUSIA, A., ALEXIOU, G., VOULGARIS, S., GIANNAKOUROS, T., KYRITSIS, A. P. & NIKOLAKAKI, E. 2016. Expression of SRPK1 in gliomas and its role in glioma cell lines viability. *Tumour Biol,* 37**,** 8699-707.

SIQUEIRA, R. P., CAETANO, M. M. M., DE SOUZA, L. A., DOS PASSOS, P. M. S., SIMAROLI, N. B., BARROS, M. V. A., DE SOUZA, A. P. M., DE OLIVEIRA, L. L., SILVA-JUNIOR, A., FIETTO, J. L. R., TEIXEIRA, R. R., TEIXEIRA, F. R. & BRESSAN, G. C. 2020. Combined SRPK and AKT pharmacological inhibition is synergistic in T-cell acute lymphoblastic leukemia cells. *Toxicol In Vitro,* 65**,** 104777.

SLACK, J. L. & YU, M. 1998. Constitutive expression of the promyelocytic leukemia-associated oncogene PML-RARalpha in TF1 cells: isoform-

specific and retinoic acid-dependent effects on growth, bcl-2 expression, and apoptosis. *Blood,* 91**,** 3347-56.

SONODA, Y., ITOH, M. & TOHDA, S. 2021. Effects of HOXA9 Inhibitor DB818 on the Growth of Acute Myeloid Leukaemia Cells. *Anticancer Res,* 41**,** 1841-1847.

STUPP, R., HEGI, M. E., MASON, W. P., VAN DEN BENT, M. J., TAPHOORN, M. J., JANZER, R. C., LUDWIN, S. K., ALLGEIER, A., FISHER, B., BELANGER, K., HAU, P., BRANDES, A. A., GIJTENBEEK, J., MAROSI, C., VECHT, C. J., MOKHTARI, K., WESSELING, P., VILLA, S., EISENHAUER, E., GORLIA, T., WELLER, M., LACOMBE, D., CAIRNCROSS, J. G., MIRIMANOFF, R. O., EUROPEAN ORGANISATION FOR, R., TREATMENT OF CANCER BRAIN, T., RADIATION ONCOLOGY, G. & NATIONAL CANCER INSTITUTE OF CANADA CLINICAL TRIALS, G. 2009. Effects of radiotherapy with concomitant and adjuvant temozolomide versus radiotherapy alone on survival in glioblastoma in a randomised phase III study: 5-year analysis of the EORTC-NCIC trial. *Lancet Oncol,* 10**,** 459-66.

SUN, H. & CHASIN, L. A. 2000. Multiple splicing defects in an intronic false exon. *Mol Cell Biol,* 20**,** 6414-25.

SUTHERLAND, H., BLAIR, A., VERCAUTEREN, S. & ZAPF, R. 2001. Detection and clinical significance of human acute myeloid leukaemia progenitors capable of long-term proliferation in vitro. *Br J Haematol,* 114**,** 296-306.

SVEEN, A., KILPINEN, S., RUUSULEHTO, A., LOTHE, R. A. & SKOTHEIM, R. I. 2016. Aberrant RNA splicing in cancer; expression changes and driver mutations of splicing factor genes. *Oncogene,* 35**,** 2413-27.

TAZI, J., BAKKOUR, N. & STAMM, S. 2009. Alternative splicing and disease. *Biochim Biophys Acta,* 1792**,** 14-26.

TWYFFELS, L., GUEYDAN, C. & KRUYS, V. 2011. Shuttling SR proteins: more than splicing factors. *FEBS J,* 278**,** 3246-55.

TZELEPIS, K., DE BRAEKELEER, E., ASPRIS, D., BARBIERI, I., VIJAYABASKAR, M. S., LIU, W. H., GOZDECKA, M., METZAKOPIAN, E., TOOP, H. D., DUDEK, M., ROBSON, S. C., HERMIDA-PRADO, F., YANG, Y. H., BABAEI-JADIDI, R., GARYFALLOS, D. A., PONSTINGL, H., DIAS, J. M. L., GALLIPOLI, P., SEILER, M., BUONAMICI, S., VICK, B., BANNISTER, A. J., RAD, R., PRINJHA, R. K., MARIONI, J. C., HUNTLY, B., BATSON, J., MORRIS, J. C., PINA, C., BRADLEY, A., JEREMIAS, I., BATES, D. O., YUSA, K., KOUZARIDES, T. & VASSILIOU, G. S. 2018. SRPK1 maintains acute myeloid leukemia through effects on isoform usage of epigenetic regulators including BRD4. *Nat Commun,* 9**,** 5378.

TZELEPIS, K., KOIKE-YUSA, H., DE BRAEKELEER, E., LI, Y., METZAKOPIAN, E., DOVEY, O. M., MUPO, A., GRINKEVICH, V., LI, M., MAZAN, M., GOZDECKA, M., OHNISHI, S., COOPER, J., PATEL, M., MCKERRELL, T., CHEN, B., DOMINGUES, A. F., GALLIPOLI, P.,

TEICHMANN, S., PONSTINGL, H., MCDERMOTT, U., SAEZ-RODRIGUEZ, J., HUNTLY, B. J. P., IORIO, F., PINA, C., VASSILIOU, G. S. & YUSA, K. 2016. A CRISPR Dropout Screen Identifies Genetic Vulnerabilities and Therapeutic Targets in Acute Myeloid Leukemia. *Cell Rep,* 17**,** 1193-1205.

UPPAL, S., GEGONNE, A., CHEN, Q., THOMPSON, P. S., CHENG, D., MU, J., MEERZAMAN, D., MISRA, H. S. & SINGER, D. S. 2019. The Bromodomain Protein 4 Contributes to the Regulation of Alternative Splicing. *Cell Rep,* 29**,** 2450-2460 e5.

UZOR, S., ZORZOU, P., BOWLER, E., PORAZINSKI, S., WILSON, I. & LADOMERY, M. 2018. Autoregulation of the human splice factor kinase CLK1 through exon skipping and intron retention. *Gene,* 670**,** 46-54.

VAN DELFT, F. W., HORSLEY, S., COLMAN, S., ANDERSON, K., BATEMAN, C., KEMPSKI, H., ZUNA, J., ECKERT, C., SAHA, V., KEARNEY, L., FORD, A. & GREAVES, M. 2011. Clonal origins of relapse in ETV6-RUNX1 acute lymphoblastic leukemia. *Blood,* 117**,** 6247-54.

VAN ROOSMALEN, W., LE DEVEDEC, S. E., GOLANI, O., SMID, M., PULYAKHINA, I., TIMMERMANS, A. M., LOOK, M. P., ZI, D., PONT, C., DE GRAAUW, M., NAFFAR-ABU-AMARA, S., KIRSANOVA, C., RUSTICI, G., HOEN, P. A., MARTENS, J. W., FOEKENS, J. A., GEIGER, B. & VAN DE WATER, B. 2015. Tumor cell migration screen identifies SRPK1 as breast cancer metastasis determinant. *J Clin Invest,* 125**,** 1648-64.

VENABLES, J. P. 2004. Aberrant and alternative splicing in cancer. *Cancer Res,* 64**,** 7647-54.

WANG, C., ZHOU, Z., SUBHRAMANYAM, C. S., CAO, Q., HENG, Z. S. L., LIU, W., FU, X. & HU, Q. 2020. SRPK1 acetylation modulates alternative splicing to regulate cisplatin resistance in breast cancer cells. *Commun Biol,* 3**,** 268.

WANG, D., WANG, C., WANG, L. & CHEN, Y. 2019. A comprehensive review in improving delivery of small-molecule chemotherapeutic agents overcoming the blood-brain/brain tumor barriers for glioblastoma treatment. *Drug Deliv,* 26**,** 551-565.

WANG, E., PINEDA, J. M. B., KIM, W. J., CHEN, S., BOURCIER, J., STAHL, M., HOGG, S. J., BEWERSDORF, J. P., HAN, C., SINGER, M. E., CUI, D., ERICKSON, C. E., TITTLEY, S. M., PENSON, A. V., KNORR, K., STANLEY, R. F., RAHMAN, J., KRISHNAMOORTHY, G., FAGIN, J. A., CREGER, E., MCMILLAN, E., MAK, C. C., JARVIS, M., BOSSARD, C., BEAUPRE, D. M., BRADLEY, R. K. & ABDEL-WAHAB, O. 2022. Modulation of RNA splicing enhances response to BCL2 inhibition in leukemia. *Cancer Cell*.

WANG, H. Y., ARDEN, K. C., BERMINGHAM, J. R., JR., VIARS, C. S., LIN, W., BOYER, A. D. & FU, X. D. 1999. Localization of serine kinases, SRPK1 (SFRSK1) and SRPK2 (SFRSK2), specific for the SR family of

splicing factors in mouse and human chromosomes. *Genomics,* 57**,** 310-5.

WANG, H. Y., LIN, W., DYCK, J. A., YEAKLEY, J. M., SONGYANG, Z., CANTLEY, L. C. & FU, X. D. 1998. SRPK2: a differentially expressed SR protein-specific kinase involved in mediating the interaction and localization of pre-mRNA splicing factors in mammalian cells. *J Cell Biol,* 140**,** 737-50.

WANG, J., TAKAGAKI, Y. & MANLEY, J. L. 1996. Targeted disruption of an essential vertebrate gene: ASF/SF2 is required for cell viability. *Genes Dev,* 10**,** 2588-99.

WANG, P., ZHOU, Z., HU, A., PONTE DE ALBUQUERQUE, C., ZHOU, Y., HONG, L., SIERECKI, E., AJIRO, M., KRUHLAK, M., HARRIS, C., GUAN, K. L., ZHENG, Z. M., NEWTON, A. C., SUN, P., ZHOU, H. & FU, X. D. 2014. Both decreased and increased SRPK1 levels promote cancer by interfering with PHLPP-mediated dephosphorylation of Akt. *Mol Cell,* 54**,** 378-91.

WEI, A. H., STRICKLAND, S. A., JR., HOU, J. Z., FIEDLER, W., LIN, T. L., WALTER, R. B., ENJETI, A., TIONG, I. S., SAVONA, M., LEE, S., CHYLA, B., POPOVIC, R., SALEM, A. H., AGARWAL, S., XU, T., FAKOUHI, K. M., HUMERICKHOUSE, R., HONG, W. J., HAYSLIP, J. & ROBOZ, G. J. 2019. Venetoclax Combined With Low-Dose Cytarabine for Previously Untreated Patients With Acute Myeloid Leukemia: Results From a Phase Ib/II Study. *J Clin Oncol,* 37**,** 1277-1284.

WORTEL, I. M. N., VAN DER MEER, L. T., KILBERG, M. S. & VAN LEEUWEN, F. N. 2017. Surviving Stress: Modulation of ATF4-Mediated Stress Responses in Normal and Malignant Cells. *Trends Endocrinol Metab,* 28**,** 794-806.

WU, Q., CHANG, Y., ZHANG, L., ZHANG, Y., TIAN, T., FENG, G., ZHOU, S., ZHENG, Q., HAN, F. & HUANG, F. 2013. SRPK1 Dissimilarly Impacts on the Growth, Metastasis, Chemosensitivity and Angiogenesis of Glioma in Normoxic and Hypoxic Conditions. *J Cancer,* 4**,** 727-35.

WU, Q., LV, T., CHEN, Y., WEN, L., ZHANG, J., JIANG, X. & LIU, F. 2015. Apoptosis of HL-60 human leukemia cells induced by Asiatic acid through modulation of B-cell lymphoma 2 family proteins and the mitogen-activated protein kinase signaling pathway. *Mol Med Rep,* 12**,** 1429-34.

WU, S., EDWARDS, H., WANG, D., LIU, S., QIAO, X., CARTER, J., WANG, Y., TAUB, J. W., WANG, G. & GE, Y. 2022. Inhibition of Mcl-1 Synergistically Enhances the Antileukemic Activity of Gilteritinib and MRX-2843 in Preclinical Models of FLT3-Mutated Acute Myeloid Leukemia. *Cells,* 11.

WU, S. Y., LEE, C. F., LAI, H. T., YU, C. T., LEE, J. E., ZUO, H., TSAI, S. Y., TSAI, M. J., GE, K., WAN, Y. & CHIANG, C. M. 2020. Opposing Functions of BRD4 Isoforms in Breast Cancer. *Mol Cell,* 78**,** 1114-1132 e10.

XU, X. & FU, X. D. 2005. Conditional knockout mice to study alternative splicing in vivo. *Methods,* 37**,** 387-92.

YANG, H., WEI, L., XUN, Y., YANG, A. & YOU, H. 2021. BRD4: An emerging prospective therapeutic target in glioma. *Mol Ther Oncolytics,* 21**,** 1-14.

YANG, X., SMITH, J. L., BECK, M. T., WILKINSON, J. M., MICHAUD, A., VASTA, J. D., ROBERS, M. B. & WILLSON, T. M. 2023. Development of Cell Permeable NanoBRET Probes for the Measurement of PLK1 Target Engagement in Live Cells. *Molecules,* 28.

YUN, S., SHARMA, R., CHAN, O., VINCELETTE, N. D., SALLMAN, D. A., SWEET, K., PADRON, E., KOMROKJI, R., LANCET, J. E., ABRAHAM, I., MOSCINSKI, L. C., CLEVELAND, J. L., LIST, A. F. & ZHANG, L. 2019. Prognostic significance of MYC oncoprotein expression on survival outcome in patients with acute myeloid leukemia with myelodysplasia related changes (AML-MRC). *Leuk Res,* 84**,** 106194.

ZHANG, H., ZHANG, Y., ZHOU, X., WRIGHT, S., HYLE, J., ZHAO, L., AN, J., ZHAO, X., SHAO, Y., XU, B., LEE, H. M., CHEN, T., ZHOU, Y., CHEN, X., LU, R. & LI, C. 2020. Functional interrogation of HOXA9 regulome in MLLr leukemia via reporter-based CRISPR/Cas9 screen. *Elife,* 9.

ZHANG, L., YANG, H., ZHANG, W., LIANG, Z., HUANG, Q., XU, G., ZHEN, X. & ZHENG, L. T. 2017. Clk1-regulated aerobic glycolysis is involved in glioma chemoresistance. *J Neurochem,* 142**,** 574-588.

ZHANG, Q., RILEY-GILLIS, B., HAN, L., JIA, Y., LODI, A., ZHANG, H., GANESAN, S., PAN, R., KONOPLEV, S. N., SWEENEY, S. R., RYAN, J. A., JITKOVA, Y., DUNNER, K., JR., GROSSKURTH, S. E., VIJAY, P., GHOSH, S., LU, C., MA, W., KURTZ, S., RUVOLO, V. R., MA, H., WENG, C. C., RAMAGE, C. L., BARAN, N., SHI, C., CAI, T., DAVIS, R. E., BATTULA, V. L., MI, Y., WANG, J., DINARDO, C. D., ANDREEFF, M., TYNER, J. W., SCHIMMER, A., LETAI, A., PADUA, R. A., BUESO-RAMOS, C. E., TIZIANI, S., LEVERSON, J., POPOVIC, R. & KONOPLEVA, M. 2022. Activation of RAS/MAPK pathway confers MCL-1 mediated acquired resistance to BCL-2 inhibitor venetoclax in acute myeloid leukemia. *Signal Transduct Target Ther,* 7**,** 51.

ZHANG, Y., SLOAN, S. A., CLARKE, L. E., CANEDA, C., PLAZA, C. A., BLUMENTHAL, P. D., VOGEL, H., STEINBERG, G. K., EDWARDS, M. S., LI, G., DUNCAN, J. A., 3RD, CHESHIER, S. H., SHUER, L. M., CHANG, E. F., GRANT, G. A., GEPHART, M. G. & BARRES, B. A. 2016. Purification and Characterization of Progenitor and Mature Human Astrocytes Reveals Transcriptional and Functional Differences with Mouse. *Neuron,* 89**,** 37-53.

ZHONG, X. Y., DING, J. H., ADAMS, J. A., GHOSH, G. & FU, X. D. 2009. Regulation of SR protein phosphorylation and alternative splicing by modulating kinetic interactions of SRPK1 with molecular chaperones. *Genes Dev,* 23**,** 482-95.

ZHOU, B., LI, Y., DENG, Q., WANG, H., WANG, Y., CAI, B. & HAN, Z. G. 2013. SRPK1 contributes to malignancy of hepatocellular carcinoma through a possible mechanism involving PI3K/Akt. *Mol Cell Biochem,* 379**,** 191-9.

ZHOU, C., KIM, S. W., REUNGWETWATTANA, T., ZHOU, J., ZHANG, Y., HE, J., YANG, J. J., CHENG, Y., LEE, S. H., BU, L., XU, T., YANG, L., WANG, C., LIU, T., MORCOS, P. N., LU, Y. & ZHANG, L. 2019a. Alectinib versus crizotinib in untreated Asian patients with anaplastic lymphoma kinase-positive non-small-cell lung cancer (ALESIA): a randomised phase 3 study. *Lancet Respir Med,* 7**,** 437-446.

ZHOU, J., GAO, G., HOU, P., LI, C. M. & GUO, D. 2017a. Regulation of the Alternative Splicing and Function of Cyclin T1 by the Serine-Arginine-Rich Protein ASF/SF2. *J Cell Biochem,* 118**,** 4020-4032.

ZHOU, Q., PHOA, A. F., ABBASSI, R. H., HOQUE, M., REEKIE, T. A., FONT, J. S., RYAN, R. M., STRINGER, B. W., DAY, B. W., JOHNS, T. G., MUNOZ, L. & KASSIOU, M. 2017b. Structural Optimization and Pharmacological Evaluation of Inhibitors Targeting Dual-Specificity Tyrosine Phosphorylation-Regulated Kinases (DYRK) and CDC-like kinases (CLK) in Glioblastoma. *J Med Chem,* 60**,** 2052-2070.

ZHOU, Y., GU, Y. & LIU, J. 2019b. BRD4 suppression alleviates cerebral ischemia-induced brain injury by blocking glial activation via the inhibition of inflammatory response and pyroptosis. *Biochem Biophys Res Commun,* 519**,** 481-488.

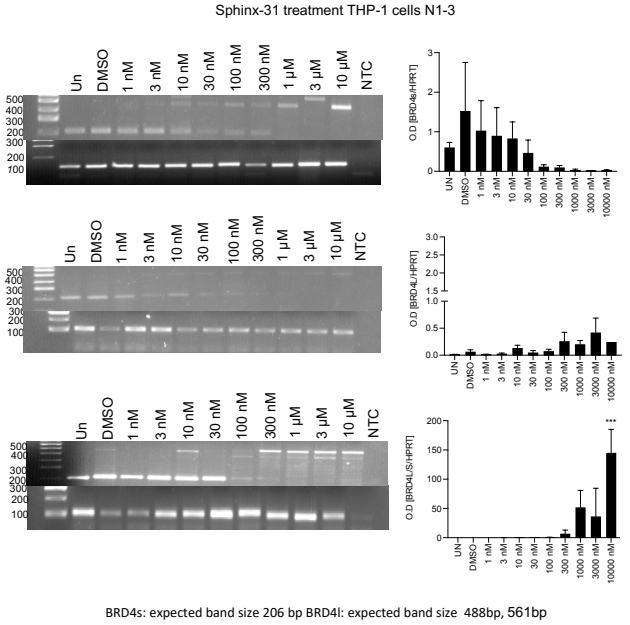
ZHOU, Y., ZHOU, J., LU, X., TAN, T. Z. & CHNG, W. J. 2018. BET Bromodomain inhibition promotes De-repression of TXNIP and activation of ASK1-MAPK pathway in acute myeloid leukemia. *BMC Cancer,* 18**,** 731.

ZHOU, Y. E., O'ROURKE, J. P., EDWARDS, J. S. & NESS, S. A. 2011. Single molecule analysis of c-myb alternative splicing reveals novel classifiers for precursor B-ALL. *PLoS One,* 6**,** e22880.

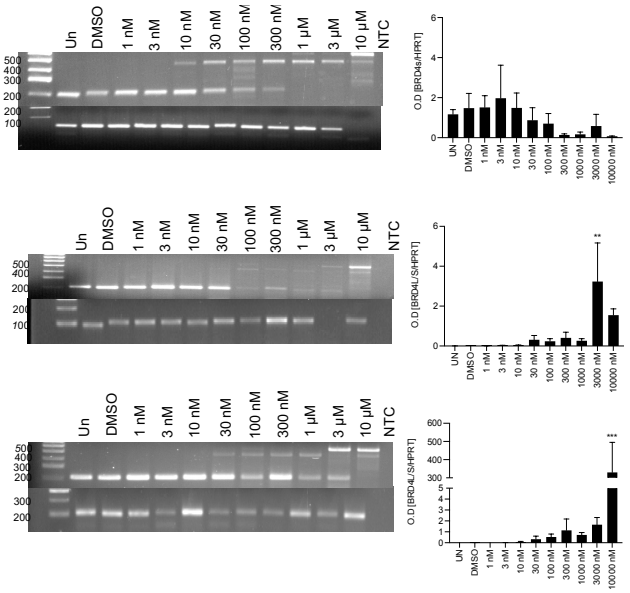
ZUBER, J., SHI, J., WANG, E., RAPPAPORT, A. R., HERRMANN, H., SISON, E. A., MAGOON, D., QI, J., BLATT, K., WUNDERLICH, M., TAYLOR, M. J., JOHNS, C., CHICAS, A., MULLOY, J. C., KOGAN, S. C., BROWN, P., VALENT, P., BRADNER, J. E., LOWE, S. W. & VAKOC, C. R. 2011. RNAi screen identifies Brd4 as a therapeutic target in acute myeloid leukaemia. *Nature,* 478**,** 524-8.

# 12. APPENDIX I.

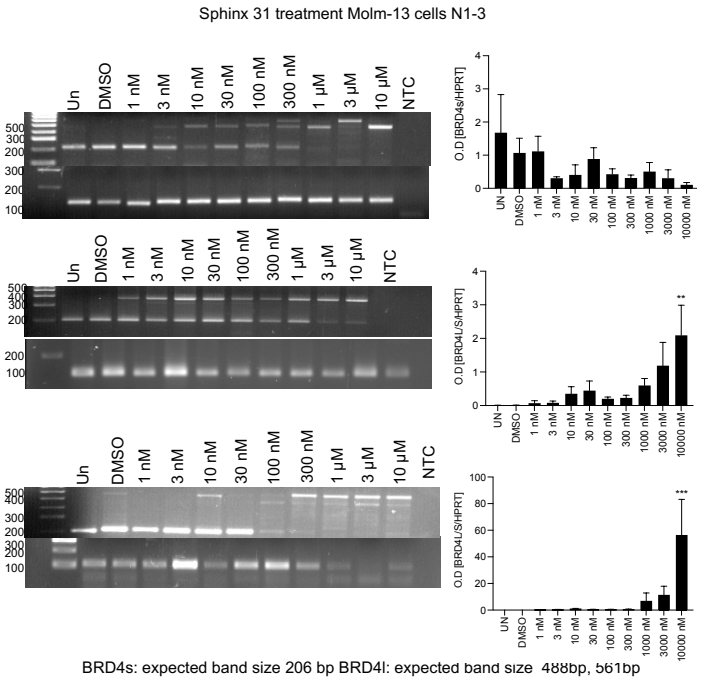
## 12.1. RT-PCR results of BRD4 splice change in response to inhibitor treatment



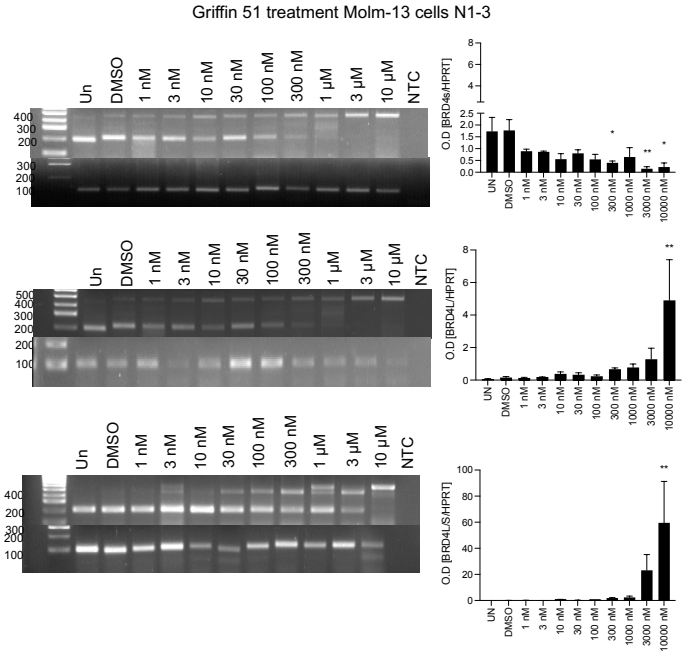

Supplementary figure of SPHINX-31 treatment on THP-1 cells. Expression of BRD4s, BRD4l and HPRT-1 in THP-1 cell line was determined by RT-PCR and visualized on a 2% gel by agarose gel electrophoresis. The expected band sizes were, BRD4s 206 bp and BRD4l: 488 bp, HPRT-1: 101 bp. The optical density was measured using Image Studio.



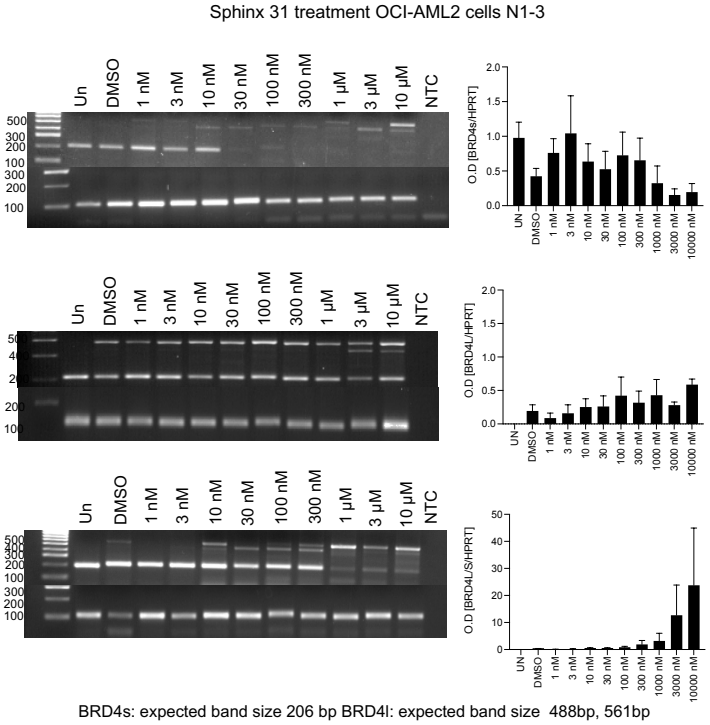

Supplementary figure of Griffin 51 treatment on THP-1 cells. Expression of BRD4s, BRD4l and HPRT-1 in THP-1 cell line was determined by RT-PCR and visualized on a 2% gel by agarose gel electrophoresis. The expected band sizes were, BRD4s 206 bp and BRD4l: 488 bp, HPRT-1: 101 bp. The optical density was measured using Image Studio.



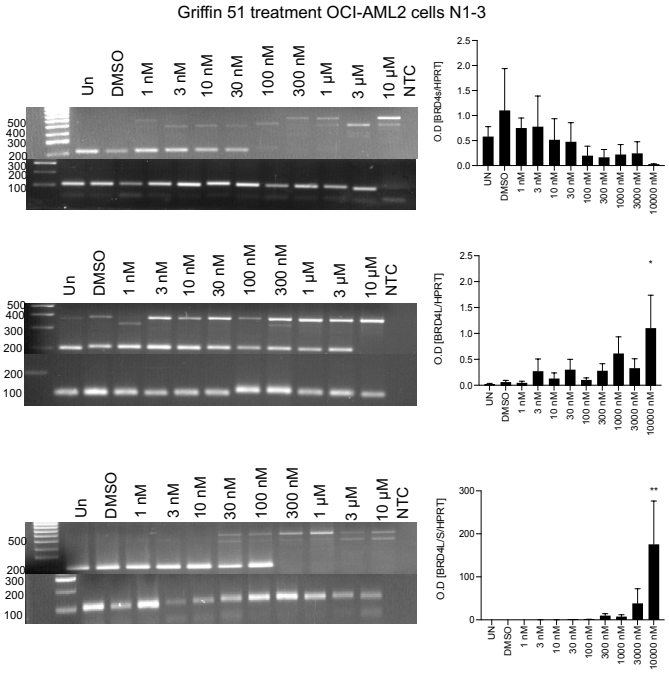

Supplementary figure of SPHINX-31 treatment on MOLM-13 cells. Expression of BRD4s, BRD4l and HPRT-1 in MOLM-13 cell line was determined by RT-PCR and visualized on a 2% gel by agarose gel electrophoresis. The expected band sizes were, BRD4s 206 bp and BRD4l: 488 bp, HPRT-1: 101 bp. The optical density was measured using Image Studio.



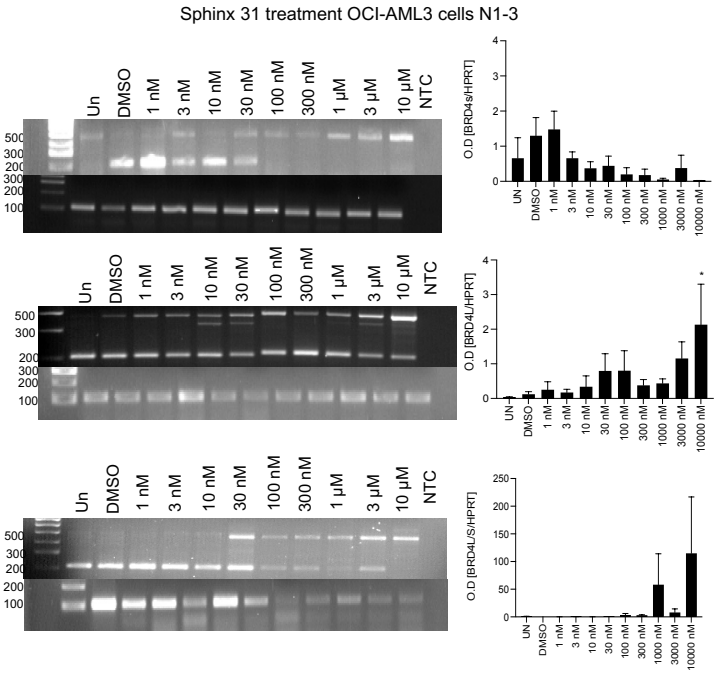

Supplementary figure of Griffin 51 treatment on MOLM-13 cells. Expression of BRD4s, BRD4l and HPRT-1 in MOLM-13 cell line was determined by RT-PCR and visualized on a 2% gel by agarose gel electrophoresis. The expected band sizes were, BRD4s 206 bp and BRD4l: 488 bp, HPRT-1: 101 bp. The optical density was measured using Image Studio.




Supplementary figure of SPHINX-31 treatment on OCI-AML2 cells. Expression of BRD4s, BRD4l and HPRT-1 in OCI-AML2 cell line was determined by RT-PCR and visualized on a 2% gel by agarose gel electrophoresis. The expected band sizes were, BRD4s 206 bp and BRD4l: 488 bp, HPRT-1: 101 bp. The optical density was measured using Image Studio.

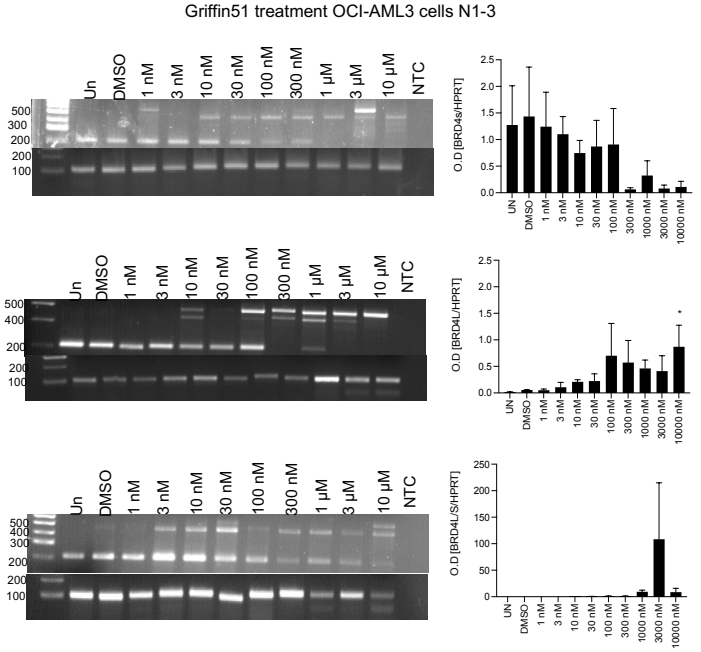



Supplementary figure of Griffin 51 treatment on OCI-AML2 cells. Expression of BRD4s, BRD4l and HPRT-1 in OCI-AML2 cell line was determined by RT-PCR and visualized on a 2% gel by agarose gel electrophoresis. The expected band sizes were, BRD4s 206 bp and BRD4l: 488 bp, HPRT-1: 101 bp. The optical density was measured using Image Studio.

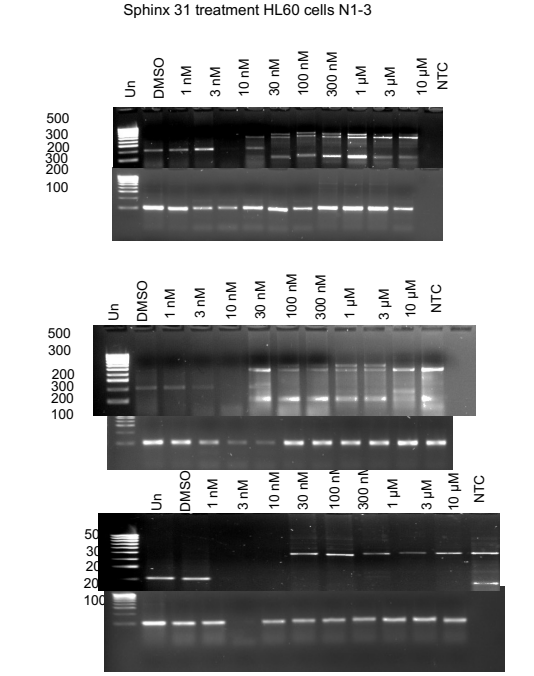



BRD4s: expected band size 206 bp BRD4l: expected band size 488bp, 561bp

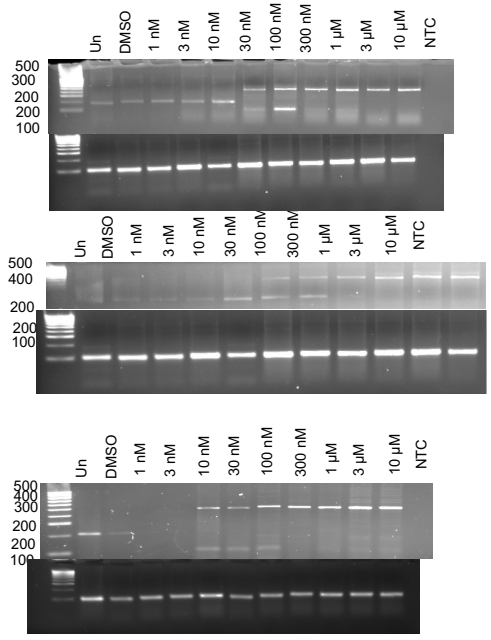
Supplementary figure of SPHINX-31 treatment on OCI-AML3 cells. Expression of BRD4s, BRD4l and HPRT-1 in OCI-AML3 cell line was determined by RT-PCR and visualized on a 2% gel by agarose gel electrophoresis. The expected band sizes were, BRD4s 206 bp and BRD4l: 488 bp, HPRT-1: 101 bp. The optical density was measured using Image Studio.



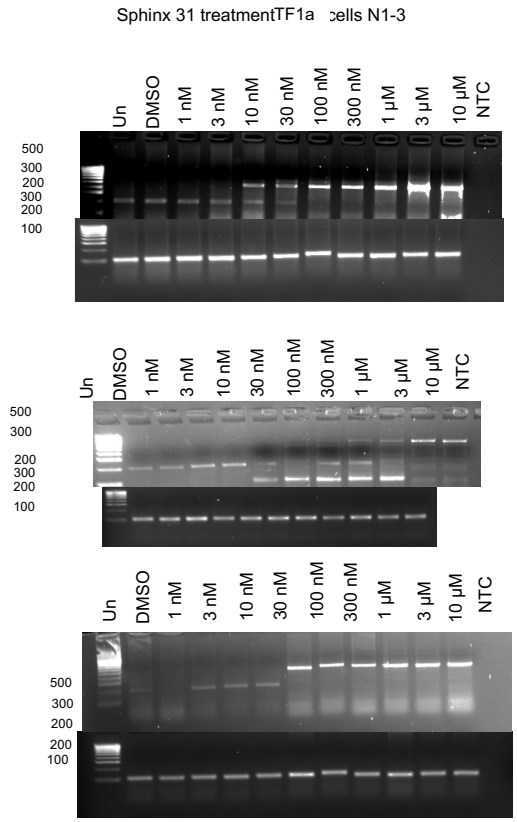

Supplementary figure of Griffin 51 treatment on OCI-AML3 cells. Expression of BRD4s, BRD4l and HPRT-1 in OCI-AML3 cell line was determined by RT-PCR and visualized on a 2% gel by agarose gel electrophoresis. The expected band sizes were, BRD4s 206 bp and BRD4l: 488 bp, HPRT-1: 101 bp. The optical density was measured using Image Studio.



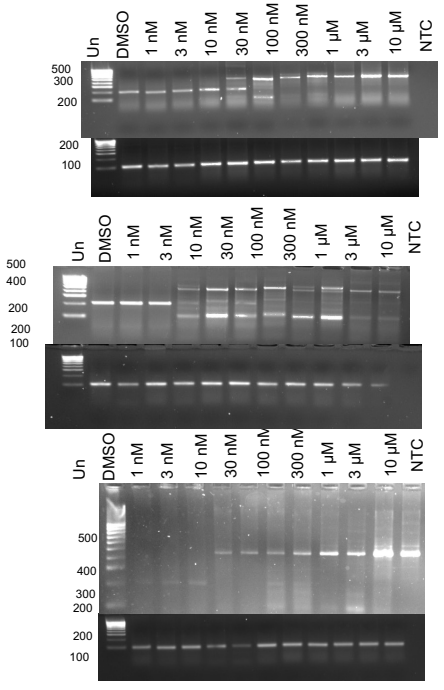

Supplementary figure of SPHINX-31 treatment on HL60 cells. Expression of BRD4s, BRD4l and HPRT-1 in HL60 cell line was determined by RT-PCR and visualized on a 2% gel by agarose gel electrophoresis. The expected band sizes were, BRD4s 206 bp and BRD4l: 488 bp, HPRT-1: 101 bp. The optical density was measured using Image Studio.




Supplementary figure of Griffin 51 treatment on HL60 cells. Expression of BRD4s, BRD4l and HPRT-1 in HL60 cell line was determined by RT-PCR and visualized on a 2% gel by agarose gel electrophoresis. The expected band sizes were, BRD4s 206 bp and BRD4l: 488 bp, HPRT-1: 101 bp. The optical density was measured using Image Studio.

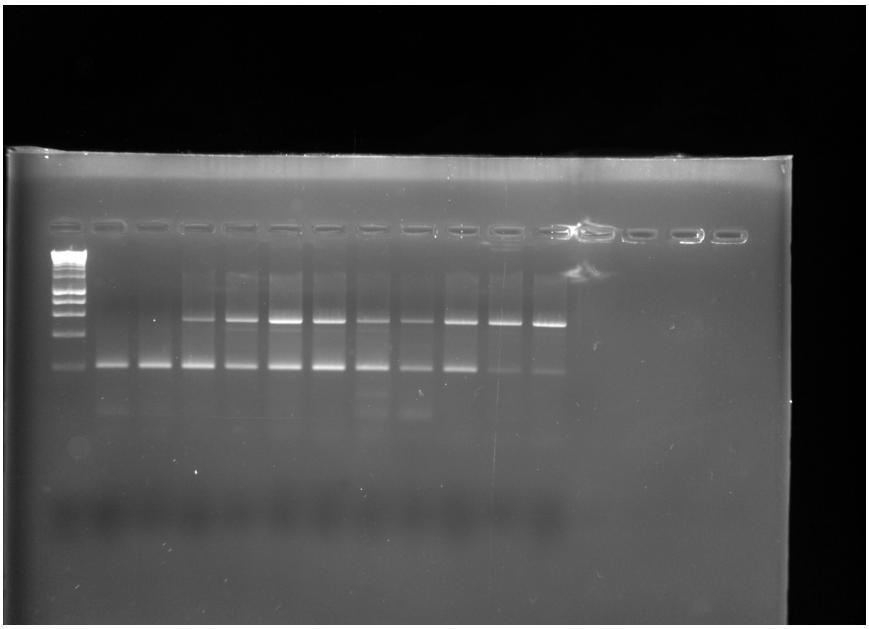



Supplementary figure of SPHINX-31 treatment on TF1a cells. Expression of BRD4s, BRD4l and HPRT-1 in TF1a cell line was determined by RT-PCR and visualized on a 2% gel by agarose gel electrophoresis. The expected band sizes were, BRD4s 206 bp and BRD4l: 488 bp, HPRT-1: 101 bp. The optical density was measured using Image Studio.

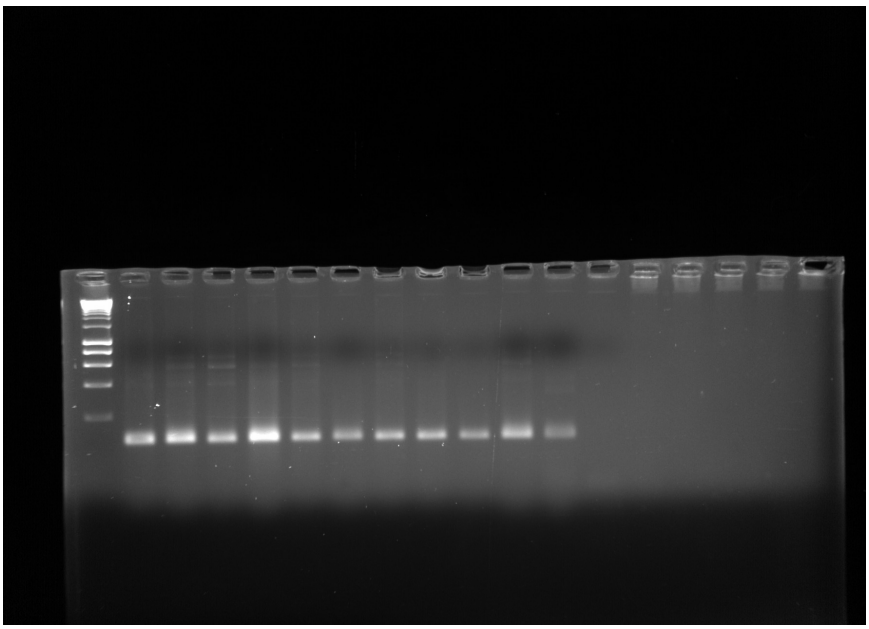



Supplementary figure of Griffin 51 treatment on TF1a cells. Expression of BRD4s, BRD4l and HPRT-1 in TF1a cell line was determined by RT-PCR and visualized on a 2% gel by agarose gel electrophoresis. The expected band sizes were, BRD4s 206 bp and BRD4l: 488 bp, HPRT-1: 101 bp. The optical density was measured using Image Studio.

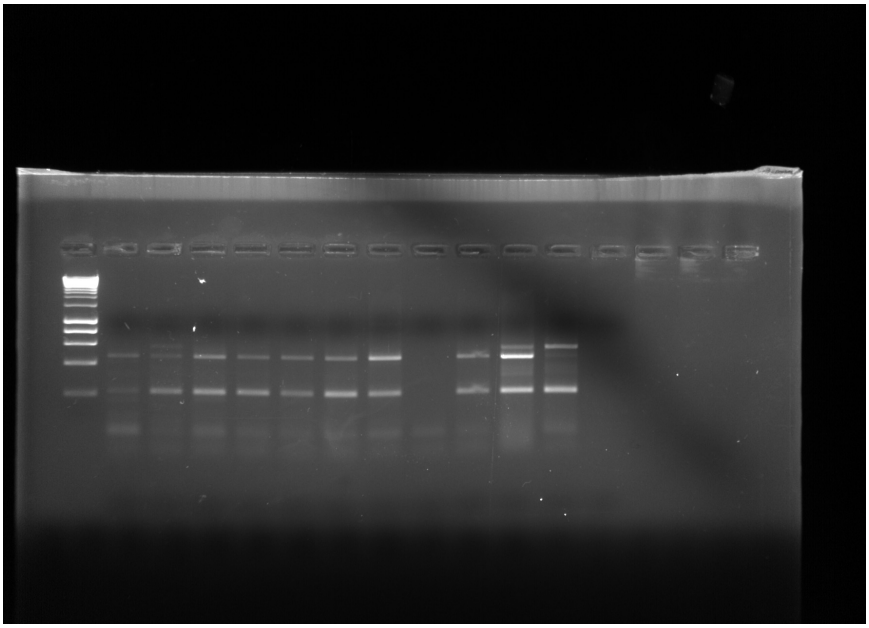
## 12.2. Full size gel images with BRD4 splice change



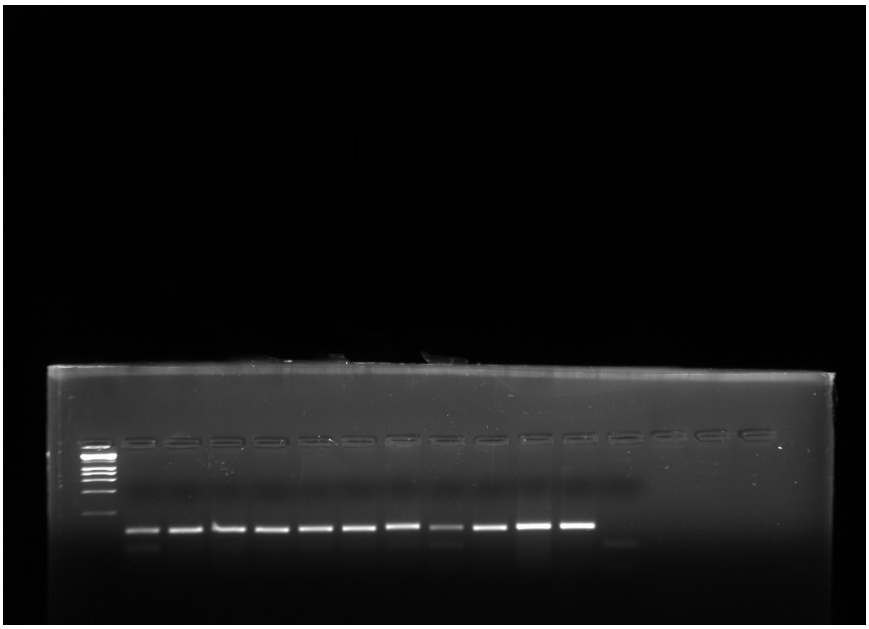
Representative example of an agarose gel showing the BRD4s and BRD4l expression levels in MOLM-13 cells after SPHINX-31 treatment. Determined by by RT-PCR and visualized on a 2% gel by agarose gel electrophoresis. The expected band sizes were, BRD4s 206 bp and BRD4l: 488 bp, HPRT-1: 101 bp. The optical density was measured using Image Studio.



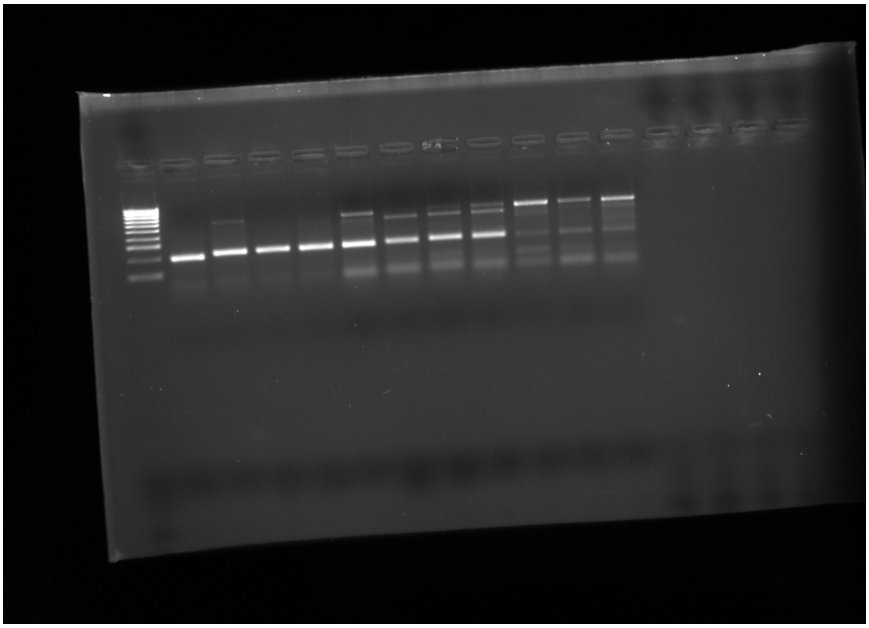
Representative example of an agarose gel showing the HPRT-1 expression levels in MOLM-13 cells after SPHINX-31 treatment. Determined by by RT-PCR and visualized on a 2% gel by agarose gel electrophoresis. The expected band sizes were, BRD4s 206 bp and BRD4l: 488 bp, HPRT-1: 101 bp. The optical density was measured using Image Studio.



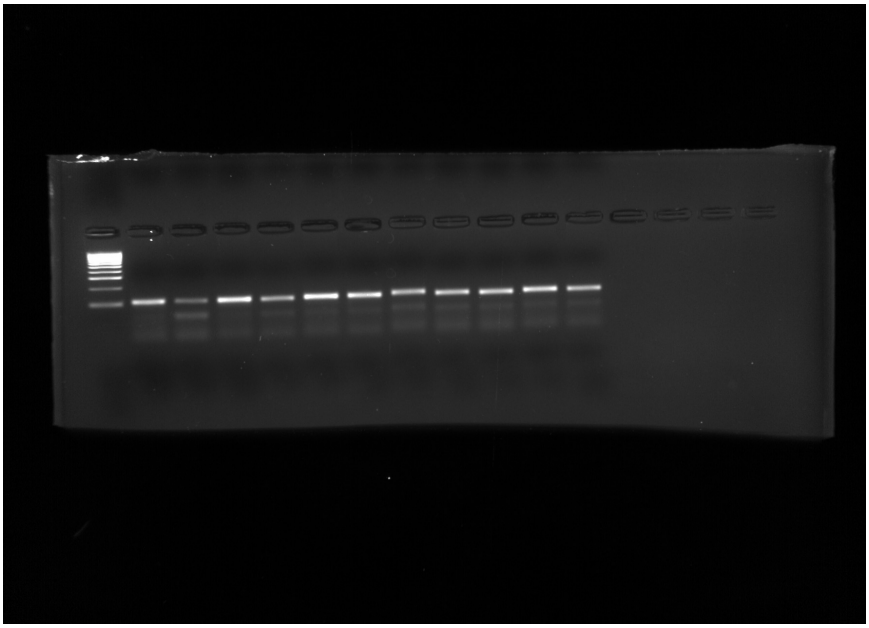
Representative example of an agarose gel showing the BRD4s and BRD4l expression levels in THP-1 cells after SPHINX-31 treatment. Determined by by RT-PCR and visualized on a 2% gel by agarose gel electrophoresis. The expected band sizes were, BRD4s 206 bp and BRD4l: 488 bp, HPRT-1: 101 bp. The optical density was measured using Image Studio.



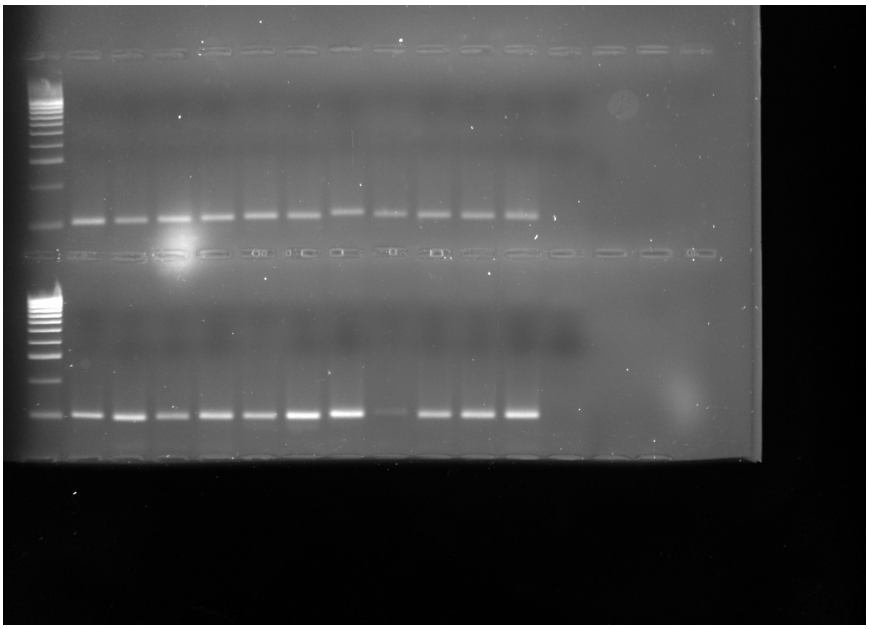
Representative example of an agarose gel showing the HPRT-1 expression levels in THP-1 cells after SPHINX-31 treatment. Determined by by RT-PCR and visualized on a 2% gel by agarose gel electrophoresis. The expected band sizes were, BRD4s 206 bp and BRD4l: 488 bp, HPRT-1: 101 bp. The optical density was measured using Image Studio.



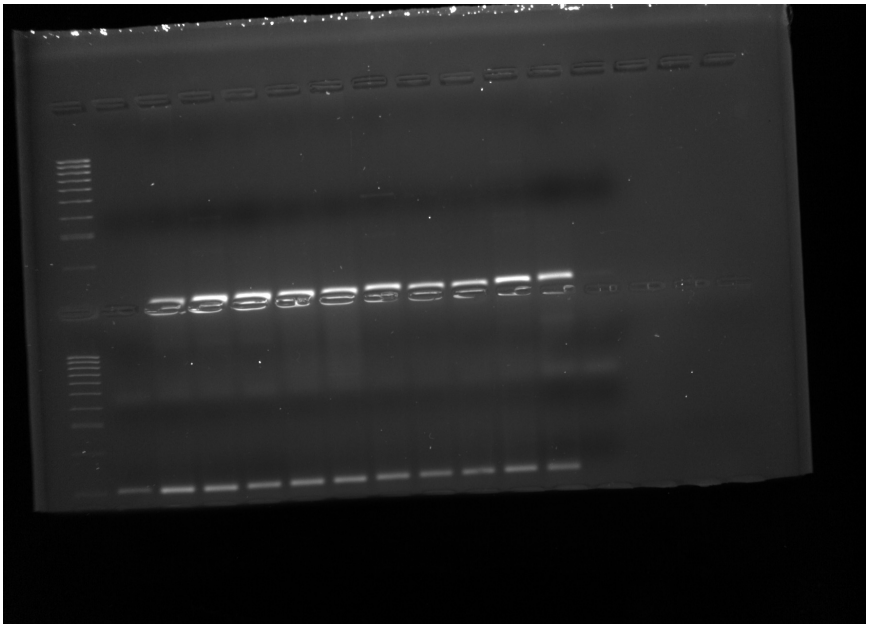
Representative example of an agarose gel showing the BRD4s and BRD4l expression levels in OCI-AML2 cells after SPHINX-31 treatment. Determined by by RT-PCR and visualized on a 2% gel by agarose gel electrophoresis. The expected band sizes were, BRD4s 206 bp and BRD4l: 488 bp, HPRT-1: 101 bp. The optical density was measured using Image Studio.



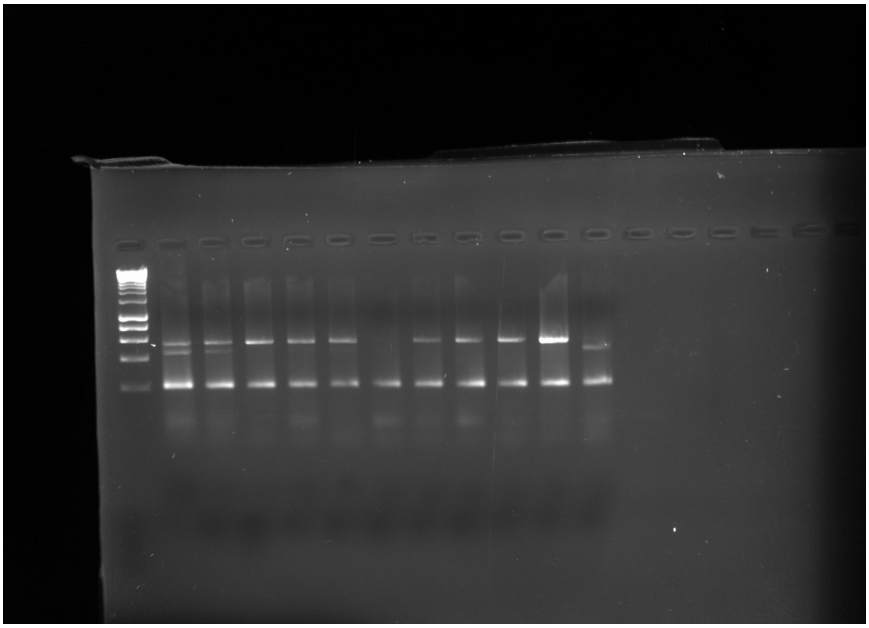
Representative example of an agarose gel showing the HPRT-1 expression levels in OCI-AML2 cells after SPHINX-31 treatment. Determined by by RT-PCR and visualized on a 2% gel by agarose gel electrophoresis. The expected band sizes were, BRD4s 206 bp and BRD4l: 488 bp, HPRT-1: 101 bp. The optical density was measured using Image Studio.



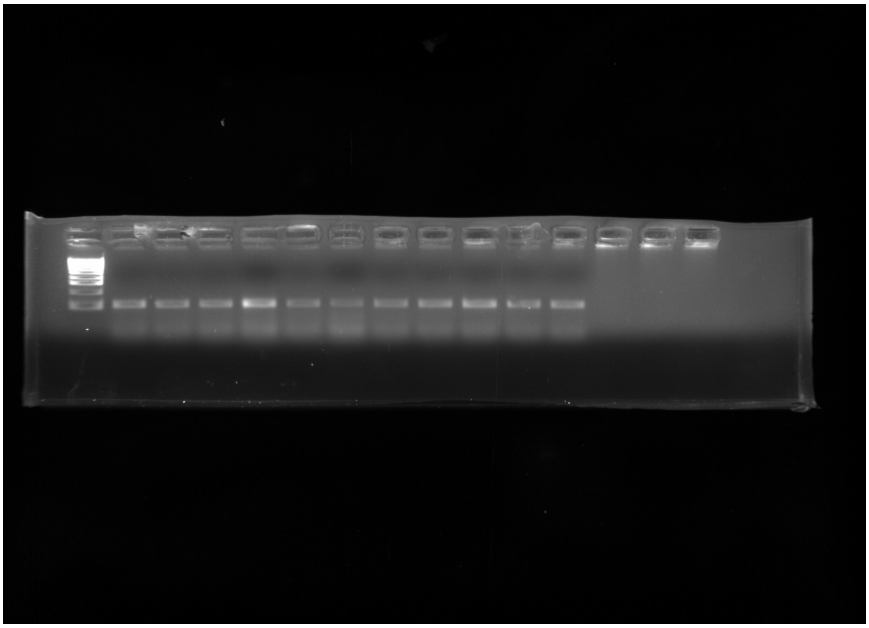
Representative example of an agarose gel showing the HPRT-1 expression levels in TF1a cells after SPHINX-31 treatment (Top) and Griffin 51 treatment (Bottom). Determined by by RT-PCR and visualized on a 2% gel by agarose gel electrophoresis. The expected band sizes were, BRD4s 206 bp and BRD4l: 488 bp, HPRT-1: 101 bp. The optical density was measured using Image Studio.



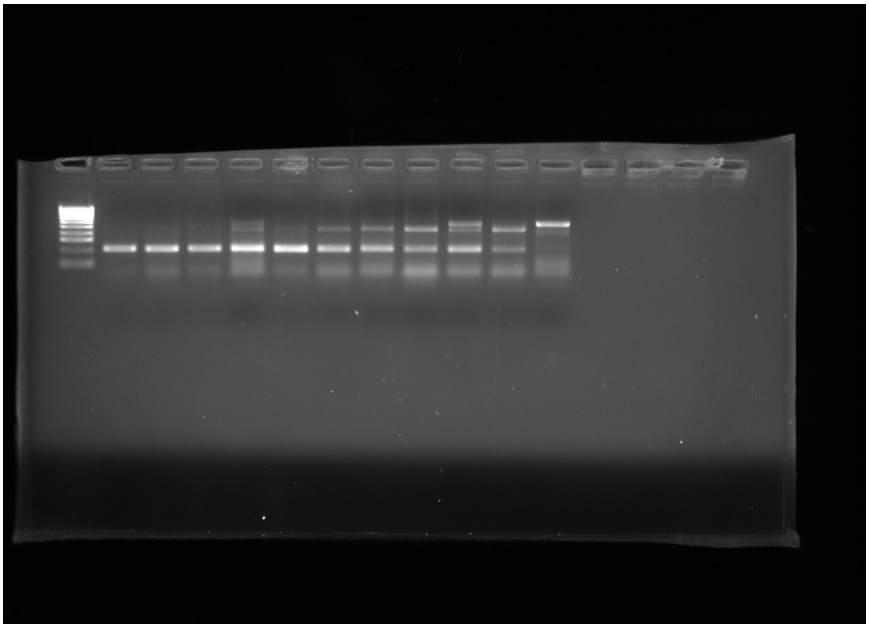
Representative example of an agarose gel showing the HPRT-1 expression levels in HL60 cells after SPHINX-31 treatment (Top) and Griffin 51 treatment (Bottom). Determined by by RT-PCR and visualized on a 2% gel by agarose gel electrophoresis. The expected band sizes were, BRD4s 206 bp and BRD4l: 488 bp, HPRT-1: 101 bp. The optical density was measured using Image Studio.



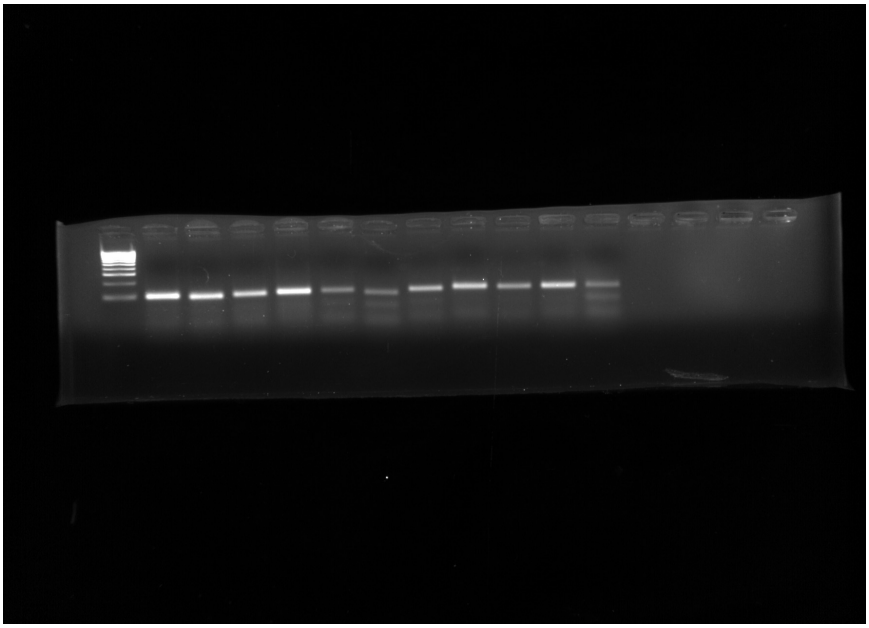
Representative example of an agarose gel showing the BRD4s and BRD4l expression levels in OCI-AML3 cells after SPHINX-31 treatment. Determined by by RT-PCR and visualized on a 2% gel by agarose gel electrophoresis. The expected band sizes were, BRD4s 206 bp and BRD4l: 488 bp, HPRT-1: 101 bp. The optical density was measured using Image Studio.



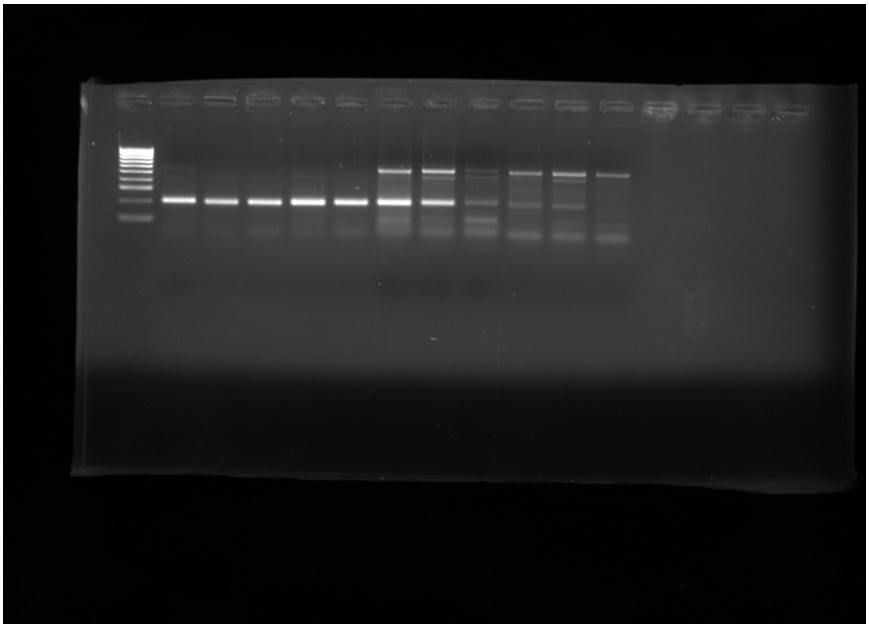
Representative example of an agarose gel showing the HPRT-1 expression levels in OCI-AML3 cells after SPHINX-31 treatment. Determined by by RT-PCR and visualized on a 2% gel by agarose gel electrophoresis. The expected band sizes were, BRD4s 206 bp and BRD4l: 488 bp, HPRT-1: 101 bp. The optical density was measured using Image Studio.



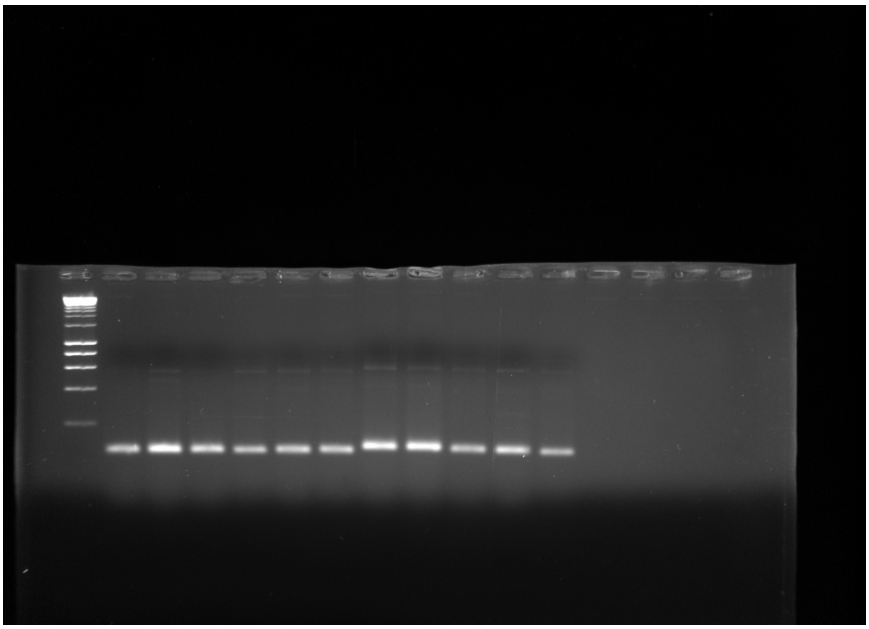
Representative example of an agarose gel showing the BRD4s and BRD4l expression levels in MOLM-13 cells after Griffin 51 treatment. Determined by by RT-PCR and visualized on a 2% gel by agarose gel electrophoresis. The expected band sizes were, BRD4s 206 bp and BRD4l: 488 bp, HPRT-1: 101 bp. The optical density was measured using Image Studio.



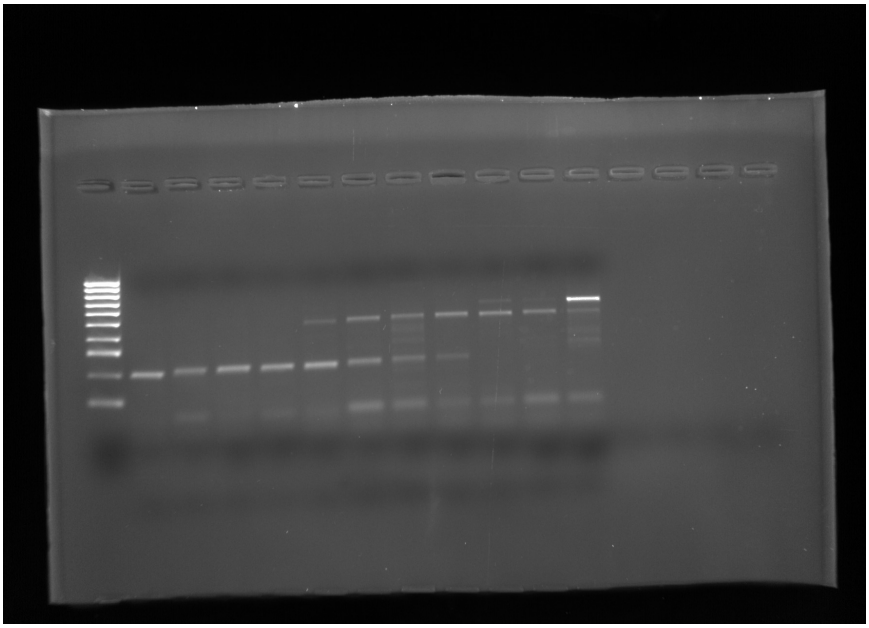
Representative example of an agarose gel showing the HPRT-1 expression levels in MOLM-13 cells after Griffin 51 treatment. Determined by by RT-PCR and visualized on a 2% gel by agarose gel electrophoresis. The expected band sizes were, BRD4s 206 bp and BRD4l: 488 bp, HPRT-1: 101 bp. The optical density was measured using Image Studio.



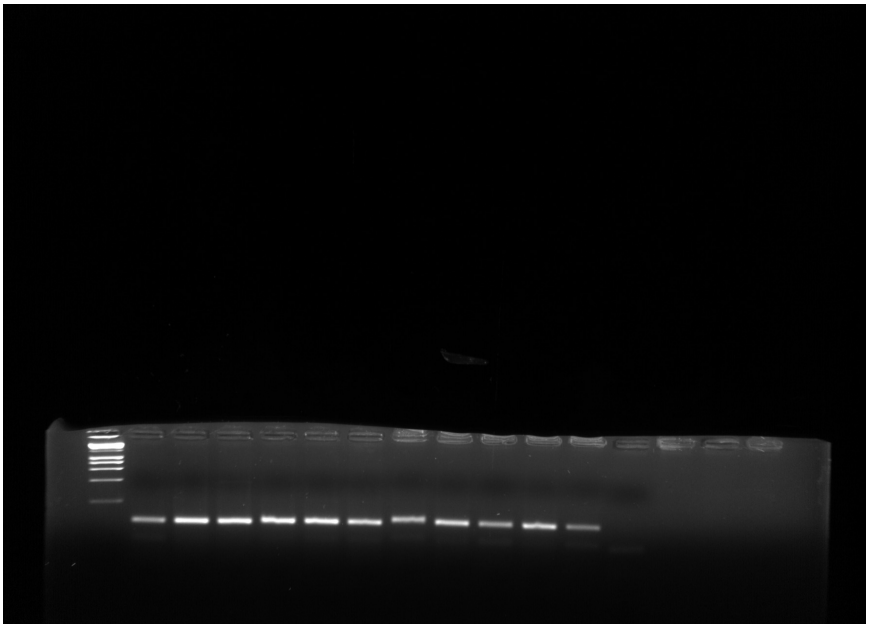
Representative example of an agarose gel showing the BRD4s and BRD4l expression levels in OCI-AML2 cells after Griffin 51 treatment. Determined by by RT-PCR and visualized on a 2% gel by agarose gel electrophoresis. The expected band sizes were, BRD4s 206 bp and BRD4l: 488 bp, HPRT-1: 101 bp. The optical density was measured using Image Studio.



Representative example of an agarose gel showing the HPRT-1 expression levels in OCI-AML2 cells after Griffin 51 treatment. Determined by by RT-PCR and visualized on a 2% gel by agarose gel electrophoresis. The expected band sizes were, BRD4s 206 bp and BRD4l: 488 bp, HPRT-1: 101 bp. The optical density was measured using Image Studio.



Representative example of an agarose gel showing the BRD4s and BRD4l expression levels in THP-1 cells after Griffin 51 treatment. Determined by by RT-PCR and visualized on a 2% gel by agarose gel electrophoresis. The expected band sizes were, BRD4s 206 bp and BRD4l: 488 bp, HPRT-1: 101 bp. The optical density was measured using Image Studio.



Representative example of an agarose gel showing the HPRT-1 expression levels in THP-1 cells after Griffin 51 treatment. Determined by by RT-PCR and visualized on a 2% gel by agarose gel electrophoresis. The expected band sizes were, BRD4s 206 bp and BRD4l: 488 bp, HPRT-1: 101 bp. The optical density was measured using Image Studio.

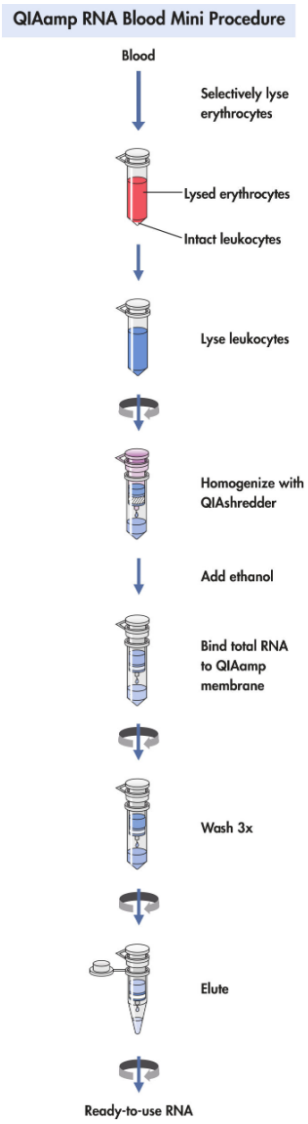
## 12.3. Primer sequences for PCR

| | **Forward** | **Reverse** |
|---|---|---|
| HOXA9 | 5'-GAATGAGAGCGGCGGAGAC- 3' | 5'-GAGCGAGCATGTAGCCAGTTG- 3' |
| MYC | 5'-AATGAAAAGGCC CCCAAGGTAGTTATCC- 3' | 5'-GTCGTTTCCGCA ACAAGTCCTCTTC- 3' |
| BCL2 | 5'-CTGCACCTGACGCCCTTCACC- 3' | 5'-CACATGACCCCA CCGAACTCAAAGA- 3' |
| BRD4 long | 5'-AGCCCCTGGTGGTAGTAAAG- 3' | 5'-CTTTTTGGGTGCCACTGGTGT- 3' |
| BRD4 short | 5'-GTGCCTCAACAAGTTCCGTT- 3' | 5'-CAAACAAACGCCCCAACCTA- 3' |
| HPRT-1 | 5'-GAACGTCTTGCTCGAGATGTGA- 3' | 5'-TCCAGCAGGTCAGCAAAGAAT- 3' |

## 12.4. Protocols

### 12.4.1. QIAamp RNA Blood Mini Kit

Brief protocol for using the QIAShredder homogenisation kit (Qiagen 79656) and QIAamp RNA Blood mini kit (Qiagen 52304). Based on the QIAamp RNA Blood Mini Handbook, published by Qiagen. (*https://www.qiagen.com/us/products/discovery-and-translational-research/dna-rna-purification/rna-purification/total-rna/qiaamp-rna-blood-mini-kit?catno=52304*).




QIAamp RNA Blood Mini procedure.

QIAamp RNA Blood Mini procedure.

# 12.4.2. CLK1-NanoLuc fusion vector sequence

NanoLuc®-CLK1 Fusion Vector

This vector can be obtained from Promega Corporation, Madison, WI. Call one of the following numbers for order or technical information.

Order or Technical 1-800-356-9526
Outside U.S. 608-274-4330

NanoLuc®-CLK1 Fusion Vector Sequence (includes open reading frame with kinase, linker and NanoLuc® luciferase):

..

ATGGTCTTCACACTCGAAGATTTCGTTGGGGACTGGCGACAGACAGCCGGCTACAACCTGGACCAAGT
CCTTGAACAGGGAGGTGTGTCCAGTTTGTTTCAGAATCTCGGGGTGTCCGTAACTCCGATCCAAAGGA
TTGTCCTGAGCGGTGAAAATGGGCTGAAGATCGACATCCATGTCATCATCCCGTATGAAGGTCTGAGC
GGCGACCAAATGGGCCAGATCGAAAAAATTTTTAAGGTGGTGTACCCTGTGGATGATCATCACTTTAA
GGTGATCCTGCACTATGGCACACTGGTAATCGACGGGGTTACGCCGAACATGATCGACTATTTCGGAC
GGCCGTATGAAGGCATCGCCGTGTTCGACGGCAAAAAGATCACTGTAACAGGGACCCTGTGGAACGGC
AACAAAATTATCGACGAGCGCCTGATCAACCCCGACGGCTCCCTGCTGTTCCGAGTAACCATCAACGG
AGTGACCGGCTGGCGGCTGTGCGAACGCATTCTGGCGGGCTCGAGCGGCGCGATCGCCATGAGACACT
CAAAGAGAACTTACTGTCCTGATTGGGATGACAAGGATTGGGATTATGGAAAATGGAGGAGCAGCAGC
AGTCATAAAAGAAGGAAGAGATCACATAGCAGTGCCCAGGAGAACAAGCGCTGCAAATACAATCACTC
TAAAATGTGTGATAGCCATTATTTGGAAAGCAGGTCTATAAATGAGAAAGATTATCATAGTCGACGCT
ACATTGATGAGTACAGAAATGACTACACTCAAGGATGTGAACCTGGACATCGCCAAAGAGACCATGAA
AGCCGGTATCAGAACCATAGTAGCAAGTCTTCTGGTAGAAGTGGAAGAAGTAGTTATAAAAGCAAACA
CAGGATTCACCACAGTACTTCACATCGTCGTTCACATGGGAAGAGTCACCGAAGGAAAAGAACCAGGA
GTGTAGAGGATGATGAGGAGGGTCACCTGATCTGTCAGAGTGGAGACGTACTAAGTGCAAGATATGAA
ATTGTTGATACTTTAGGTGAAGGAGCTTTTGGAAAAGTTGTGGAGTGCATCGATCATAAAGCGGGAGG
TAGACATGTAGCAGTAAAAATAGTTAAAAATGTGGATAGATACTGTGAAGCTGCTCGCTCAGAAATAC
AAGTTCTGGAACATCTGAATACAACAGACCCCAACAGTACTTTCCGCTGTGTCCAGATGTTGGAATGG
TTTGAGCATCATGGTCACATTTGCATTGTTTTTGAACTATTGGGACTTAGTACTTACGACTTCATTAA
AGAAAATGGTTTTCTACCATTTCGACTGGATCATATCAGAAAGATGGCATATCAGATATGCAAGTCTG
TGAATTTTTTGCACAGTAATAAGTTGACTCACACAGACTTAAAGCCTGAAAACATCTTATTTGTGCAG
TCTGACTACACAGAGGCGTATAATCCCAAAATAAAACGTGATGAACGCACCTTAATAAATCCAGATAT
TAAAGTTGTAGACTTTGGTAGTGCAACATATGATGACGAACATCACAGTACATTGGTATCTACAAGAC
ATTATAGAGCACCTGAAGTTATTTTAGCCCTAGGGTGGTCCCAACCATGTGATGTCTGGAGCATAGGA
TGCATTCTTATTGAATACTATCTTGGGTTTACCGTATTTCCAACACACGATAGTAAGGAGCATTTAGC
AATGATGGAAAGGATTCTTGGACCTCTACCAAAACATATGATACAGAAAACCAGGAAACGTAAATATT
TTCACCACGATCGATTAGACTGGGATGAACACAGTTCTGCCGGCAGATATGTTTCAAGACGCTGTAAA
CCTCTGAAGGAATTTATGCTTTCTCAAGATGTTGAACATGAGCGTCTCTTTGACCTCATTCAGAAAAT
GTTGGAGTATGATCCAGCCAAAAGAATTACTCTCAGAGAAGCCTTAAAGCATCCTTTCTTTGACCTTC
TGAAGAAAAGTATAGTTTAA

Sequence file prepared 12-Oct-2017.